IRE Transactions on ANTENNAS and PROPAGATION

Volume AP-9 MARCH, 1961 Number 2

Published Bimonthly

In This Issue

PUBLISHED BY THE

Professional Group on Antennas and Propagation

IRE TRANSACTIONS® PGAP IS A PUBLICATION DEVOTED TO EXPERIMENTAL AND THEORETICAL PAPERS ON RADIO ANTENNAS, ON GUIDED OR UNGUIDED PROPAGATION OF RADIO WAVES, AND ON ALLIED FIELDS OF RADIO PHYSICS SUCH AS RADIO ASTRONOMY

MANUSCRIPTS should be submitted to Sidney A. Bowhill, *Editor*, 222 Electrical Engineering, Pennsylvania State University, University Park, Pa. Manuscripts should be original typewritten copy, double-spaced, plus one carbon copy and two sets of copies of illustrations. Original illustrations will be called for if the paper is accepted. References should appear as footnotes and include author's name, title, journal, volume, initial and final page numbers, and date.

CONTRIBUTIONS, which should average 15 double-spaced typewritten pages in length, are subjected to review by the Associate Editors and their readers. Each paper must have a summary of less than 200 words.

COMMUNICATIONS should not exceed five double-spaced typewritten pages in length, together with not more than three illustrations. Accepted at the Editor's discretion, they appear in the first available issue.

NEWS ITEMS concerning PGAP members and group activities should be sent to the News Editor, R. C. Hansen, Space Technology Laboratories, P.O. Box 95001, Los Angeles 45, Calif.

ORIGINAL ILLUSTRATIONS should be submitted as follows: All line drawings (graphs, charts, block diagrams, cutaways, etc.) should be inked uniformly and ready for reproduction. If commercially printed grids are used in graph drawings, author should be sure printer's ink is of a color that will reproduce. Photographs should be glossy prints. Call-outs or labels should be marked on a registered tissue overlay, not on the illustration itself. No illustration should be larger than 8 x 10 inches.

Copies can be purchased from **the INSTITUTE OF RADIO ENGINEERS, 1 East 79th St., New York 21, N.Y.** Individual copies of this issue, and all available back issues, except Vols. AP-5, No. 1; AP-6, No. 1; AP-7, Special Supplement, may be purchased at the following prices: IRE members (one copy) $2.25, libraries and colleges $3.25, all others $4.50. Yearly subscription rate: non-members $17.00; colleges and public libraries $10.00. IRE TRANSACTIONS ON ANTENNAS AND PROPAGATION. Printed in U.S.A. Printed by George Banta Co., Inc., Curtis Reed Plaza, Menasha, Wisconsin.

Second-class postage paid at MENASHA, WISCONSIN, and additional mailing offices under the act of August 24, 1912. Acceptance for mailing at a special rate of postage is provided for in the act of February 28, 1925, embodied in Paragraph 4, Section 412, P. L. & R., authorized October 26, 1927.

IRE Transactions on Antennas and Propagation

Volume AP-9 MARCH, 1961 Number 2
Published Bimonthly

TABLE OF CONTENTS

CONTRIBUTIONS

COMMUNICATIONS

contributions

A Triangular Arrangement of Planar-Array Elements that Reduces the Number Needed*

EUGENE D. SHARP†, MEMBER, IRE

Summary—**In this paper, it is shown that by arranging the elements of a beam-scanning planar antenna array in a triangular pattern rather than a rectangular pattern, the number of elements needed in the array is reduced. (The number of elements needed in an array is determined from the requirement that no spurious beams form in the array pattern.) The reduction in the number of elements depends upon the solid angle over which the main beam is positioned. If the main beam is positioned within a constant angle about the array normal, then the number of elements can be reduced by 13.4 per cent by arranging the elements in a pattern of equilateral triangles rather than in a square pattern. If the main beam is positioned within a "pyramid," centered about the array normal, then the reduction is usually less than 13.4 per cent. Graphs are included showing for both element arrangements the solid angle over which the main beam can be scanned without the formation of spurious beams.**

Introduction

In the design of large-aperture, electronic-scanning, antenna arrays, the number of antenna elements, phase shifters, and associated components becomes extremely large. If the number of antenna elements can be reduced by spacing them farther apart, the number of phase shifters and associated components can also be reduced, resulting in a sizable decrease in the cost and complexity of a scanning array.

In this paper, it is shown that if the main beam is positioned throughout the interior of a cone whose axis is the array normal, the number of array elements can be reduced by 13.4 per cent by arranging the elements in a pattern of equilateral triangles rather than squares. If the main beam is positioned throughout the interior of a "pyramid" whose axis is the array normal, the reduction in the number of elements is less than 13.4 per cent. The reduction in the number of elements applies to arrays of uniformly-spaced elements. Arrays of nonuniformly-spaced elements are not considered here.

The spacing between elements is limited by the formation of spurious beams in the array pattern. To prevent spurious beams from forming, the element spacing must be less than a certain maximum. This maximum element spacing can be determined by examining the array pattern and finding the element spacing at which a spurious beam just begins to form.

* Received by the PGAP, February 22, 1960; revised manuscript received, July 29, 1960. The work reported in this paper was done at Stanford Res. Inst. on Contract AF (19(604)-2240 from the AF Cambridge Res. Center, Cambridge, Mass.

† Stanford Res. Inst., Menlo Park, Calif.

When the array elements are arranged in a triangular pattern, we find that the maximum element spacing is larger than when the array elements are arranged in a rectangular pattern; and thus fewer elements are needed to complete an antenna aperture when the elements are arranged in a triangular pattern.

Location of Spurious Beams

The array pattern for an array of isotropic radiators excited with equal amplitude and arranged in the rectangular pattern of Fig. 1 is

$$S_R = \sum_n e^{jn(2\pi/\lambda)a_z(\cos\theta - \cos\theta_0)} \cdot \sum_m e^{jm(2\pi/\lambda)a_x(\cos\phi\sin\theta - \cos\phi_0\sin\theta_0)}. \quad (1)$$

In this expression λ is the free-space wavelength, and (θ_0, ϕ_0) defines the angle to which the main beam is scanned. A beam forms whenever all the terms of the array pattern add up in phase, or at the angle (θ, ϕ) defined by the two simultaneous equations:

$$\cos\theta = \cos\theta_0 + p(\lambda/a_z) \quad (p = 0, \pm 1, \pm 2, \cdots),$$
$$\cos\phi\sin\theta = \cos\phi_0\sin\theta_0 + q(\lambda/a_x) \quad (q = 0, \pm 1, \pm 2, \cdots). \quad (2)$$

When $p = q = 0$, the solution of (2) gives $\theta = \theta_0$ and $\phi = \phi_0$, which is the main-beam angular position. Spurious-beam angular positions (if they exist) are given by using other combinations of p and q.

An array of elements arranged in the triangular pattern is shown in Fig. 2. For purposes of calculation, this array pattern can be thought of as a sum of the patterns of two subarrays. The triangularly arranged array can be separated into the subarrays of circles and crosses shown in Fig. 2. The subarray of crosses is displaced from the subarray of circles by b_x and b_z along the x and z coordinates, respectively. The element spacing for both subarrays is $2b_x$ along the x coordinate and $2b_z$ along the z coordinate. The pattern of the subarray of circles is that of (1) with $2b_x$ and $2b_z$ replacing a_x and a_z, respectively. The pattern of the subarray of crosses is also that of (1), multiplied by a phase factor to take into account the displacement of the subarray of crosses from the subarray of circles. Summing the two subarray patterns, we find that the array pattern of the triangularly arranged array of Fig. 2 phased to direct a beam in the (θ_0, ϕ_0) direction, is

$$S_T = \left[1 + e^{j(2\pi/\lambda)b_z(\cos\theta - \cos\theta_0)} \cdot e^{j(2\pi/\lambda)b_x(\cos\phi\sin\theta - \cos\phi_0\sin\theta_0)}\right] \cdot \left[\sum_n e^{j2n(2\pi/\lambda)b_z(\cos\theta - \cos\theta_0)} \cdot \sum_m e^{j2m(2\pi/\lambda)b_x(\cos\phi\sin\theta - \cos\phi_0\sin\theta_0)}\right]. \quad (3)$$

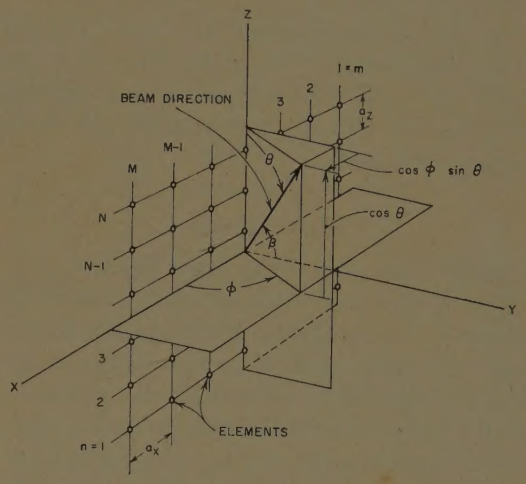

Fig. 1—Array of elements arranged in a rectangular pattern.

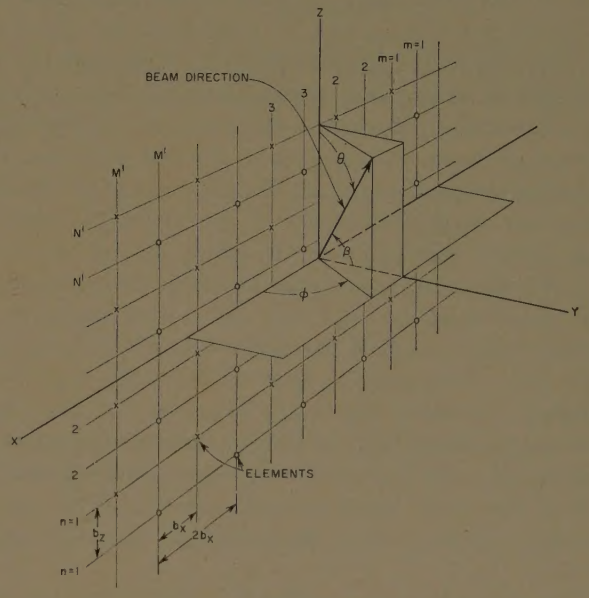

Fig. 2—Array of elements arranged in a triangular pattern.

S_T is very similar to S_R except for the additional factor multiplying the summations over n and m and the multiplier 2 appearing in the exponents. As with array pattern S_R, spurious beams may form in the array pattern S_T when all the terms in the second factor are in phase. This situation occurs at the angles (θ, ϕ) defined by the simultaneous equations

$$\cos\theta = \cos\theta_0 + p(\lambda/2b_z) \quad (p = 0, \pm 1, \pm 2, \cdots),$$
$$\cos\phi\sin\theta = \cos\phi_0\sin\theta_0 + q(\lambda/2b_x) \quad (q = 0, \pm 1, \pm 2, \cdots)$$
$$(p + q) \text{ even}. \quad (4)$$

The first factor of S_T is equal to either 0 or 2, depending on the value of p and q in (4). Thus, if $(p+q)$ is odd, it equals zero, and if $(p+q)$ is even, it equals two. In this way a spurious beam forms in the array pattern S_T only when $(p+q)$ is even and not when $(p+q)$ is odd.

The location of the spurious beams is independent of the array aperture size and shape. The array aperture may be of any reasonable shape such as rectangular, circular, elliptical, and (2) and (4) apply for the location of the spurious beams.

Scan Angles

The region over which the main beam can be positioned without the formation of spurious beams can be determined for rectangular or triangular element arrangements using (2) and (4), respectively. As the main beam is positioned away from the array normal ($\beta=0$), an angle is reached at which a spurious beam just begins to form. This spurious beam always begins to form in the plane of the array. This plane is defined by the condition that $\beta=90°$, or the equivalent conditions that $\phi=0°$ or 180°. Therefore, in order to find the region over which the main beam can be positioned for given element spacings, one sets $\cos\phi=\pm1$ in (2) and (4) and solves for θ_0 vs ϕ_0 using appropriate values of p and q. The solution θ_0 vs ϕ_0 defines the boundary of the region over which the main beam can be positioned without the formation of spurious beams. If the center of the beam is positioned on the boundary of this region, a spurious beam forms completely in the plane of the array. To keep the spurious beam from forming, the peak of the main beam must be kept just inside the boundary by approximately one half the null beamwidth. As the size of the array increases, the beamwidth of the main beam decreases, allowing the main beam to be positioned closer to the boundary. In this paper the statement, to position the main beam within a region, implies that the peak of the main beam should come no closer to the boundary of the region than one half the null beamwidth.

If the elements are arranged in a square pattern with an element spacing of $a_x=a_z=0.585\ \lambda$, the region over which the main beam can be positioned is shown in Fig. 3. If the elements are arranged in a pattern of equilateral triangles in which $2b_x=0.676\ \lambda$ and $b_z=0.585\ \lambda$, the region over which the main beam can be positioned without the formation of spurious beams is shown in Fig. 4. For both Fig. 3 and Fig. 4, the main beam can be positioned to an angle approaching 45° from the array normal in any direction. However, when the elements are arranged in a square pattern, the main beam can be positioned throughout a larger solid angle than when the elements are arranged in a triangular pattern.

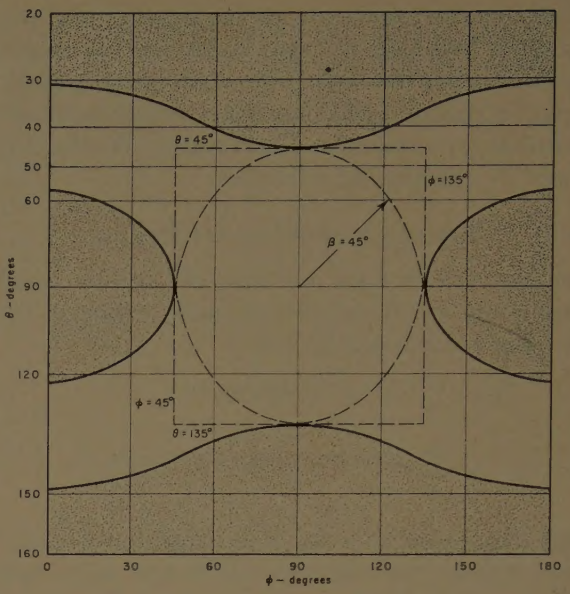

Fig. 3—Solid angle over which the main beam can be scanned for an array of elements arranged in a square pattern with $a_x=a_z=0.585\ \lambda$.

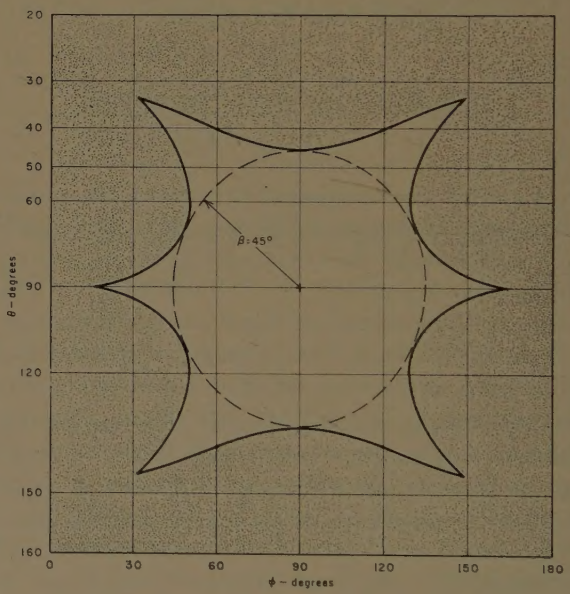

Fig. 4—Solid angle over which the main beam can be scanned for an array of elements arranged in a pattern of equilateral triangles with $2b_x=0.676\ \lambda$ and $b_z=0.585\ \lambda$ (reduction in the number of elements is 13.4 per cent).

Reduction in the Number of Antenna Elements

If we calculate the number of elements needed to complete an antenna array of a given size when the elements are arranged first in a rectangular pattern, and then in a triangular pattern, we find that, in general, fewer elements are needed when the elements are arranged in the triangular pattern. For a large array, the number of elements in the rectangularly arranged array of Fig. 1 is approximately

$$N_R=\frac{A}{a_x a_z} \tag{5}$$

where A is the area of the array aperture. For a large array, the number of elements in the triangularly arranged array of Fig. 2 is approximately

$$N_T=\frac{A}{2b_x b_z}. \tag{6}$$

The per cent reduction in the number of elements comparing (6) to (5) is

$$\frac{N_R - N_T}{N_R} \times 100 \text{ per cent.} \qquad (7)$$

A calculation of the number of elements required by the arrays of Fig. 3 and Fig. 4 shows that the triangularly arranged array contains 13.4 per cent fewer elements than the squarely arranged array. The main beam of both these arrays can be scanned within a cone defined by $\beta = 45°$. The result is that if the main beam is to be positioned within any cone defined by $\beta = \beta_0$, the number of elements can always be reduced 13.4 per cent by arranging them in a pattern of equilateral triangles instead of squares. In this case, the altitude of the equilateral triangle in the triangularly arranged array is equal to the element spacing of the squarely arranged array, or $b_z = a_z$ and $2b_x = a_x/0.866$. Therefore, $(N_R - N_T)/N_R = 0.134$.

Another application may require that the main beam be positioned not within a cone, but within the region bounded by the four surfaces $\phi = 90° \pm \beta_\phi$, $\theta = 90° \pm \beta_\theta$. For this case, the number of elements can still be reduced by arranging them in a triangular pattern instead of a rectangular pattern, but the reduction here is less than the previous 13.4 per cent. For instance, if $\beta_\theta = \beta_\phi = 45°$, the element spacing for an array of elements arranged in a square pattern need not be changed from that of Fig. 3; however, for an array of elements arranged in a triangular pattern, the element spacing of Fig. 4 cannot be used because the main beam is to be positioned in regions in which a spurious beam forms. If $2b_x$ is decreased to 0.645 λ, then the main beam can be positioned throughout the required region bounded by the four surfaces $\theta = 45°$, 135° and $\phi = 45°$, 135° shown in Fig. 5. In comparing the number of elements required for the array of Fig. 5 to the number required for the array of Fig. 3, the per cent reduction in the number of elements is 9.2 per cent. The reduction in the number of elements when other values of β_θ and β_ϕ, keeping $\beta_\theta = \beta_\phi$, are chosen, is shown in Fig. 6. The reduction in the number of elements is a maximum when the main beam is not scanned at all and when the main beam is scanned throughout a hemisphere. A minimum occurs when $\beta_\theta = \beta_\phi = 20°$.

Similar calculations can be made when other values of β_θ and β_ϕ are chosen such that $\beta_\theta \neq \beta_\phi$. For instance, when $\beta_\theta = 45°$ and $\beta_\phi = 25°$, the number of elements can be reduced by 7.7 per cent by arranging the elements in a triangular pattern instead of a rectangular pattern.

The reduction in the number of elements resulting from the use of the triangular array depends upon the region through which the main beam is positioned. If the main beam is positioned within the interior of a cone whose axis is the array normal, the number of array elements can be reduced by 13.4 per cent by arranging them in a pattern of equilateral triangles instead of squares. If the main beam is positioned throughout the interior of a "square pyramid" whose axis is the array normal, the reduction in the number of elements may vary from 13.4 per cent to 5.7 per cent, depending upon the maximum main-beam angular position from the array normal. The possible reduction in the number of phase shifters and associated components in the phasing network feeding the array elements would be similar to the reduction in the number of elements.

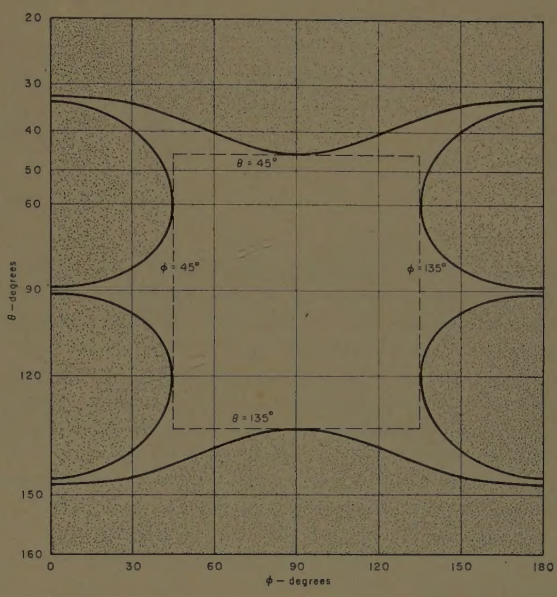

Fig. 5—Solid angle over which the main beam can be scanned for an array of elements arranged in a triangular pattern with $2b_x = 0.645\lambda$ and $b_z = 0.585\lambda$ (reduction in the number of elements is 9.2 per cent).

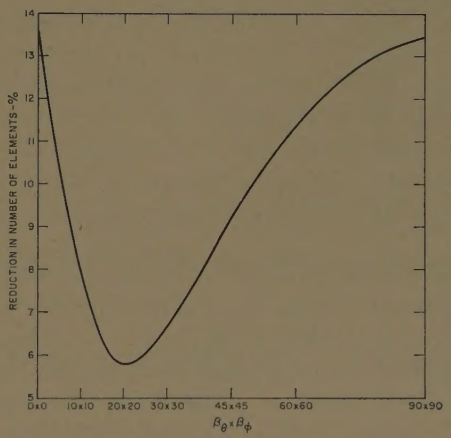

Fig. 6—Reduction in the number of elements resulting from the arrangement of elements in a triangular pattern, instead of a square pattern when the main beam is to be scanned within a region bounded by the four surfaces $\theta = 90° \pm \beta_\theta$ and $\phi = 90° \pm \beta_\phi$.

A Study of the Coma-Corrected Zoned Mirror by Diffraction Theory*

S. DASGUPTA† AND Y. T. LO‡

Summary—A two dimensional coma-corrected zoned mirror has been investigated by a rigorous integral equation formulation, for whose solution a procedure of successive approximation can be established. For computational convenience, the exact first order solution is again approximated. The error committed in this approximation is investigated. The higher order solutions due to couplings between zones are not significant so far as the image field is concerned.

In the example studied, it is found that for a system with small *F*-number and an illumination of small taper the coma aberration of this zoned mirror is practically eliminated for scan angles up to 25°, in sharp contrast to a smooth parabola whose scanning characteristics are also presented for comparison. However, the chromatic aberration overshadows this advantage for a wide-band application; the total bandwidth of this example is only a few per cent.

I. Introduction

FOR wide angle scanning, the aperture of a microwave reflector is always limited by the progressive deterioration of the image as the aperture of the system is increased. The correction of aberrations by placing the surface of one curvature on the surface of another has been suggested by various workers. In particular, the zoned mirror[1–4] recently has received much attention, probably because of the development of large aperture antenna systems for radio astronomy research.

A zoned mirror consists of sections of a set of confocal paraboloids with focus at c and axis vc defined by $r=2(f-n\lambda/2)/[1+\cos\Psi]$, $n=0, 1, 2\cdots$, where f is the focal length of the paraboloid with largest focal length (Fig. 1). This family of paraboloids will intersect the spherical surface Σ with c as center and f as radius at circles represented by P_1, P_2, etc. If a set of planes perpendicular to the axis vc is drawn through the vertices of paraboloids, N_1, N_2, $\cdots$, they will cut the spherical surface in another set of circles represented by Q_1, Q_2; by passing through this set of circles, a family of cylinders coaxial with vc can be drawn. Then the paraboloidal surfaces cut out by these cylinders form a zoned mirror as shown by the solid line in Fig. 1.

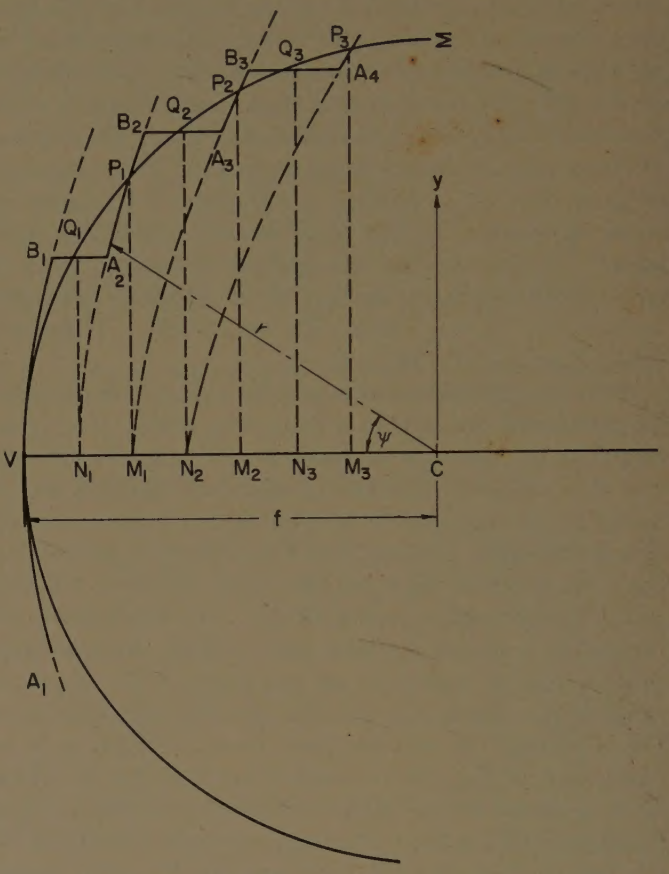

Fig. 1—Construction and geometry of zoned mirror.

Ramsay and Jackson[2] compared the measured gains, sidelobe levels and beamwidths of the radiation pattern of a zoned mirror with those of a spherical mirror with a feed offset of 15°. They found that the zoned mirror is not much better than the spherical mirror. However, it should be pointed out that they worked with a case where the advantages of a zoned mirror are greatly suppressed since their mirror had a large *F*-number with a 15 db-tapered illumination, and the zones were not exactly on the coma-circle as shown above.

Provencher,[3] on the other hand, investigated a zoned mirror with a smaller *F*-number and also with the zones properly located. He has demonstrated the vast superiority of a zoned mirror over a smooth parabola or a spherical mirror in scanning performance.

* Received by the PGAP, March 8, 1960; revised manuscript received by July 14, 1960. This work was supported by Wright Air Development Center under contract No. AF 33(616)3220 and No. AF 33(616)-6079.

† Government College of Engineering and Technology, Raipur, M.P., India. Formerly Antenna Lab., Dept. of Elec. Engrg., University of Illinois, Urbana, Ill.

‡ Antenna Laboratory, Dept. of Elect. Engrg., University of Illinois, Urbana, Ill.

[1] D. W. Fry and F. K. Goward, "Aerials for cm Wavelength," Cambridge University Press, Cambridge, England; 1950.

[2] J. F. Ramsay and J. A. C. Jackson, "Wide angle scanning performance of mirror aerials," *Marconi Review*, vol. 19, No. 122, pp. 119–140; 1956.

[3] J. H. Provencher, "Experimental Study of a Diffraction Reflector," Air Force Cambridge Research Center, Cambridge, Mass.; April, 1959.

[4] A. L. Ronchi and G. Toraldo di Francia, "An application of parageometrical optics to the design of a microwave mirror," IRE TRANS. ON ANTENNAS AND PROPAGATION, vol. AP-6, pp. 129–133; January, 1958.

Toraldo di Francia *et al.*,[4] have shown by parageometrical optics that coma aberration is greatly reduced in a zoned mirror. They have obtained expressions for the fifth order coma and astigmatism for this type of mirror (the third order coma is absent as a result of the satisfaction of the sine condition). Very recently they also reported[5] that their experimental results are in good agreement with the theoretical predictions of the best focal surface for scanning purposes.

Aberrations of a system are generally studied by geometrical optics or by obtaining the diffraction pattern at the image space with a known aberration function at the aperture.[6] For a practical system it is in general extremely difficult to determine the aberration function except by experiment. On the other hand, geometrical optics provides only an asymptotic solution which becomes powerless to describe the deterioration of a diffraction pattern in the microwave region. This is particularly true for the region of nulls and minor lobes where, because of increased sensitivity to aberration, even physical optics begin to show errors. For a system like the zoned mirror, which has a large number of discontinuities in structure, even the physical optics method seems to need further justification. It is reasonable to assume that the diffraction due to the edges and the coupling between zones could be important particularly in the regions of nulls and minor lobes upon which the coma aberration has a dominant effect.

The purpose of this investigation is, therefore:

1) to analyze the performance of the zoned mirror as a wide angle scanning antenna by employing a more rigorous boundary value problem approach, and

2) to provide a comparative study of various approximations in the analysis.

For mathematical convenience, a two-dimensional zoned mirror is studied where each zone except the first is approximated by a flat strip. In fact, this system is of more interest, since, being free from astigmatism, it enables one to evaluate its ability in coma correction exclusively.

II. Formulation

Let a two-dimensional zoned mirror consist of n perfectly conducting plane strips infinite extent in the z-direction, and let an incident plane electromagnetic wave with its electric field E_{inc} be polarized parallel to the edges of the strips. Then the current $I_1, I_2, \cdots, I_n$ induced on the zones 1, 2, $\cdots$, n respectively satisfy the following equation

$$-E_{\text{inc}}(s') = \sum_{i=1}^{n} G_i^* I_i \tag{1}$$

where

$$G \equiv -\frac{k^2}{4\omega\epsilon} H_0^{(2)}(k|s|),$$

$$k \equiv 2\pi/\lambda,$$

$$j \equiv \sqrt{-1},$$

$$G_i^* I_i = \text{convolution integral over strip } i$$

$$= \frac{k^2}{4\omega\epsilon} \int_{\text{strip } i} I_i(s) H_0^{(2)}(k|s - s'|)\, ds;$$

s' is a point on any of the n strips.

Eq. (1) represents a set of n simultaneous integral equations for n unknown functions $I_i(s)$. Let[7]

$$I_i = I_{ii} + \sum_{\substack{j=1 \\ j\neq i}}^{n} I_{ij} \tag{2}$$

where I_{ii} is the current induced on strip i due to E_{inc} in the absence of other strips, and I_{ij} is the current on strip i due to the field of I_j of the strip j. Then by definition

$$G_i^* I_{ii} = -E_{\text{inc}}(s'), \qquad s' \text{ on strip } i. \tag{3}$$

It follows that

$$\sum_{\substack{j=1 \\ j\neq i}}^{n} \left[G_i^* I_{ij} + G_j^* I_{jj} + \sum_{\substack{k=1 \\ k\neq j}}^{n} G_j^* I_{kj} \right] = 0. \tag{4}$$

Since s' is on strip i, $|G|$ in the first integral of (4) is much greater than that in second and third, and further $I_{jj} \gg I_{jk}$. Thus an iterative procedure can be established by solving

$$\sum_{\substack{j=1 \\ j\neq i}}^{n} \left[G_i^* I_{ij}^{(1)} + G_j^* I_{jj} \right] = 0, \qquad s' \text{ on strip } i, \tag{5}$$

where $I_{ij}^{(1)}$, the first order solution of I_{ij}, represents the current induced in strip i due to I_{jj}. In effect, (5) represents an independent linear integral equation for each strip. Hence, the set of n simultaneous integral equations denoted by (1) has been reduced to independent equations for each order of solutions. Since (5) is linear, it follows that

$$G_i^* I_{ij}^{(1)} + G_j^* I_{jj} = 0, \qquad \text{for all } j \neq i. \tag{6}$$

Eq. (6) can be solved if I_{jj} is known. Indeed, it represents the integral equation of the current distribution on a strip i due to a known source distribution I_{jj} on strip j. Further, by definition I_{jj} is the current induced on strip j due to an incident plane wave as given by (3). Thus the problem is reduced to the solution of (3) and thereafter to that of (6). In fact, (3) is a special case of

[5] G. Toraldo di Francia, *et al.*, "Experimental test of a stepped zoned mirror for microwaves," IRE Trans. on Antennas and Propagation, vol. AP-7, pp. 125–133; December, 1959.

[6] B. R. Nijboer, "Diffraction Theory of Aberrations," Ph.D. Dissertation, Univ. of Groningen, Netherlands; 1942.

[7] It is clear that the summation indices j and k in (2) and (4) etc. should not be confused with the imaginary number $j = \sqrt{-1}$ and the phase shift constant $k = 2\pi/\lambda$.

(6). The rigorous solutions for both equations lead to a series solution involving Mathieu functions with the width of the strips (among other factors) as the argument.[8] However, this solution loses its importance for practical purposes due to slow convergence when the width of the strip is large, as in the present case, where large aperture is of main interest. It can also be shown that even the asymptotic expansion of the Mathieu functions for such arguments leads to solutions, the accuracy of which is not the same at all points on the strip, and at certain points the accuracy is very low. An approximate solution with reasonable accuracy is therefore to be obtained.

III. Approximate Solution

There are numerous works[9] on approximate solutions to (3) and (6), most of which have justified their theory by showing the small numerical difference between the approximate and exact solutions for a certain set of parameters, for which the latter is available. The first order term in their solutions is, in fact, the same as that obtained by Schwarzchild (namely, the half plane solutions for each edge, which is sufficiently accurate for strips of the order of a wavelength wide or more). Thus, the current distribution I_{ii} across a strip AB of Fig. 2

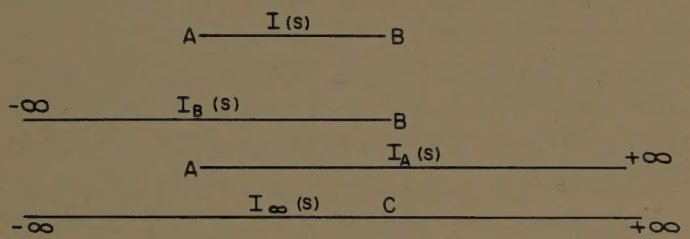

Fig. 2—Approximation of a strip by two half-planes and an infinite plane.

can, for the present purpose, be approximated in the following way:

$$I_{ii} = \begin{cases} I_A + I_B - I_C, & s \text{ on } AB, \\ 0, & s \text{ outside of the strip } AB, \end{cases}$$

where I_A and I_B are the current distributions across a halfplane extending from A to ∞, and from B to $-\infty$ respectively, and I_C is the current across an infinite plane. I_A, I_B and I_C are known exactly in terms of Fresnel integrals and simple functions. Thus, I_{ii} can be computed without resorting to complicated Mathieu functions as follows. Let

$$E_{\text{inc}} = e^{jkr\cos(\alpha'-\alpha)}$$

be the incident electric field polarized parallel to z-axis where r, α are the coordinates of the point of observation and α' is the direction of the incident wave, all measured from the half-plane ax with edge A as origin as shown in Fig. 3. Then by Sommerfeld's half-plane

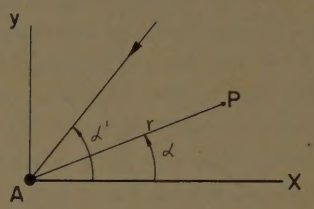

Fig. 3—A plane wave incident on a half-plane.

solution,[10]

$$\begin{aligned} I_A = \frac{2}{\eta}\Bigg[& \sin\alpha'\{(C_A+S_A)\cos(kr\cos\alpha') \\ & -(C_A-S_A)\sin(kr\cos\alpha')\} \\ & +\frac{\sin\alpha'/2}{\sqrt{\pi kr}}(\cos kr-\sin kr)\Bigg] \\ & +\frac{2j}{\eta}\Bigg[\sin\alpha'\{(C_A+S_A)\sin(kr\cos\alpha') \\ & +(C_A-S_A)\cos(kr\cos\alpha')\} \\ & -\frac{\sin\alpha'/2}{\sqrt{\pi kr}}(\cos kr+\sin kr)\Bigg] \end{aligned} \tag{7}$$

where

$$C_A - jS_A = \int_0^u e^{-j\pi t^2/2}dt,$$

$$u = 2\sqrt{\frac{kr}{\pi}}\cos\alpha'/2 \quad \text{and} \quad \eta = \sqrt{\mu/\epsilon}.$$

I_B can be obtained by putting $(\pi-\alpha')$ for α' and r' for r in (7) if $(r', \pi-\alpha)$ is the observation point referred to origin B. I_C is given by $I_C = (2/\eta)\sin\alpha\, e^{jkr\cos\alpha'}$.

For the solution of (6), let the Green's function, namely the current in strip i due to a unit line source at (r_0, θ_0) be K_{ij}; then based on the same procedure, K_{ij} can be approximated by $K_A+K_B-K_C$ where K_A, K_B and K_C are currents in the half-planes A, B and infinite

[8] S. Dasgupta and Y. T. Lo, "A Study of the Coma-Corrected Zoned Mirror by Diffraction Theory," Antenna Lab., Univ. of Ill., Urbana, Ill., Tech. Rept. No. 40; July, 1959.

[9] K. Schwarzchild, "Die bungung und polarisation des lichtsdurch einen spalt," *Math. Ann.*, vol. 55, pp. 177; 1902.
S. Skavlem, "On the differention of scaler plane waves by a slit of infinite length," *Arch. Math. Maturvid.* vol. 51, p. 161; 1951.
S. N. Karp and A. Russek, "Diffraction by a wide slit," *J. Appl. Phys.*, vol. 27, No. 8, p. 186; August, 1956.
R. F. Millar, "Diffraction by a wide slit and complementary strip," Ph.D. Dissertation, Cambridge University, Cambridge, England, 1957.
P. M. Morse and P. J. Rubenstein, "Diffraction of waves by ribbons and slots," *Phys. Rev.*, vol. 54, p. 895; December, 1938.
E. B. Moullin and P. M. Phillips, "On the current induced in a conducting ribbon by the incidence of a plane electromagnetic wave," *Proc. IEE*, vol. 99, Pt. IV, No. 3, p. 137; 1952.
E. B. Moullin, "On the current induced in a conducting ribbon by a current filament parallel to it," *Proc. IEE*, Monograph No. 71 R, p. 7; 1953.

[10] B. B. Baker and E. T. Copson, "The Mathematical Theory of Huygens Principle," Clarendon Press, Oxford, England; 1950.
A. Sommerfeld, "Optics," Academic Press, New York, N. Y.; 1954.

plane C respectively as shown in Fig. 2. Since the field at any point $P(r, \theta)$ due to a unit filament S in presence of a half plane as in Fig. 4 is given by[11]

$$E_z(P) = \frac{j\omega\mu}{4\pi}\left\{\int_{-\infty}^{\xi_0} e^{-jkR\cosh\xi}d\xi - \int_{-\infty}^{\xi_1} e^{-jkR_1\cosh\xi}d\xi\right\} \quad (8)$$

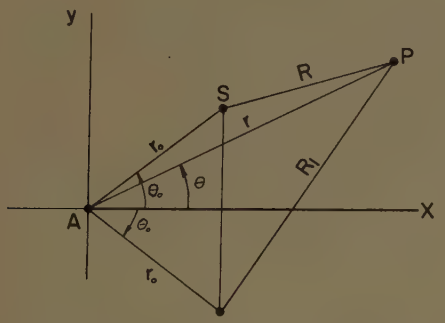

Fig. 4—A line source above a half-plane.

where

$$\sinh\xi_0 = \frac{2\sqrt{rr_0}}{R}\cos\frac{\theta-\theta_0}{2}, \qquad \sinh\xi_1 = \frac{2\sqrt{rr_0}}{R_1}\cos\frac{\theta+\theta_1}{2},$$

$$R = \sqrt{r^2 + r_0^2 - 2rr_0\cos(\theta-\theta_0)},$$

and

$$R_1 = \sqrt{r^2 + r_0^2 - 2rr_0\cos(\theta+\theta_0)}.$$

Then

$$K_A = -\frac{1}{\pi}\left[\sqrt{\frac{r_0}{r}}\frac{(r+r_0)}{R^2}\sin\frac{\theta_0}{2}e^{-jk(r+r_0)} + \frac{jkr_0}{2R_e}\sin\theta_0\int_{(-2\sqrt{rr_0}/R)\cos\theta_0/2}^{(2\sqrt{rr_0}/R)\cos\theta_0/2} e^{-jkr\sqrt{1+z^2}}dz\right]. \quad (9)$$

Similarly K_B can be obtained by replacing r, r_0, θ, θ_0, by r', r_0', θ' and θ_0' respectively. Furthermore

$$K_C = \frac{jkr_0}{2R}\sin\theta_0 H_1^{(2)}(kR). \quad (10)$$

Since (6) is linear in I_{ij} and I_{jj},

$$I_{ij}(s) = \int_{\text{strip } j} K_{ij}(s', s)I_{jj}(s')ds', \qquad s \text{ on strip } i.$$

IV. Investigation of the Error Due to Approximation of the Current Distribution

To determine precisely the error committed in the approximation to the solutions of (3) and (6) obviously requires a knowledge of the exact solutions to these equations; but these exact solutions have purposely not been sought owing to the difficulty of computation as discussed previously. However, the tangential field due to the exact current is known; therefore, it is possible to determine the degree of approximation by evaluating the closeness of the boundary condition satisfied.

Let the exact current distribution at any point x on the strip AB be $I_e(x)$, here the origin $x=0$ being the center of the strip; then, since the total tangential E-field at any point x on the strip of width $2h$ is zero, we have the integral equation for I_e given by

$$G * I_e = -E_{\text{inc}}(x), \qquad -h \le x \le h, \quad (11)$$

where

$$G \equiv \frac{-k^2}{4\omega\epsilon}H_0^{(2)}(k|x|),$$

$$I_e(x) \equiv 0 \quad \text{if} \quad |x| > h, \quad \text{and}$$

$$G * I_e = -\frac{k^2}{4\omega\epsilon}\int_{-\infty}^{\infty} I_e(x')H_0^{(2)}(k|x-x'|)dx'.$$

The approximate current distribution $I(x)$ will, in general, satisfy a slightly different equation given by

$$G * [I] = -E_{\text{inc}}(x) + \Delta E(x), \quad -h \le x \le h, \quad (12)$$

where

$$[I(x)] = I(x)\{U(x+h) - U(x-h)\},$$

$$U(x) \equiv 1, \qquad x > 0,$$

$$\equiv 0, \qquad x < 0;$$

hence

$$G * (I_e - [I]) = -\Delta E(x), \quad -h \le x \le h. \quad (13)$$

Thus, ΔE indicates the error committed in the boundary condition by taking the approximate current distribution $I(x)$ for the problem of the strip.

Now $I(x) = I_A(x) + I_B(x) - I_C(x)$ for $-h \le x \le h$ and they satisfy the following equations

$$G * I_B = -E_{\text{inc}}, \qquad -\infty \le x \le h,$$

$$G * I_A = -E_{\text{inc}}, \qquad -h \le x \le \infty,$$

$$G * I_C = -E_{\text{inc}}, \qquad -\infty \le x \le \infty. \quad (14)$$

By breaking the range of the above integrations into $-\infty$ to $-h$, $-h$ to h, and h to ∞ using (11) and (12), one obtains

$$\Delta E(x) = G * \{(I_B - I_C)U(-x'-h) + (I_A - I_C)U(x'-h)\}, \quad -h \le x \le h, \quad (15)$$

where I_A, I_B and I_C are known. This method of determining error is different from others in that it is not restricted by the width of the strip.

For the observation point near the center of the strip or at the edges, the integral can be evaluated asymptotically in $2h$. For other points, an upper bound can be found. The results, reported elsewhere,[8] indicate that the asymptotic series for ΔE is of an order at least $(kh)^{-2}$.

[11] This form of solution is preferred to the series solution in Bessel functions so far as computation is concerned.

Fig. 5 shows $|\Delta E|$ as expressed in $|\Delta E/E_{inc}| \times 100$ for various width $l=2h$, and normal incidence. It is seen that even for a strip of $\lambda/2$ wide, the error is less than 1 per cent. Fig. 6 shows $|\Delta E|$ for $l=\lambda$ but with incident angle $=0$, 15°, 25°, 45°. On the average $|\Delta E|$ increases with α, but it is always less than 1.7 per cent. For all the strips used in the zoned mirror in the present investigation, the average $|\Delta E|$ is less than 0.5 per cent for $\alpha=0$, and less than about 2 per cent for the highest oblique incidence. It is therefore clear that the approximate current distributions provided a rather high accuracy solution.

V. Numerical Computations

For the purpose of computation the dimensions chosen are:

a) $F=f/D=0.556$, b) $f=10$, c) total number of zones $=11$, where f is the focal length and D is the diameter of the aperture.

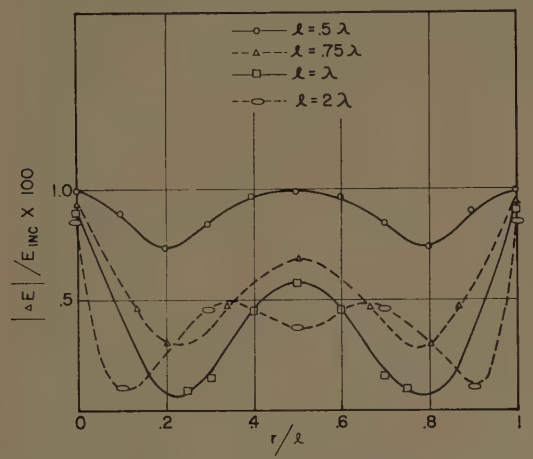

Fig. 5—Error $|\Delta E|$ in per cent of incident field vs point of observation on the strip with incident angle $\alpha=0$.

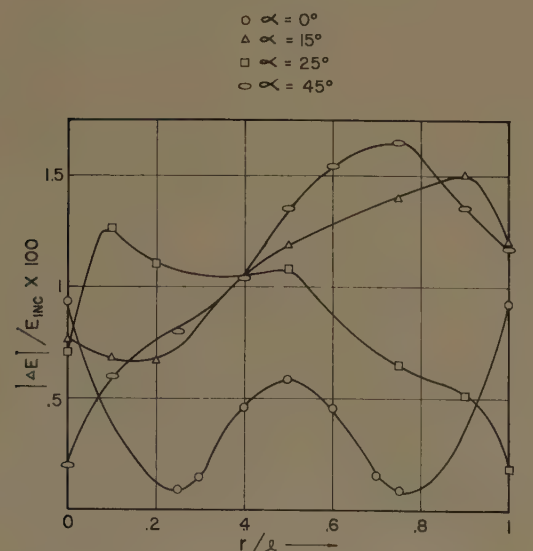

Fig. 6—Error $|\Delta E|$ in per cent of incident field vs point of observation on a strip of one wavelength in width for various incident angles.

The first zone is a smooth parabola of finite dimension, the rigorous solution of which is unknown. However, if the parabolic zone is replaced by a flat strip of the same aperture, it is possible to compute I_{11}, I_{1j} and fields due to I_{11} and $I_{11}+I_{1j}$. It is found that not only is I_{1j} very small compared to I_{11}, but the fields due to I_{11} and $I_{11}+I_{1j}$ are practically the same. If it may be conjectured that the order of magnitude of both I_{11} and I_{1j} of the first zone remains the same whether it is made of a flat strip or a smooth parabola, then it can be concluded that $I_{11}+I_{1j}$ and I_{11} produce almost the same field for a smooth parabola also. However, I_{11}, the current induced on a finite smooth parabola due to an incident plane wave is still unknown; but it is generally known that the physical optics solution for a finite parabola agrees closely with experimental results. Further, according to the computation[8] the physical optics solution for the corresponding flat strip does not differ significantly from that including the edge effect, since the first strip is quite wide in terms of wavelengths (6.245 λ in the present case). Therefore, it seems reasonable to use the physical optics solution for the smooth parabola representing the central zone. In other words, the significant contribution of the first strip is that due to the geometrical optics current, regardless of whether the first zone is a flat strip or a portion of a smooth parabola. However, this does not imply that the contribution due to the flat strip is the same as that due to an equivalent smooth parabola. This becomes clear if one observes that in the present case the optical path difference at the edge between the two is of the order of $\lambda/4$. The difference in over-all contribution is indicated in Fig. 7 for normal incidence. In fact, it shows that in actual construction the first zone should not be approximated by a flat strip.

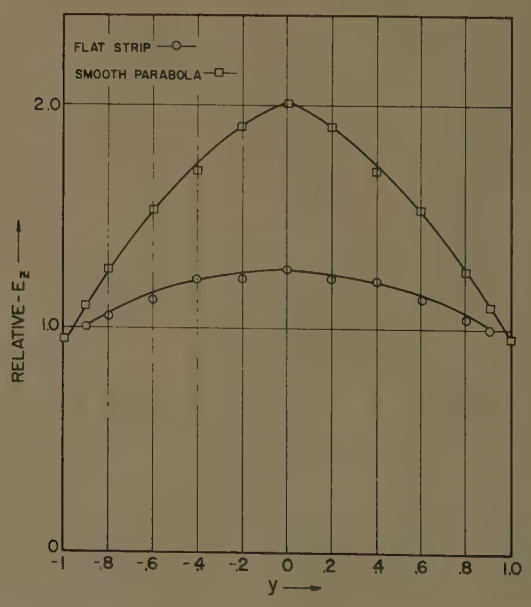

Fig. 7—Comparison of field intensity in the focal plane due to the first zone of different constructions, with normal incidence.

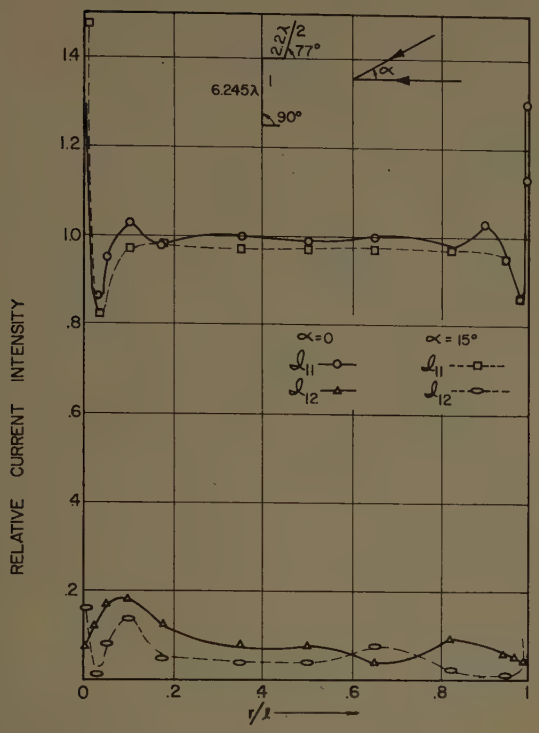

Fig. 8—Self-induced and mutual-induced current distributions of strip no. 1.

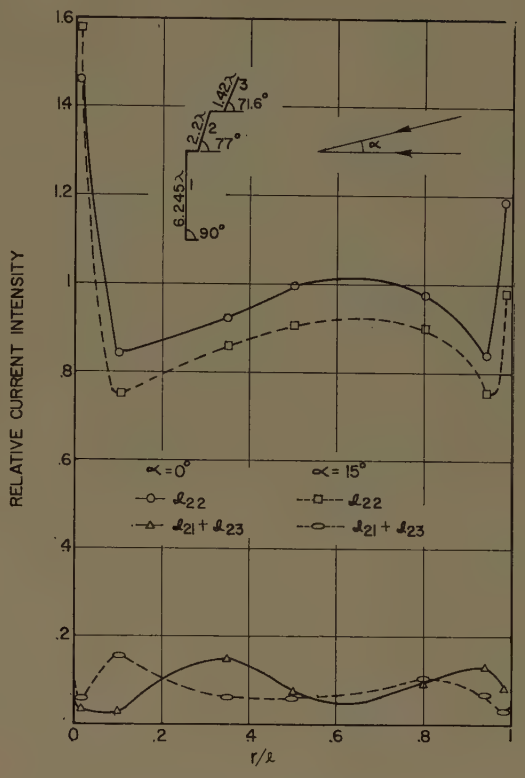

Fig. 9—Self-induced and mutual-induced current distributions of strip no. 2.

A) *Current Distribution:* The surface current density I_{ii} and I_{ij} have been obtained. For most strips the first order induced current due to coupling between adjacent strips, $(I_{i,i-1}+I_{i,i+1})$, is about 10 to 15 per cent of I_{ii} in the average. It may be conjectured that the second order solution is probably in the order of 1 or 2 per cent of I_{ii}. Only the currents for strip 1 (assumed flat) and 2 with $\alpha=0°$ and 15° are shown in Figs. 8 and 9. More complete information is given in the referenced report.[8]

B) *Image Patterns:* The image pattern of the zoned mirror has been studied with the following current distributions on the strips due to a plane wave at various incident angles:

1) The geometrical optics current distribution, *i.e.*, the truncated distribution I_G for an infinite plane. In this case the effects of both the edges and coupling between strips are neglected.

2) A current distribution which takes into account the edge effect but ignores couplings between strips, *i.e.*, the zero order solution of the integral equation given by (4).

3) A current distribution which considers both the edge effect and the first order coupling between adjacent strips as given by (6).

All computations are done by ILLIAC, the electronic high speed computer at the University of Illinois. The time required for computing an image pattern with one angle of incidence for three different current approximations is about 14, 16 and 60 minutes for 1), 2) and 3) respectively.

For comparative study, the image pattern of an equivalent smooth parabola, *i.e.*, a smooth parabola with the same focal length and aperture as the zoned mirror, is also computed. These patterns are all shown in Figs. 10–15.

With normal incidence, the maximum intensities due to a smooth parabola and case 1 of the above, are almost identical, while cases 2 and 3, which yield almost identical patterns, have a maximum about four per cent less than that of a smooth parabola. Thus, the edge effect reduces the gain slightly. The value of the secondary maxima is the largest for the smooth parabola, while for the zoned mirror in all three cases they are the same, having a value approximately 60 per cent of that of the smooth parabola.

As the angle of incidence is changed from normal, the maximum intensity falls off rapidly for the smooth parabola. Case 1 also shows a drop, while for cases 2 and 3 the drop is very small until the angle of incidence exceeds 15°. The locations of the primary and secondary maxima for all three cases of the zoned mirror remain the same while those of the smooth parabola change considerably. The sharpness of the field intensity distribution curves (*i.e.*, the focusing capability) for the smooth parabola drops off considerably.

The ratio of the magnitude of the two secondary maxima for the three cases of the zoned mirror remain constant and equal to unity up to an incident angle of about 20°, while it changes rapidly from 1 to 4.25 for a

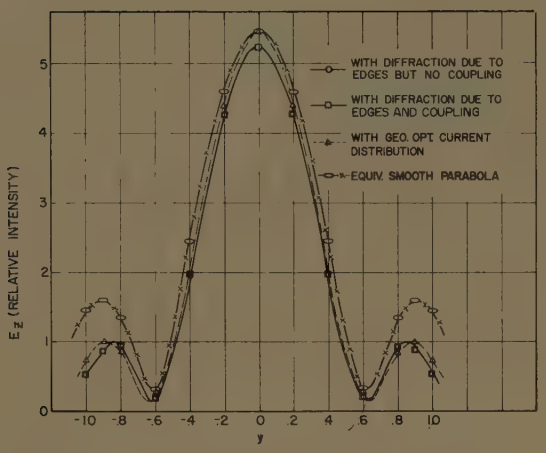

Fig. 10—Image patterns in the focal plane for normal incidence, $\alpha=0$.

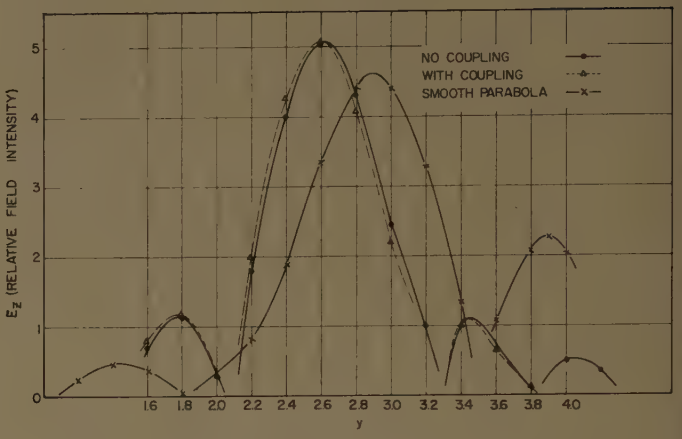

Fig. 13—Image patterns in the focal plane for $\alpha=15°$.

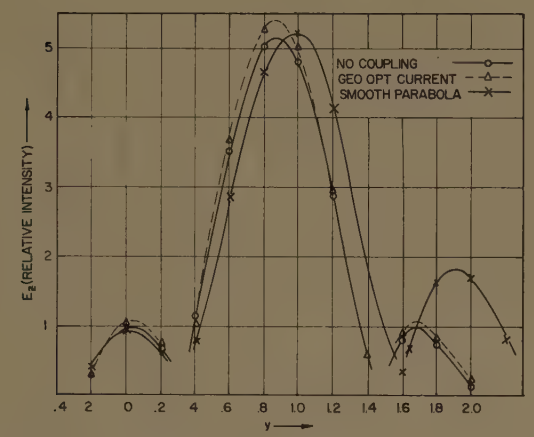

Fig. 11—Image patterns in the focal plane for $\alpha=5°$.

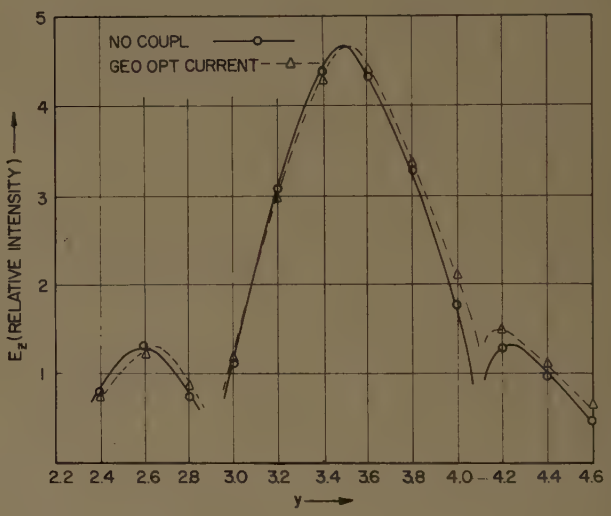

Fig. 14—Image patterns in the focal plane for $\alpha=20°$.

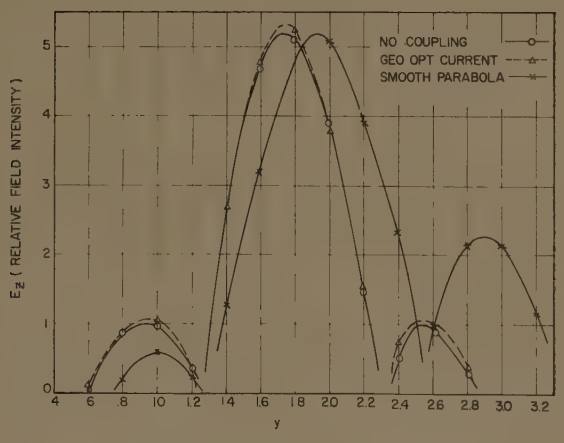

Fig. 12—Image patterns in the focal plane for $\alpha=10°$.

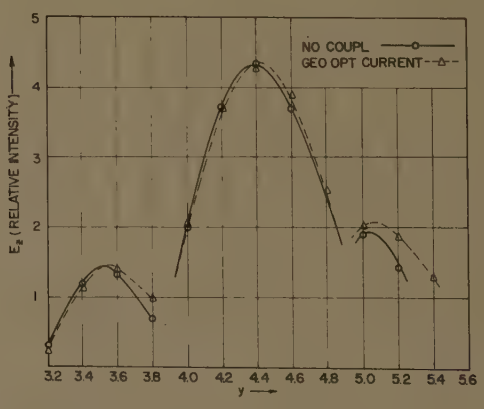

Fig. 15—Image patterns in the focal plane for $\alpha=25°$.

smooth parabola as the angle of incidence is changed from 0° to 15° (see Fig. 21).

The absolute value of the secondary maximum for the zoned mirror shows a slight increase as the angle of incidence is changed from normal and also the secondary maxima for Case 1 deviate more and more from those of Cases 2 and 3 as the angle of incidence is increased; with an incident angle of 20°, the two secondary maxima for Case 1 give a ratio of 1.2 as against 1.01 for Case 2.

The fact that the intensity distributions of the electric field for Cases 2 and 3 are very nearly the same, indicates that the contribution of the coupled current to the total field is negligible. These results indicate that the coupling effect between strips can be ignored without sacrificing much accuracy. It is significant because the coupling effect, which is the result of the first order iteration, is the most time consuming step in the computation as indicated in the beginning of this section.

Though there is some difference in the results between Case 1 and Case 2, particularly for oblique incidence, the physical optics solution, as given by Case 1, yields a reasonably good approximation, even with 22 discontinuities due to the edges in the present system, and the simplification in computation is quite considerable.

It is interesting to note that the two secondary maxima on either side of the principal are more symmetrical for Cases 2 and 3 than for Case 1, indicating that the effect of the edges seems to reduce the "coma" somewhat.

C) *Scanning Performance:* The curves in Figs. 16–20, which are derived with the aid of the reciprocity theorem from the intensity distribution curves discussed before, show the important and interesting properties of the zoned mirror as an antenna in comparison with a smooth parabola with an isotropic feed. It is clear from Fig. 16, that for a zoned mirror the deflection of the beam of the radiation pattern from the axis is proportional to the displacement of the feed. For the same scan angle, a larger displacement of the feed is required for a smooth parabola than for a zoned mirror and the difference in displacement increases as the scan angle is increased. Fig. 17(a) shows the maximum field intensity on the focal plane for various angles of incidence while Fig. 17(b) shows the variation of the relative gain against the scan angle. The gain of the zoned mirror is substantially constant over a 20° scan. For a 15° scan angle, the loss in gain is only 0.27 db, while for a parabola it is 1.36 db.

Fig. 18 shows approximately the change in half-power beamwidth[12] for 0° to 15° scan angle to be roughly 30 per cent for the smooth parabola against 5 per cent for the zoned mirror. Fig. 19 is a plot of the magnitude of the first two secondary maxima of the image pattern against their positions in the focal plane. This provides the information of the minor lobe level of the radiation pattern, as shown in Fig. 20, against the scan angle.[13] It may be noted that the minor lobe level is smaller for the smooth parabola than that of the zoned mirror for the on-focus feed case, the figures being about −15.8 db and −14.6 db respectively. This is expected since the zoned mirror, having reflecting strips at a constant distance from the focus, is uniformly illuminated while the smooth parabola is not. The minor lobe level of the radiation pattern goes up rapidly as the off-setting of the feed is increased for the smooth parabola whereas it increases very slowly for the zoned mirror.

A more interesting result, so far as the coma correction is concerned, is shown in Fig. 21. It is seen that the ratio of the two first secondary maxima of the image pattern (a function of coma aberration only in the present system) is substantially constant for a zoned mirror in contrast with that for a smooth parabola. It clearly indicates that the zoned mirror considered here is very effective in the reduction of coma aberration.

D) *Chromatic Aberration Study:* It is to be expected that such a system would be very frequency sensitive. The image patterns for frequencies 6.25 per cent and 11.25 per cent higher than the designed value f_0 are computed. A typical pattern for $\alpha = 15°$ is shown in Fig. 22 against that for the smooth parabola at $1.0625f_0$. It is seen that for a deviation of about 6 per cent from the design frequency the secondary maxima of the zoned mirror become so strong that they are merged with the main beam. For a frequency 11.25 per cent higher, the maximum intensity drops further so that there is practically no distinction between the main and secondary beams. This is also true for other angles of incidence.[14] This result indicates that the chromatic aberration is so overwhelming that there is no necessity to evaluate the coma. The drop in maximum field intensity and gain at $1.0625f_0$, may be obtained from Fig. 17. On the other hand, by comparison the smooth parabola is a wide-

---

[12] The image pattern is calculated with an incident plane wave of unity intensity at a certain incident angle α. By the theorem of reciprocity, a feed of unity intensity at a position y will produce in the direction of angle α a radiation field equal to the intensity of the image pattern at y. Thus, with a set of image patterns for various incident angles, the radiation patterns for various feed positions can be found. Since the image patterns of the zoned mirror remains almost unchanged in a moderate range of scan angle, these two patterns (radiation and image) become approximately the same with their abscissas related by $y = c\alpha$ where the constant c is given by the slope of the curve in Fig. 16. Therefore, the beamwidth of one pattern can be approximately obtained from the other through this relation. As expected, this approximation becomes worse for very large scan angle and also becomes less accurate for the smooth parabola.

[13] As the incident angle of the plane wave changes continuously, the field intensity at a fixed observation point in the image plane will undergo a series of maxima which correspond to the peaks of the major and minor lobes of the radiation pattern. Thus, by using Fig. 19 the minor lobe level of the radiation pattern for various scan angles can be obtained in the following manner. Let a feed be at a position y in the image plane, then minor lobes at levels shown in Fig. 19 will be produced somewhere in the space. At the same time the major lobe field intensity corresponding to this feed displacement can be found by first using Fig. 16 to obtain the scan angle α for this value of y, then referring to Fig. 17(a) for the intensity. The ratio of these two intensities is the sidelobe level of the radiation pattern for this feed displacement.

[14] Y. T. Lo, "A Study of the Chromatic Aberration of a Coma-Corrected Zoned Mirror," Antenna Lab., Univ. of Illinois, Urbana, Ill., Tech. Rept.; 1960.

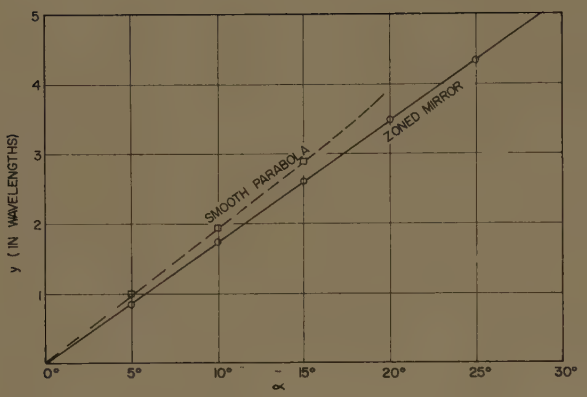

Fig. 16—Relation between the position of off-axis feed and the beam deflection angle α.

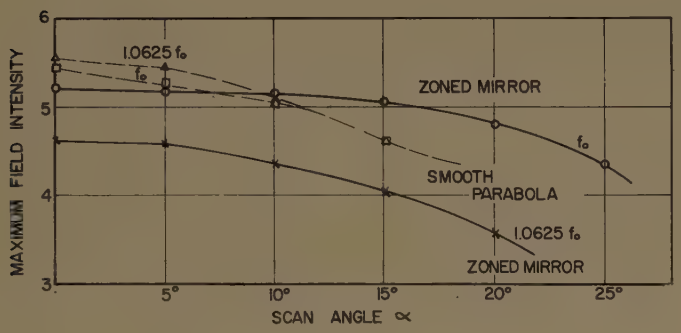

(a)

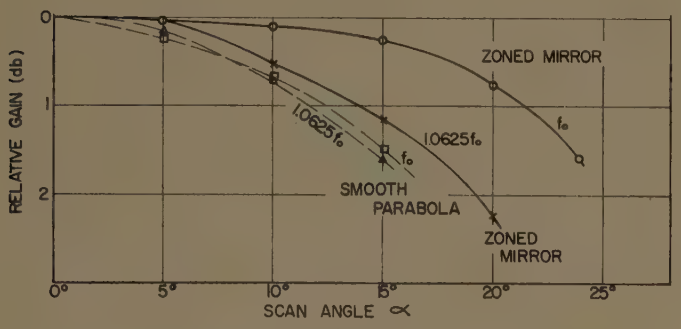

(b)

Fig. 17—(a) Maximum field intensity of the image vs scan angle α. (b) Variation of directive gain vs scan angle α; for the designed frequency f_0 and $1.0625f_0$.

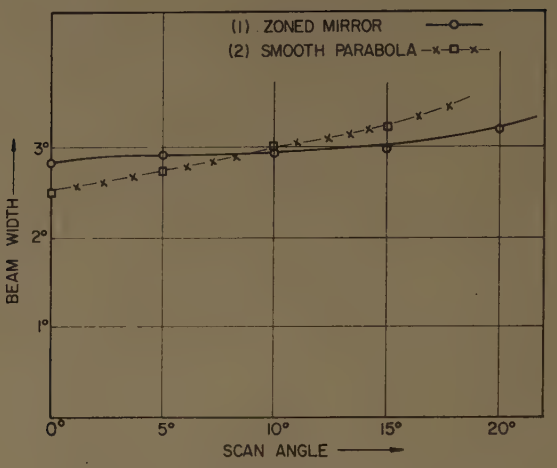

Fig. 18—Half-power beamwidth of the radiation pattern vs scan angle.

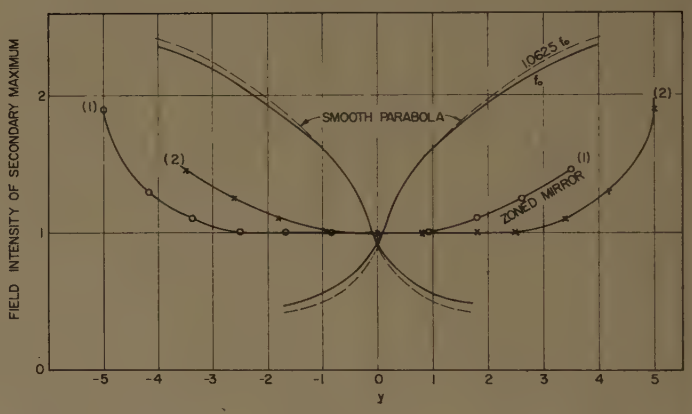

Fig. 19—Magnitude of two first secondary maxima vs their positions in the focal plane for the designed frequency f_0 and $1.0625f_0$.

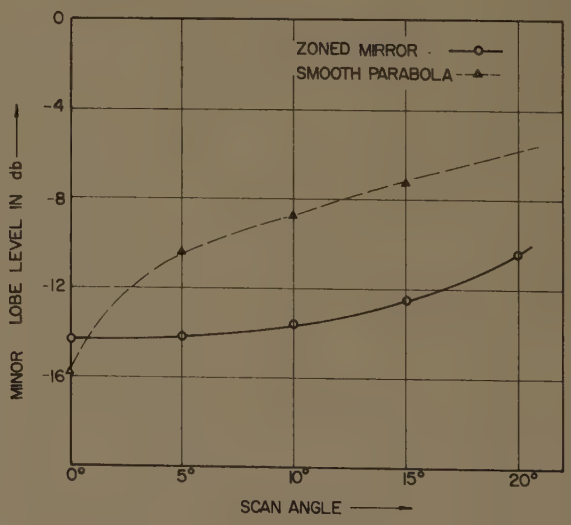

Fig. 20—Minor lobe level of the Radiation pattern vs scan angle.

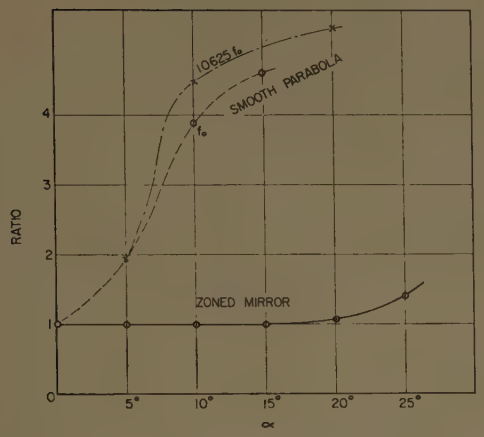

Fig. 21—Ratio of two first secondary maxima vs scan angle α for the designed frequency f_0 and $1.0625f_0$.

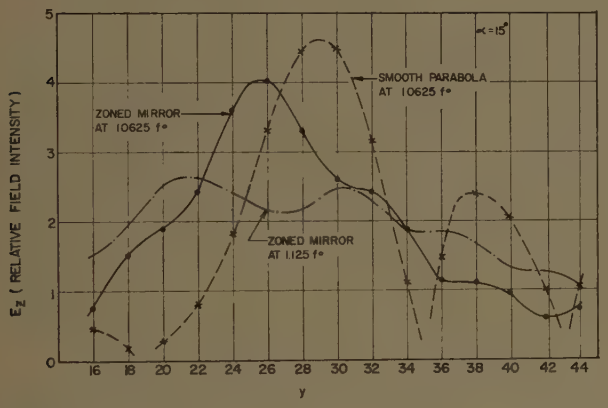

Fig. 22—Image patterns in the focal plane for zoned mirror at $1.0625f_0$ and $1.125f_0$ and for smooth parabola at $1.0625f_0$, with $\alpha=15°$.

band device, whose maximum intensity gain, minor lobe level and position, and ratio of two secondary maxima for $1.0625f_0$ are essentially the same as those at f_0, as shown in Figs. 17, 19, and 21.

VI. Discussion and Conclusion

A study of the $|\Delta E|$-curves reveals that the approximate solution is very close to the exact one. Because of the relative ease of computation, it has more practical value than the exact solution. Indeed, the latter becomes impractical in such a complex problem.

In spite of a large number of discontinuities in the structure, the generally used physical optics solution seems to offer a rather accurate result. For higher accuracy the edge effect should be considered, but the coupling effect seems to be of less importance.

The effectiveness of a coma-corrected zoned mirror has been a subject of controversy for some time. The present investigation, made on a two-dimensional cylindrical zoned mirror which is free from astigmatism, enables us to evaluate its effectiveness in correction of "coma" without complications of other aberrations.

A comparison with the performance of an equivalent smooth parabola has indicated that the zoned mirror with small F-number and uniform illumination has a performance much superior to that of a smooth parabola in the reduction of the coma aberration. The beamwidth, gain and minor lobe level of the radiation pattern and also the ratio of the two first minor lobe levels of the image distribution in the focal plane are relatively constant for a zoned mirror for scan angles up to 25°, while for a smooth parabola the ratio of the first minor lobe level increases drastically.

On the other hand, the zoned mirror is a very frequency-sensitive device; at a frequency about 6 per cent higher than the design value, the image and also the scanning performance are worse than those of corresponding smooth parabola. The zoned mirror probably has a total useful bandwidth of only a few per cent.

The method of solution used in this paper provides a detailed and fairly accurate picture of results to be expected in a region where geometrical optics fails. The approach may be particularly valuable in radio-telescope applications where the structure is often so huge that an experimental study, even on a scaled down model, is impractical.

VII. Acknowledgment

These authors are indebted to Professors E. C. Jordan and G. A. Deschamps for their valuable comments on this paper. They are also indebted to N. E. Wiseman for his assistance in programming the computation.

Microwave Antennas Derived from the Cassegrain Telescope*

PETER W. HANNAN†, SENIOR MEMBER, IRE

Summary—A microwave antenna can be designed in the form of two reflecting dishes and a feed, based on the principle of the Cassegrain optical telescope. There are a variety of shapes and sizes available, all described by the same set of equations. The essential performance of a Cassegrain double-reflector system may be easily analyzed by means of the equivalent-parabola single-reflector concept.

Techniques are available for reducing the aperture blocking by the sub dish of the Cassegrain system: one method minimizes the blocking by optimizing the geometry of the feed and sub dish; other methods avoid the blocking by means of polarization-twisting schemes. The former method yields good performance in a simple Cassegrain antenna when the beamwidth is about 1° or less. The latter methods are available for any application not requiring polarization diversity, and an optimized set of polarization-operative surfaces has been developed for these twisting Cassegrain antennas.

Experimental results, presented for practical antennas of both types, illustrate the feasibility of these principles. A number of unusual benefits have been obtained in the various Cassegrain antenna designs, and additional interesting features remain to be exploited.

I. Introduction

FOR THE DESIGN of an optical telescope, the Cassegrain double-reflector system has often been utilized [1]–[4]. Compared with the single-reflector type, it achieves a high magnification with a short focal length, and allows a convenient rear location for the observer.

Recently, a number of microwave antennas have been developed which employ double-reflector systems similar to that of the Cassegrain telescope. Each of these antennas has achieved one or more particular benefits not obtainable with the ordinary single-reflector type. While the various designs may differ from each other to a considerable degree, there are certain basic features which are common to all.

It is the purpose of this paper to outline the design principles and essential properties of the Cassegrain antenna, and to discuss its advantages and limitations. Some of the techniques available for minimizing its limitations are described, and experimental results illustrating the practical nature of two particular designs are presented. Finally, a number of interesting applications for the Cassegrain antenna are mentioned.

II. Telescope vs Antenna

A Cassegrain telescope consists of two mirrors and an observing optical instrument, as indicated in Fig. 1. The primary mirror, which is a large concave mirror in the rear, collects the incoming light and reflects it toward the secondary mirror, which is a small convex mirror out in front. The secondary mirror then reflects the light back through a hole in the center of the primary mirror. When the incoming rays of light are parallel to the telescope axis, the final bundle of light rays is focused toward a point; at this location the observer places his eye or his camera.

The basic microwave antenna derived from the Cassegrain telescope is shown in Fig. 2. The microwave reflectors, which will be called the main dish and the sub dish, respectively, have surfaces similar in shape to those of the telescope. The microwave feed is a small antenna which, together with a transmitter or receiver, replaces the optical instrument of the telescope.

Analysis of the operation of a Cassegrain antenna system may be performed with the same semi-optical approximation commonly employed with an ordinary single-dish antenna. Usually the feed is sufficiently small so that the wave radiated by the feed can be described by the far-field pattern of the feed before reach-

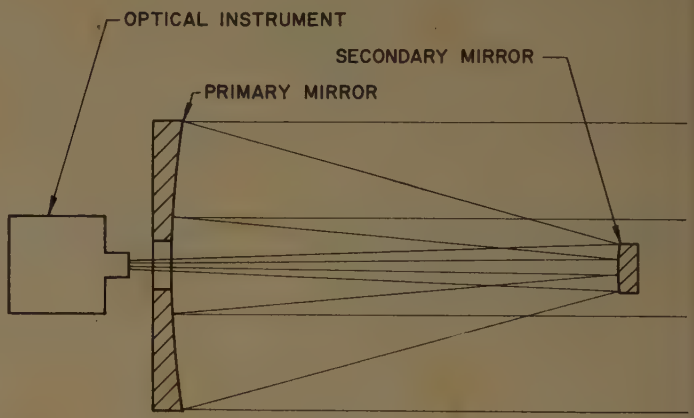

Fig. 1—Cassegrain telescope.

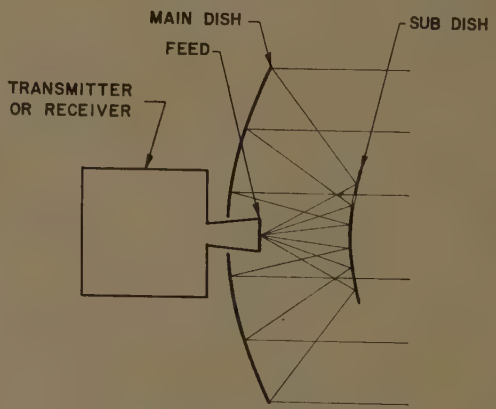

Fig. 2—Cassegrain antenna.

* Received by the PGAP, March 12, 1960. Revised manuscript received, July 5, 1960. Presented at the URSI-IRE Spring Meeting, Washington, D. C., May 2–5, 1960.

† Wheeler Labs., Smithtown, N. Y.

ing the sub dish, and the wave incident on the sub dish appears to travel along the rays originating from a point centered on the feed. The sub dish, which must be large enough to intercept the useful portion of the feed radiation, ordinarily reflects this wave essentially according to ray optics. On reaching the main dish, the wave is again reflected according to ray optics; and because of the geometry of the antenna elements, the rays emerge parallel and the wavefront has the flat shape which is usually desired. The amplitude of the emergent wave across the aperture has a taper which is determined by the radiation pattern of the feed, modified by the additional tapering effect of the antenna geometry. The far-field pattern of the antenna is, of course, a diffraction pattern whose characteristics depend on the amplitude taper of the emergent wave.

III. Geometry

The geometry of the Cassegrain system is simple and well-known, but it is helpful to have at hand those formulas describing the dish contours in terms of the significant antenna parameters. The classical Cassegrain geometry, shown in Fig. 3, employs a parabolic contour for the main dish and a hyperbolic contour for the sub dish. One of the two foci of the hyperbola is the real focal point of the system, and is located at the center of the feed; the other is a virtual focal point which is located at the focus of the parabola. As a result, all parts of a wave originating at the real focal point, and then reflected from both surfaces, travel equal distances to a plane in front of the antenna.

To completely describe a Cassegrain system, four fixed parameters are required, two for each dish. Since seven parameters are shown in Fig. 3, three are dependent on the other four, and three equations exist which describe this dependency. In the case of the main dish, the relationship is

$$\tan \tfrac{1}{2}\phi_v = \pm \frac{1}{4}\frac{D_m}{F_m}. \tag{1}$$

As will be discussed later, the positive sign in the above formula applies to the Cassegrain forms, and the negative sign to the Gregorian forms. In the case of the sub dish, the relationships are

$$\frac{1}{\tan \phi_v} + \frac{1}{\tan \phi_r} = 2\frac{F_c}{D_s}, \tag{2}$$

$$1 - \frac{\sin \tfrac{1}{2}(\phi_v - \phi_r)}{\sin \tfrac{1}{2}(\phi_v + \phi_r)} = 2\frac{L_v}{F_c}. \tag{3}$$

In a typical case, the parameters D_m, F_m, F_c, and ϕ_r might be determined by considerations of antenna performance and space limitations; ϕ_v, D_s, and L_v would then be calculated. It is interesting to note that a value for the parameter ϕ_r, which determines the beamwidth required of the feed radiation, may be specified independently of the ratio F_m/D_m, which determines the shape of the main dish.

The contour of the main dish is given by the equation

$$x_m = \frac{{y_m}^2}{4F_m}. \tag{4}$$

The contour of the sub dish is given by the equation

$$x_s = a\left[\sqrt{1 + \left(\frac{y_s}{b}\right)^2} - 1\right] \tag{5}$$

where

$$e = \frac{\sin \tfrac{1}{2}(\phi_v + \phi_r)}{\sin \tfrac{1}{2}(\phi_v - \phi_r)},$$

$$a = \frac{F_c}{2e} \qquad b = a\sqrt{e^2 - 1}.$$

The quantities e, a, and b are the parameters of the hyperbola: e is eccentricity, a is half the transverse axis, and b is half the conjugate axis.

So far, only the geometry of the classical Cassegrain system has been considered. However, the system may easily be extended to include a variety of forms, all obeying the basic formulas presented above. In Fig. 4, two series are shown in which the curvature of the sub dish is modified from the classical convex shape to a flat, and finally a concave shape. As this is done, the diameter of the sub dish increases. The first series shows the case in which the main dish is held invariant; this yields a progressive increase in the required feed beamwidth, and a progressive decrease in the axial dimension of the antenna. In the second series the feed beamwidth is held invariant; in this case, the main dish becomes progressively flatter, and the axial dimension of the antenna progressively increases.

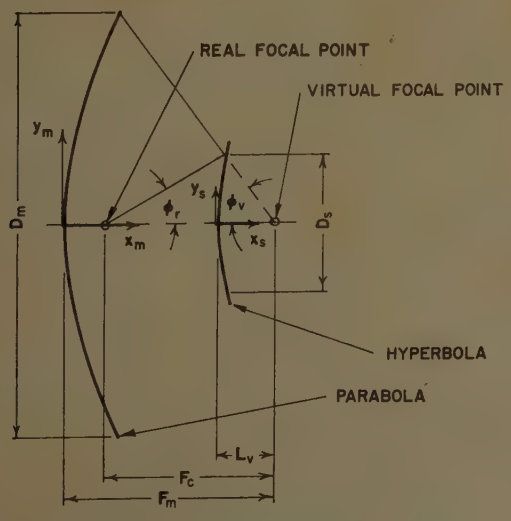

Fig. 3—Geometry of Cassegrain system.

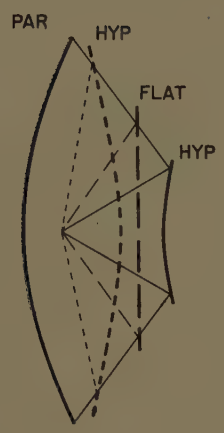

(a) Invariant main dish.

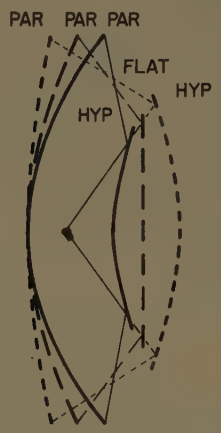

(b) Invariant feed.

Fig. 4—Cassegrain modifications.

In Fig. 5, a series is presented in which the beamwidth of the feed is progressively increased while the overall dimensions of the antenna are held fixed. The range of values of some of the parameters previously mentioned are indicated alongside the sketches, together with the distinguishing characteristic of each case. (In each sketch an additional dish and some additional rays are shown in dashed lines, and one column has an additional parameter F_e/F_m; these will be discussed in the next section of this paper, and should be disregarded at this point.) The first three cases are similar to those shown in Fig. 4. In the fourth case, the main dish has degenerated to a flat contour and the sub dish has degenerated to a parabolic contour; here, the flat main dish may be placed at any distance from the sub dish, out to the region where the ray-optical approximation begins to fail. The final case carries the progression to the ridiculous extreme of a concave elliptical sub dish and a convex parabolic main dish, with the former being larger than the latter. It should be mentioned that in the two cases having one flat dish, the formulas presented before, while valid, are overly complicated and contain indeterminate factors; since the focusing is accomplished entirely by the curved parabolic surface, it is preferable to employ the simple formulas for an antenna having a single parabolic dish.

A further extension of the Cassegrain system is shown in Fig. 6. Here, the focal point of the main dish moves to a region between the two dishes, and the contour of the sub dish becomes concave elliptical. In the first of the two cases shown, the system is identical with that of the Gregorian telescope; however, both cases obey the formulas given previously for the Cassegrain system, if the proper values are employed. The ranges allowable for some of the parameters are indicated in the figure. In addition, the negative sign must be employed in (1) so as to maintain a positive F_m with the negative ϕ_v which occurs in the Gregorian forms. The first case, or classical Gregorian, is drawn so as to have the same over-all size and the same feed beamwidth as the classical

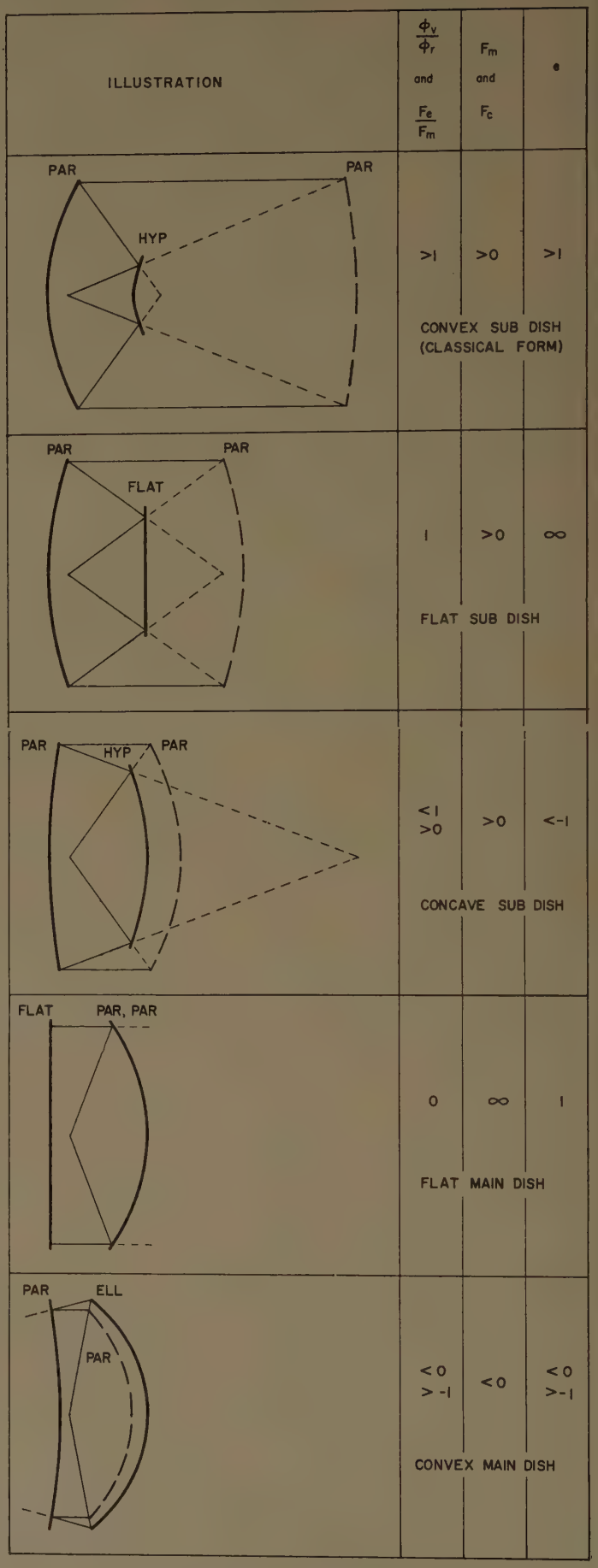

Fig. 5—Series of Cassegrain forms.

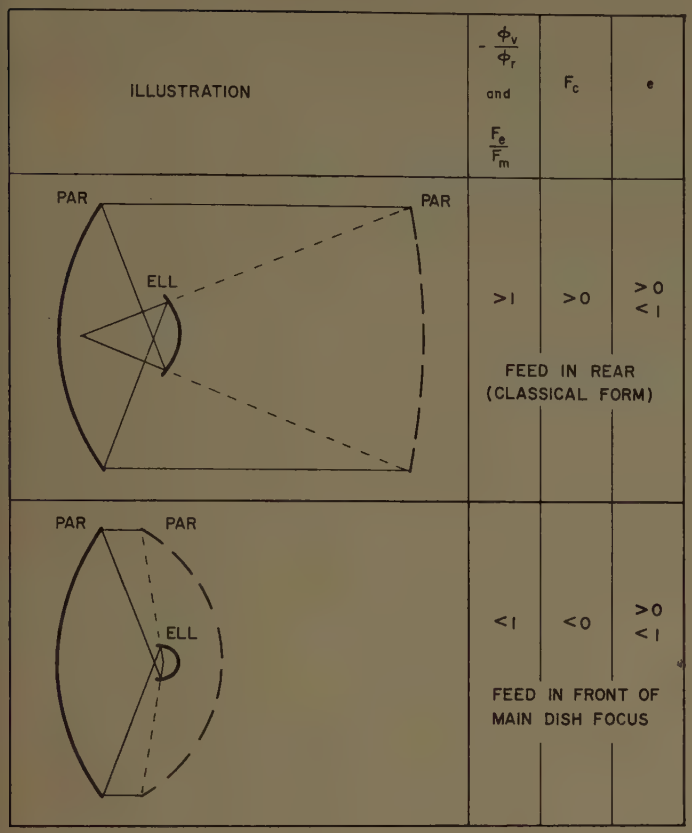

Fig. 6—Series of Gregorian forms.

Cassegrain in the first case of the previous figure. Under these conditions, the Gregorian form requires a shorter focal length for the main dish. In the second of the Gregorian forms shown, the feed has been moved to a location between the main dish focus and the sub dish, with the main dish kept the same as in the first case. This form would have several major disadvantages that would make it unattractive in most antenna applications.

All of the above-mentioned forms are members of the same family, which might be called the Cassegrain family. In every case, incoming rays collected by the main dish are focused toward a point. It should be mentioned that a further extension of the Cassegrain system can be made by modifying the contours of both dishes in such a way that incoming rays collected by the main dish are not focused exactly toward a point, while the final bundle of incoming rays, after reflection from the sub dish, remain focused toward a point. Although this may be a useful technique for achieving certain kinds of performance [5]–[7], it is beyond the scope of this paper.

IV. Equivalence Concepts

A. Virtual Feed

One concept which is helpful in understanding and predicting the essential performance of a Cassegrain antenna is that of a virtual feed. As shown in Fig. 7, the combination of real feed and sub dish is considered as being replaced by a virtual feed at the focal point of the main dish. Thus the antenna becomes an ordinary single-dish design, having the same main dish but a different feed.

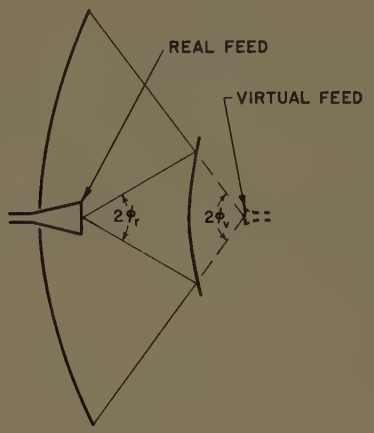

Fig. 7—Virtual-feed concept.

If both the real and virtual feeds had dimensions much larger than a wavelength, the configuration of the virtual feed could be determined by finding the optical image of the real feed in the sub dish. This condition seldom exists for a microwave antenna; however, if only the effective apertures of the feeds are considered, it is found that the imaging process yields approximately the correct results. For the classical Cassegrain configurtion shown in Fig. 7, the virtual feed has an effective aperture smaller than that of the real feed, and has a correspondingly broader beamwidth. The beamwidth increase is, of course, the result of the convex curvature of the sub dish; the ratio of virtual-feed to real-feed beamwidth is indicated by the quantity ϕ_v/ϕ_r.

For the various Cassegrain modifications, the range of values that the quantity ϕ_v/ϕ_r may achieve is given in the first column of Figs. 5 and 6, and from this the relative sizes of the effective apertures of the real and virtual feeds may be inferred. When the sub dish is flat, the virtual and real feeds are, of course, identical. For the Cassegrain system having a concave sub dish, the virtual feed has a beamwidth smaller than that of the real feed, and has a larger effective aperture. However in the classical Gregorian form, the concave sub dish results in an effective aperture of the virtual feed which is smaller than that of the real feed, just as in the classical Cassegrain system.

There are several situations in the design of microwave antennas in which the ability to obtain a different effective aperture of the virtual feed from that of the real feed is quite helpful. One such case occurs with a monopulse antenna, where it is difficult to reduce the overall size of the feed aperture to a wavelength or less, while maintaining efficient and wideband performance. On the other hand, a large feed aperture ordinarily requires a long focal length for effective utilization of the main aperture, thereby increasing the size of the

antenna structure. This problem may be solved by means of the classical Cassegrain system of Fig. 7, which can incorporate a large feed while employing a short focal length for the main dish. Actually, the axial dimension of such an antenna is often less than the main focal length, because the virtual feed is beyond the sub dish. In addition, of course, there are no waveguide components required in this forward region.

B. Equivalent Parabola

The concept of a virtual feed furnishes a useful qualitative means for analyzing a Cassegrain antenna, but, in general, it is not convenient for an accurate quantitative analysis. In addition, the virtual feed assumes ridiculous proportions for certain of the Cassegrain configurations. A second concept, that of the equivalent parabola, overcomes these limitations.

As shown in Fig. 8, the combination of main dish and sub dish is considered as being replaced by an equivalent focusing surface, drawn with dashed lines in the figure, at a certain distance from the real focal point. The properties of this focusing element can be determined from a study of the "principal surface" of the Cassegrain system. This surface [8] is defined here as the locus of intersection of incoming rays parallel to the antenna axis with the extension of the corresponding rays converging toward the real focal point, as indicated in Fig. 8. It happens that for the Cassegrain system, the "principal surface" has a parabolic contour, and the focal length of this parabola exactly equals the distance from its vertex to the real focal point. As a result, this surface could be employed as a reflecting dish which would focus an incoming plane wave toward the real focal point in exactly the same manner as does the combination of main dish and sub dish. (Actually, the plane wave would have to be incident from the opposite direction; this is of no significance in the principles of this concept.) Thus the antenna again becomes an ordinary single-dish design, but this time having the same feed and a different main dish.

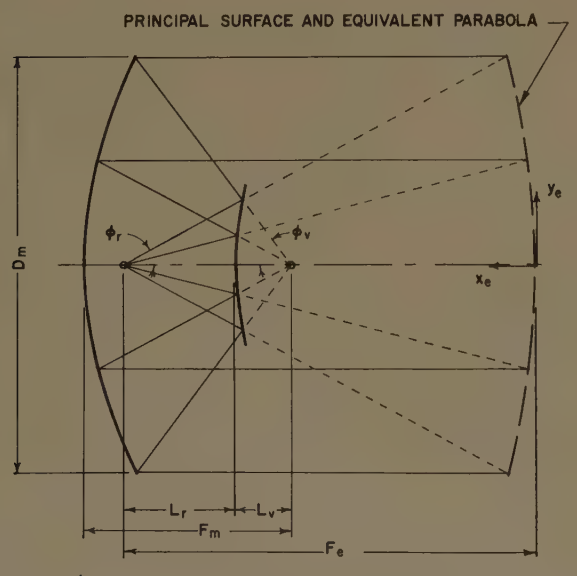

Fig. 8—Equivalent-parabola concept.

It should be mentioned that the equivalent parabola is based on simple ray analysis, rather than on an exact analysis of the wave action. This ray approximation is made throughout the paper, and is accurate enough for most purposes except when the sub dish is only a few wavelengths in diameter. When the wave analysis is necessary, consideration would have to be given to the Fresnel diffraction pattern formed at the main dish after reflection of the feed radiation by the sub dish.

The following equations provide the relationship between the equivalent parabola, the antenna parameters shown in Fig. 8, and some of the parameters previously mentioned:

$$\frac{1}{4}\frac{D_m}{F_e} = \tan \tfrac{1}{2}\phi_r, \tag{6}$$

$$x_e = \frac{y_e^2}{4F_e}, \tag{7}$$

$$\pm \frac{F_e}{F_m} = \frac{\tan \frac{1}{2}\phi_v}{\tan \frac{1}{2}\phi_r} = \frac{L_r}{L_v} = \frac{e+1}{e-1}. \tag{8}$$

In (8), the positive sign applies to the Cassegrain forms, and the negative sign to the Gregorian forms. Eqs. (6) and (7) describe the equivalent parabola itself, in terms of its *equivalent focal length*, F_e. Eq. (8) presents the various alternate expressions for the quantity F_e/F_m the ratio of equivalent focal length to focal length of the main dish. It is evident that with the classical Cassegrain system, the equivalent focal length is greater than the focal length of the main dish.

As might be expected, the equivalent-parabola concept also applies to the extended Cassegrain forms, and to the Gregorian forms, as well. The equivalent parabola for each of these cases is indicated by the dashed curves in Figs. 5 and 6, and the range of values for the quantity F_e/F_m is indicated in the first column of these figures. When the sub dish is flat, the equivalent focal length equals the focal length of the main dish. For the Cassegrain system having a concave sub dish, the equivalent focal length is shorter than that of the main dish. For the case of a flat main dish, the equivalent parabola is identical with the sub dish. In the classical Gregorian form, the equivalent focal length is greater than that of the main dish, as is also the case in the classical Cassegrain system.

In describing the magnifying properties of a Cassegrain optical telescope, it has become customary to employ the concept of the equivalent focal length [1], [2], [4]. It has also been recognized that the coma aberration of a Cassegrain telescope is the same as that of a telescope having a single parabolic mirror of focal length equal to the equivalent focal length of the Cassegrain [2]. These two aspects are readily explainable in terms of the equivalent parabola. It may be noted that since

the Cassegrain optical telescope has an equivalent focal length greater than that of its large mirror, it has greater magnifying power and reduced coma compared with that obtained with only the single large mirror.

In the case of a microwave antenna, the equivalent-parabola concept yields properties similar to those mentioned above. The effective aperture of the feed should be such that the equivalent parabola is properly illuminated: when the equivalent focal length is greater than the focal length of the main dish, the optimum feed aperture is larger than that which would be optimum for a single-dish antenna having the same focal length as the main dish. This result is analogous to the magnifying properties [1]–[3] of the optical telescope; it also corresponds to the result obtained with the virtual-feed concept. Indeed, the ratio F_e/F_m is sometimes called the *magnification*. This is a valid approximation when applied to the relative sizes of the real and virtual feeds or images. However, it should not be confused with the magnification of an optical telescope containing an eyepiece, in which the term usually applies to the relative sizes of the image and the object.

As regards coma aberration, the equivalent-parabola concept yields the same results as in the optical case, when the off-axis beam angle is small. However, when this angle becomes appreciable, as may be necessary in a microwave antenna, the feed is sufficiently offset from the dish axes so that the principal surface is no longer closely approximated by the original equivalent parabola; therefore, the wide-angle coma may differ considerably from that calculated by the equivalent-parabola concept. Of course, other aberrations may become appreciable at the same time.

There are some significant uses of the equivalent-parabola concept in the microwave antenna which appear to have no application in the optical telescope. One such case involves the determination of amplitude taper across the main aperture of the antenna. For an ordinary single-dish antenna, the illumination is determined by the radiation pattern of the feed, modified by a "space-attenuation" characteristic which is a simple function of the F/D ratio [9]. For a Cassegrain antenna, exactly the same process is applicable, with the F/D ratio now being the ratio of equivalent focal length to main-dish diameter, F_e/D_m. In other words, the illumination is exactly the same as that which would exist across a single dish having the equivalent focal length and being illuminated with the same feed. When the equivalent focal length is greater than the diameter, the "space-attenuation" characteristic modifies the feed radiation only slightly; with a practical feed, such an antenna can have high efficiency even though it may have a physically short axial length.

V. Reduction of Aperture Blocking

The principal limitation on the application of the historical Cassegrain system to microwave antennas is the blocking of the main aperture by the sub dish [10], [11]. This problem has not been serious with optical telescopes because the requirements on characteristics of the diffraction pattern have not been severe, and because, for the relatively short wavelength of light, the size of the small reflector can be made very much less than that of the large reflector. With a microwave antenna, neither of these conditions ordinarily exists.

The presence of an opaque sub dish in the main aperture of the antenna creates a "hole" in the illumination which causes decreased gain and increased sidelobe levels. To analyze this effect, the resulting illumination may be resolved into two components [9], the original illumination plus a negative center, or "hole," as shown in Fig. 9(a). The resulting antenna pattern, shown in Fig. 9(b), can be determined by adding together the two pattern components, the original pattern plus a broad, low, negative pattern radiated by the "hole."

Although the above method facilitates an exact calculation of the shadowing effect for any case, it is instructive to apply the method to a particular simple case

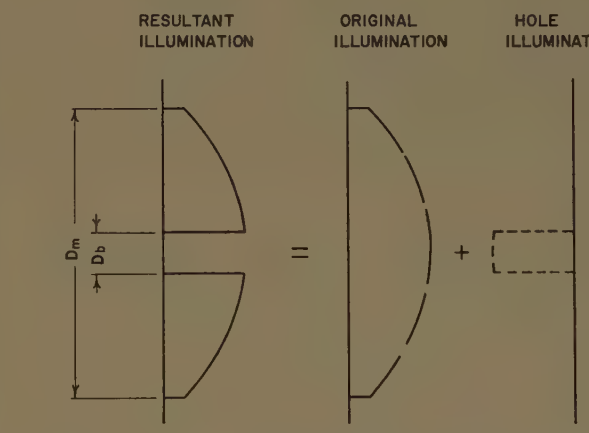

(a) Illumination.

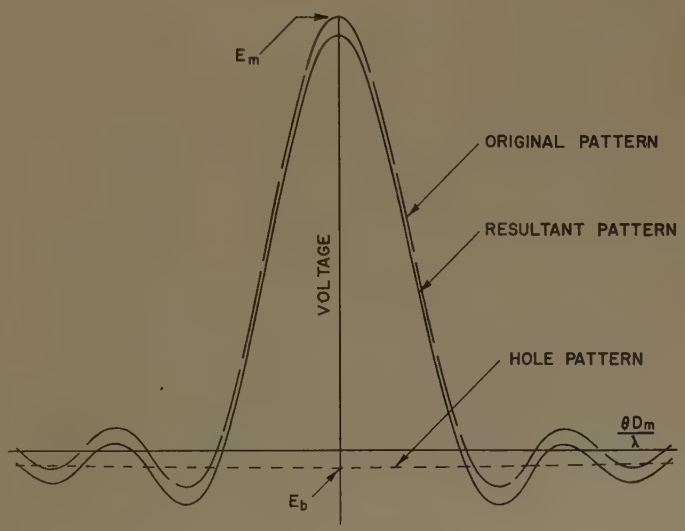

(b) Patterns.

Fig. 9—Effect of aperture blocking.

which approximates many practical cases. If the main aperture is circular, and is assumed to have a completely tapered parabolic illumination, a small circular obstacle in the center of the aperture will create a "hole" pattern whose peak voltage relative to the peak voltage of the original pattern is

$$\frac{E_b}{E_m} = 2\left(\frac{D_b}{D_m}\right)^2. \tag{9}$$

where D_b is the diameter of the blocked portion of the aperture. This relative voltage is then subtracted from unity to yield the resultant relative peak voltage, and is added to the relative level of the first sidelobe to yield the resultant relative level.

The illumination hole is not the only effect created by the presence of an obstacle in the main aperture; the power which strikes the obstacle must also be accounted for. Usually this power reradiates and contributes an additional component to the sidelobes. For a particular sub dish and antenna configuration, it is often a straightforward process to estimate the amplitude pattern of this radiation. However the manner in which it combines with the original pattern is more complicated, and is likely to vary radically with a change of frequency. A further consideration of this effect is beyond the scope of this paper, and, even though it may sometimes be an important one, the effect will be neglected henceforth.

A. Minimum Blocking with Simple Cassegrain

In order to determine the degree of aperture blocking to be expected in a Cassegrain antenna having an ordinary reflecting sub dish, it is necessary to consider those factors which influence the size of the sub dish. Essentially, the minimum size of the sub dish is determined by the directivity of the feed, and the distance between the feed and the sub dish. By making the feed more directive, or by decreasing its distance to the sub dish, the size of the sub dish may be reduced without incurring a loss caused by spillover of the feed radiation beyond the edge of the sub dish. However, as indicated in Fig. 10, a continuation of this process can eventually result in the feed itself creating a shadow in the main illumination which is greater than that created by the sub dish. It is evident that there is some intermediate condition in which neither the sub-dish nor the feed shadow predominates, and which would yield the least amount of aperture blocking; this may be termed the *minimum-blocking condition.*

In Fig. 11, the minimum blocking condition is shown, together with some approximate equations describing the basic relations between certain parameters. By combining these equations, a relationship is obtained which specifies the geometry for the minimum-blocking condition; it is as follows:

$$\frac{F_c}{F_m} \approx \frac{1}{2}\,\frac{kD_f^2}{F_c\lambda} \approx \frac{D_f}{D_s'} \tag{10}$$

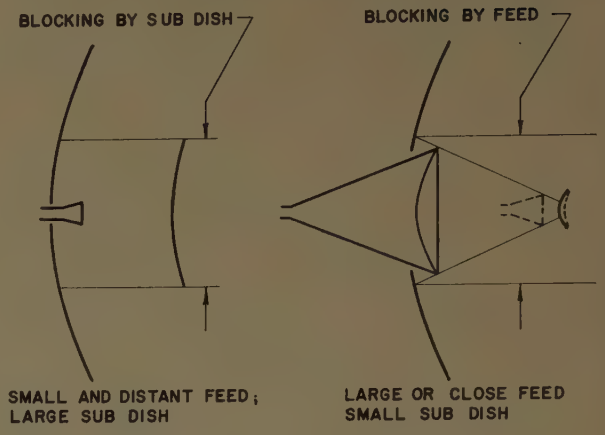

Fig. 10—Types of aperture blocking.

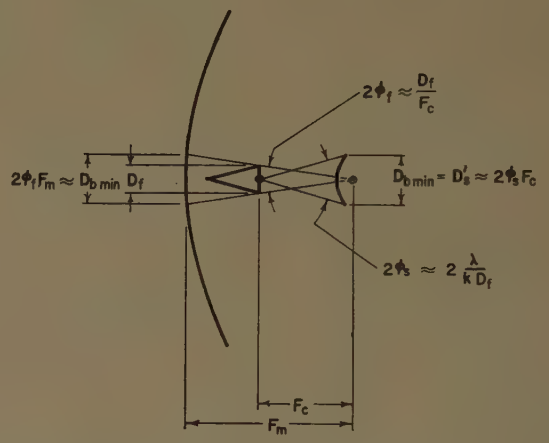

Fig. 11—Condition for minimum blocking by sub dish and feed.

where D_s' is the physical or blocking diameter of the sub dish, D_f is the physical or blocking diameter of the feed aperture, and k is the ratio of the effective feed-aperture diameter to its blocking diameter.[1] This approximate relationship assumes that the angles ϕ_s and ϕ_f, shown in Fig. 11, are small; and that the sub dish is much closer to the focus of the main dish than it is to the feed (F_c/F_m much larger than one). It also assumes that ray optics can describe the feed shadow; this is a good approximation when the feed is far from the sub dish. Within these limitations, minimum aperture blocking is obtained for a practical case in which there is essentially no spillover of the main lobe of the feed pattern past the edge of the sub dish. Although shown for the classical Cassegrain system, the above approximate analysis also applies for the classical Gregorian system [13].

It can be seen that the minimum-blocking condition

[1] Ordinarily k is slightly less than one; however, where a cluster of many feeds is employed to obtain a cluster of antenna beams, k can become quite small.

is not limited to a particular set of antenna dimensions, but includes a series ranging from the case of a feed located near the vertex of the main dish and having a diameter about equal to that of the sub dish, to the case of a feed located far in front of the main dish and having a diameter much smaller than the sub dish. In the former case, the feed should be focused approximately toward the focal point of the main dish in order that the illumination of the main aperture be characterized by a Fraunhofer diffraction pattern rather than a Fresnel pattern. In the latter case this is not necessary, but the feed must, of course, be excited by a length of transmission line and supported in its extended location; in an extreme form the latter case resembles a single-dish antenna with a splash-plate feed, although the principle of operation is quite different.

The diameter of the aperture blocking for the minimum-blocking condition is given by the following approximate equation:

$$D_{b\,\min} \approx \sqrt{\frac{2}{k} F_m \lambda} \tag{11}$$

where the limitations are the same as those mentioned previously. This equation also assumes that the total amount of aperture blocking is no greater than either of the two equal and coincident shadows; actually the blocking would be somewhat greater, particularly for the case of a small feed located close to the sub dish. It should also be mentioned that the approximation given in (11) implies that a classical Gregorian would have slightly less blocking than a classical Cassegrain of the same axial dimension, because of the shorter F_m of the former; however, a more exact formulation would show that just the reverse is true. The significant fact to note from (11) is that the minimum blocking diameter can be computed before determining the feed size and location, these latter dimensions finally being related by (10).

It is of interest to express (11) in some alternate approximate forms which more clearly illustrate the basic relationships;

$$\left(\frac{D_{b\,\min}}{D_m}\right)^2 \approx \frac{2}{k}\,\frac{\lambda}{D_m}\,\frac{F_m}{D_m} \approx \frac{\pi}{2k}\,2\theta_{p/2}\,\frac{F_m}{D_m} \approx \frac{\pi}{2k}\,\frac{2\theta_{p/2}}{2\phi_v} \tag{12}$$

where $2\theta_{p/2}$ is the approximate half-power beamwidth of the antenna pattern in radians, and $2\theta_v$ is the approximate included angle formed by the main dish at the virtual feed in radians. (Actually the first and second forms of (12) are almost exactly equal when the main aperture is circular and has a completely tapered parabolic illumination, and the second and third forms are equal when $2\phi_v$ is small.) It is apparent from (12) that an antenna with a narrow beamwidth can have less relative aperture blocking than one with a wide beamwidth. This might be expected on the basis that the optical case, which has a very narrow beamwidth, has the capability for very small relative aperture blocking. Also apparent is the desirability of a small F/D ratio for the main dish, and an efficient feed aperture (k approaching one).

As an example, consider an antenna which is to have a pencil beam of one-degree half-power beamwidth, $F_m/D_m = 0.3$, $k = 0.7$, and which is to be optimized for the minimum-blocking condition. The second form of (12) yields a value of about .012 for $(D_{b\min}/D_m)^2$, which may then be applied in (9) to yield a value of about .024 for E_b/E_m. The aperture blocking in this antenna would therefore reduce the gain by about $\frac{1}{4}$ db and would increase a -23 db sidelobe[2] to about -20.5 db. This effect might be acceptable for some applications, but not for others. Thus a one-degree beamwidth might be considered as a rough boundary above which the simple Cassegrain design, even though optimized, would be unattractive.

B. Twisting Cassegrains for Least Blocking

The preceding discussion of a minimum-blocking design has assumed that, similar to an optical telescope, operation in all polarizations is required. However, many microwave antennas need operate in only one polarization, and in this event a considerable reduction of aperture blocking is possible. Fig. 12 presents one scheme for accomplishing this, by means of a polarization-twisting technique which avoids the sub-dish shadowing.

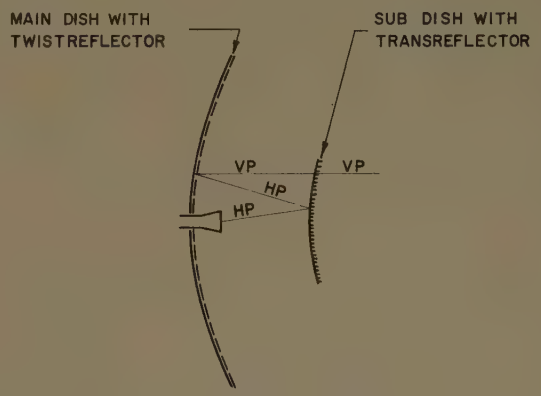

Fig. 12—Polarization twist for non-blocking sub dish.

In this scheme as shown, the sub dish comprises a horizontal grating, called a transreflector, which reflects a horizontally-polarized wave radiated by the feed. The main dish incorporates a surface design, called a twistreflector, which twists the horizontally-polarized wave to a vertically-polarized one as it reflects the wave back. The portion of this wave which is now incident on the

[2] The -23 db figure is a value which is typical for the first-sidelobe level when the illumination is tapered to about 11 db for maximum gain with a circular aperture.

sub dish is transmitted through unaffected, because the sub dish is transparent to a vertically-polarized wave. Thus there is no blocking by the sub dish at all. The feed does, of course, create aperture blocking; however, its size can be made quite small, and the blocking can be comparable with that of an ordinary single-dish design. In this scheme, therefore, it is advantageous to use a large sub dish with a small feed.

While the above process is theoretically perfect in the cardinal regions of the antenna aperture, the three-dimensional geometry of the system is such that there can be some loss into cross-polarized radiation toward the outer portion of the intercardinal regions. It is beyond the scope of this paper to consider this effect in detail, but some general comments can be made. One part of this effect occurs with the wave radiated from the sub dish to the main dish; for any but the most extreme Cassegrain forms, the loss here is usually so small as to be negligible. The other part occurs with the wave radiated from the feed to the sub dish, and the results are dependent on the polarization characteristics of the feed. There is often a moderate amount of loss here; however it is usually not greatly different from the loss in an ordinary single-dish antenna caused by the same effect.

Another scheme for reducing aperture blocking is indicated in Fig. 13; here, a polarization-twisting technique is employed to render the feed invisible. Two configurations are possible, both involving a sub dish which incorporates a twistreflector. In one case, a vertically-polarized feed is located behind the main dish, and the central portion of the main dish includes a transreflector having a horizontal grating. The feed radiates through the transreflector toward the sub dish, the sub dish reflects this wave and twists its polarization to horizontal, and the horizontally-polarized wave is then completely reflected by the main dish. In the other case, the feed is composed of thin horizontal elements and is located out in front of a simple main dish. When the feed radiates toward the sub dish, the vertically-polarized wave returned by the sub dish passes through the feed unaffected, is completely reflected by the main dish, and again passes through the feed. In both of these configurations, it is evident that the sub dish causes aperture blocking but the feed does not. Consequently, the feed may be greatly enlarged so that its increased directivity allows the sub dish to become quite small. As mentioned previously, when the feed becomes equal to or larger than the sub dish, the phase front across the feed aperture should be curved so as to focus the feed toward the vicinity of the main dish focus. It should also be mentioned that when this condition exists, the simple geometry of the Cassegrain system and the equivalence concepts no longer apply; however the basic operation of the antenna remains similar.

Of the two basic polarization-twisting schemes, the one having a twistreflecting main dish is of general applicability to many antenna developments [14]–[17],

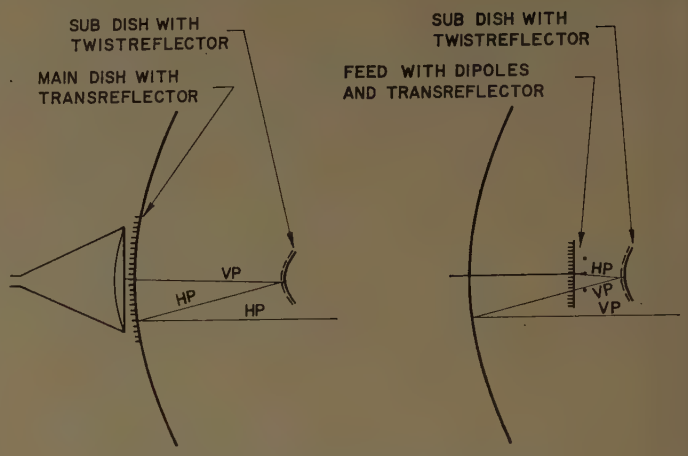

Fig. 13—Polarization twist for non-blocking feed.

while the one having a twistreflecting sub dish is useful in some special circumstances. For example, the former may be efficiently employed with any of the Cassegrain extensions shown in Fig. 5, and with the classical Gregorian form, as well. On the other hand, the latter should be limited to those forms in which the sub dish is small compared with the main dish. In either case it is essential, of course, to have suitable designs for the twist-reflector and transreflector. One particular technique [16] involving thin metal wires embedded in fiberglass skins, has proven most satisfactory. While it is not the purpose of this paper to discuss these designs in detail, a brief description is in order as an indication of their practical nature.

For the transreflector design, a grating of thin wires, closely-spaced compared with a wavelength, has the property of being essentially a perfect reflector for parallel polarization, and being essentially invisible to perpendicular polarization. The cross-section of a practical structure which incorporates a quarter-wave sandwich support is indicated in Fig. 14(a). The wires may be placed all in one skin, or else they may be divided equally between the two skins as shown; either technique usually yields about the same result.

For the twistreflector design, a grating of metal wires oriented at 45° to the incident polarization may be placed in front of a reflecting surface. When the spacing between the grating and the reflecting surface is about three-eighths of a wavelength, and the grating is designed to allow about one-half of the parallel-polarized power to pass through, the twistreflector operates over a broad frequency band and over a wide range of incidence angles. The cross-section of a practical structure is shown in Fig. 14(b).

It is perhaps interesting to note in passing, that there are a number of uses for a twistreflector in addition to those already discussed. One such use occurs in an ordinary single-reflector antenna during transmission, when it is desired to prevent any of the wave reflected by the dish from getting back into the feed. This can be accomplished with a twistreflector on the dish [12].

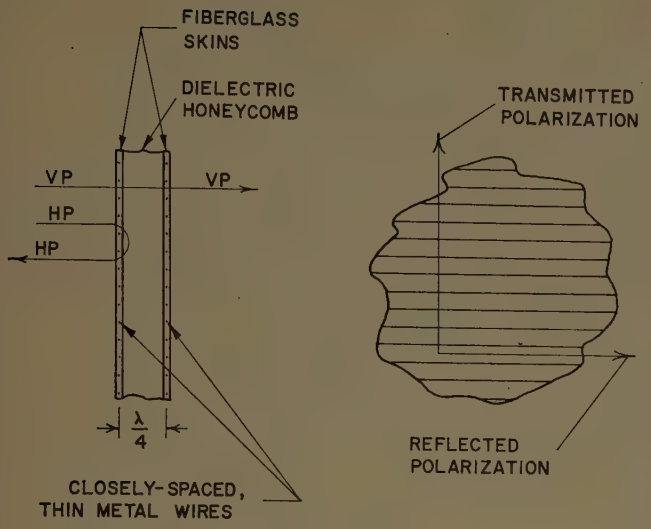

(a) Transreflector.

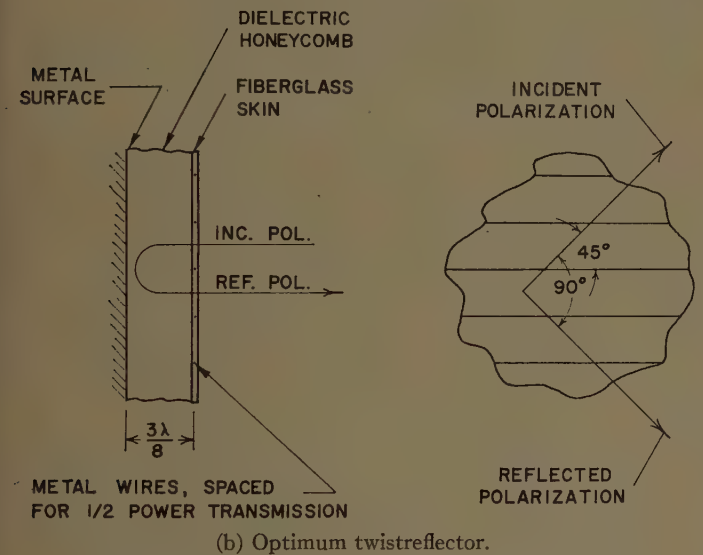

(b) Optimum twistreflector.

Fig. 14—Designs for polarization-operative surfaces.

Another use applies to a simple Cassegrain, in which it is desired to eliminate what may sometimes be an appreciable reflection by the sub dish back into the feed. Incorporation of a twistreflector on the sub dish achieves this result, and may create other advantages as well.

VI. Experimental Results

A number of Cassegrain antennas have been designed at Wheeler Laboratories, and their performance has been highly satisfactory. By way of illustration, the radiation patterns of two different antennas are presented; these two were designed for the Bell Telephone Laboratories on Army Ordnance projects.

One design is shown by the photograph in Fig. 15. It employs simple reflecting surfaces, and its geometry approaches that of the minimum-blocking configuration indicated in Fig. 11. Actually, as may be seen from the picture, the sub dish is appreciably larger than the feed shadow, and the blocking area is greater than the minimum possible by a factor of almost 3. The antenna is

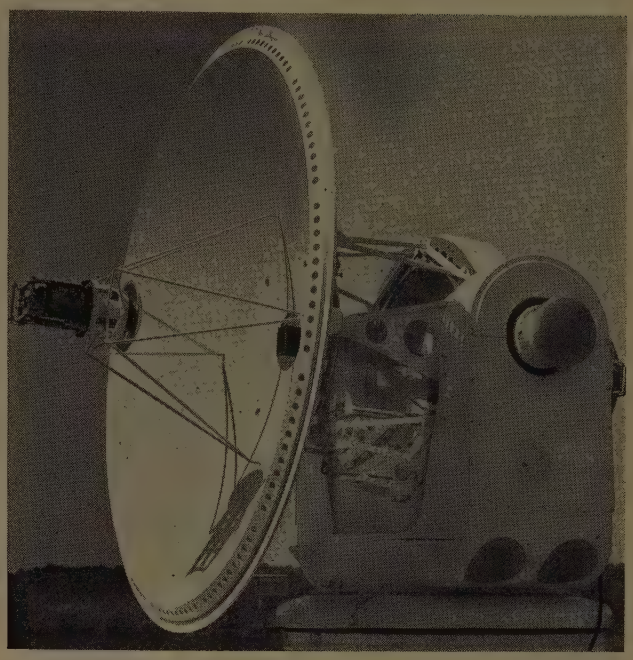

Fig. 15—Photograph of a simple Cassegrain.

shown in location on the roof of the antenna-development facility of Wheeler Laboratories at Smithtown, Long Island. Also visible in the picture are the precision mount for the antenna, and the versatile positioning devices for the feed and sub dish; these items were provided by the Bell Telephone Laboratories.

The radiation pattern and efficiency[3] of this Cassegrain antenna are shown by the solid curve in Fig. 16(a). The half-power beamwidth is 0.6 degrees; this is narrow enough so that the simple Cassegrain system without twisting is adequate for the intended application, even without complete optimization of the aperture blocking. As may be seen, the efficiency[3] of this Cassegrain is fairly high in spite of aperture blocking by both the sub dish and its rigid supporting system. This is probably a result of the efficient aperture utilization obtained with a long equivalent focal length. As expected, the near sidelobes are raised several db by the sub dish blocking; however this effect would also have occurred in the intended application had an ordinary single-reflector antenna been employed.

The dashed curve in Fig. 16(a) shows the radiation pattern which is obtained when the antenna is intentionally defocused by moving the sub dish a small distance toward the main dish. If desired, this technique might be used to provide a variable beamwidth. Alternatively, by moving the sub dish away from the main dish the antenna can be focused toward a point nearer than the far field; this would permit a greater concentration of power at such a point than could otherwise be obtained. Of course these focusing techniques are also

[3] The "efficiency" is used here as the ratio of measured gain to the gain which would be obtained if the same main aperture were uniformly illuminated, with no spillover or other losses.

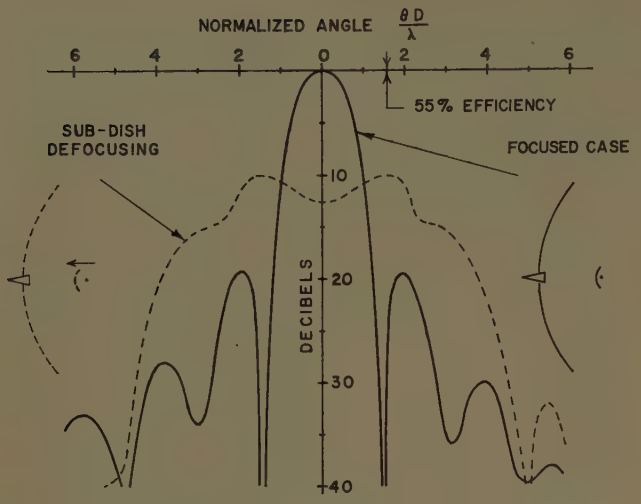

(a) Focused and defocused cases.

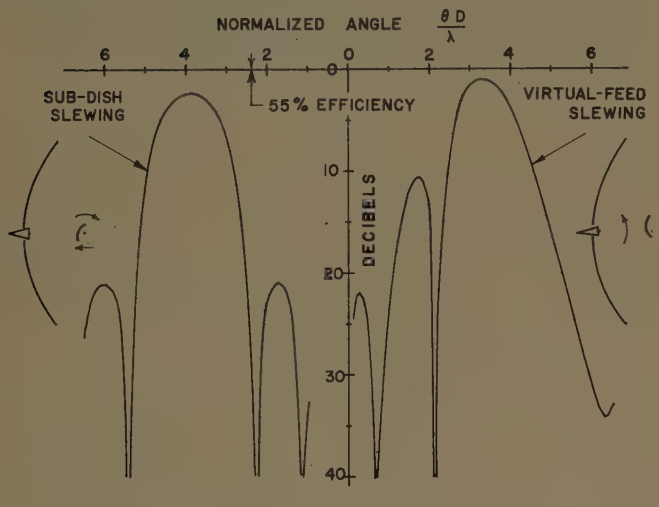

(b) Off-axis scanning methods.

Fig. 16—Radiation patterns of a simple Cassegrain.

available in the ordinary single-reflector antenna, as well as most other types. With this Cassegrain, however, it is possible to perform these operations by motion of a relatively small, passive device.

In Fig. 16(b), the patterns of this same antenna are shown for two cases in which the beam is scanned off axis by approximately three beamwidths. The pattern on the left is obtained by a movement of only the sub dish; the motion involves a substantial tilt about the main dish focus, plus a small axial motion to regain the focused condition in the plane of scan. It is evident that no appreciable coma is introduced by this process, since the pattern remains quite symmetrical. On the other hand, there is a considerable amount of astigmatism created; the pattern in the plane normal to the scan plane, not shown here, is quite broad. This defect is partly responsible for the decrease of gain which is apparent. The results presented above are typical of a Cassegrain system with a large F_e/F_m. It is perhaps instructive to mention that similar effects are obtained with this system when the scanning is accomplished by offsetting the feed and refocusing.

The pattern on the right side of Fig. 16(b) is obtained by tilting both the feed and the sub dish as a unit about the vertex of the main dish. This is equivalent to rotating the virtual feed about the same point. As can be expected, this results in a substantial degree of coma distortion, about the same as would be obtained by offsetting the feed in an ordinary single-reflector antenna of the same main focal length.

The other antenna design chosen as an example incorporates a twist-reflecting main dish and a transreflecting sub dish, such that the sub dish creates no aperture blocking, as illustrated in Fig. 12. The equivalent focal length of this antenna is designed to be just long enough so that a monopulse feed system can be employed in a size just large enough to utilize a simple cluster of four horns as the feed. The complicated monopulse plumbing is located in a convenient region behind the antenna.

The patterns of this antenna are shown in Fig. 17 for the sum and one difference channel. Also indicated are the computed points, determined from a knowledge of the feed pattern, and including a contribution from aperture blocking by the feed. The close correspondence between the two patterns is evident. Similar good agreement exists in the other properties of this antenna. The efficiency[3] of 54 per cent in the sum pattern is rather high for a monopulse system; this is a result of the inherent advantage of a Cassegrain system with a long equivalent focal length and very small aperture blocking. All of the above results confirm the nearly lossless behavior of the polarization-twisting technique and the surface designs of Fig. 14. While the twisting type of antenna requires additional effort during design and construction of the polarization-operative surfaces, it has proven practical to build in large quantities, and has yielded the expected good performance in the field.

VII. Benefits of Cassegrain Systems

In concluding the discussion of Cassegrain optics applied to microwave antennas, it is appropriate to outline some of the benefits obtainable. Perhaps most important is the ability to place the feed in a convenient position, while utilizing reflectors as the focusing elements. The rear location and forward direction for the feed are most desirable in various applications involving complicated feeds and associated plumbing.

One example of this advantage occurs in the case of an antenna intended for low-noise operation, as illustrated in Fig. 18. At present, a low-noise receiver is likely to be bulky and require a number of auxiliary connections as well as occasional adjustments; it is therefore inconvenient to mount it close to the feed out in front of a single-reflector antenna. Yet this is often done, because the attenuation in a waveguide from the

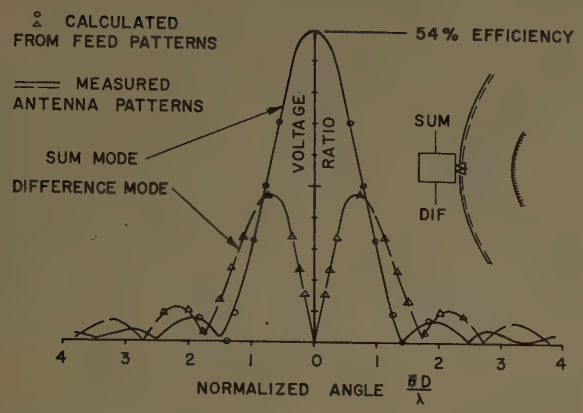

Fig. 17—Radiation patterns of a twisting Cassegrain.

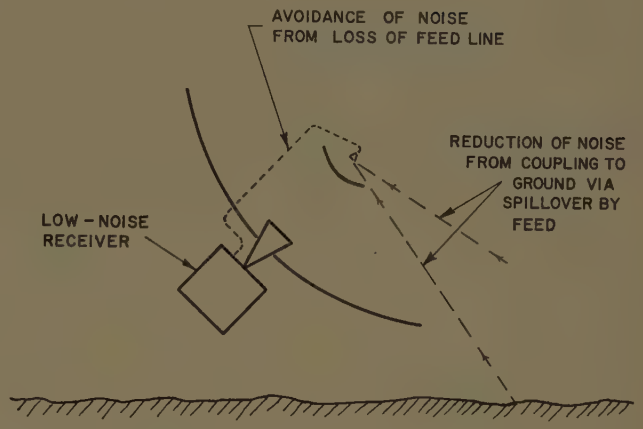

Fig. 18—Simple Cassegrain antenna for low-noise applications.

feed back to a receiver located behind the dish would introduce an excessive amount of noise power. The Cassegrain system furnishes the opportunity to avoid most of these difficulties.

There is another benefit obtainable with the Cassegrain system in a low-noise application. With the ordinary single-reflector antenna, there is usually a considerable amount of wide-angle sidelobe response caused by spillover radiation from the small feed out in front. This may introduce a very substantial amount of noise power into the antenna, by coupling to the radiation from the warm ground. In the case of a Cassegrain antenna, spillover radiation from the virtual feed can be very much less. This is because of the essentially ray-optic behavior of reflection from the sub dish, which results from its relatively large diameter in wavelengths. There remains to be considered, of course, spillover from the real feed past the edge of the sub dish. Although the total amount of this spillover power may be comparable with that in a single-reflector antenna, it is likely to be confined to direction relatively close to the antenna axis. There is also to be considered the sidelobe radiation created by the aperture blocking by the sub dish; here again, this is usually appreciable only in forward directions. As a result of these directional properties, the spillover and aperture blocking couple to the ground only when the antenna is pointed at a low elevation angle. In comparison, the ordinary single-reflector antenna is likely to have appreciable coupling to the ground even at high elevation angles.

It is possible in the case of a polarization-twisting Cassegrain system to reduce even this relatively narrow-angle sidelobe response. Fig. 19 illustrates this effect, for the scheme which involves a twistreflector at the main dish and a transreflector at the sub dish. Since the feed is horizontally polarized, it is essentially isolated from any vertically-polarized source, such as the normal ground reflection of the incoming wave, or one component of thermal ground radiation. If the transreflector is extended from the sub dish to the main dish in

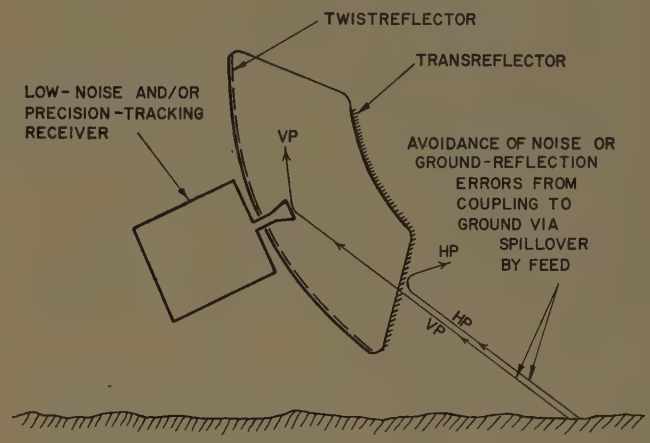

Fig. 19—Twisting Cassegrain antenna for further reduction of coupling to ground.

the lower portion of the antenna, isolation may also be achieved for the other polarization. Such an antenna, then, has effectively only those sidelobes which would be inherent in the illumination distribution of its main aperture. As a result, the antenna could provide accurate tracking of a target, as well as low-noise performance, down to elevation angles determined only by the decay rate of the inherent sidelobes.

In continuing the outline of benefits obtainable with a Cassegrain system, mention can be made of the ability to obtain an equivalent focal length much greater than the physical length; as discussed previously in this paper, various advantages may be obtained in this way. A third aspect is the capability for scanning or broadening the beam by moving one of the antenna surfaces. One case involving a small moving sub dish has been described here; there have also been designs utilizing a moving flat main dish for wide-angle scanning [15], [17].

The existence of two dishes and two focal points in the Cassegrain system gives rise to interesting methods for incorporating the separate functions of two antennas into one structure. On the left side of Fig. 20 a simple scheme is shown which provides a full-size plus a re-

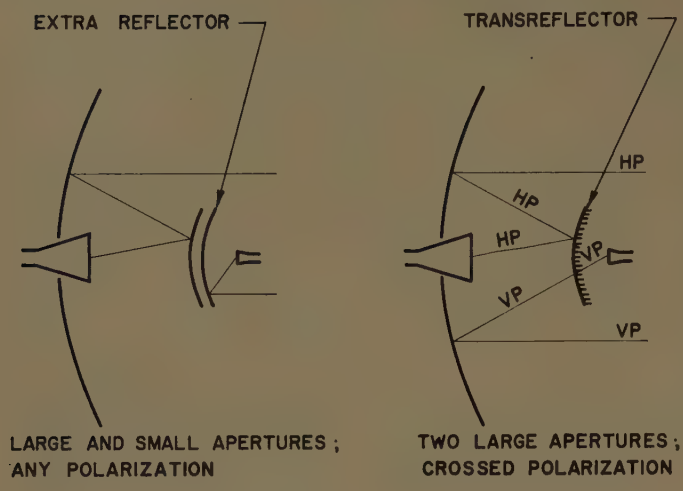

Fig. 20—Dual antennas, blocking sub dishes.

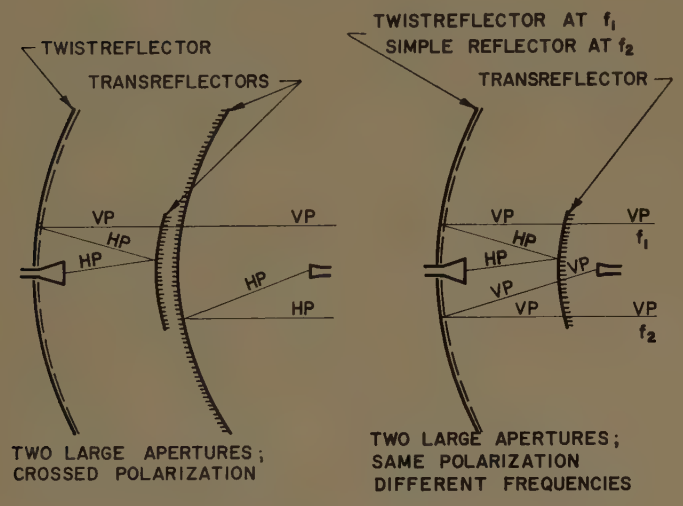

Fig. 21—Dual antennas, non-blocking sub dishes.

duced-size antenna combination, while on the right side there is illustrated a scheme for obtaining two full-size antennas having crossed polarizations. In both of these cases, the sub dish causes some blocking of one of the two apertures. On the left side of Fig. 21 an alternate scheme is shown for obtaining two full-size antennas having crossed polarizations; here, the polarization-twisting process eliminates any blocking by the sub dish. On the right side of Fig. 21, a scheme is indicated whereby two full-size antennas are obtained having the same polarization but operating at different frequencies, without any blocking by the sub dish. This case relies on a surface design for the main dish which is a twist-reflector at one frequency and an ordinary reflector at the other frequency.

VIII. Conclusion

To summarize the discussion of the principles and features of Cassegrain antennas, it has been shown that a simple set of formulas describe a number of forms, and that the essential performance can be calculated by means of simple equivalence concepts. The basic defect, aperture blocking by the sub dish, can be minimized or virtually eliminated by certain techniques. The Cassegrain system has proven both practical and advantageous in a number of operational antennas, and the tested performance has agreed closely with the computed predictions. A variety of benefits are obtainable with the Cassegrain system, and it provides a highly versatile form of microwave antenna capable of achieving good performance in a number of unusual applications. The second reflecting surface which is available in this system provides an extra degree of freedom to the antenna designer for application to his particular problem.

IX. Symbols

D_m = effective diameter of circular main dish (to edge rays).
D_s = effective diameter of circular sub dish (to edge rays).
D_s' = blocking diameter of sub dish.
D_f = diameter of feed.
D_b = diameter of aperture blocking.
$D_{b\,\min}$ = diameter of aperture blocking for minimum-blocking geometry.
F_m = focal length of main dish.
F_c = distance between foci of sub dish.
F_e = equivalent focal length of Cassegrain system.
L_v = distance from virtual focus (or main dish focus) to sub dish.
L_r = distance from real focus (or feed) to sub dish.
ϕ_v = angle between axis and edge ray, at virtual focus.
ϕ_r = angle between axis and edge ray, at real focus.
$2\phi_s$ = included angle between rays from real focus to physical edges of sub dish, in radians.
$2\phi_f$ = included angle between rays from virtual focus to edges of feed, in radians.
e = eccentricity of conic section.
a = transverse half-axis of conic section.
b = conjugate half-axis of conic section.
x_m, y_m = coordinates of main dish (axial, radial).
x_s, y_s = coordinates of sub dish (axial, radial).
x_e, y_e = coordinates of equivalent parabola (axial, radial).
λ = wavelength.
f = frequency.
k = ratio of effective diameter to blocking diameter of the feed.
θ = antenna pattern angle, in radians.
$2\theta_{p/2}$ = half-power beamwidth of antenna, in radians.
E = pattern voltage.
E_b = peak voltage of the supplemental negative pattern caused by aperture blocking.
E_m = peak voltage of the pattern of the main aperture without blocking.

X. Acknowledgment

The principles and geometry of the double-reflector systems described in this paper are based entirely on the principles developed for the optical telescope. This work originated in the 17th century, with particular forms being attributed to Gregory, Newton, and Cassegrain. It seems very probable that the simple concept of an equivalent parabola has long been known to those involved in the theory of optical reflecting telescopes; however the writer, having only a limited acquaintance with the optical literature, has not found any reference to this.

The existence of a minimum-blocking design was suggested by H. A. Wheeler, for the case of a feed located at the vertex of the main dish. This suggestion led to the general case of a feed located anywhere, and the basic relationship of minimum blocking as a function of beamwidth.

During the design of a radar antenna for the Bell Telephone Laboratories, the system involving a transreflecting sub dish and twistreflecting main dish was conceived [16] as the solution to the problem at hand. Later it was learned that the basic concept had already occurred to C. A. Cochrane [14] of Elliott Brothers, London. The scheme involving a twistreflecting sub dish and a transreflecting main dish or feed was devised in connection with the design of another antenna for the Bell Telephone Laboratories.

The use of thin wires in fiberglass for the polarization-operative surfaces was worked out in cooperation with K. B. Woodard of the Bell Telephone Laboratories. The particular set of dimensions which achieve wideband, wide-angle twistreflector performance was derived by H. Jasik, as a consultant to Wheeler Laboratories.

Of the four dual-antenna schemes mentioned in Section VII, it is of interest to note that the first has also been perceived and utilized by the Ryan Aeronautical Co., and the second by both Sperry Gyroscope Co., and Melpar, Inc.

The writer would like to express his appreciation for the support of Wheeler Laboratories in the preparation of this paper. He would also like to acknowledge the permission of the Bell Telephone Laboratories and the Army Ordnance Corps for the inclusion of experimental results obtained on certain antennas developed for them, and the helpful cooperation of R. L. Mattingly of the Bell Telephone Laboratories in this respect.

XI. Bibliography

[1] A. G. Ingalls, "Amateur Telescope Making," Scientific American, Inc., New York, N. Y., vol. 1, pp. 62–65, 215–218, 444–453; 1953.
[2] J. B. Sidgewick, "Amateur Astronomer's Handbook," Faber and Faber, Ltd., London, Eng., pp. 161–165; 1955.
[3] L. C. Martin, "Technical Optics," Sir Isaac Pitman and Sons, Ltd., London, Eng., vol. 2, pp. 75–78; 1954.
[4] D. O. Woodbury, "The Glass Giant of Palomar," Dodd Mead and Co., New York, N. Y.; 1957.
[5] W. M. Cady, M. B. Karelitz, and L. A. Turner, "Radar Scanners and Radomes," M.I.T. Rad. Lab. Ser., McGraw-Hill Book Co., Inc., New York, N. Y., vol. 26, pp. 55–61; 1948.
[6] W. Rotman, "A Study of Microwave Double-Layer Pillboxes, Part II—Multiple-Reflector Systems," AF Cambridge Res. Ctr., Bedford, Mass., Rept. No. TR-56-101; January, 1956.
[7] A. K. Head, "A new form for a giant radio telescope," *Nature*, vol. 179, pp. 692–693; April 6, 1957.
[8] F. A. Jenkins and H. E. White, "Fundamentals of Optics," McGraw-Hill Book Co., Inc., New York, N. Y., p. 156; 1957.
[9] C. C. Cutler, "Parabolic-antenna design for microwaves," Proc. IRE, vol. 35, pp. 1285–1286, 1288; November, 1947.
[10] K. S. Kelleher, "Microwave optics at naval research laboratory," *Proc. Symp. on Microwave Optics*, McGill University, Montreal, Canada, vol. 2, Paper No. 34; June, 1953.
[11] B. Woodward, "The Cassegrain Antenna," Advertisement by Airborne Instruments Lab., Proc. IRE, vol. 46, p. 2A; March, 1958.
[12] S. Silver, "Microwave Antenna Theory and Design," M.I.T. Rad. Lab. Series, McGraw-Hill Book. Co., Inc., New York, N. Y., vol. 12, pp. 190–192, 447–448; 1949.
[13] Advertisement by D. S. Kennedy and Co., *Aviation Week*, vol. 71, p. 4; July 27, 1959.
[14] C. A. Cochrane, "Improvements in or Relating to High Frequency Radio Aerials," British Patent No. 700,868, February, 1952–December, 1953; "High Frequency Radio Aerials," U. S. Patent No. 2,736,895, February, 1952–February, 1956.
[15] P. F. Mariner and C. A. Cochrane, "Improvements in or Relating to High Frequency Radio Aerials," British Patent No. 716,939; August, 1953–October, 1954.
[16] Wheeler Laboratories reports available through ASTIA: WL No. 658, ASTIA No. AD 116479, January, 1955; and WL No. 666, ASTIA No. AD 306000, April, 1955.
[17] R. W. Martin and L. Schwartzman, "A Rapid Wide Angle Scanning Antenna with Minimum Beam Distortion," *Proc. 1958 East Coast Conf. on Aeronautical and Navigational Electronics*, Baltimore, Md., pp. 47–51.

Multiple Beams from Linear Arrays*

J. P. SHELTON†, MEMBER, IRE AND K. S. KELLEHER‡, SENIOR MEMBER, IRE

Summary—**The problem of devising a passive RF transmission line feed system to provide independent multiple outputs from a linear array is considered. It is shown that a lossless, matched feed network is possible only for uniform aperture distribution. The general feed system for connecting 2^n inputs to 2^n elements is shown to consist of conventional hybrid junctions with associated phase shifters. In order to increase the possible number of elements in the array, the problem of finding applicable junctions more complex than the hybrid is considered. Junctions with three inputs and three outputs and with four inputs ond four outputs are derived for use in multiple feed networks, expanding the number of elements in the array to $2^l 3^m 4^n$.**

I. Introduction

THE array-type antenna was in use many years before adoption of the microwave optics techniques for forming directive beams. However, it had only a limited number of elements and seldom, if ever, produced more than a single directive beam simultaneously. The microwave optics techniques, on the other hand, provided capability for large apertures and were adaptable to producing multiple beams. Since, in many applications, the array has advantages over the microwave optics counterpart, it is desirable to develop techniques permitting the use of a large number of array elements and providing multiple beams from such an array.

The microwave optics systems were those capable of yielding wide-angle performance. The inputs to this system were simple feed horns. Many different techniques were employed. The early units consisted of parabolic reflectors with large F/D ratios. Later work involved Schmidt systems, Luneberg lenses and the parabolic torus reflector.

In all of the systems, with the exception of the Luneberg lens, some phase error existed in the apertures forming the majority of the beams. In general, the wide-angle capability of the system or the number of multiple beams that the system could produce was limited by this inherent phase error. Since the Luneberg lens showed the most promise, it was found that this structure, or some related configuration, would be most desirable for achieving multiple beams.

It is well known that all microwave optics structures employ a feed and focusing objective. In such a system, inefficiency is introduced due to spillover of energy from the feed which is not captured by the objective. A more serious problem is a decreased aperture efficiency, due to the requirement that the multiple beams cross over at a very high level. If levels as high as 3 db are required, problems in isolation among the various elements are introduced. This is particularly severe with regard to the isolation between an element and its neighbors. Variations in the impedance match in neighboring feeds can drastically affect the radiated beam associated with a given feed.

Considerations of efficiency, beam overlap, and element isolation indicate the difficulties that are encountered in obtaining a microwave optics system producing multiple beams. Since the work done on obtaining multiple beams from an array has, to the greatest extent, involved complex feed structures employing active elements, it is desirable to consider the problem anew and to determine how this might be achieved entirely with a passive transmission-line network, so that the antenna system is capable of both transmitting and receiving with a minimum of complexity.

This paper is organized into four major divisions. The first one, Section II, is concerned with the possible pattern characteristics of a set of beams from a linear array. It is found that, for uniform amplitude distribution, the best configuration achieves one input and beam position for each element of the array. The same relationship is shown to hold for aperture distributions other than uniform. In Section III, the limitations on the feed network are established and it is found that the only lossless feed system is the one for uniform illumination. In Section IV, the details of the hybrid feed networks are presented, and a table presents the possible array sizes. Finally, the design of the more complex hybrids that can be used is treated in the appendices.

Research on multiple-beam arrays is in progress at the W. L. Maxson Corporation with significant results.[1] The approach used, however, although simpler in geometry, consists basically of traveling-wave arrays and is inherently somewhat inefficient. The purpose of this paper is to explore the fundamental limitations on multiple-feed systems before giving detailed attention to design aspects.

II. Multiple-Beam Pattern Characteristics

Before the problem of realizing the multiple-feed system is considered, it is necessary to evaluate the multiple-beam radiation pattern characteristics that are at-

* Received by the PGAP, March 25, 1960; revised manuscript received, July 27, 1960. The research was sponsored by the Electronics Research Directorate of the Air Force Cambridge Research Center, Air Research and Development Command, under contract AF19(604)-5217.

† Radiation Systems, Inc., Alexandria, Va. Formerly with AGA Corp., Alexandria, Va.

‡ AGA Corp., Alexandria, Va.

[1] M. Carroll, W. Kahn, and E. Shubel, "Multidirectional Beam Scanning Antenna Array—First Interim Report," prepared for RADC by W. L. Maxson Corp., New York, N. Y., Contract No. AF30(603)-1920; July, 1958–April, 1959.

tainable from a linear array. It would be desirable to find the relationships among beam spacing and aperture distribution with its associated aperture efficiency, beamwidth, and sidelobe level.

The desirable feed network would be one in which the array attains maximum effective aperture for every angle of incidence; that is, the feed system would be matched as seen from both the inputs and from the elements.

The problem of beam spacing is best approached by considering the case of the uniform distribution, a typical array factor of which is shown in Fig. 1 for a six-

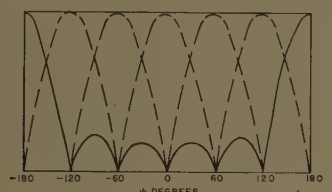

(a)

(b)

Fig. 1—Overlapping array factors for uniform six-element array. (a) Outermost beam split evenly. (b) Outermost beams split at crossover points.

element array. Array or space factors are expressed in terms of ψ, the relative phase at adjacent elements for an incident wave, which can easily be converted to angle in any specific application with the equation $\psi = (2\pi d/\lambda) \sin \theta$, where d is element spacing and θ is angle relative to the normal to the array. It can be seen that the nulls are evenly spaced, so that six beams can be overlapped without repetition, the maxima being located at the nulls of the other beams. Any other arrangement of the beams or a greater number of beams would mean reduced aperture efficiency, since the maximum gain of a given beam would be reduced by the absorption of energy by other beams. On this basis there should be one beam for each element of the array, and the beams are spaced $2\pi/N$ in ψ, where N is the number of elements.

On this basis, the required phase relationships are as shown below. For six elements, the successive element phases are seen to be $\pm 30°$, $\pm 90°$, $\pm 150°$.

Element	1	2	3	4	5	6	Beam Numbers
Phase	0°	± 30°	± 60°	± 90°	±120°	±150°	3 and 4
	0°	± 90°	±180°	±270°	±360°	±450°	2 and 5
	0°	±150°	±300°	±450°	±600°	±750°	1 and 6

The question now is whether it is possible to use the same beam positions for aperture amplitude distributions other than uniform. The most general case is the one in which the element distribution is in phase but the amplitudes are arbitrary. If the amplitudes are denoted by $a_1, a_2, \cdots, a_N$, the distribution can be broken down into even and odd components, the even distribution being

$$\frac{a_1 + a_N}{2}, \frac{a_2 + a_{N-1}}{2}, \frac{a_3 + a_{N-2}}{2} \cdots$$

and the odd being

$$\frac{a_1 - a_N}{2}, \frac{a_2 - a_{N-1}}{2}, \frac{a_3 - a_{N-2}}{2} \cdots.$$

The array factors can be written

$$E_e(\psi) = (a_1 + a_N) \cos (N-1)\psi/2 + (a_2 + a_{N-1}) \cos (N-3)\psi/2 + \cdots$$

$$jE_0(\psi) = (a_1 - a_N) \sin (N-1)\psi/2 + (a_2 - a_{N-1}) \sin (N-3)\psi/2 + \cdots.$$

Since the even and odd array factors are in phase quadrature, the power pattern can be written as the sum of their squares,

$$P(\psi) = E_e^2(\psi) + E_0^2(\psi),$$

$$E_e^2(\psi) = (a_1 + a_N)^2 \cos^2 (N-1)\psi/2 + 2(a_1 + a_N)(a_2 + a_{N-1}) \cos (N-1)\psi/2 \cdot \cos (N-3)\psi/2 + (a_2 + a_{N-1})^2 \cdot \cos^2 (N-3)\psi/2 + \cdots$$

$$E_0^2(\psi) = (a_1 - a_N)^2 \sin^2 (N-1)\psi/2 + 2(a_1 - a_N)(a_2 - a_{N-1}) \sin (N-1)\psi/2 \cdot \sin (N-3)\psi/2 + (a_2 - a_{N-1})^2 \cdot \sin^2 (N-3)\psi/2 + \cdots.$$

Straightforward trigonometric manipulation yields expressions of the following form:

$$E_e^2(\psi) = \frac{(a_1 + a_N)^2}{2} + \frac{(a_2 + a_{N-1})^2}{2} + \cdots + b_1 \cos (N-1)\psi + b_2 \cos (N-2)\psi + \cdots$$

$$E_0^2(\psi) = \frac{(a_1 - a_N)^2}{2} + \frac{(a_2 - a_{N-1})^2}{2} + \cdots + c_1 \cos (N-1)\psi + c_2 \cos (N-2)\psi + \cdots.$$

Thus, the power pattern assumes the form

$$P(\psi) = a_1^2 + a_2^2 + \cdots a_N^2 + d_1 \cos (N-1)\psi + d_2 \cos (N-2)\psi + \cdots. \quad (1)$$

As one shifts from beam to beam, the variable ψ used in the above equations is altered by the appropriate phase, which may be written $m\phi$, where m assumes integral values from one to the total number of beams M (not necessarily equal to the number of elements N). In order to insure a generally symmetrical phase distribution and beam coverage, $\phi = 2\pi/M$. For optimum coverage by the array, it is required that

$$\sum_{m=1}^{M} P(\psi, m) = \text{constant}.$$

Referring to (1) and inserting the appropriate phases, the expression for the total power radiated in a direction ψ by all beams can be written,

$$\sum_{m=1}^{M} P(\psi, m) = M(a_1^2 + a_2^2 + \cdots a_N^2) + d_1 \sum_{m=1}^{M} \cos (N-1)\left(\psi + m\frac{2\pi}{M}\right) + d_2 \sum_{m=1}^{M} \cos (N-2)\left(\psi + m\frac{2\pi}{M}\right) + d_n \sum_{m=1}^{M} \cos\left(\psi + m\frac{2\pi}{M}\right). \quad (2)$$

Now, the periods of ψ in the arguments, $(N-1)\psi$, $(N-2)\psi$, $\cdots$, in (2) are $2\pi/N-1$, $2\pi/N-2$, $\cdots$, 2π, while the change in the variable ψ introduced by traversing from one beam to another is $2\pi/M$. If the period coincides with the change in ψ for any of the terms in (2), then the sum for that term will be nonzero and a function of ψ. For example, if $M = N-1$,

$$\sum_{m=1}^{N-1} \cos [(N-1)\psi + m2\pi] = (N-1) \cos [(N-1)\psi],$$

but if $M = N$,

$$\sum_{m=1}^{N} \cos\left[(N-1)\left(\psi + m\frac{2\pi}{N}\right)\right] = 0.$$

Thus, the number of beams, M, cannot fall in the range one through $N-1$, and must assume a value of at least N, the number of elements in the array. As was the case with the uniform array, a value of M greater than N does not improve the coverage of the system but merely reduces the maximum possible gain of each beam through increased beam overlap. It is, therefore, seen that the number of beams is independent of the illumination.

It is interesting to note that, as the sidelobes are reduced and the beamwidth broadens, the beam crossover level becomes higher for two reasons. First, the aperture efficiency of the individual beam decreases, so that relative crossover can easily increase. Second, the lower sidelobe characteristic results in less received energy distributed to other inputs, so that the absolute crossover can also be expected to increase some before too much gain is lost.

III. Limitations on the Feed Network

The previous discussion had as its starting point the assumption of a given aperture distribution, with appropriate phase characteristics for the multiple-beam radiation pattern coverage. No consideration was given to the realizability of the network required to connect the array elements with the inputs so as to provide the assumed aperture distributions.

A diagram of the network inputs and outputs is shown in Fig. 2. If it is required that the transmission

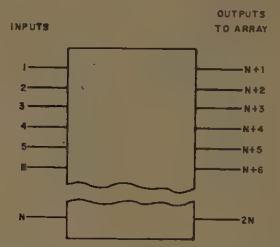

Fig. 2—General $2N$-port network for multiple-beam application.

loss from an input to the outputs to the elements be zero and that the inputs be isolated from one another, the scattering matrix is of the following form:

$$\left(\begin{array}{ccc|ccc} 0 & \cdots & 0 & S_{1\,N+1} & \cdots & S_{1\,2N} \\ \vdots & & \vdots & \vdots & & \vdots \\ 0 & \cdots & 0 & S_{N\,N+1} & \cdots & S_{N\,2N} \\ \hline S_{N+1\,1} & \cdots & S_{N+1\,N} & 0 & \cdots & 0 \\ \vdots & & \vdots & \vdots & & \vdots \\ S_{2N\,1} & \cdots & S_{2N\,N} & 0 & \cdots & 0 \end{array}\right).$$

The upper left quadrant indicates that the inputs are matched and isolated. The upper right and lower left quadrants represent transmission coefficients between the inputs and outputs, and the lower right quadrant is the reflection and transmission coefficients among the outputs to the array, as yet undetermined, but assumed to be 0.

It has recently been pointed out that the length (the sum of the squares of the magnitudes) of any row or column of a scattering matrix must be less than or equal

to unity.[2] In view of this limitation, the maximum transfer coefficient for amplitude distributions differing only in phase is given by

$$\sum_{b=1}^{N} |S_{ab}|^2 = N|S_{ab}|^2 \leqq 1$$

$$|S_{ab}| \leqq 1/\sqrt{N}. \tag{3}$$

Since some transfer coefficients must be greater than $1/\sqrt{N}$ in a tapered distribution, (3) forces the conclusion that any tapered distribution is achieved only at the expense of net transmission loss from inputs to outputs. Thus, the feed system for uniform illumination is the only lossless one, so far as achieving maximum array efficiency is concerned.

Of course, if the feed system were to have fewer inputs than the number of elements in the array, (3) would be altered to read

$$S_{ab} \leqq 1/\sqrt{P}, \qquad P < N$$

where P is the number of inputs. In this event, the conclusion of Section II, that the number of beams is equal to the number of elements, would be violated.

Although it appears that efficient feed networks giving tapered illuminations may be realized at the expense of over-all beam coverage, such possibilities will not be further investigated at this time, and the following sections are devoted to feed networks connecting N inputs to N elements with uniform illumination.

IV. Synthesis of Multiple-Feed Networks

The required microwave network has $2N$ ports and is matched at all ports. The N outputs on one side of the network that are excited by any of the N inputs on the other side possess a progressive phase characteristic that is a function of the input.

The first step is to determine just what phase characteristic is required. It is possible to select any 360° portion of the ψ coordinate in which to place the beams. Referring to Fig. 1, the problem can be reduced to whether a beam maximum or a crossover point should be located at $\psi = 0$. If the feed system is to be symmetrical, it is preferable to locate the beams symmetrically, with a crossover point at zero. On the other hand, such an arrangement results in excessive backlobes from the outermost beams due to the second-order maximum which is beginning to form. These two beams can be discarded, or if the patterns were shifted so that one is located at $\psi = 0°$ and one at $\psi = \pm 180°$ with a beam split between the edges of the coverage region, then only the split pattern need be discarded. These problems can best be dealt with, when the practical design is undertaken. For present purposes, it is best to locate the beams with the symmetry corresponding to that expected of the multiple-feed network.

The solution will be shown to depend upon building blocks, the simplest of which is the hybrid junction. The hybrid junction is a building block because it can provide two overlapping beams from a two-element array, as shown in Fig. 3. It should be noted that there are

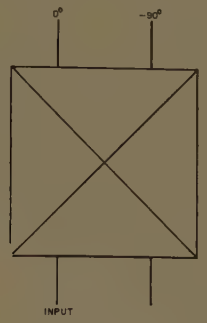

Fig. 3—Operation of hybrid coupler.

various configurations which provide hybrid operation. Hybrids that rely on symmetry, such as the magic tee hybrid, have in-phase and out-of-phase outputs. Directional-coupler hybrids have outputs that are 90° out of phase. Some couplers give a phase lag to the coupled arm and some a phase lead. In the following discussion the hybrid junction is a phase-lag coupler. Similar techniques would be applicable for use with the other components.

A single hybrid junction supplies rudimentary multiple-beam operation from a two-element array. The significance of the element, however, lies in its use as a building block for arrays with more elements and beams. Figs. 4 and 5 indicate feed systems for four and eight elements, respectively, and the pattern for extending the number to any power of two is clear. The critical aspects of the arrangements are the interconnections among the hybrids and to the elements and the added phase shifts. All transmission lines in a given cross section are assumed equal in length except for the phase shifters.

The principal limitation on the use of hybrids is the restriction of the number of elements to powers of two. The alternative to this difficulty would be to find more building blocks. The next larger building block would be one in which three inputs and outputs are connected so that three beams could be obtained from a three-element array. This case is treated in Appendix I, and such a component consists of three lines equally coupled to one another so as to effect equal power division, followed by a 120° phase shifter on the output that will feed the central element.

An additional limitation on the use of small building blocks is the great number that are required to feed large arrays. For this reason, a network of four inputs

[2] L. Joseph and W. K. Saunders, "A theorem on lossy nonreciprocal n-port junctions," Proc. IRE, vol. 47, p. 102; January, 1959.

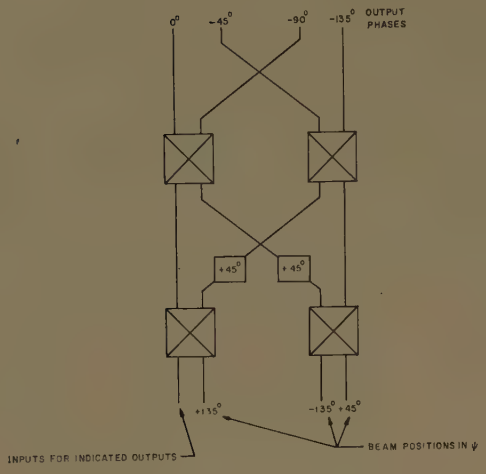

Fig. 4—Four-element feed system.

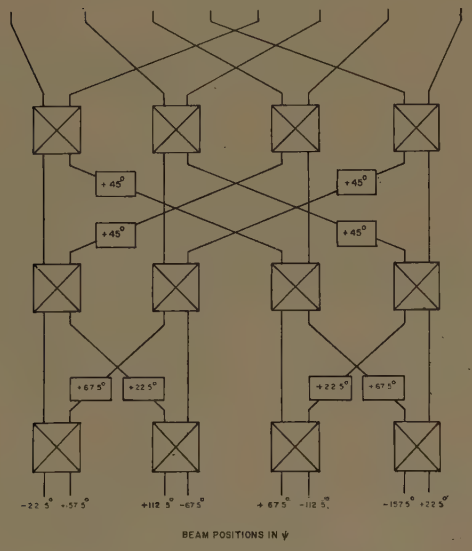

Fig. 5—Eight-element feed system.

TABLE I

RELATIONSHIP BETWEEN INPUTS AND JUNCTIONS

Number of Elements $N=2^l 3^m 4^n$	l	m	n	2×2 Hybrids	3×3 Junctions	4×4 Junctions	Total Junctions
2	1	0	0	1	0	0	1
3	0	1	0	0	1	0	1
4	0	0	1	0	0	0	1
6	1	1	0	3	2	0	5
8	1	0	1	4	0	2	6
9	0	2	0	0	6	0	6
12	0	1	1	0	4	3	7
16	0	0	2	0	0	8	8
18	1	2	0	9	12	0	21
24	1	1	1	12	8	6	26
27	0	3	0	0	27	0	27
32	1	0	2	16	0	16	32
36	0	2	1	0	24	9	33
48	0	1	2	0	16	24	40
54	1	3	0	27	54	0	81
64	0	0	3	0	0	48	48
72	1	2	1	36	48	18	102
81	0	4	0	0	108	0	108
96	1	1	2	48	32	48	128
108	0	3	1	0	108	27	135
128	1	0	3	64	0	96	160

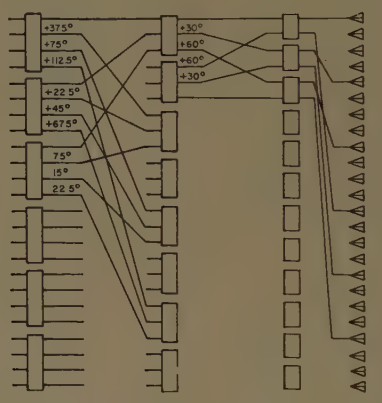

Fig. 6—24-element system using three types of junctions.

and four outputs is desirable, although it does not introduce any further flexibility in the number of elements. The derivation for such a junction is given in Appendix II.

Listed in Table I are the arrays with elements up to the number 128 that are available, with information on the number of hybrids required.

An example of how the different types of junctions are used to feed an array of 24 elements is shown in Fig. 6.

V. Conclusions

It has been shown that maximum space coverage is obtained by feeding an array of N elements with N feeds to provide N beams. Maximum efficiency is obtained by uniform illumination of all elements by all inputs; in fact, any illumination other than uniform, under the condition of maximum space coverage, is obtained only at the expense of transmission loss through the feed network.

Methods for synthesizing multiple-feed networks from building block junctions have been indicated. The simplest building block is the hybrid junction, and two other more complex junctions have been derived. At this point the number of beams is limited to $N=2^l3^m4^n$.

Although the geometrical shape factor of the feed systems is somewhat complicated by overlapping lines, it is felt that this type of system represents an optimum case. Further study is indicated on modifications in this approach to allow reduction in space coverage or greater pattern control at the expense of reduced efficiency.

Appendix I

Six-Port Junction For Multiple-Feed Arrays

No systematic design procedure was used in deriving the designs for the six-port and eight-port junctions. In this appendix some of the considerations involved in finding networks to match the desired scattering ma-

trices are given. The scattering matrices for six- and eight-port junctions are as follows:

$$1/\sqrt{3}\begin{bmatrix} 0 & 0 & 0 & e^{j(2\pi/3)} & 1 & e^{-j(2\pi/3)} \\ 0 & 0 & 0 & 1 & 1 & 1 \\ 0 & 0 & 0 & e^{-j(2\pi/3)} & 1 & e^{j(2\pi/3)} \\ e^{j(2\pi/3)} & 1 & e^{-j(2\pi/3)} & 0 & 0 & 0 \\ 1 & 1 & 1 & 0 & 0 & 0 \\ e^{-j(2\pi/3)} & 1 & e^{j(2\pi/3)} & 0 & 0 & 0 \end{bmatrix}$$

$$1/2\begin{bmatrix} 0 & 0 & 0 & 0 & e^{j(9\pi/8)} & e^{j(3\pi/8)} & e^{-j(3\pi/8)} & e^{-j(9\pi/8)} \\ 0 & 0 & 0 & 0 & e^{j(3\pi/8)} & e^{j(\pi/8)} & e^{-j(\pi/8)} & e^{-j(3\pi/8)} \\ 0 & 0 & 0 & 0 & e^{-j(3\pi/8)} & e^{-j(\pi/8)} & e^{j(\pi/8)} & e^{j(3\pi/8)} \\ 0 & 0 & 0 & 0 & e^{-j(9\pi/8)} & e^{-j(3\pi/8)} & e^{j(3\pi/8)} & e^{j(9\pi/8)} \\ e^{j(9\pi/8)} & e^{j(3\pi/8)} & e^{-j(9\pi/8)} & e^{-j(9\pi/8)} & 0 & 0 & 0 & 0 \\ e^{j(3\pi/8)} & e^{j(\pi/8)} & e^{-j(\pi/8)} & e^{-j(3\pi/8)} & 0 & 0 & 0 & 0 \\ e^{-j(3\pi/8)} & e^{-j(\pi/8)} & e^{j(\pi/8)} & e^{j(3\pi/8)} & 0 & 0 & 0 & 0 \\ e^{-j(9\pi/8)} & e^{-j(3\pi/8)} & e^{j(3\pi/8)} & e^{j(9\pi/8)} & 0 & 0 & 0 & 0 \end{bmatrix}$$

The form of the scattering matrices suggests the use of parallel-coupled transmission lines.[3] If a set of parallel coupled transmission lines is used, with all inputs on one side and outputs on the other, the requirements for match and isolation are automatically met. The simplest procedure is to find configurations that divide the input energy equally among all outputs, and then to try to arrive at proper phase outputs through trial and error.

Before the possible configurations are analyzed, it is worthwhile to consider the various types of coupling mechanisms. Shown in Fig. 7 are branch coupling, waveguide narrow-wall and broad-wall coupling. The normal modes are the same for all cases, even and odd, but the coupling characteristics yield different propagation constants for the modes. The following coupling relationships are deduced:

$\beta E_1 = \beta_0 E_1 + cE_2$ for branch coupling

$\beta E_1 = \beta_0 E_1 + c(E_2 + E_1)$ for side-wall coupling

$\beta E_1 = \beta_0 E_1 + c(E_2 - E_1)$ for broad-wall coupling,

where

β is the phase constant, $2\pi/\lambda$, in the coupled region
β_0 is the phase constant in uncoupled transmission line
c is the coupling coefficient
E_1 and E_2 are the voltages on the two lines.

In conventional transmission-line analysis, the wave equation is

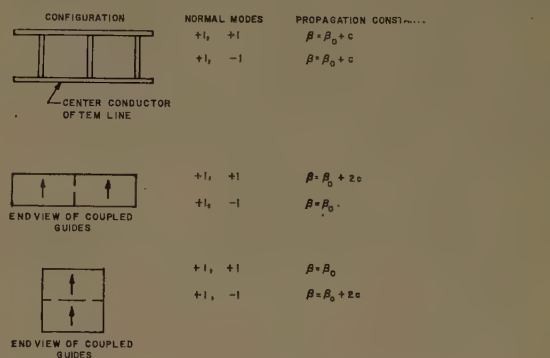

Fig. 7—Various types of coupling mechanisms.

$$c^2 \frac{\partial^2 E}{\partial x^2} = \frac{\partial^2 E}{\partial t^2}.$$

Assuming a time dependence, $e^{j\omega t}$, the equation simplifies to

$$\frac{\partial^2 E}{\partial x^2} = -\beta^2 E.$$

If the propagation is limited to one direction, further simplification to

$$\frac{\partial E}{\partial x} = j\beta E$$

is achieved, and the following analysis is based upon this relationship.

If the network of Fig. 8 is assumed, in which the input line is coupled to $N-1$ other lines, it is of interest to determine the limitation on N for equal energy division among all outputs. The propagation constant matrix is

[3] J. P. Shelton, Jr., "Multiple-line directional couplers," 1957 IRE National Convention Record, pt. 1, pp. 254–262.

found to be, for broad-wall coupling,[3]

$$\begin{pmatrix} \beta_0-\beta+(N-1)c & -c & -c & -c\cdots \\ -c & \beta_0-\beta+c & 0 & 0 \\ -c & 0 & \beta_0-\beta+c & 0 \\ -c & 0 & 0 & \beta_0-\beta+c \\ \cdots & & & \end{pmatrix}.$$

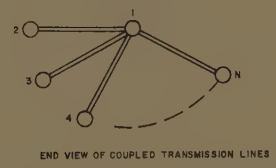

Fig. 8—Case for $N-1$ lines coupled to input line.

Since, for input at E_1, all other outputs are identical in amplitude and phase, it is possible to reduce the matrix to

$$\begin{pmatrix} \beta_0-\beta+(N-1)c & -(N-1)c \\ -c & \beta_0-\beta+c \end{pmatrix}.$$

Solution of the equation formed by setting the determinant of the propagation matrix equal to zero,

$$(\beta_0-\beta)^2+(\beta_0-\beta)Nc=0,$$

yields the two normal mode constants for the simplified system,

$$\beta_0-\beta=0$$

$$\beta_0-\beta+Nc=0.$$

The normal modes are found to be

$$E_1=E_2 \quad \text{for} \quad \beta=\beta_0$$

$$E_1=-(N-1)E_2 \quad \text{for} \quad \beta=\beta_0-Nc.$$

For an initial input amplitude $E_1=N$, E_2 through $E_N=0$, it is found that the outputs are

$$E_1=(N-1)+e^{-iNcx}$$

$$E_2\cdots E_N=e^{-iNcx}-1$$

where x is the length of the coupling region. Since the total input power is N^2, the output power in each arm must be N, and the output amplitudes are $\sqrt{N}$.

It is seen that the output amplitude for the coupled lines is, with the exception of phase, $2\sin Ncx/2$. Thus, the condition for achieving equal power division is

$$2\sin\frac{Ncx}{2}\leqq\sqrt{N}.$$

For

$$N=2, \quad cx=\pi/4$$
$$N=3, \quad cx=2\pi/9$$
$$N=4, \quad cx=\pi/4.$$

For $N\leq 4$, the condition cannot be satisfied since the sine function is limited to unity and $\sqrt{N}$ becomes greater than two; it is, therefore, seen that the arrangement of Fig. 8 is limited to four lines.

If three lines are all coupled by an amount $cx=2\pi/9$, as shown in Fig. 9, the relative phases of the outputs are

	1	2	3
Input at 1	0°	+120°	+120°
Input at 2	+120°	0°	+120°
Input at 3	+120°	+120°	0°

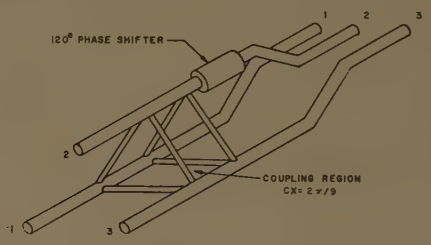

Fig. 9—Three-line junction for multiple-feed arrays.

If a phase shift of +120° is introduced into the output of line 2, the relative phases become

	1	2	3
Input at 1	0°	−120°	−240°
Input at 2	0°	0°	0°
Input at 3	−240°	−120°	0°

and this is desired phase relationship.

It can be shown that the other two types of coupling mechanisms can be used to realize the same type of network, except that the required added phase shift may be positive or negative, depending on the type of coupling.

Appendix II

Four-Input Four-Output Junction For Multiple-Feed Arrays

The two coupling configurations shown in Fig. 10 can be shown to give equal output amplitudes for coupling regions having $cx=\pi/4$. The phase relationship of the outputs for input at line 1 is

	1	2	3	4
Case A	0°	− 90°	− 90°	−180°
Case B	0°	−180°	−180°	−180°

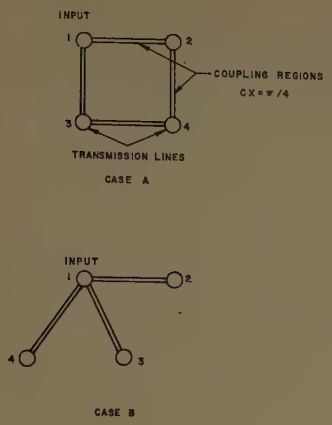

Fig. 10—Coupling configurations for equal power division with four lines.

It is impossible to achieve the required phase characteristics using only one coupling configuration. The network of Fig. 11 combines both types and gives the following phases:

	1	2	3	4
Input at 1	0°	− 90°	− 90°	−180°
Input at 2	−180°	0°	−180°	−180°
Input at 3	−180°	−180°	0°	−180°
Input at 4	−180°	− 90°	− 90°	0°

If the outputs are rearranged as shown and the indicated phase shifts are added, the resultant behavior provides multiple-feed capability.

	1	2	4	3
Added phase shift	0°	− 45°	− 90°	+ 45°
Input at 1	0°	−135°	−270°	−405°
Input at 2	0°	+135°	+270°	+405°
Input at 3	0°	− 45°	− 90°	−135°
Input at 4	0°	+ 45°	+ 90°	+135°

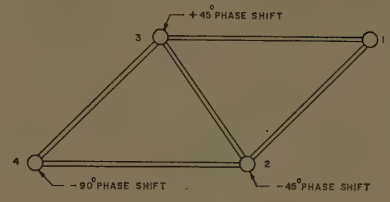

Fig. 11—Four-line network with multiple-feed capability.

It will be noted that a lagging phase shift has been assumed in this case. The reason is that the two coupling arrangements of Fig. 10 may be combined so that they operate essentially independently. That is, for an input to line 1, lines 2 and 3 are uncoupled, and for an input to line 2, lines 1, 3 and 4 are uncoupled. This is achieved only for difference coupling, for which the coupling term is of the form $c(E_2-E_1)$, so that when the amplitudes are the same, the coupling is zero.

Difference coupling is characteristic of broad-wall connection between waveguides. It can be obtained with branch networks only at the expense of an awkward increase in complexity. Some of the possible waveguide cross sections for the three-line junction and the two cross sections for a four-line junction are shown in Fig. 12.

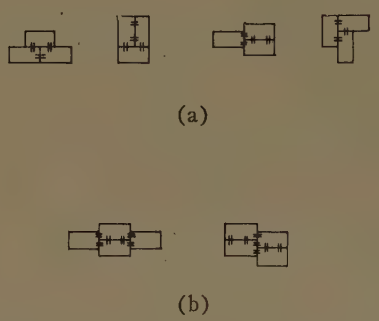

Fig. 12—Allowable waveguide arrangements for couplers of three and four lines. (a) Waveguide orientations for three-line couplers. (b) Orientations for four-line coupler.

A New Technique for Electronic Scanning*

H. E. SHANKS†

Summary—**The concept of time-modulated antennas has recently been demonstrated as a means of overcoming many of the limitations currently restricting advances in the antenna art. Of special importance is the mathematical possibility of generating a pattern complex capable of providing simultaneous scan operation. This characteristic is realized by periodic time modulation of the aperture distribution. This paper discusses the theory of simultaneous "scanning" using time modulation techniques and shows that the required pattern complex is generated by a progressive-pulse aperture excitation. The fundamental equations and relationships concerning the form of pulse excitation and "scanning" coverage are derived. In addition, practical methods of physically generating the proper pulse-excited aperture are described, and the necessary detection requirements are delineated.**

Introduction

ONE of the most desirable features of modern radar systems is the capability of performing beam scanning by electronic methods. As a result, a considerable amount of effort has been expended in the investigation of methods for electronic scanning of antenna systems. Techniques which have been studied in this connection include frequency variation, phase shift scan (ferrites, TWT's, delay lines, etc.), and in a minor way, the ideas of space time equivalence. In spite of these investigations, a system which realizes the optimum objectives in terms of simplicity, reliability and versatility has yet to be devised. In a recent paper,[1] the application of time domain techniques to antenna systems was described, and in a preliminary way shown to provide a means for quasi-electronic scanning. It is the purpose of this paper to elaborate on this application and to demonstrate the practical nature of this method of electronic "scanning."

The basic philosophy of time domain antennas is centered around the recognition that if some parameter of an antenna (length, shape, aperture excitation, etc.) is modulated in a periodic manner, the time varying radiation pattern can be written in one form as

$$g(\theta, t) = A\{b_0(\theta) + b_1(\theta)\cos\omega_0 t + b_2(\theta)\cos 2\omega_0 t + \cdots\}e^{j\omega t}; \quad (1)$$

where the $b_n(\theta)$ are in general different spatial dependent patterns, ω_0 is the modulation frequency and it is assumed that $\omega_0 \ll \omega$. Because of the independent nature of the ω_0 harmonics, each term in the series can be independently detected to provide a series of signals, each having different spatial pattern characteristics. For the special case in which the spatial patterns are pencil beams pointing in different directions, the strength of a given harmonic $n\omega_0$ will give a direct indication of the presence and strength of a target in the corresponding direction. It is this particular characteristic which is of importance for electronic "scanning."

Theory of Time Domain "Scanning"

The basic features of utilizing the time domain philosophy to achieve electronic scanning can be seen by consideration of a continuously excited linear array. Suppose that $2N+1$ pencil beams are desired from an array of length $2l_0$, with the spacing between beams of the order of θ_0. In addition, each of these patterns is associated (*i.e.*, "tagged") with a different frequency component. In mathematical language, these conditions are expressed by

$$g(\theta, t) = \sum_{n=-N}^{N} \frac{\sin[kl_0(\nu - n\nu_0)]}{\nu - n\nu_0} e^{j(\omega + n\omega_0)t}, \quad (2)$$

where $g(\theta, t)$ is the desired time varying pattern complex, ω_0 is the fundamental modulation frequency and ν and ν_0 are, respectively, $\sin\theta$ and $\sin\theta_0$. In a practical system, the value of ν_0 and the number of beams, $2N+1$, would be chosen to give the desired angular coverage and detection accuracy. Examination of (2) gives an excellent picture of the scanning mechanism; a target in the vicinity of the angular direction $n\nu_0$ will be directly associated with the frequency $n\omega_0$. From another viewpoint, (2) represents a frequency spectrum in which the upper and lower sideband magnitudes indicate the strength of targets in the associated directions. This viewpoint, as well as the problem of detecting the individual frequency components, will be discussed more fully later. The above pattern characteristics are indicated in symbolic fashion in Fig. 1.

The aperture distribution to give the pattern characteristics of (2) may be found by the application of Fourier integral theory. This distribution is

$$f(x, t) = \sum_{n=-N}^{N} e^{-j(k\nu_0 nx - n\omega_0 t)}, \quad (3)$$

which may be rewritten as

$$f(x, t) = 1 + 2\sum_{n=1}^{N} \cos n[k\nu_0 x - \omega_0 t]. \quad (4)$$

This expression can be considered as a series of traveling amplitude waves moving from left to right along the array. Because of the equality of these wave amplitudes, the complete sum will resemble an exciting pulse travel-

* Received by the PGAP, May 16, 1960; revised manuscript received, July 22, 1960. This work was performed while the author was with the Hughes Aircraft Co.

† American Systems, Inc., Hawthorne, Calif.

[1] H. E. Shanks and R. W. Bickmore, "Four-dimensional electromagnetic radiators," *Canad. J. Phys.*, vol. 37, pp. 263–275; March, 1959.

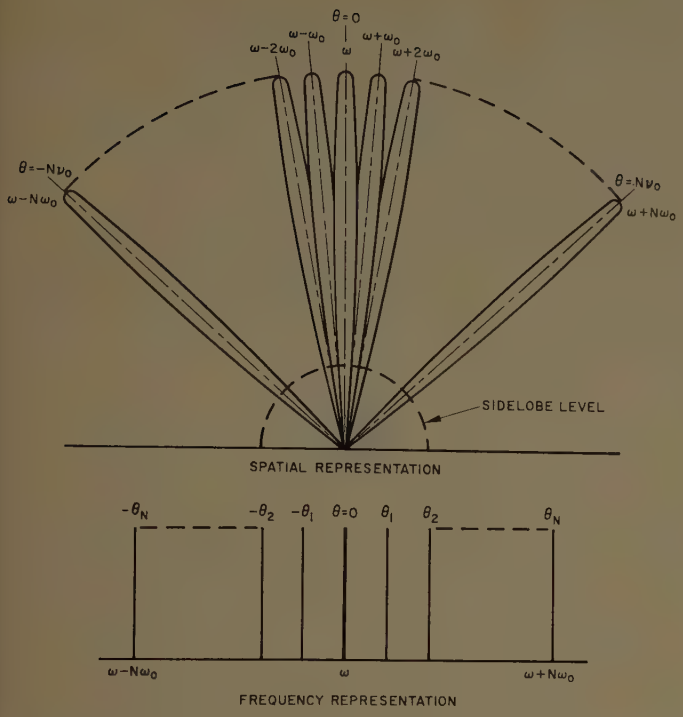

Fig. 1—Graphical illustration of time domain electronic scanning.

ing across the array. As a matter of fact, (4) becomes a traveling Dirac delta function in the limit as $N \to \infty$.

Thus it is seen that in order to realize the pattern complex of (2), the linear array must be excited progressively, a small portion at a time. Because of the choice of a finite number of terms in (2), the pulse shape as determined by (4) is not of simple form. The problem of synthesizing a reasonably simple pulse shape which achieves a practical distribution will not be discussed at the present time. Instead, a rectangular pulse excitation will be analyzed and shown to represent the opposite extreme in which an infinite number of beams exist.

Rectangular Pulse Excitation

As mentioned above, here we disregard the synthesis problem and assume a pulse shape which is consistent with state-of-the-art capabilities. The resulting radiation complex is then determined to see whether it demonstrates scanning capability. For this purpose, a discrete array of N elements will be considered. The assumed aperture excitation is such that each element is progressively turned on for a time T/N and then switched off. This excitation cycle is repeated periodically with period T. These conditions are equivalent to a coherent rectangular pulse, of width T/N, traveling down the array in a time T.

If the elements are numbered by the symbol m with $m = 0, 1, 2, \cdots, N-1$, the mth element will be assumed to be turned on with an amplitude A_m during the time defined by

$$\frac{mT}{N} \leq t \leq (m+1)\frac{T}{N}.$$

This excitation will give rise to a pattern

$$g(\theta, t) = h_m(\theta)e^{j\omega t};$$

$$\frac{mT}{N} - \frac{md}{c}\sin\theta \leq t \leq \frac{(m+1)T}{N} - \frac{md}{c}\sin\theta, \quad (5)$$

where the $m(d/c)\sin\theta$ term arises because of the differential in time required for the pulse to travel to the observation point from a given element. For the array under consideration,

$$h_m(\theta) = A_m e^{jkmd\sin\theta}, \quad (6)$$

where d is the interelement spacing along the array.

Because of the periodic nature of the resulting pattern, it may be expanded in a Fourier series of the form

$$g(\theta, t) = \sum_{n=-\infty}^{\infty} f_n(\theta)e^{j2\pi nt/T}e^{j\omega t}, \quad (7)$$

where the coefficients are readily found from

$$f_n(\theta) = \frac{1}{T}\int_0^T g(\theta, t)e^{-j\omega t}e^{-j2\pi nt/T}dt. \quad (8)$$

Substituting (5) and (6) into (8) results in

$$f_n(\theta) = \frac{1}{T}\sum_{m=0}^{N-1} A_m e^{jkmd\sin\theta} \cdot \int_{(mT/N)-(md/c)\sin\theta}^{(m+1)(T/N)-(md/c)\sin\theta} e^{-j(2\pi nt/T)}dt. \quad (9)$$

This expression is readily integrated, term by term, to give,

$$f_n(\theta) = (-1)^n \frac{\sin\left(\frac{n\pi}{N}\right)}{n\pi}\sum_{m=0}^{N-1} A_m \cdot \exp\left\{jm\left[\frac{(\omega + n\omega_0)}{c}d\sin\theta - \frac{2n\pi}{N}\right]\right\}. \quad (10)$$

The sum

$$\sum_{m=0}^{N-1}$$

in (10) is just the conventional radiation pattern of an array, of N elements, which has a maximum in the direction

$$\sin\theta = \frac{2n\pi}{N(k + nk_0)d},$$

or if $nk_0 \ll k$, which is true for practical cases of interest,

$$\sin\theta = \frac{2n\pi}{Nkd}. \quad (11)$$

It should be noted that the beam pointing direction is controlled by the frequency mode number n. This characteristic is just what is desired to realize simultaneous scanning.

By properly choosing the A_m coefficients, the individual pattern characteristics can be controlled as desired. For definiteness, it will be assumed here that the array is uniformly excited ($A_m=1$) and that the inter-element spacing $d=\lambda/2$. Under this condition, (10) can be expressed in closed form as

$$f_n(\theta) = (-1)^n \frac{\sin\left(\frac{n\pi}{N}\right)}{\left(\frac{n\pi}{N}\right)} \cdot e^{j(N-1/2)\pi \sin\theta} \frac{\sin\frac{N\pi}{2}\left[\sin\theta - \frac{2n}{N}\right]}{\sin\frac{\pi}{2}\left[\sin\theta - \frac{2n}{N}\right]}, \quad (12)$$

where the beam pointing direction is now given by $\sin\theta=2n/N$. Substituting this result in (7) gives the complete pattern complex

$$g(\theta,t) = \sum_{n=-\infty}^{\infty} (-1)^n \frac{\sin\left(\frac{n\pi}{N}\right)}{\left(\frac{n\pi}{N}\right)} \cdot e^{j(N-1/2)\pi \sin\theta} \frac{\sin\frac{N\pi}{2}\left\{\sin\theta - \frac{2n}{N}\right\}}{\sin\frac{\pi}{2}\left\{\sin\theta - \frac{2n}{N}\right\}} e^{j(\omega+n\omega_0)t}. \quad (13)$$

This expression demonstrates the desired characteristics; namely, an infinite number of beams pointed in various directions, each associated with a different frequency component $n\omega_0$. It should be noted that as n gets very large, the associated beams will be directed into imaginary space, causing accompanying reactive fields. Although in practice only a finite number of terms will be used, it is inefficient to permit a significant portion of the total power to remain in the unused region of space (either real or imaginary). This difficulty can be partially corrected by controlling the modulation parameters (pulse shape, pulse period and number of elements). An ideal example of this was given earlier in this paper. In that situation, it was specified that a prescribed number of beams exist only in a certain angular region. This procedure, it will be recalled, gave rise to a complicated form of pulse excitation. These two extremes indicate the possible trade-offs between simplicity of construction and efficiency which are available.

In the above analysis, only the one way pattern has been considered. An extension of this analysis, to the two way problem, is readily carried out and results in similar characteristics. In this case, a time separation is used between the switching off of one element and the turning on of the next element. During this period the returning pulse is received by the appropriate element. By this procedure the analysis of two way transmission is identical to one way transmission except for a factor of two which occurs in the phase and time delay associated with the observation range.

It is important to consider how some of the antenna parameters affect the over-all system capabilities. Therefore, suppose that 100 beams are desired distributed from $-50°$ to $50°$, approximately one degree apart. In this case n ranges from -50 to 50 and for $|n|=50$ it is necessary that

$$\frac{2n}{N} = \sin\theta,$$

where $\theta=50°$. Solving for the number of elements gives $N=130$. In other words, an array containing 130 elements is required to meet the above specifications. Under this condition, the nominal beamwidth of all patterns will be approximately one degree. It should be mentioned that as in other electronic scanning methods, the beamwidth of the pattern away from broadside will be degraded because of the projected aperture effect. For example, if the beamwidth at broadside is one degree, at 50° the beamwidth will be 1.5°. When operating in a two way fashion, the required number of elements is reduced by a factor of two.

In terms of practical antennas, another characteristic of this technique is of importance. This feature concerns the variation in amplitude of the various frequency components. In order to achieve equal detection probabilities from all beams, each of the frequency components should appear with approximately the same amplitude. The controlling amplitude factor in (13) is

$$\frac{\sin\left(\frac{n\pi}{N}\right)}{\left(\frac{n\pi}{N}\right)}.$$

For the above design example, $n\pi/N$ ranges from zero to 1.2 and $\sin x/x$ ranges between one and 0.78. Thus the decrease in amplitude over all used frequencies is not a significant factor. Because of the slow rate of decrease of beam amplitudes, however, a considerable amount of the total energy will be radiated in regions which are not used. This, of course, is inefficient, and must be remedied in a practical design. What is desired is a uniform distribution of beams in the region of interest and a rapid fall-off in beam amplitudes outside of this region. This characteristic can be achieved by careful control of the pulse shape, pulse separation and other modulation parameters. The problem is similar to the synthesis problem met in conventional array studies.

The preceding discussion demonstrates that from an antenna viewpoint, a time varying radiation pattern can be readily achieved which has the inherent capabil-

ity of providing angular detection information similar to that received from a sequentially scanned antenna. However, in order to make use of this capability, a system must be devised to process the data properly.

Detection System Analysis

It will be assumed that a normal superheterodyne receiver is an integral part of the system. The complete signal incident on the receiver from the antenna will be of the following form:

$$E(\theta, t) = \sum_{n=-\infty}^{\infty} f_n(\theta) e^{j\Phi(\theta)} e^{j(\omega+n\omega_0)t}, \qquad (14)$$

where $f_n(\theta)e^{j\Phi(\theta)}$ is a symbolic notation for the pattern information contained in (13). This signal is processed by the receiver and the IF output is

$$E(\theta, t) = \sum_{n=-\infty}^{\infty} f_n(\theta) \cos\left[(\omega_{IF} + n\omega_0)t + \Phi(\theta)\right]. \qquad (15)$$

As mentioned earlier, this expression represents a frequency spectrum centered about the carrier ω_{IF} in which the sideband amplitudes are proportional to the pattern return in the associated directions.

A method for selecting a particular sideband from this spectrum is desired. The straightforward technique for accomplishing this is to utilize a single tunable filter or a bank of filters to select the frequencies $(\omega_{IF}+n\omega_0)$. Although this can probably be done, a more elegant method is available. This method consists of mixing the signal of (15) with a local oscillator of about the IF frequency. Such a system is depicted in Fig. 2. It is assumed that the local oscillator is swept over a band of frequencies $(\omega_{IF}+\omega_A)-N\omega_0 \leq \omega_{LO} \leq (\omega_{IF}+\omega_A)+N\omega_0$, and the output of the mixer fed to a narrow band filter tuned to ω_A. The frequency ω_A is inserted into the system to eliminate the need for operation with dc signals. Without this frequency the system operates as a phase detector. Under this condition an output pulse will be produced by the filter whenever the swept frequency differs from $(\omega_{IF}+n\omega_0)$ by ω_A. Moreover, the magnitude of this pulse will be proportional to the signal return from the direction associated with the sideband frequency $n\omega_0$.

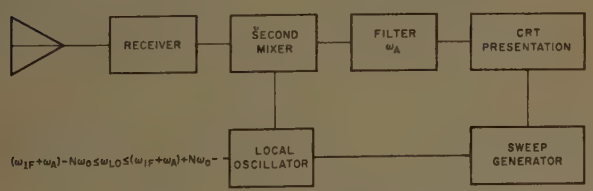

Fig. 2—Detection system for electronic scanning.

Thus, the above method provides a series of sequentially related pulses whose magnitude is directly related to the target return in a progressive set of directions. By feeding these pulses to a display device, such as a CRT whose sweep rate is synchronized with the swept oscillator, a conventional presentation is achieved. It is interesting to consider some practical values of the various frequencies used in the analysis. Assume an X-band radar with an array modulation frequency of $\omega_0=100$ cps. With a conventional IF of 30 Mc, and assuming 100 beams, as in the example above, the sweep bandwidth will be 10 kc centered at 30 Mc. The output filter might reasonably be tuned to 1000 cps with a bandwidth sufficient to reject 900 and 1100 cps by 20–30 db. It should be pointed out that these specifications are consistent with the current state-of-the-art in filter techniques.

As in all types of simultaneous scan systems, the question naturally arises as to how the power in a given direction compares with other scanning systems. This question has been studied from the standpoint of signal-to-noise ratios as determined at the receiver in two-way operation. It can thus be stated that the signal-to-noise ratio for the present scanning scheme is equivalent to that in a conventional scanning system. Hence, the detection range is also equivalent.

Possible Array Configuration

A number of methods can be visualized for realizing the proper pulse-excited linear array. One scheme might make use of a dispersive structure of sufficient length so that a pulsed carrier would illuminate one element at a time. This method is not particularly attractive because of the accurate tolerances required in construction. The most attractive method comprises an array in which each element is fed through a simple on-off switch, perhaps a ferrite rotation device. Such a system is illustrated in Fig. 3. Since the over-all system is a phase coherent device, the transmitter is of a phase coherent type. The transmitter can either be a CW type or a pulsed system. In the first case, the ferrite programming is free running, while in the second case it is synchronized with the modulation character of the pulsed carrier.

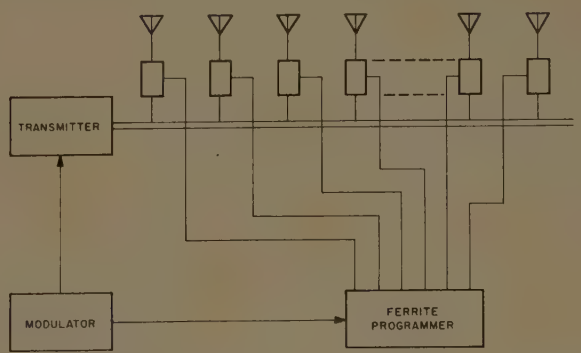

Fig. 3—Possible linear array for time domain electronic scanning.

Conclusion

The "scanning" system described in this paper has been shown to be a practical scheme which may overcome many limitations in present techniques. In particular, it is no longer necessary to control the phase between elements to "scan"; instead simple on-off switching in a progressive fashion is utilized. This characteristic will greatly relax the component problem, as well as simplify the programming network. In addition to simplifying the antenna system, no major increase in complexity is necessary for detection and display. Also, no sacrifice in detection range is produced by this method of operation.

Although the examples used in this work are based on a discussion of the linear array, this is by no means a restriction. In fact, a straightforward extension is seen for 2-dimensional arrays. In this case, the 2-dimensional element lattice would be pulse excited in a raster fashion much like the scanning of a television tube. The result would be a volumetric distribution of directive beams with the beam positions controlled in one principal plane by the Fourier Harmonics with one period, and the beam position in the other principal plane controlled by a second series of harmonics with differing period. Needless to say, the technique can be applied in all frequency bands where switching components are available.

Cylindrical Shields*

R. W. P. KING†, fellow, ire, and C. W. HARRISON, JR.‡, senior member, ire

Summary—**The effectiveness of an imperfectly-conducting cylindrical shield of small cross section depends on both the attenuation through the metal wall of the externally maintained field and the amplitude of the current that is induced in the cylinder. When the length of the cylinder, which behaves like a linear scattering antenna, approaches a resonant value, the currents induced in the walls and the field inside the tube are relatively large. Under these conditions, large currents may be induced in a thin dipole placed coaxially within the shield.**

Introduction

In a recent paper,[1] a general theory of shielding by imperfectly conducting walls enclosing a region of finite size was formulated and applied specifically to the response of a dipole probe in a metal cylinder that is electrically small, both in cross section and in length. It is the purpose of this investigation to consider shielding by cylinders that are electrically small in cross section but may be up to a wavelength long. Two problems are considered. First, the determination of the axial electric field in a metal cylinder of length $2l$, inner radius b and outer radius c, when immersed in an incident field E^i parallel to its axis, is outlined. Second, the response of a thin dipole antenna of length $2h$ and radius a, placed coaxially within the shield, is investigated.

In order to permit the application of the theory of cylindrical antennas, the following conditions are imposed:

$$c \ll l, \qquad \beta_0 c \ll 1, \tag{1}$$

$$a \ll h, \qquad \beta_0 a \ll 1, \tag{2}$$

where $\beta_0 = \omega\sqrt{\mu_0\epsilon_0} = 2\pi/\lambda_0$ is the free space wave number. The conductivity of the metal walls and of the dipole[2] is σ, the permeability $\mu = \mu_0\mu_r$. The complex propagation constant in the metal is

$$k = j^{-1/2}\beta, \qquad \beta = \sqrt{\omega\mu\sigma}. \tag{3}$$

In most cases it may be assumed that

$$\beta b \geqq 10, \tag{4}$$

so that the simpler asymptotic forms of the Bessel functions may be used. Formally, the general case may be carried through without difficulty. Note that the inequalities (1) and (4) are compatible since

$$(\beta/\beta_0) = \sqrt{\mu_r\sigma/\omega\epsilon_0} \gg 1, \tag{5}$$

by definition of a good conductor.

The coaxial cylinders to be analyzed are shown in Fig. 1. They are equivalent to a coaxial line with two electrically open ends but with a completely closed

* Received by the PGAP, May 23, 1960.

† Consultant to the Sandia Corp., Sandia Base, Albuquerque, N. M., and Gordon McKay Professor of Applied Physics, Harvard University, Cambridge, Mass.

‡ Sandia Corp., Sandia Base, Albuquerque, N. M.

[1] C. W. Harrison, Jr. and R. W. P. King, "Response of a loaded dipole in an imperfectly conducting cylinder of finite length," *J. Res. NBS*, sect. D, vol. 64D, pp. 289–293; May–June, 1960.

[2] For simplicity, the conductivities of the dipole and the shield are assumed to be the same, since the numerical value of the conductivity of the dipole is unimportant as long as it is in the range of metals used as electrical conductors. If desired, separate values may be used with no difficulty.

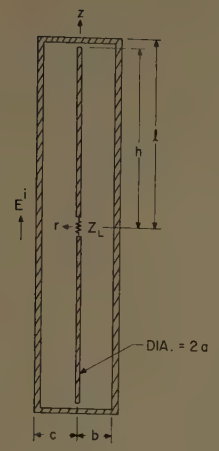

Fig. 1—Dipole in cylindrical shield.

shield. The electrically open ends are obtained by means of gaps between the ends of the inner conductor and the metal disks that close the ends of the shield. A lumped load Z_L is shown connected in series with the inner conductor at its center. The electric field E^i parallel to the axis of the cylinders is maintained by an external source.

For completeness, a brief summary of the relevant parts of the earlier work[1] is given together with the appropriately generalized formulas.

The Electric Field in a Closed Tubular Conductor

The first problem is to determine the ratio of the axial field inside the shield to the incident field when there is no inner conductor.

Since the tubular shield satisfies the conditions (1) of linear antenna theory, it may be treated as an unloaded receiving antenna in a uniform field. The total axial current $I_c(z)$ has the following leading term,[3]

$$I_c(z) = I_c(0)\left[\frac{\cos\beta_0 z - \cos\beta_0 l}{1 - \cos\beta_0 l}\right], \tag{6}$$

where

$$I_c(0) = 2l_e E^i/Z_{cin}. \tag{7}$$

In (7), $2l_e$ is the effective length of an antenna of actual length $2l$ and Z_{cin} is the input impedance of the antenna when cut in two at the center and driven by a delta-function generator. Curves of l_e/λ are in King;[3] an approximate formula when $\beta_0 l < \pi$ is

$$\beta_0 l_e = \tan(\beta_0 l/2). \tag{8}$$

The input impedance of an imperfectly conducting antenna is given by

$$Z_{cin} = Z_{c0} + Z_c^i, \tag{9}$$

where Z_{c0}, the impedance of a perfectly conducting antenna, is given in tabular and graphical form in King,[4] and

$$Z_c^i = (z_c^i/\beta_0)(\beta_0 l \csc^2\beta_0 l - \cot\beta_0 l) \tag{10}$$

is the contribution from ohmic resistance.[5] The internal impedance z_c^i per unit length of a tube of outer radius c is given below. In general, Z_c^i is negligible compared with Z_{c0}.

The general formula for the internal impedance per unit length of a tubular conductor of outer radius c and inner radius b is[6]

$$z_c^i = \frac{E(c,z)}{I_c(z)} = \frac{k}{2\pi c\sigma}\left[\frac{J_0(kc)N_1(kb) - N_0(kc)J_1(kb)}{J_1(kc)N_1(kb) - N_1(kc)J_1(kb)}\right]. \tag{11a}$$

When (4) is satisfied, (11a) reduces to

$$z_c^i = \frac{k}{2\pi c\sigma}\sqrt{\frac{\cosh 2A_c + \cos 2A_c}{\cosh 2A_c - \cos 2A_c}}\, e^{i(\Phi_c+\psi_c-\pi/4)}. \tag{11b}$$

If the additional condition, $A_c \geqq 4$, is imposed (which is equivalent to requiring the wall thickness to be at least four times the skin depth) the following simple formula is obtained:

$$z_c^i = \frac{\beta}{2\pi c\sigma}\, e^{i\pi/4}. \tag{11c}$$

In the above formulas:

$$\tan\Phi_c = \tanh A_c \tan A_c \tag{12a}$$

$$\tan\psi_c = \tanh A_c \cot A_c \tag{12b}$$

and

$$A_c = (c-b)/d_s \tag{13}$$

where

$$d_s = \sqrt{2/\omega\mu\sigma} \tag{14}$$

is the skin depth.

With (11) and (7), it follows that,

$$E(c,0)/E^i = 2l_e z_c^i/Z_{cin}. \tag{15}$$

This is the fundamental relation between the field at the outer surface of the tube and the incident field.

The relation between the tangential field at the inner surface ($r=b$) to that at the outer surface ($r=c$) has been given in the literature.[1,6] It is,

$$\frac{E(b,z)}{E(c,z)} = \frac{J_0(kb)N_1(kb) - N_0(kb)J_1(kb)}{J_0(kc)N_1(kb) - N_0(kc)J_1(kb)}. \tag{16a}$$

[3] R. W. P. King, "Theory of Linear Antennas," Harvard University Press, Cambridge Mass., ch. 4, p. 469, (18) and p. 492; 1956.

[4] *Ibid.*, pp. 154–179.

[5] *Ibid.*, p. 147, (11) and (12).

[6] R. W. P. King, "Electromagnetic Engineering," McGraw-Hill Book Co., Inc., New York, N. Y., p. 356; 1945.

Subject to (4) this becomes,

$$\frac{E(b,z)}{E(c,z)} = \sqrt{\frac{c}{b}}\left(\frac{e^{-j\Phi_c}}{\sqrt{\tfrac{1}{2}[\cosh 2A_c + \cos 2A_c]}}\right) \quad (16b)$$

with the additional restriction, $A_c \geqq 4$, the following simple result is obtained;

$$\frac{E(b,z)}{E(c,z)} = 2\sqrt{\frac{c}{b}}\, e^{-A_c(1+j)}. \quad (16c)$$

The condition $\beta_0 b \ll 1$, which is implied in (1), has as a consequence the relation

$$\frac{E(r,z)}{E(b,z)} = \frac{J_0(\beta_0 r)}{J_0(\beta_0 b)} \doteq 1 \quad \text{for} \quad r \leqq b. \quad (17)$$

The combination of (17) with (16) and (15) and the use of (11) leads to the following formulas for the ratio of the axial electric field in the air within the conducting tube to the incident field outside the tube: ($r \leqq b$)

$$\delta = \frac{E(r,0)}{E^i} = \frac{l_e k}{\pi c \sigma Z_{cin}}\left[\frac{J_0(kb)N_1(kb) - N_0(kb)J_1(kb)}{J_1(kc)N_1(kb) - N_1(kc)J_1(kb)}\right], \quad (18a)$$

when $\beta b \geqq 10$,

$$\delta = \frac{E(r,0)}{E^i} = \frac{l_e \beta}{\pi\sigma\sqrt{bc}\, Z_{cin}} \frac{e^{j(\Psi_c - \pi/4)}}{\sqrt{\tfrac{1}{2}[\cosh 2A_c - \cos 2A_c]}}. \quad (18b)$$

When, in addition, $A_c \geqq 4$,[7]

$$\delta = \frac{E(r,0)}{E^i} = \frac{2l_e\beta}{\pi\sigma\sqrt{bc}\, Z_{cin}} e^{-A_c(1+j)} e^{j\pi/4}; \quad (18c)$$

where $A_c = (c-b)/d_s$. Except near the ends at $z = \pm l$, the axial distribution of the electric field is obtained from the relation $E = z^i I$ with (6). It is approximately

$$E(r,z) = E(r,0)\left[\frac{\cos\beta_0 z - \cos\beta_0 l}{1 - \cos\beta_0 l}\right], \quad (19)$$

when $\beta_0 l < 2\pi$. This completes the determination of the axial electric field in the interior of the imperfectly conducting tube when it contains no inner conductor.

The Current in a Dipole within the Shield

When a conducting dipole is placed along the axis in the air within the shield, the axial field that exits there induces currents in the dipole. These currents in turn set up a field that induces additional currents in the shield and, since the shield is imperfectly conducting, a field is also maintained outside the shield. It will be assumed that this is much smaller than the incident field as, indeed, it will be if the ratio in (18) is small. Let the field maintained by the current in the dipole be denoted by $E'(r, z)$. At the outer surface of the shield it is $E'(c, z)$. It follows that the current that must be maintained on the shield in order to satisfy the boundary condition for the continuity of the tangential component of the electric field at $r = c$ is given by (6) and (7) with $E^i + E'(c, 0)$ substituted for E^i in (7). Since it is assumed that

$$\left|\frac{E'(c,0)}{E^i}\right| \ll 1, \quad (20)$$

no serious error is made by replacing $E'(c, z)$ by the constant value $E'(c, 0)$ at the center. However, if (20) is satisfied the resulting change in the small ratio δ is of higher order and may be neglected. In other words, it is assumed that the attenuation through the shield is sufficiently great so that what might be described as multiple reflections from the dipole back through the shield may be neglected.

Subject to (20), the field $E(a, z)$ given by (19) with (18) and $r = a$ at the surface of the dipole is independent of the current in the dipole. This latter is then given by

$$I_a(z) = I_a(0)\frac{\cos\beta_0 z - \cos\beta_0 h}{1 - \cos\beta_0 h} \quad (21)$$

with

$$I_a(0) = 2h_e E(a,0)/(Z_{ain} + Z_L), \quad (22)$$

if the approximation is made of replacing $E(a, z)$ by $E(a, 0)$. Since for dipoles of length $2h < \lambda$ the large currents are all induced near the center, no large error is involved in this simplification. In (22) $2h_e$ is the effective length of the dipole as if it were in free space, Z_{ain} is its input impedance, and Z_L is a load that may be connected in series at its center.

The input impedance of the dipole in the imperfectly conducting shield is not the same as it would be if it were either in a perfectly conducting shield or in free space. Its approximate value may be obtained as follows. Consider the dipole center driven by a delta-function voltage V that maintains a current $I(z)$. This current may be separated into two parts,

$$I(z) = I_A(z) + I_T(z), \quad (23)$$

where $I_T(z)$ is the part for which an equal and opposite current is induced in the shield, and $I_A(z)$ is the part for which no current is induced in the shield. If the shield were perfectly conducting, $I_A(z)$ would be zero. In other words, $I_A(z)$ is the algebraic sum of the currents in the dipole and the induced currents in the shield. Since the electromagnetic field outside the shield due to $I_T(z)$ and the current induced in the shield is zero, the entire field outside the shield is that maintained by $I_A(z)$, just as if there were no shield and $I_A(z)$ were the total current on the dipole. It follows that

$$V = I(0)Z_{ain} = I_A(0)Z_{a0} + I_T(0)Z_T, \quad (24)$$

where Z_{a0} is the input impedance of the dipole in free

[7] For example, with an aluminum shield ($\sigma = 3.54 \times 10^7$ 1/ohm-m) at a frequency of 10 kc, this condition leads to $c - b \geqq 4d_s = 4\sqrt{2/\omega\mu\sigma} = 0.338$ cm.

space and Z_T is the input impedance of two sections of transmission line in series. That is,

$$Z_T = 2R_c \coth [\alpha h + j(\beta_0 h + \Phi_h)], \tag{25}$$

where R_c is the characteristic impedance of the coaxial line, $\alpha = 2r_a{}^i/R_c$ is the attenuation constant, and $\Phi_h \doteq 0$ is the terminal phase function of the ends which are open-circuited. With (23), the input impedance of the dipole in the shield may be expressed in the form

$$Z_{a\text{in}} = Z_T + \frac{I_A(0)}{I(0)}(Z_{a0} - Z_T). \tag{26}$$

The ratio of currents in (26) may be replaced by a ratio of fields in the following manner. The field $E'(c, 0)$ maintained on the outer surface of the shield is due entirely to $I_A(z)$ and is, in fact, proportional to it. The field $E^i(b, 0)$ incident on the inner surface of the shield is proportional to the total current $I(z)$ in the dipole. Both fields are those that would be maintained in the absence of the shield. Since the wall thickness $(c-b)$ is a very small fraction of a free-space wavelength, it follows that

$$\frac{I_A(0)}{I(0)} = \frac{E'(c, 0)}{E^i(b, 0)} = \delta'. \tag{27}$$

It may now be argued that the attenuation through the shield of a field that is incident from the outside must be essentially the same as the attenuation through the same shield of a field incident from the inside, provided βb is sufficiently great to satisfy (4). That is,

$$\delta' = \delta. \tag{28}$$

With (27) and (28) it follows that

$$Z_{a\text{in}} = Z_T + \delta(Z_{a0} - Z_T), \tag{29}$$

where δ is given by (18b) or (18c). Note that if the walls of the shield are perfectly conducting $\delta = 0$ and $Z_{a\text{in}} = Z_T$; similarly, when the shield is absent, $\delta = 1$ and $Z_{a\text{in}} = Z_{a0}$.

The final expression for the current at the center of the dipole when enclosed by the imperfectly conducting cylindrical shield may now be expressed as follows,

$$\frac{I_a(0)}{E^i} = \frac{2h_e\delta}{Z_T + \delta(Z_{a0} - Z_T) + Z_L}, \tag{30}$$

where δ is given by (18b) or (18c) and it is assumed that (4) is satisfied together with (20).

Numerical Examples

In order to obtain a quantitative estimate of the magnitude of the ratio δ of the field in a cylindrical shield of finite length and of the current that may be induced in a conductor along the axis of such a shield, consider the following numerical examples. These involve an aluminum shield of given wall thickness and cross-sectional size but two different lengths, the one very short compared with the wavelength, the other a half wavelength long.

The subscripts 1 and 2 appearing on the various parameters entering the problem refer to the short and half-wavelength long shields, respectively. The cylinder and inner conductor are made of aluminum. $\sigma = 3.54 \times 10^7$ (ohm-meter)$^{-1}$. In both illustrations, $f = 10$ kc, $\omega = 2\pi f = 6.283 \times 10^4$, $\lambda_0 = 3 \times 10^4$ meter, $\beta_0 = 2\pi/\lambda_0 = 2.094 \times 10^{-4}$ meter^{-1}.

The Cylinder as an Antenna

$$c = 6.8 \text{ cm}, \; b = 6.7 \text{ cm}, \; (c - b) = 1 \text{ mm}$$

$$l_1 = 5m, \; \beta_0 l_1 = 1.047 \times 10^{-3}, \; \Omega_{1c} = 2 \ln \frac{2l_1}{c} = 9.98$$

$$l_2 = 7.5 \text{ km}, \; \beta_0 l_2 = 1.571, \; \Omega_{2c} = 2 \ln \frac{2l_2}{c} = 24.61$$

$$\beta = \sqrt{\omega\mu\sigma} = 1.672 \times 10^3 \text{m}^{-1}$$

$$\mu = 4\pi \times 10^{-7} \text{ henry} - \text{m}^{-1}$$

$$\beta b = 112.02, \; d_s = \sqrt{\frac{2}{\omega\mu\sigma}} = 0.846 \text{ mm}$$

$$A_c = \frac{(c - b)}{d_s} = 1.182$$

$$Z_{c\text{ in }1} = -j3.78 \times 10^5 \text{ ohms}^{8}$$

$$Z_{c\text{ in }2} \approx 77.3 + j43.6 = 88.75e^{j0.514} \text{ ohms}^{9}$$

$$l_{e1} \approx \tfrac{1}{2} l_1 = 2.5\text{m}^{10}$$

$$l_{e2} = 5.04 \times 10^3 \text{m}^{11}$$

Computed Field Ratio

$$\delta_1 = \frac{E(a, 0)}{E^i} = j0.845 \times 10^{-9} e^{-j0.458}$$

$$= (0.374 + j0.758)10^{-9} \qquad \text{[from (18b)]}$$

$$\delta_2 = \frac{E(a, 0)}{E^i} = 7.25 \times 10^{-3} e^{-j0.972}$$

$$= (4.08 - j5.98)10^{-3} \qquad \text{[from (18b)]}$$

Interior Data

Center Conductor:

$$a = 2 \times 10^{-3}\text{m}, \; h_1 = 5\text{m}, \beta_0 h_1 = 1.047 \times 10^{-3},$$

$$\Omega_1 = 2 \ln \frac{2h_1}{a} = 17.03,$$

$$h_2 = 7.5 \text{ km}, \; \beta_0 h_2 = 1.571, \; \Omega_2 = 2 \ln \frac{2h_2}{a} = 31.66$$

$$h_{e1} \approx \tfrac{1}{2} h_1 = 2.5\text{m}^{10}$$

$$h_{e2} \approx 4.77 \times 10^3 \text{m}^{12}$$

$$Z_{0a1} = -j7.817 \times 10^5 \text{ ohms}^{13}$$

[8] King, *op. cit.*, footnote 3, p. 192 (46b).
[9] *Ibid.*, by extrapolation of Table 30.1, p. 168.
[10] *Ibid.*, p. 496.
[11] *Ibid.*, p. 492, Fig. 9.6b; $h_e/\lambda_0 = 0.168$ for $\Omega_{2c} = 24.61$.
[12] *Ibid.*, p. 492, Fig. 9.6b; $h_e/\lambda \approx 0.159$ for $\Omega \approx \infty$.
[13] *Ibid.*, p. 184, (6c) with $\Omega = 17.03$.

$$Z_{0a2} \approx 74 + j42.5 = 85.3e^{j0.521\,14}$$

$$Z_{T1} = 2R_c \coth (\alpha + j\beta_0)h_1 \approx \frac{-j2R_c}{\beta_0 h_1}$$

$$R_c = 60 \ln \frac{b}{a} = 210.7 \text{ ohms. Hence}$$

$$Z_{T1} = -j4.03 \times 10^5 \text{ ohms.}$$

$$Z_{T2} = 2R_c \tanh \alpha h_2 = 2R_c \alpha h_2 \approx r^i h_2$$

$$= (r_a{}^i + r_c{}^i)h_2, \text{ since } \alpha = \frac{r^i}{2R_c}.$$

Also[15]

$$r^i = \frac{\beta a}{2\pi a^2 \sigma} \frac{M_0(\beta a)}{M_1(\beta a)} \cos \left[\frac{3\pi}{4} + \theta_0(\beta a) - \theta_1(\beta a) \right]$$

$$\beta a = 3.3$$

$$M_0(3.3) = 2.301, \theta_0(3.3) = 109°.25^{16}$$

$$M_1(3.3) = 2.124, \theta_1(3.3) = 206°.83^{17}$$

$$r_a{}^i = 3.23 \times 10^{-3\,18}$$

$$r_c{}^i = 9.59 \times 10^{-5} \text{ [(11b) with (12a) and (12b)]}$$

$$r^i = r_a{}^i + r_c{}^i = 3.33 \times 10^{-3}$$

$$Z_{T2} = r^i h_2 = 24.95 \text{ ohms.}$$

Ratio of the Current at the Middle of the Unloaded Center Conductor to the Incident Field

$$\frac{I_{a1}(0)}{E^i} = 1.05 \times 10^{-14} e^{j2.683} \text{ [(30) with } Z_L = 0]$$

$$\frac{I_{a2}(0)}{E^i} = 2.72e^{-j0.967} \text{ [(30) with } Z_L = 0]$$

Thus, for an incident field E^i of 10 volts/meter the magnitude of the current at the center of the inner conductor is only 1.05×10^{-13} amperes for the case of the short cylinder. However, for the half-wave cylinder the current is 27.2 amperes for the same incident field.

[14] *Ibid.*, p. 168, by extrapolation with Table 30.1, noting that for $\Omega \approx \infty$, $Z = 73.1 + j\,42.5$.
[15] King. *op, cit.*, footnote 6, p. 346, (2).
[16] *Ibid.*, p. 523.
[17] *Ibid.*, p. 524.
[18] *Ibid.*, p. 346, (2).

Conclusion

The field in the interior of a cylindrical shield depends on the attenuation through the shield and on the amplitude of the current that can be induced on it by the external field. When a closed cylindrical shield is very short compared with the wavelength, the effective length is small and the impedance is enormous. It follows that the induced current is very small, and with it the field in the interior of the shield. When the shield approaches a resonant length, the effective length is relatively large and the impedance quite small. It follows that a rather large current is induced in the cylinder and a correspondingly large field is maintained in the interior.

If a dipole is placed inside the shield with its ends not connected to the metal end surfaces of the shield, the current induced in it depends on its length and on the magnitude of the surrounding field. When the field in the shield is small and the length of the dipole is far from a resonant value, the current induced in the dipole is extremely small. On the other hand, when the field in the shield is more intense and the dipole has a resonant length, surprisingly large induced currents are possible.

Similar results may be expected if the dipole in a shield is replaced by a conventional coaxial line with a load at one end and a generator at the other. If the length of the line is resonant at the frequency of an external field and the wall thickness is not very great compared with the skin depth, significant fields may be maintained within the shield. These may induce relatively large currents in the coaxial line, particularly if a resonant condition obtains. Evidently, all of the conclusions reached for solid metal shields also apply to the practically important case of braided shields of comparable thickness.

Although somewhat idealized, the assumed numerical values are not physically unreasonable under special circumstances. The short cylinder in a uniform field is obviously realizable. A cable 15 km long in a uniform field is not easily realized. However, a long cable on dry sand near a high-powered VLF transmitter might not be very different in its response.

Folded Dipoles and Loops*

C. W. HARRISON, JR.†, SENIOR MEMBER, IRE, AND R. W. P. KING‡, FELLOW, IRE

Summary—**In Section I the theory of linear arrays consisting of two or more closely spaced elements that are interconnected by lumped reactances is reviewed. Specific application is made to two-element end-loaded folded dipoles and monopoles constructed of conductors with different diameters, to series tuned three-wire folded dipoles and monopoles, and to a three-wire-line reactor and impedance transformer. In Section II the circular folded dipole or Halo antenna is treated.**

I. Linear Elements

Introduction

A TWO-WIRE line driven and loaded in various ways is shown in Figs. 1(a)–1(d). Although constructed of the same pair of parallel, closely-spaced conductors, the four structures shown in Fig. 1 have quite different properties.

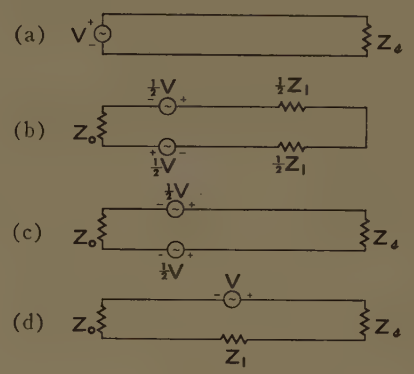

Fig. 1—Shunt- and series-loaded two-wire lines and folded-dipole antennas.

Fig. 1(a) is a schematic diagram of the conventional balanced two-wire transmission line. It is driven at one end, and loaded at the other. The currents in the two conductors of the line are equal in amplitude and opposite in phase, so that radiation is very small if the distance between the two conductors is a sufficiently small fraction of a wavelength.

The circuit in Fig. 1(b) is also that of a balanced two-wire line. In this case generators that maintain equal and opposite voltages are connected in series with the two conductors at an arbitrary point along their length. The line is loaded on the one hand by two identical impedances $\frac{1}{2}Z_1$ in series with the two conductors and, on the other hand, by an impedance Z_0 across the left end. Note that owing to the symmetry of the generators and the lumped impedance, the currents in the line are again equal and opposite.

The line in Fig. 1(b) is unbalanced if either of the generators or either of the impedances $\frac{1}{2}Z_1$ is replaced by a short circuit. Owing to the geometrical asymmetry, the currents in the two conductors of the line are not equal and opposite.

From the point of view of transmission line theory, the circuit of Fig. 1(c) is completely unbalanced. The two symmetrically placed generators maintain equal voltages in phase. Since the impedances are symmetrically arranged, the currents in the two conductors are equal and in the same direction. This structure is not a transmission line at all, but a two-element cage antenna that is driven off center. Note that the impedances Z_0 and Z_s are not of interest since no potential difference is maintained across them. They may be replaced by short circuits or removed and the ends left open with very little effect on the currents in the two long conductors. An analysis of the circuit in Fig. 1(c) has been made by King,[1] when the generators are located at the center and Z_0 and Z_s are replaced by straight conductors.

The circuit in Fig. 1(d) may be reduced to that of the conventional folded dipole[2–5] if the three impedances are replaced by straight conductors and the over-all length is a half-wavelength. The more general circuit given by Fig. 1(d) with Z_0 and Z_s replaced by short- or open-circuits and with Z_1 an arbitrary impedance has also been treated in detail.[5] By the theorem of images, these analyses include the corresponding folded monopoles[6] over a conducting ground plane. One purpose of this paper is to treat the general case illustrated in Fig. 1(d), the end-loaded series-tuned folded dipole and its image equivalent, the end-loaded folded monopole when the two conductors have different radii. Aspects of this general case have been treated by Harrison[7,8] and King,[5,9] but the methods and results have not been published in a tech-

* Received by the PGAP, May 25, 1960; revised manuscript received, July 5, 1960.

† Sandia Corp., Albuquerque, N. M.
‡ Consultant to Sandia Corp. and Gordon McKay Professor of Applied Physics, Harvard University, Cambridge, Mass.

[1] R. W. P. King, "The rectangular loop antenna as a dipole," IRE TRANS. ON ANTENNAS AND PROPAGATION, vol. AP-7, pp. 53–61; January, 1959.
[2] R. W. P. King, H. R. Mimno, and A. H. Wing, "Transmission Lines, Antennas and Wave Guides," McGraw-Hill Book Co., Inc., New York, N. Y., p. 224; 1945.
[3] W. V. B. Roberts, "Input impedance of folded dipoles," *RCA Rev.*, vol. 8, pp. 289–300; June, 1947.
[4] R. Guertler, "Impedance transformation in folded dipoles," PROC. IRE, vol. 38, pp. 1042–1047; September, 1950.
[5] R. W. P. King, "Theory of Linear Antennas," Harvard University Press, Cambridge, Mass.; pp. 334–343; 1956.
[6] J. Leonhardt, R. D. Mattuck, and A. J. Pote, "Folded unipole antennas," IRE TRANS. ON ANTENNAS AND PROPAGATION, vol. AP-3, pp. 111–117; July, 1955.
[7] C. W. Harrison, Jr., "Folded Antennas," Ph.D. dissertation, Harvard University, Cambridge, Mass., published as Cruft Lab. Tech. Rept. No. 193; 1954.
[8] C. W. Harrison, Jr., "Theory of End-Loaded Monopole," Sandia Corp., Albuquerque, N. M., Tech. Memorandum 275–57(14); October, 1957.
[9] R. W. P. King, *op. cit.*, footnote 5, pp. 358–361.

nical journal. The related problem represented by Fig. 1(d), when the generator is moved from the center of one of the long sides of the rectangle to the end of the line in series with Z_0—which is equivalent to Fig. 1(a) if an impedance Z_1 is connected in series at the center of one of the line wires[10]—is also considered. The closely related problem of the correspondingly unbalanced shielded-pair line has been analyzed.[11]

The loading and driving arrangements illustrated in the several parts of Fig. 1 may be extended in a generalized sense to any multiwire line. A number of different folded wire structures have been studied by Harrison;[7] a generalization of Harrison's theory to an N-element folded antenna has been given by King.[9] Owing to the great variety of possible locations of generators, series impedances, and reactive interconnections, a general formulation of the arbitrarily loaded and interconnected multiwire line or folded antenna structure is impractical. For this reason the analytical procedure is illustrated in several relatively simple structures with practical interest. These include the series-tuned three-wire folded dipole and monopole, and a three-element transmission-line reactor, in addition to the end-loaded two-wire folded dipole.

As a final related problem, a folded dipole that is bent into a circle to form a Halo antenna is analyzed in Section II.

General Principle of the Theory

The mathematical formulation of problems that involve unbalanced multiwire lines with series and interconnecting impedances is more easily followed if the underlying principle is first understood. This is simple. It consists of the separation of those currents that can be treated by conventional transmission-line theory from radiating currents that must be analyzed by antenna theory. Clearly, such a separation is meaningful only if there are indeed currents that do not contribute significantly to the far-zone field. In simple two-wire structures such as those shown in Fig. 1, the radiating currents are the equal and codirectional, or unbalanced, currents; the currents that contribute negligibly to radiation are the conventional equal and opposite, or balanced, line currents. (Note that these latter contribute negligibly to radiation only if the maximum distance between the several conductors of the multiwire configuration is a very small fraction of a wavelength.) In the more complicated folded and variously interconnected circuits, the separation of the currents into two groups that, respectively, do and do not contribute significantly to the far-zone field is not achieved as easily as for the relatively simple unbalanced two-wire line. However, the two groups are readily separated in principle by imagining all of the parallel conductors superimposed without altering the currents in them. The net current that remains uncancelled is the total radiating part, the currents that cancel are the nonradiating or transmission-line part. The analytical procedure for rearranging the N individual currents in the N conductors of a multiwire structure into one radiating component and $N-1$ transmission-line components is first to achieve a corresponding separation of the vector potentials due to the radiating and nonradiating currents. In this manner one integral equation is obtained for the radiating current in an equivalent dipole and $N-1$ equations for the transmission-line currents. Since the integral equation for the radiating current in the dipole is of familiar form with a known solution, and the $N-1$ integral equations for the nonradiating currents reduce to simple simultaneous algebraic equations that may be solved directly, it is possible to evaluate the individual currents by imposing conditions appropriate to the locations and properties of both generators and lumped series or interconnecting impedances. The details depend upon the characteristics of each individual configuration of conductors.

The following general conditions and principles apply.

1) If the over-all length of the structure is $2h$, the radius of conductor i is a_i and the distance between conductors i and k is b_{ik}, the following inequalities are assumed to be satisfied for all values of i and k:

$$a_i \ll h; \qquad a_i < b_{ik}; \qquad (\beta b_{ik})^2 \ll 1. \tag{1}$$

Note that $\beta = 2\pi/\lambda$ is the wave number.

2) All conductors are assumed to be perfect so that the tangential component of the electric field on the surface of each wire is zero.

3) The scalar potential is continuous except across the terminals of generators and lumped impedances. Generators are treated as discontinuities in scalar potential[12] (δ-function source) with driving voltage defined according to the pattern:

$$V = \lim_{z \to 0} \{\phi(z) - \phi(-z)\}. \tag{2}$$

The voltage drop across an impedance Z_L carrying a current I_L is given by $I_L Z_L$. An equivalent generator has the emf

$$V_L = -I_L Z_L. \tag{3}$$

4) The sum of the currents directed toward the junction of two or more wires is zero. The current is zero at the open end of any wire.

[10] C. W. Harrison, Jr., "Hybrid Transmission Lines," Sandia Corp., Albuquerque, N. M., Tech. Memorandum 157-58(14); May, 1958.

[11] R. W. P. King, "Transmission-Line Theory," McGraw-Hill Book Co., Inc., New York, N. Y.; pp. 203–224; 1955.

[12] The infinite current required to charge the knife-edge capacitance across the terminals of the δ-function generator (which do not exist in physically available methods of driving) is automatically subtracted out in iterated solutions of the type obtained in this paper. This has been shown by T. T. Wu and R. W. P. King, "Driving point and input admittance of linear antennas," *J. Appl. Phys.*, vol. 30, pp. 74–76; January, 1959.

5) Contributions to the far-zone fields by short connecting impedances with lengths b_{ik} and by equal and opposite currents in conductors separated by distances b_{ik} are neglected. The radiation resistance referred to maximum current due to these currents in a general two-wire-line circuit[13] has the order of magnitude $30\beta^2b^2$. It is assumed that βb is small enough to make this resistance negligible compared with the radiation resistance of the folded structure.

End-Loaded Folded Dipoles and Monopoles

The Vector Potential and the Integral Equations: The first structures to be analyzed are the closely related end-loaded folded dipole shown in Fig. 2 and the end-loaded folded monopole shown in Fig. 3.[8] The more general case with two conductors with different radii a_1 and a_2 is treated. Each conductor has the length $2h$; the distance between centers is b.

The boundary condition, $E_z=0$, on the conductors 1 and 2 is equivalent to the following equation[14] for the vector potential $\boldsymbol{A}=\hat{z}A$:

$$\frac{d^2A(z)}{dz^2}+\beta^2A(z)=0 \tag{4}$$

which has the solutions:

$$A_1(z)=\frac{-j}{v_0}\left\{C_1\cos\beta z+\frac{V_0}{2}\sin\beta|z|\right\} \tag{5a}$$

$$A_2(z)=\frac{-j}{v_0}C_2\cos\beta z, \tag{5b}$$

if the driving voltage V_0 is defined as in (2) and the symmetry condition, $A(z)=A(-z)$ is imposed; v_0 is the velocity of light; C_1 and C_2 are arbitrary constants. The vector potential on the surface of conductor 1 is[15,16]

$$A_1(z)=A_{11}(z)+A_{12}(z)=\frac{\mu_0}{4\pi}\int_{-h}^{h}I_1(z')K_{a_1}(z,z')dz'$$
$$+\frac{\mu_0}{4\pi}\int_{-h}^{h}I_2(z')K_b(z,z')dz', \tag{6}$$

where

$$K_c(z,z')=\frac{e^{-j\beta R_c}}{R_c},\qquad R_c=\sqrt{(z-z')^2+c^2} \tag{7}$$

and $\mu_0=4\pi\times10^{-7}$ henry/m. The vector potential $A_2(z)$ on conductor 2 is given by (6) with subscripts 1 and 2 interchanged. The substitution of the integrals for $A_1(z)$ and $A_2(z)$ in (5a) and (5b) yields two simultaneous

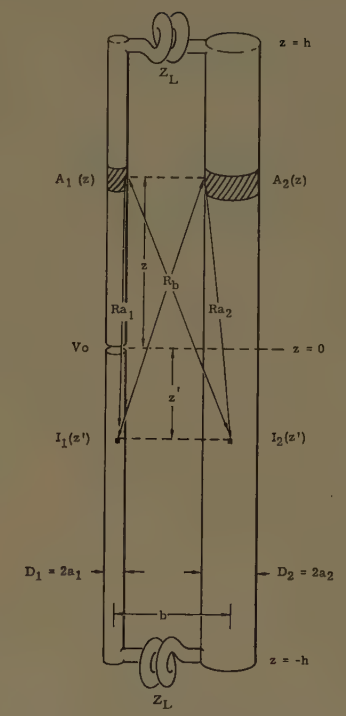

Fig. 2—End-loaded folded dipole.

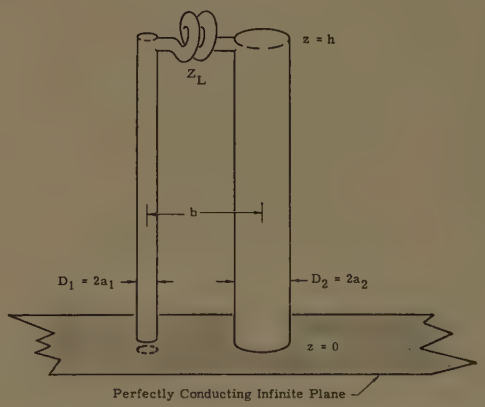

Fig. 3—End-loaded folded monopole.

integral equations for the two unknown currents, $I_1(z)$ and $I_2(z)$.

The first step in the solution of these equations is to rearrange them in such a manner that the radiating antenna currents are separated from the transmission-line currents. This is accomplished with

$$A_{1d}(z)=\frac{\mu_0}{4\pi}\int_{-h}^{h}I_1(z')K_d(z,z')dz' \tag{8a}$$

$$A_{2d}(z)=\frac{\mu_0}{4\pi}\int_{-h}^{h}I_2(z')K_b(z,z')dz' \tag{8b}$$

where $K_d(z,z')$ is defined by (7) with $c=d$ and d is the as yet undefined effective radius of the equivalent radiating dipole. However, it is anticipated that d must satisfy (1), in the same manner as a_i. The integrals (8a)

[13] R. W. P. King, C. W. Harrison, Jr., and D. H. Denton, Jr., "Transmission-line missile antennas," IRE Trans. on Antennas and Propagation, vol. AP-8, pp. 88–90; January, 1960. Also Sandia Corp., Albuquerque, N. M., Tech. Memorandum 436-58(14): November, 1958.
[14] R. W. P. King, *op. cit.*, footnote 5, p. 73.
[15] *Ibid.*, p. 264, 4.
[16] *Ibid.*, pp. 15–20.

and (8b) are added to and subtracted from (6). Thus,

$$A_{11}(z) = A_{1d}(z) + [A_{11}(z) - A_{1d}(z)]. \tag{9}$$

The difference term in (9) may be evaluated as follows:

$$A_{11}(z) - A_{1d}(z) = \frac{\mu_0}{4\pi}\int_{-h}^{h} I_1(z')[K_{a1}(z,z') - K_d(z,z')]dz'$$

$$\doteq \frac{\mu_0}{4\pi} I_1(z)\int_{-\infty}^{\infty}[K_{a_1}(z,z') - K_d(z,z')]dz'$$

$$\doteq \frac{\mu_0 I_1(z)}{4\pi} r_{a_1} \tag{10}$$

where

$$r_{a_1} = 2\ln\left(\frac{d}{a_1}\right). \tag{11}$$

The justification for the approximations involved in (10) depends on the fact that with βd and βa_1 both small, the integrand has a significant value only when z' has values near z. It follows that in a small range near $z'=z$, the current is sensibly constant at $I_1(z') \doteq I_1(z)$ and that with (1) the limits may be changed as shown.[17]

It follows that

$$A_{11}(z) = A_{1d}(z) + \frac{\mu_0}{4\pi} I_1(z) r_{a_1} \tag{12a}$$

$$A_{12}(z) = A_{2d}(z) + \frac{\mu_0}{4\pi} I_2(z) r_b \tag{12b}$$

where

$$r_b = 2\ln\frac{d}{b}. \tag{13}$$

Corresponding formulas for $A_{22}(z)$ and $A_{21}(z)$ are obtained from (12a) and (12b) by writing 2 for 1 and 1 for 2 in the subscripts. With (12a) and (12b) it follows that

$$A_1(z) = \frac{\mu_0}{4\pi}[J_d(z) + I_1(z)r_{a1} + I_2(z)r_b] \tag{14}$$

where

$$J_d(z) = \frac{4\pi}{\mu_0}[A_{1d}(z) + A_{2d}(z)]$$

$$= \int_{-h}^{h} I_T(z) K_d(z,z')dz'. \tag{15}$$

In (15) $I_T(z) = I_1(z) + I_2(z)$ is the total radiating current. In the same manner,

$$A_2(z) = \frac{\mu_0}{4\pi}[J_d(z) + I_1(z)r_b + I_2(z)r_{a_2}] \tag{16}$$

where

$$r_{a_2} = 2\ln\frac{d}{a_2}. \tag{17}$$

When (14) and (16) are substituted in (5a) and (5b), the following equations are obtained:

$$J_d(z) + I_1(z)r_{a_1} + I_2(z)r_b = \frac{-j4\pi}{\zeta_0}[C_1\cos\beta z + \tfrac{1}{2}V_0\sin\beta|z|] \tag{18a}$$

$$J_d(z) + I_1(z)r_b + I_2(z)r_{a_2} = \frac{-j4\pi}{\zeta_0} C_2\cos\beta z \tag{18b}$$

where

$$\zeta_0 = \left(\frac{\mu_0}{\epsilon_0}\right)^{1/2} \doteq 120\pi \text{ ohms}.$$

The Equivalent Dipole: The general form of the integral equation for the current in a dipole with an effective radius d is

$$J_d(z) = \frac{-j4\pi}{\zeta_0}[C_d\cos\beta z + \tfrac{1}{2}V_d\sin\beta|z|] \tag{19}$$

where $J_d(z)$ is defined in (15), V_d is the effective driving voltage at $z=0$ and C_d is an arbitrary constant that is ultimately evaluated from the condition $I_T(h)=0$. It is necessary to express d and V_d in terms of the constants occurring in (18a, b). This may be accomplished by multiplying (18b) by an arbitrary parameter m and adding it to (18a). The result is

$$(m+1)J_d(z) + I_T(z)[r_{a_1} + mr_b] + I_2(z)[r_b - r_{a_1} + m(r_{a_2} - r_b)]$$

$$= \frac{-j4\pi}{\zeta_0}[(C_1 + mC_2)\cos\beta z + \tfrac{1}{2}V_0\sin\beta|z|]. \tag{20}$$

Note that use has been made of the expression for the total radiating current, $I_T(z) = I_1(z) + I_2(z)$, in order to eliminate $I_1(z)$. The next step is to reduce (20) to the form (19) by assigning proper values to m and the effective radius d. This is accomplished by setting the coefficients of $I_T(z)$ and $I_2(z)$ in (20) equal to zero. Thus,

$$r_{a_1} + mr_b = 0 \tag{21a}$$

$$r_b - r_{a_1} + m(r_{a_2} - r_b) = 0. \tag{21b}$$

It follows that

$$r_b^2 = r_{a_1}r_{a_2} \tag{22}$$

$$m = -\frac{r_{a_1}}{r_b} = -\frac{r_b}{r_{a_2}}. \tag{23}$$

The substitution of (11), (13), and (17) in (22) gives

$$\ln d = \frac{(\ln b)^2 - \ln a_1 \ln a_2}{\ln\dfrac{b^2}{a_1 a_2}} \tag{24}$$

[17] A detailed discussion of this integral, which is precisely the one occurring in the derivation of the transmission-line equations from electromagnetic theory, is given in R. W. P. King, *op. cit.*, footnote 5, pp. 60–64.

or

$$d = \exp\left[\frac{(\ln b)^2 - \ln a_1 \ln a_2}{\ln \dfrac{b^2}{a_1 a_2}}\right]. \tag{25}$$

An alternative form is obtained by subtracting $\frac{1}{4}\ln b^2 a_1 a_2$ from both sides in (24). This gives

$$\ln d = \tfrac{1}{4}\ln(b^2 a_1 a_2) + \frac{\left(\ln \dfrac{a_1}{a_2}\right)^2}{4 \ln \dfrac{b^2}{a_1 a_2}}, \tag{26}$$

so that

$$d = b^{1/2}(a_1 a_2)^{1/4} e^{p} \tag{27a}$$

where

$$p = \frac{\left(\ln \dfrac{a_1}{a_2}\right)^2}{4 \ln \dfrac{b^2}{a_1 a_2}}. \tag{27b}$$

Note that when the two conductors have equal radii, $a_1 = a_2 = a$,

$$d = \sqrt{ab} \tag{28}$$

in agreement with earlier work[2,3] on the simple folded dipole.

A comparison of (19) and (20) shows that

$$V_d = \frac{V_0}{1+m} \tag{29a}$$

where

$$\frac{1}{1+m} = \frac{r_{a_2}}{r_{a_2} - r_b} = \frac{\ln \dfrac{b}{a_2}}{\ln \dfrac{b^2}{a_1 a_2}}. \tag{29b}$$

The solution of an equation like (19) has been discussed in detail for a dipole of radius a, length $2h$, and with a driving voltage V_0. Extensive theoretical and experimental data are available[18] for the distribution of current in the normalized form $I(z)/V_0$ and for the impedance defined by $Z_0 = V_0/I(0)$. Evidently $I_T(z)/V_d$ and

$$Z_d = \frac{V_d}{I_T(0)} \tag{30}$$

correspond exactly to these quantities if the effective radius d is used in place of a. The available data for currents and impedances are given, respectively, as functions of βz and βh with $\Omega = 2\ln 2h/a$ as parameter. All of these data, and in particular, the tables of impedances,[19] apply directly with $\Omega = 2\ln 2h/d$.

The Currents: With $I_T(z)$ and Z_d determined, it is a simple matter to obtain expressions for the individual currents $I_1(z)$ and $I_2(z)$. This is accomplished by subtracting (18b) from (18a) to obtain

$$I_1(z)\alpha_1 - I_2(z)\alpha_2 = \frac{-j4\pi}{\zeta_0}\left[D_1 \cos\beta z + \tfrac{1}{2}V_0 \sin\beta\,|\,z\,|\,\right] \tag{31}$$

where

$$\alpha_1 = r_{a_1} - r_b = 2\ln\frac{b}{a_1} \tag{32a}$$

$$\alpha_2 = r_{a_2} - r_b = 2\ln\frac{b}{a_2} \tag{32b}$$

$$D_1 = C_1 - C_2. \tag{32c}$$

If $I_2(z)\alpha_1$ is added and subtracted on the left in (31) and use is made of the total current $I_T(z) = I_1(z) + I_2(z)$, the following expression for $I_2(z)$ is obtained:

$$I_2(z) = I_T(z)\left(\frac{\alpha_1}{\alpha_1 + \alpha_2}\right) + \frac{j4\pi}{\zeta_0(\alpha_1 + \alpha_2)}\left(D_1 \cos\beta z + \tfrac{1}{2}V_0 \sin\beta\,|\,z\,|\,\right). \tag{33a}$$

It follows directly that

$$I_1(z) = I_T(z)\left(\frac{\alpha_2}{\alpha_1 + \alpha_2}\right) - \frac{j4\pi}{\zeta_0(\alpha_1 + \alpha_2)}\left(D_1 \cos\beta z + \tfrac{1}{2}V_0 \sin\beta\,|\,z\,|\,\right). \tag{33b}$$

The Scalar Potential and the Driving-Point Admittance: The scalar potential is related to the vector potential by the Lorentz condition which defines the divergence of the vector potential in the form

$$\operatorname{div} \boldsymbol{A} + j\frac{\beta^2}{\omega}\phi = 0. \tag{34}$$

Since significant contributions to ϕ near $z = \pm h$ are from charges associated with the radiating current $I_T(z)$ which maintains a maximum of charges at the ends of the structure, it is sufficient to set $\mathbf{A} \doteq A_z$. It follows with (5a, b) that

$$\phi_1(h) \doteq \frac{j\omega}{\beta^2}\left[\frac{\partial A_1(z)}{\partial z}\right]_{z=h} = -C_1 \sin\beta h + \frac{V_0}{2}\cos\beta h \tag{35a}$$

$$\phi_2(h) \doteq \frac{j\omega}{\beta^2}\left[\frac{\partial A_2(z)}{\partial z}\right]_{z=h} = -C_2 \sin\beta h. \tag{35b}$$

[18] R. W. P. King, *op. cit.*, footnote 5, Ch. II.

[19] R. W. P. King, *op. cit.*, footnote 5, pp. 168–182.

Hence, the voltage drop is

$$I_1(h)Z_L = \phi_1(h) - \phi_2(h) = -D_1 \sin \beta h + \frac{V_0}{2} \cos \beta h. \quad (36)$$

Since $I_2(h) = -I_1(h)$, (31) gives

$$I_1(h) = \frac{-j4\pi}{\zeta_0(\alpha_1 + \alpha_2)} \left[D_1 \cos \beta h + \frac{V_0}{2} \sin \beta h \right]. \quad (37)$$

By elimination from (36) and (37), and with

$$Z_c = \frac{\zeta_0(\alpha_1 + \alpha_2)}{4\pi} = \frac{\zeta_0}{2\pi} \ln \frac{b^2}{a_1 a_2}, \quad (38)$$

it follows that

$$D_1 = \frac{V_0}{2} \left[\frac{\cos \beta h + j\left(\frac{Z_L}{Z_c}\right) \sin \beta h}{\sin \beta h - j\left(\frac{Z_L}{Z_c}\right) \cos \beta h} \right]. \quad (39)$$

Since $I_T(z)$ is known from the solution of (30) and D_1 is given in (39), $I_1(z)$ and $I_2(z)$ as expressed in (33a) and (33b) are determined.

The current at the driving point is $I_1(0)$. It is obtained from (33b) as follows:

$$I_1(0) = I_T(0) \frac{\alpha_2}{\alpha_1 + \alpha_2} + \frac{V_0}{2Z_c} \left[\frac{Z_c + jZ_L \tan \beta h}{Z_L + jZ_c \tan \beta h} \right]. \quad (40)$$

The input admittance is

$$Y_{\text{in}} = \frac{I_1(0)}{V_0} = \frac{F}{Z_d} + \frac{1}{Z_t} \quad (41)$$

where

$$F = \frac{\alpha_2}{\alpha_1 + \alpha_2} = \left[\frac{\ln \frac{b}{a_2}}{\ln \frac{b^2}{a_1 a_2}} \right]^2 \quad (42)$$

$$Z_t = 2Z_c \left[\frac{Z_L + jZ_c \tan \beta h}{Z_c + jZ_L \tan \beta h} \right], \quad (43)$$

and Z_d is the input impedance of a center-driven isolated cylindrical antenna of radius d given by (27a), Z_c is given by (38). This completes the analysis of the end-loaded folded dipole shown in Fig. 2. The admittance of the end-loaded monopole shown in Fig. 3 is $2Y_{\text{in}}$ where Y_{in} is given by (41). If the two radii, a_1 and a_2, are equal, $Z_c = (\zeta_0/\pi) \ln (b/a)$, $F = \frac{1}{4}$, and $d = \sqrt{ab}$. If the end loads are straight conductors of radius a and length b, Z_L may be set equal to zero provided h is replaced by $(h + b/2)$ in (43). If $Z_L = \infty$, the circuit in Fig. 2 reduces to that of a center-driven dipole with a parallel parasitic element.

In the important special case with $\beta h = \pi/2$, $Z_L \doteq 0$, and $a_1 = a_2$, $Y_{\text{in}} = 1/4Z_d$ or $Z_{\text{in}} = 4Z_d$—a familiar formula.

Series Tuned Three-Wire Dipoles and Monopoles

The Vector Potential, the Integral Equations, and the Equivalent Dipole: As an application of the general theory developed in the analysis of the end-loaded two-wire antenna to multi-wire structures, consider the three-wire dipole shown in Fig. 4 and the corresponding monopole in Fig. 5.[20] The lumped load Z_L is now connected in series with one of the elements—in this case conductor 3—instead of as an end connection between two of them. Such a load is most easily handled by replacing it by an equivalent generator with emf V_3 given by[21]

$$V_3 = -I_3(0)Z_L. \quad (44)$$

The vector potential on the surface of each of the three conductors satisfies (4). The solutions that take account of symmetry and driving voltages and correspond to (5a) and (5b) are

$$A_1(z) = \frac{-j}{v_0} \left\{ C_1 \cos \beta z + \frac{V_1}{2} \sin \beta |z| \right\} \quad (45a)$$

$$A_2(z) = \frac{-j}{v_0} C_2 \cos \beta z \quad (45b)$$

$$A_3(z) = \frac{-j}{v_0} \left\{ C_3 \cos \beta z + \frac{V_3}{2} \sin \beta |z| \right\}. \quad (45c)$$

The vector potentials are also given by the following integrals that correspond to (6):

$$A_1(z) = \frac{\mu_0}{4\pi} \left\{ \int_{-h}^{h} I_1(z') K_a(z, z') dz' + \int_{-h}^{h} I_2(z') K_b(z, z') dz' + \int_{-h}^{h} I_3(z') K_{2b}(z, z') dz' \right\} \quad (46a)$$

$$A_2(z) = \frac{\mu_0}{4\pi} \left\{ \int_{-h}^{h} I_1(z') K_b(z, z') dz' + \int_{-h}^{h} I_2(z') K_a(z, z') dz' + \int_{-h}^{h} I_3(z') K_b(z, z') dz' \right\} \quad (46b)$$

$$A_3(z) = \frac{\mu_0}{4\pi} \left\{ \int_{-h}^{h} I_1(z') K_{2b}(z, z') dz' + \int_{-h}^{h} I_2(z') K_b(z, z') dz' + \int_{-h}^{h} I_3(z') K_a(z, z') dz' \right\}. \quad (46c)$$

The kernels are defined by (7) with $c = a$, b, or $2b$. The substitution of these expressions in (45a)–(45c) yields three simultaneous integral equations in the three unknown currents $I_1(z)$, $I_2(z)$, and $I_3(z)$.

[20] C. W. Harrison, Jr., "Theory of Shunt-Tuned Three-Wire Monopole," Sandia Corp., Albuquerque, N. M., Tech. Memorandum 301-57(14); October, 1957.

[21] Note that the negative sign occurs in (44) since the equivalent emf is the negative of the voltage drop across the impedance.

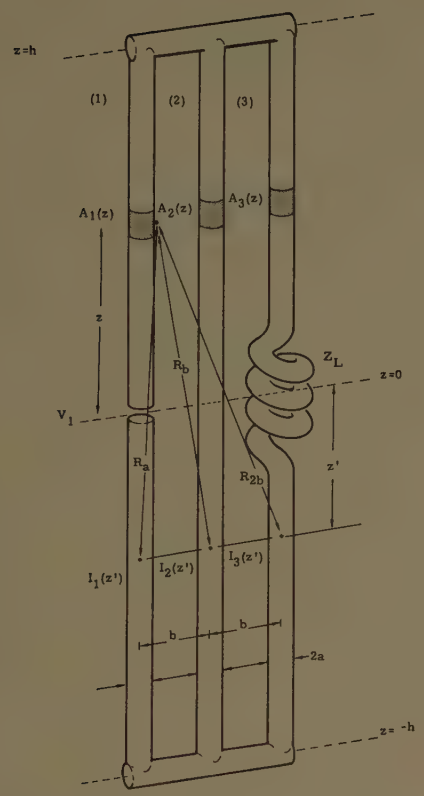

Fig. 4—Series-loaded coplanar three-wire dipole.

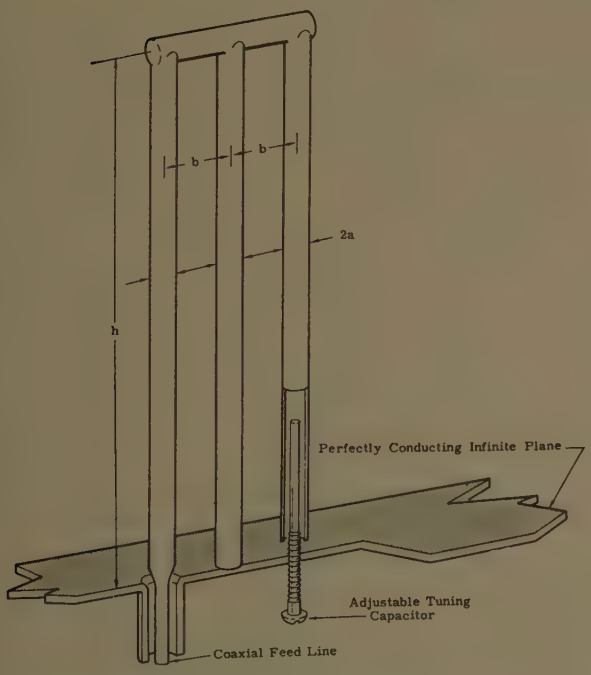

Fig. 5—Series-loaded coplanar three-wire monopole.

The integrals (45a)–(45c) are transformed by introducing the auxiliary potentials $A_{1d}(z)$ and $A_{2d}(z)$ defined by (8a) and (8b) and

$$A_{3d}(z) = \frac{\mu_0}{4\pi}\int_{-h}^{h} I_3(z')K_d(z,z')dz' \tag{47}$$

where $K_d(z,z')$ is defined by (7) with $c=d$. These auxiliary integrals are added and subtracted in (46a)–(46c) according to the pattern (9). The evaluation given in (10) is carried out for each, and steps paralleling (12a)–(12b) are carried out to obtain expressions like (14). Thus

$$A_1(z) = \frac{\mu_0}{4\pi}\left[J_d(z) + I_1(z)r_a + I_2(z)r_b + I_3(z)r_{2b}\right] \tag{48a}$$

$$A_2(z) = \frac{\mu_0}{4\pi}\left[J_d(z) + I_1(z)r_b + I_2(z)r_a + I_3(z)r_b\right] \tag{48b}$$

$$A_3(z) = \frac{\mu_0}{4\pi}\left[J_d(z) + I_1(z)r_{2b} + I_2(z)r_b + I_3(z)r_a\right]. \tag{48c}$$

When $J_d(z)$ is defined by the integral on the right in (15) with the total radiating current given by $I_T(z)=I_1(z)+I_2(z)+I_3(z)$ and with the r-parameters defined by

$$r_a = 2\ln\frac{d}{a}, \qquad r_b = 2\ln\frac{d}{b}, \qquad r_{2b} = 2\ln\frac{d}{2b}. \tag{49}$$

When (48a)–(48c) are substituted in (45a)–(45c) three simultaneous integral equations are obtained in a form corresponding to (18a)–(18b). In order to combine them in such a manner that an equation of the type (19) may be obtained for the total current

$$I_T(z) = I_1(z) + I_2(z) + I_3(z), \tag{50}$$

they may be multiplied respectively by 1, m, and n, and then added. The result is

$$\begin{aligned}(1+m+n)J_d(z) &+ I_T(z)\left[r_a + mr_b + nr_{2b}\right]\\ &+ I_2(z)\left[r_b - r_a + m(r_a - r_b) + n(r_b - r_{2b})\right]\\ &+ I_3(z)\left[r_{2b} - r_a + n(r_a - r_{2b})\right]\\ &= \frac{-j4\pi}{\zeta_0}\left[(C_1 + mC_2 + nC_3)\cos\beta z\right.\\ &\qquad \left. + \tfrac{1}{2}(V_1 + nV_3)\sin\beta\,|\,z\,|\,\right].\end{aligned} \tag{51}$$

Note that (50) has been used to eliminate $I_1(z)$. The integral equation (51) may be reduced to the form of (19) by setting the coefficients of $I_T(z)$, $I_2(z)$, and $I_3(z)$ equal to zero and using the three equations so obtained to determine m, n, and the effective radius d. The three equations are:

$$r_a + mr_b + mr_{2b} = 0 \tag{52a}$$

$$r_b - r_a + m(r_a - r_b) + n(r_b - r_{2b}) = 0 \tag{52b}$$

$$r_{2b} - r_a + n(r_a - r_{2b}) = 0. \tag{52c}$$

From (52c) it follows at once that $n=1$. Accordingly,

$$m = -\frac{(r_a + r_{2b})}{r_b} = -\frac{(2r_b - r_{2b} - r_a)}{r_a - r_b}. \quad (53)$$

The second equation reduces to

$$2r_b^2 - r_a r_{2b} - r_a^2 = 0. \quad (54)$$

With (49) and considerable algebraic manipulation, it follows that

$$\ln d = \frac{2(\ln b)^2 - \ln 2b \ln a - (\ln a)^2}{3(\ln b - \ln a) - \ln 2} \quad (55)$$

or

$$\ln d = \ln (2ab^2)^{1/3} - \frac{\ln 4 \ln \dfrac{b}{2a}}{6 \ln \dfrac{b^3}{2a^3}}. \quad (56)$$

Hence

$$d = (2ab^2)^{1/3} e^{-q}, \qquad q = \frac{\ln 4 \ln \dfrac{b}{2a}}{6 \ln \dfrac{b^3}{2a^3}}. \quad (57)$$

This is the effective radius of the equivalent dipole.

$$\frac{n}{1+m+n} = \frac{1}{2+m} = \frac{r_b}{2r_b - r_a - r_{2b}} = \frac{\ln \dfrac{b}{a}}{\ln \dfrac{b^3}{2a^3}} = \left(\frac{\alpha_0}{\alpha_1}\right) \quad (58a)$$

where

$$\alpha_0 = 2 \ln \frac{b}{a} \quad (58b)$$

$$\alpha_1 = 2 \ln \frac{b^3}{2a^3} = 3\alpha_0 - 2 \ln 2. \quad (58c)$$

The equation (51) may now be expressed as follows:

$$J_d(z) = \frac{-j4\pi}{\zeta_0} \left[C_d \cos \beta z + \tfrac{1}{2} V_d \sin \beta \left| z \right| \right] \quad (59)$$

where

$$V_d = \frac{V_1 + nV_3}{1+m+n} = \frac{\alpha_0}{\alpha_1}(V_1 + V_3). \quad (60)$$

Clearly (59) is in the standard form for determining the current $I_T(z)$ in a dipole of radius d and center driven by an effective voltage V_d. The constant C_d is evaluated from the condition $I_T(h)=0$. The effective impedance of the dipole is

$$Z_d = \frac{V_d}{I_T(0)} = \frac{\alpha_0}{\alpha_1}\left(\frac{V_1 - I_3(0)Z_L}{I_T(0)}\right). \quad (61)$$

Its numerical value may be obtained directly from extensive available tables[19] as explained in conjunction with (30). Note, however, that Z_d is *not* the driving point impedance of the three-wire antenna now under study.

The Currents and the Input Admittance: Explicit expressions for the individual currents in the three elements of the antenna may be obtained by solving the two difference equations obtained from (45a)–(45c) with (48a)–(48c) by forming

$$\frac{4\pi}{\mu_0}[A_1(z) - A_2(z)] \quad \text{and} \quad \frac{4\pi}{\mu_0}[A_2(z) - A_3(z)]$$

together with the definition of the total current. The three simultaneous relations are

$$I_1(z) + I_2(z) + I_3(z) = I_T(z), \quad (62a)$$

$$I_1(z)\alpha_0 - I_2(z)\alpha_0 - I_3(z) \ln 4 = \frac{-j4\pi}{\zeta_0}\left[D_1 \cos \beta z + \tfrac{1}{2} V_1 \sin \beta \left| z \right| \right] \quad (62b)$$

$$I_1(z) \ln 4 + I_2(z)\alpha_0 - I_3(z)\alpha_0 = \frac{-j4\pi}{\zeta_0}\left[D_2 \cos \beta z - \tfrac{1}{2} V_3 \sin \beta \left| z \right| \right] \quad (62c)$$

where α_0 is defined in (58b) and

$$D_1 = C_1 - C_2, \qquad D_2 = C_2 - C_3. \quad (63)$$

In terms of the additional notation

$$\alpha_2 = \alpha_4 \alpha_1 \quad (64a)$$

$$\alpha_3 = \alpha_0 - 2 \ln 2 = 2 \ln \frac{b}{2a} \quad (64b)$$

$$\alpha_4 = \alpha_0 + 2 \ln 2 = 2 \ln \frac{2b}{a} \quad (64c)$$

the solutions of (62a)–(62c) are as follows:

$$I_1(z) = I_T(z)\frac{\alpha_0 \alpha_4}{\alpha_2} - \frac{j4\pi}{\zeta_0}\left[\left(\frac{2\alpha_0 D_1 + \alpha_3 D_2}{\alpha_2}\right)\cos \beta z + \frac{1}{2}\left(\frac{2\alpha_0 V_1 - \alpha_3 V_3}{\alpha_2}\right)\sin \beta \left| z \right| \right] \quad (65a)$$

$$I_2(z) = I_T(z)\frac{\alpha_3 \alpha_4}{\alpha_2} + \frac{j4\pi}{\zeta_0}\frac{\alpha_4}{\alpha_2}\left[(D_1 - D_2)\cos \beta z + \tfrac{1}{2}(V_1 + V_3)\sin \beta \left| z \right| \right] \quad (65b)$$

$$I_3(z) = I_T(z)\frac{\alpha_0 \alpha_4}{\alpha_2} + \frac{j4\pi}{\zeta_0}\left[\left(\frac{\alpha_3 D_1 + 2\alpha_0 D_2}{\alpha_2}\right)\cos \beta z + \frac{1}{2}\left(\frac{\alpha_3 V_1 - 2\alpha_0 V_3}{\alpha_2}\right)\sin \beta \left| z \right| \right]. \quad (65c)$$

The arbitrary constants D_1 and D_2 may be evaluated by requiring the continuity of the scalar potential at $z=\pm h$. Since there are no impedances connecting the conductors at $z=\pm h$ it follows that

$$\phi_1(h) = \phi_2(h) = \phi_3(h) \tag{66}$$

where the potentials are obtained as in (35a),(35b). Thus

$$\phi_1(h) = -C_1 \sin \beta h + \tfrac{1}{2}V_1 \cos \beta h \tag{67a}$$

$$\phi_2(h) = -C_2 \sin \beta h \tag{67b}$$

$$\phi_3(h) = -C_3 \sin \beta h + \tfrac{1}{2}V_3 \cos \beta h. \tag{67c}$$

It follows that

$$D_1 = C_1 - C_2 = \tfrac{1}{2}V_1 \cot \beta h \tag{68a}$$

$$D_2 = C_2 - C_3 = -\tfrac{1}{2}V_3 \cot \beta h. \tag{68b}$$

If these values are substituted in (65a)–(65c) together with (44), *viz.*, $V_3=-I_3(0)Z_L$, all currents are completely determined. The part of $I_T(z)$ that contributes to each is obtained from the well-known solution of (59).

The driving point admittance of the series-loaded three-wire folded antenna shown in Fig. 4 is defined by

$$Y_{\text{in}} = \frac{I_1(0)}{V_1} \tag{69}$$

where, from (65a), and with (64a), (68a), (68b) and $V_3=-I_3(0)Z_L$,

$$I_1(0) = \frac{\alpha_0}{\alpha_1} I_T(0) - \frac{jB_h}{\alpha_2}[2\alpha_0 V_1 + \alpha_3 I_3(0) Z_L]. \tag{70a}$$

Note that from (65c)

$$I_3(0) = \frac{\alpha_0}{\alpha_1} I_T(0) + \frac{jB_h}{\alpha_2}[\alpha_3 V_1 + 2\alpha_0 I_3(0) Z_L]. \tag{70b}$$

Also,

$$I_T(0) = \frac{\alpha_0}{\alpha_1 Z_d}[V_1 - I_3(0) Z_L]. \tag{70c}$$

In (70a) and (70b), the following shorthand is used:

$$B_h = \frac{2\pi}{\zeta_0} \cot \beta h = \frac{\cot \beta h}{60} \text{ mho}. \tag{71}$$

An explicit formula for $I_1(0)$ is readily obtained if (70c) is substituted in (70a) and (70b) and if the value of $I_3(0)$ obtained from (70b) is also substituted in (70a). The result may be expressed as follows

$$Y_{\text{in}} = \frac{I_1(0)}{V_1} = \frac{\alpha_4 \eta_2 - jB_h Z_L(\eta_2 + \eta_1)}{\alpha_4(1 + Z_L \eta_2)} \tag{72}$$

where Y_{in} is the driving-point admittance of the three-wire antenna and

$$\eta_1 = \frac{1}{Z_d}\left(\frac{\alpha_0}{\alpha_1}\right)^2 + jB_h \frac{\alpha_3}{\alpha_1 \alpha_4} \tag{73a}$$

$$\eta_2 = \frac{1}{Z_d}\left(\frac{\alpha_0}{\alpha_1}\right)^2 - jB_h\left(\frac{2\alpha_0}{\alpha_1 \alpha_4}\right). \tag{73b}$$

The several α's are defined in (58b)–(58c) and (64a)–(64c); they involve only the dimensions b and a. Z_d is the impedance of a cylindrical antenna with effective radius d and length $2h$. It may be obtained from the extensive tables[19] to which reference has already been made.

The input admittance of the three-conductor series-tuned folded dipole antenna shown in Fig. 4 is given by (72). Note that when $Z_L=0$, (72) reduces simply to

$$Y_{\text{in}} = \eta_2 \tag{74}$$

where η_2 is given by (73b).

The input impedance of the folded three-wire monopole with load $Z_L/2$ over a conducting plane (Fig. 5), is $2Y_{\text{in}}$ where Y_{in} is given by (72).

If the three conductors of the folded dipole are arranged with a delta cross section as shown in Fig. 6 instead of in a plane as shown in Fig. 4, the input admittance may be obtained directly from (72). In this case the distance b replaces $2b$ in r_{2b} so that $r_{2b}=r_b$, which is equivalent to setting

$$\alpha_3 = \alpha_4 = \alpha_0 = 2 \ln \frac{b}{a}; \qquad \alpha_1 = 3\alpha_0 \tag{75}$$

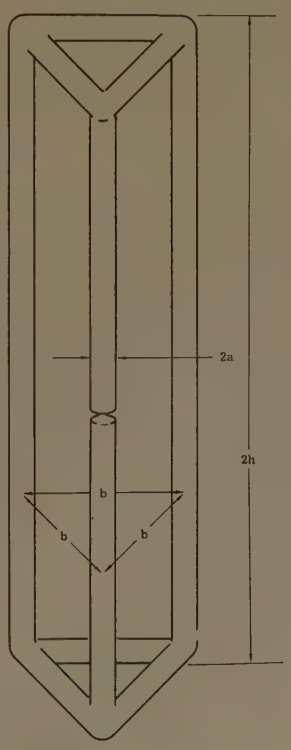

Fig. 6—Three-wire folded dipole with delta cross section.

and from (54)

$$d = (ab^2)^{1/3}. \tag{76}$$

It follows that the admittance is given by (72) with

$$\eta_1 = \frac{1}{9Z_d} + j\frac{B_h}{3\alpha_0}; \qquad \eta_2 = \frac{1}{9Z_d} - j\frac{2B_h}{3\alpha_0}. \tag{77}$$

When the load $Z_L = 0$, this reduces to (74) with η_2 given by (77).

Another related three-conductor folded antenna is shown in Fig. 7. It differs from the circuit in Fig. 4 in that $Z_L = 0$ and that the generator is in series with the middle conductor (No. 2) instead of with the outer conductor (No. 1). By the same procedure used in deriving (72) it is readily shown that

$$Y_{\text{in}} = \frac{I_2(0)}{V_2} = \frac{1}{Z_d}\left[\frac{\alpha_3}{\alpha_1}\right]^2 - jB_h\frac{2}{\alpha_1}, \tag{78}$$

where α_1 and α_2 are given in (58c) and (64b), and B_h is defined in (71). As usual Z_d is the impedance of a dipole of half-length h and effective radius d, in this case also given by (57). The admittance of the corresponding monopole over a conducting plane is twice the value for the dipole.

Summary—Multituned Antennas: The analysis of the series-tuned three-wire antenna may be generalized to any number of wires, each series-tuned by an arbitrary impedance provided the maximum transverse dimension is sufficiently small compared with the wavelength as required in (1). For simplicity the present analysis has been restricted to the three-element antenna with only one wire series-tuned. The effect of the series tuning is readily seen in the expression (72) for the input admittance. Since there is no restriction on the length of the antennas, the theory applies directly to the electrically short multituned antennas useful in VLF transmission.[22]

Multiwire Transmission Lines

End-driven circuits of the types shown in Figs. 8 and 9 may be analyzed by methods similar to those described in the preceding sections. The circuit of Fig. 8 may be called a hybrid transmission line since the series load in one side unbalances the line and thus makes it radiate like a folded antenna. Although such unbalanced or hybrid lines can be analyzed formally[10] to determine the driving-point impedance in terms of a driving voltage consisting of a discontinuity in scalar potential—$V(-h)$ in Fig. 8—this may be of little practical significance owing to the fact that it is not possible to approximate such a voltage by coupling to a tank coil or connecting a transmission line across the terminals without thereby more or less completely altering the circuit. Such a coupled coil or feeding line cannot be located in the neutral plane of the radiated field, and thus must become an integral part of the radiating system. In other words, the circuit to be analyzed is, in fact, not that of Fig. 8, but that of Fig. 8 *augmented by whatever conductors are attached to the lower end of the circuit.* (Note that in the case of the folded antennas analyzed in con-

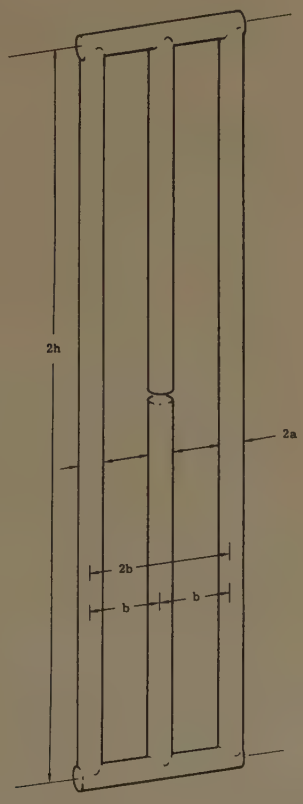

Fig. 7—Three-wire coplanar folded dipole with center conductor driven.

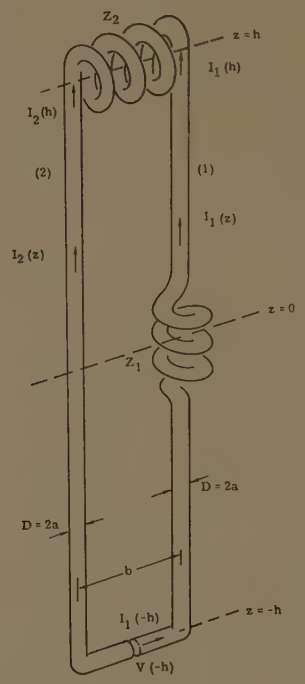

Fig. 8—Two-wire side- and end-loaded hybrid transmission line.

[22] An alternative procedure is discussed in C. W. Harrison, Jr., "Approximate Theory of Multituned Antenna for VLF Transmission," Sandia Corp., Tech. Memorandum 362–58(14); September, 1958.

junction with Figs. 2, 4, 6, and 7, a two-wire line connected to the driving terminals is easily arranged in the neutral plane of the radiated field—such a location is implied in the analysis.)

Balanced circuits such as that shown in Fig. 9 are true sections of essentially nonradiating, multi-wire transmission lines. For them the methods used to analyze the circuits of Figs. 2–7 are applicable, but are greatly simplified owing to the absence of a radiating $I_T(z)$. This may be illustrated specifically for the circuit shown in Fig. 9 which is useful as a top-loading reactor and impedance transformer in the so-called "wedge" antenna in the field of missile telemetry.

The essential condition that there be no radiation is

$$I_T(z) = I_1(z) + I_2(z) + I_3(z) = 0; \quad J_d(z) = 0. \tag{79}$$

The location of the generator at one end of the line and the absence of any unbalancing load along its full length assures that (79) applies to the circuit in Fig. 9. In addition, symmetry assures that

$$I_1(z) = I_3(z). \tag{80}$$

Continuity conditions for the scalar potential are:

$$\text{at } z = h: \qquad \phi_1(h) = \phi_2(h) = \phi_3(h) \tag{81a}$$

$$\text{at } z = -h: \qquad V(-h) = \phi_2(-h) - \phi_1(-h) = \phi_2(-h) - \phi_3(-h) \tag{81b}$$

where $V(-h)$ is the driving voltage between the lower end of conductor 2 and the transverse short-circuit leading to conductors 1 and 3.

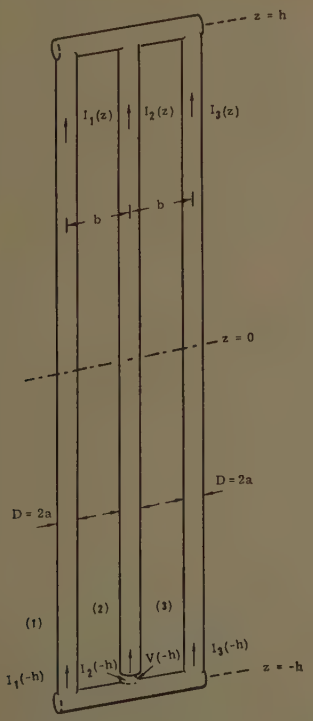

Fig. 9—Balanced three-wire line reactor.

Expressions for the vector potentials are solutions of (4) with arbitrary coefficients. Thus,

$$A_3(z) = A_1(z) = \frac{-j}{v_0}\left[C_1 \cos \beta z + C_1' \sin \beta z\right] \tag{82a}$$

$$A_2(z) = \frac{-j}{v_0}\left[C_2 \cos \beta z + C_2' \sin \beta z\right]. \tag{82b}$$

Since $I_T(z) = 0$, the determination of the properties of an equivalent dipole is irrelevant and the entire solution is obtained, in this case, directly from the difference equations (62a)–(62c). Moreover, since $I_3(z) = I_1(z)$, $A_3(z) = A_1(z)$, there is only one such equation, viz.

$$I_1(z)\alpha_0 - I_2(z)\alpha_0 - I_3(z) \ln 4 = I_1(z)\alpha_1 = \frac{-j4\pi}{\zeta_0}\left[D_1 \cos \beta z + D_1' \sin \beta z\right], \tag{83}$$

where $\alpha_0 = 2 \ln (b/a)$, $\alpha_1 = 3\alpha_0 - \ln 4 = 2 \ln (b^3/2a^3)$, as defined in (58b), (58c), and where $D_1 = C_1 - C_2$, $D_1' = C_1' - C_2'$. It follows that

$$I_1(z) = \frac{-j4\pi}{\zeta_0 \alpha_1}\left[D_1 \cos \beta z + D_1' \sin \beta z\right] \tag{84a}$$

$$I_2(z) = -2I_1(z) = \frac{j8\pi}{\zeta_0 \alpha_1}\left[D_1 \cos \beta z + D_1' \sin \beta z\right]. \tag{84b}$$

The constants D_1 and D_1' are readily evaluated from (81a), (81b) with

$$\phi_3(z) = \phi_1(z) = -C_1 \sin \beta z + C_1' \cos \beta z \tag{85a}$$

$$\phi_2(z) = -C_2 \sin \beta z + C_2' \cos \beta z. \tag{85b}$$

Thus, from the equations obtained from (85a) and (85b) with $z = \pm h$, it follows directly that

$$D_1 = C_1 - C_2 = -\frac{V(-h)}{2 \sin \beta h} \tag{86a}$$

$$D_1' = C_1' - C_2' = -\frac{V(-h)}{2 \cos \beta h}. \tag{86b}$$

Hence, the final solutions for the individual currents are:

$$I_1(z) = \frac{j4\pi}{\zeta_0 \alpha_1} \frac{V(-h)}{\sin 2\beta h} \cos \beta(h - z) \tag{87a}$$

$$I_2(z) = \frac{-j8\pi}{\zeta_0 \alpha_1} \frac{V(-h)}{\sin 2\beta h} \cos \beta(h - z). \tag{87b}$$

The driving-point admittance is

$$Y_{in} = \frac{I_2(-h)}{V(-h)} = -j\frac{8\pi}{\zeta_0 \alpha_1} \cot 2\beta h = \frac{-j \cot 2\beta h}{30 \ln\left(\frac{b^3}{2a^3}\right)} \text{ mho}. \tag{88}$$

This completes the analysis of the three-wire transmission-line reactor shown in Fig. 9. Note that transmission-line end effects and the finite length of the connecting terminations have been neglected together with ohmic losses and the small radiation losses from a balanced, closely spaced line.

II. Circular Elements

The Loop Antenna

The analysis in Section I is concerned with antennas that consist of parallel, closely-spaced and variously interconnected and loaded linear elements. They are shown to be equivalent to a single dipole and a combination of sections of transmission line. In this part the analogous problem of antennas that consist of parallel, closely-spaced, and variously interconnected and loaded circular elements is considered in terms of a simple special case, the circular folded dipole and monopole. Such circuits are equivalent to a single loop antenna and reactive sections of transmission line curved into a circle. A folded circular loop or Halo antenna is shown in Fig. 10, and a folded half loop over a highly conducting plane in Fig. 11.

The distribution of current in a single-turn loop antenna and its driving-point admittance have been studied by Storer,[23] for loops that satisfy the following conditions:

$$a^2 \ll b^2; \qquad \beta^2 a^2 \ll 1; \qquad \beta b \leq 2.5 \tag{89}$$

where a is the radius of the wire, b the radius of the loop, and $\beta = 2\pi/\lambda$. His formula for the current as a function of the polar angle ϕ measured from the delta function generator at $\phi = 0$ is the following fairly complicated expression:

$$I(\phi) = \frac{V}{j\pi\zeta_0}\left\{\frac{1}{\alpha_0} + 2\sum_1^4 \frac{\cos n\phi}{\alpha_n} - \frac{2\pi}{\ln\left(\frac{n_0}{4.5}\right)} \cdot \left[\left(\frac{\beta b}{4.5}\right)J_1(\phi) + \left(\frac{\beta b}{4.5}\right)^3 J_2(\phi)\right]\right\} \tag{90}$$

where

$$\ln\left(\frac{n_0}{4.5}\right) = \frac{\Omega}{2} - 3.226; \qquad \Omega = 2\ln\left(\frac{2\pi b}{a}\right) \tag{91}$$

and $\alpha_0 \cdots \alpha_n$, $J_1(\phi)$ and $J_2(\phi)$ are parameters that are defined and represented graphically in the Appendix;

[23] J. E. Storer, "Impedance of Thin Wire Loop Antenna," Cruft Lab. Harvard University, Cambridge, Mass., Tech. Rept. No. 212; May, 1955. Extensive curves and tables of admittances and impedances are given in this report.

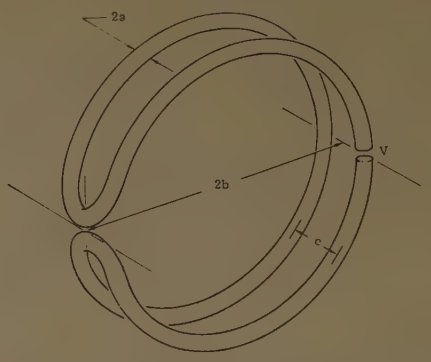

Fig. 10—Isolated folded circular loop or Halo antenna.

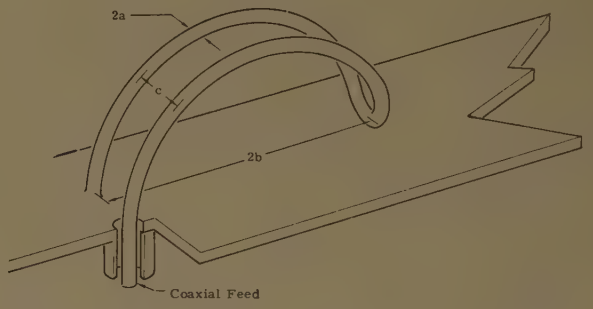

Fig. 11—Folded half loop over a highly conducting plane.

$I(\phi)$ is also shown for $\Omega = 10$. The driving-point admittance of the unloaded loop is

$$Y_{l0} = \frac{1}{j\pi\zeta_0}\left\{\frac{1}{\alpha_0} + 2\sum_1^4 \frac{1}{\alpha_n} - \frac{2\pi}{\ln\left(\frac{n_0}{4.5}\right)} \cdot \left[\left(\frac{\beta b}{4.5}\right)J_1(0) + \left(\frac{\beta b}{4.5}\right)^3 J_2(0)\right]\right\}. \tag{92}$$

The admittance Y_{lL} of a single-turn loop that is driven at $\phi = 0$ by a voltage V_1 and is loaded at $\phi = \pi$ by a lumped impedance Z_L in series with the loop may be obtained from that of the unloaded loop by replacing the negative voltage drop across the load by an equivalent generator with voltage

$$V_2 = -I_3(\pi)Z_L \tag{93}$$

where $I_3(\pi)$ is the total current through Z_L and then superimposing the currents $I_1(\phi)$ and $I_2(\phi)$ maintained by V_1 and V_2. This procedure is represented schematically in Fig. 12. If

$$k = \frac{I(\pi)}{I(0)} \tag{94}$$

it follows from Fig. 12 that

$$I_3(0) = I_1(0) + I_2(\pi) = I_1(0) + kI_2(0) \tag{95a}$$

$$I_3(\pi) = I_1(\pi) + I_2(0) = I_2(0) + kI_1(0). \tag{95b}$$

The driving point admittance Y_{1L} of the loaded loop in Fig. 13 is obtained by solving (95a) and (95b) together with (93) and the relation

$$V_2 = \frac{I_2(0)}{Y_{10}} \cdot \tag{96}$$

The result is

$$Y_{1L} = Y_{10}\left[\frac{1 + Z_L Y_{10}(1 - k^2)}{1 + Z_L Y_{10}}\right] \tag{97}$$

where Y_{10} is given by (92) and k [as defined in (94)] is obtained from (90) with $\phi = 0$ and $\phi = \pi$. Y_{1L} in (97) is the final expression for the driving-point admittance of a circular loop antenna when a load Z_L is connected in series at the point diametrically opposite the driving point. Such a load may be in the form of a tuning reactor or it may be the input impedance of a section of two-wire line.

If the loop is open-circuited at $\phi = \pi$, $Z_L = \infty$ and (97) reduces to

$$Y_{1\infty} = Y_{10}(1 - k^2). \tag{98}$$

The Admittance of the Halo Antenna

The Halo antenna consists of a conventional two-conductor folded dipole antenna bent into a circular form as shown in Fig. 15(a). Such an antenna may be analyzed by superposition as shown schematically in Fig. 15. It is assumed that (89) is satisfied, and, in addition, that the distance c between parallel loops is sufficiently small so that

$$\beta^2 c^2 \ll 1. \tag{99}$$

The folded dipole loop in Fig. 15(a) is driven by a voltage $2V$ at $\phi = 0$ in one of the loops. It may be treated as the superposition of the loops in Figs. 15(b) and 15(c).

In Fig. 15(b) the two parallel loops are driven by identical generators in phase and with voltage V. Equal symmetrical currents $I_1^s(\phi) = I_2^s(\phi)$ are excited and the potential difference between the two loops at any given value of ϕ is zero. Accordingly, the presence of a short circuit joining them at $\phi = \pi$ is of no consequence. The two loops individually correspond to the open-circuited loop in Fig. 14 and, just as in the case of symmetrically driven dipoles,[24] the two together are equivalent to a single loop with effective radius.

$$d = \sqrt{ac}. \tag{100}$$

[24] R. W. P. King, *op. cit.*, footnote 5, p. 275.

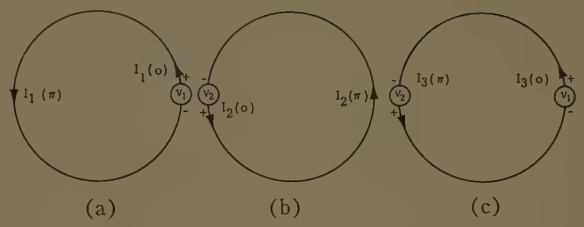

Fig. 12—Superposition of two loops each driven at a single point to obtain a loop driven at two points.

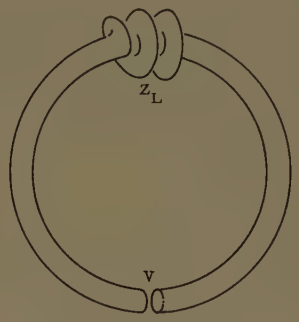

Fig. 13—Impedance-loaded single conductor loop.

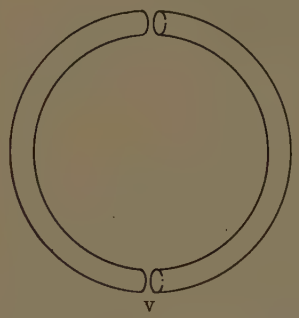

Fig. 14—Single-conductor loop with gap.

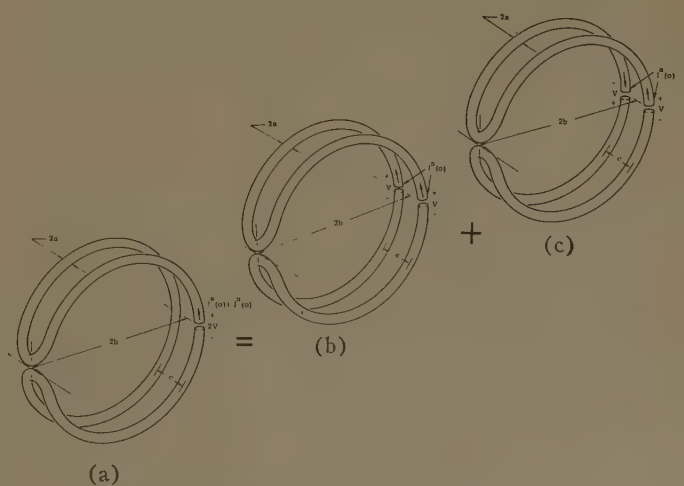

Fig. 15—Principle of superposition applied to obtain the admittance of a folded-circular loop or Halo antenna.

The symmetrical admittance seen by each voltage V is

$$Y^s = \frac{I^s(0)}{V} = \frac{1}{2} Y_{l\infty} \tag{101}$$

where $Y_{l\infty}$ is given by (98) for a loop with radius d.

In the circuit in Fig. 15(c) the two parallel loops are driven by voltages V that are equal in magnitude but opposite in phase. For such voltages the antisymmetrical currents in the two loops are equal and opposite $I_2^a = -I_1^a$ so that the loops behave like two short-circuited sections of transmission line connected in series with each other and the two generators. If $c^2 \ll b^2$, the admittance of each section is approximately the same as if it were straight. That is, and neglecting ohmic resistance,

$$Y^{(a)} = \frac{I^{(a)}(0)}{V} \doteq \frac{-j}{R_c} \cot \beta\pi b \tag{102}$$

where $R_c = (\zeta_0/\pi) \ln (c/a) = 120 \ln (c/a)$ ohms.

The admittance of the Halo antenna in Fig. 15(a) is defined by

$$Y_H = \frac{I_1}{2V} = \frac{I^s(0) + I^a(0)}{2V} = \frac{1}{2}[Y^{(s)} + Y^{(a)}]. \tag{103}$$

With (101) and (102)

$$Y_H = \tfrac{1}{4} Y_{l0}(1 - k^2) - \frac{j}{2R_c} \cot \beta\pi b \tag{104}$$

where Y_{l0} is given by (92) for a loop antenna of radius d; k is obtained from (94) with (90).

For some applications it is advantageous to connect a lumped tuning impedance Z_L between the adjacent ends at $\phi = \pi$ of the circular folded dipole. Such an impedance has no effect on the transmission-line currents $I^a(\theta)$ as obtained in Fig. 15(c). On the other hand, instead of the open-circuited loop of effective radius d represented by Fig. 15(b), a similar loop with a connecting impedance Z_L is involved in determining $I^s(\phi)$. In the determination of the admittance of the loaded Halo antenna, the formula

$$Y^{(s)} = \tfrac{1}{2} Y_{lL} \tag{105}$$

must be used instead of (101). Y_{lL} is given by (97). It follows that

$$Y_{HL} = \tfrac{1}{4} Y_{l0} \left[\frac{1 + Z_L Y_{l0}(1 - k^2)}{1 + Z_L Y_{l0}} \right] - \frac{j}{2R_c} \cot \beta\pi b \tag{106}$$

is the driving-point admittance of the series loaded Halo antenna.

Numerical Analysis of a Halo Antenna

A Halo antenna is formed by bending into circular shape a conventional folded dipole (but with the outer extremities of the structure not brought in contact). Therefore, it is of interest to compare the input admittance and impedance of a folded dipole before and after it is bent into a Halo antenna. For this purpose consider a folded dipole of length $2h = \lambda/2$, or $\beta h = \pi/2$, and effective radius $d = \sqrt{ac}$ such that $\Omega = 2 \ln 2h/d = 10$. When the dipole is bent into the Halo configuration the corresponding dimensions are $2\pi b = \lambda/2$ or $\beta b = 0.5$, $\Omega = 2 \ln 2\pi b/\sqrt{ac} = 10$. The admittance Y_0 and impedance Z_0 of a straight dipole with $\beta h = \pi/2$ and $\Omega = 10$ are[20]

$$Y_0 = (9.38 - j\,4.52) \times 10^{-3} \text{ mho} \tag{107a}$$

$$Z_0 = 86.5 + j41.7 \text{ ohms.} \tag{107b}$$

The corresponding admittance of a single circular loop with $\beta b = 0.5$ and $\Omega = 10$ is obtained from (92). Reference to Figs. 16–18 in the Appendix shows that for these values of Ω and βb, the α coefficients are

$$\frac{1}{\alpha_0} = 1.870 + j0.033 \qquad \frac{1}{\alpha_3} = -0.09 + j0.0$$

$$\frac{1}{\alpha_1} = -0.675 + j0.050 \qquad \frac{1}{\alpha_4} = -0.052 + j0.0 \tag{108}$$

$$\frac{1}{\alpha_2} = -0.15 + j0.0.$$

Also

$$J_1(0) = 1.25 \qquad J_1(\pi) = -0.07 \tag{109a}$$

$$J_2(0) = 0.34 \qquad J_2(\pi) = -0.05. \tag{109b}$$

With these values,

$$Y_{l0} = \frac{-0.558 + j0.133}{j120\pi^2}$$

$$= (0.112 + j0.471) \times 10^{-3} \text{ mho} \tag{110a}$$

$$Z_{l0} = 478.6 - j2008 \text{ ohms} \tag{110b}$$

The admittance and impedance of the open-circuited loop are obtained from (98) with

$$k = \frac{3.024 - j0.067}{-0.558 + j0.133} = -5.15 - j1.11. \tag{111}$$

Thus,

$$Y_{l\infty} = (0.112 + j0.471)10^{-3}(-24.29 - j11.43)$$

$$= (2.66 - j12.72) \times 10^{-3} \text{ mho} \tag{112a}$$

$$Z_{l\infty} = 15.7 + j75.3 \text{ ohms.} \tag{112b}$$

A comparison of (112b) with (107b) shows that the impedance of a straight dipole is greatly altered when it is bent into a circle with its open ends close together but not in contact. The resistance is decreased to about one fifth, the reactance almost doubled.

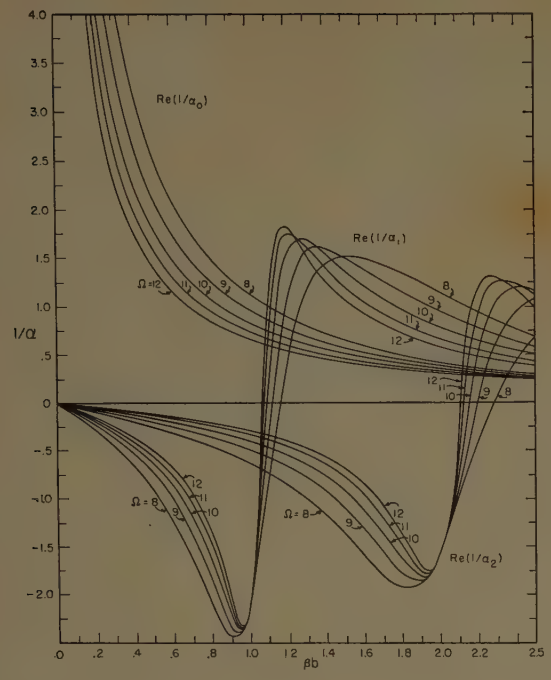

(a)

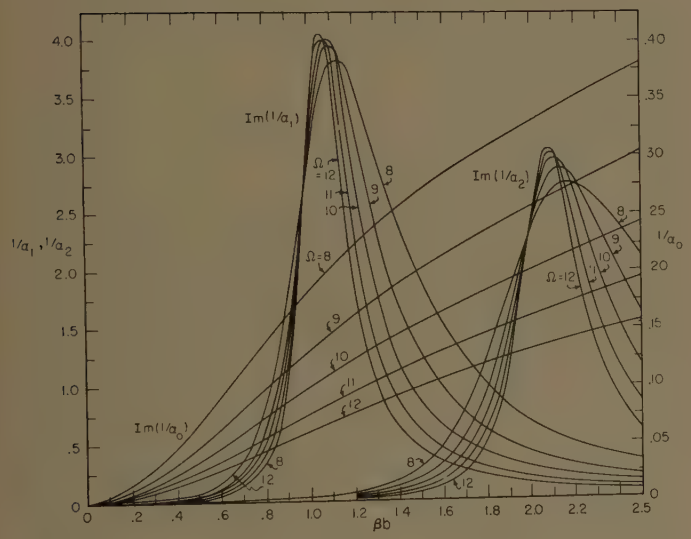

(b)

Fig. 16—(a) Real parts of the functions $1/\alpha_0$, $1/\alpha_1$, $1/\alpha_2$. (b) Imaginary parts of the functions $1/\alpha_0$, $1/\alpha_1$, $1/\alpha_2$.

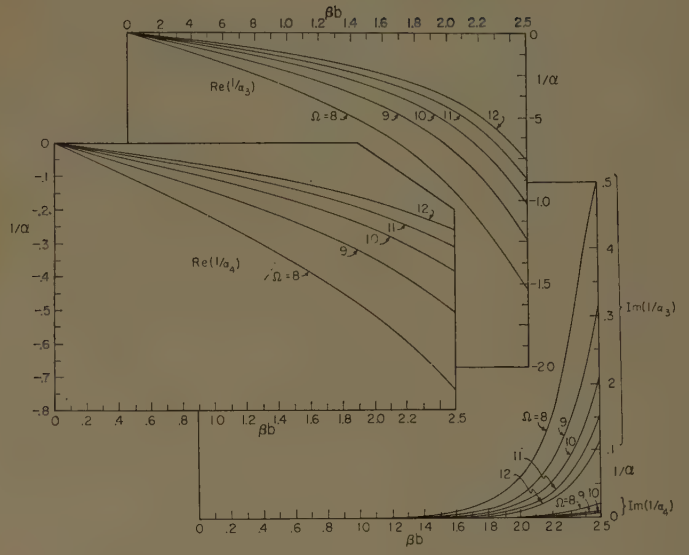

Fig. 17—Real and imaginary parts of the functions $1/\alpha_3$ and $1/\alpha_4$.

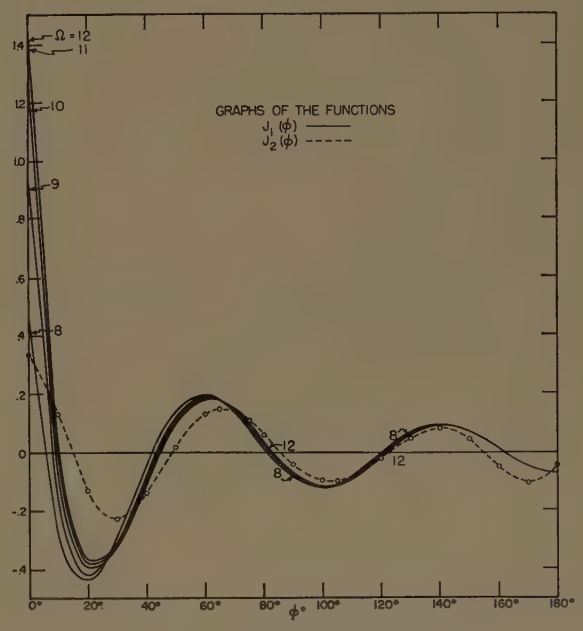

Fig. 18—The functions $J_1(\phi)$ and $J_2(\phi)$.

The admittance and impedance of the Halo antenna when $\beta b = 0.5$ and $Y^{(a)} = 0$ are obtained from (104). They are simply

$$Y_H = \tfrac{1}{4} Y_{l\infty} = (0.665 - j3.18) \times 10^{-3} \text{ mho} \quad (113a)$$

$$Z_H = 62.9 + j301 \text{ ohms.} \quad (113b)$$

The corresponding values for the straight folded dipole are

$$Y_{in} = \tfrac{1}{2} Y^{(s)} \doteq \tfrac{1}{4} Y_0 = (2.34 - j1.13) \times 10^{-3} \text{ mho} \quad (114a)$$

$$Z_{in} \doteq 4Z_0 = 346 + j167 \text{ ohms.} \quad (114b)$$

The numerical values of the admittance and impedance of the Halo antenna may be modified by changing the values of the radius a of the wire and the distance c between the parallel circular loops. Alternatively, a lumped series tuning reactance $Z_L = jX_L$ may be used in place of an open circuit between the adjacent ends of the Halo structure. In this case the admittance is obtained from (106) instead of from (104).

This completes the analysis of the Halo antenna shown in Fig. 10. The impedance of one half of this structure over a conducting plane as shown in Fig. 11 is obtained by dividing the impedance of the Halo antenna by two.

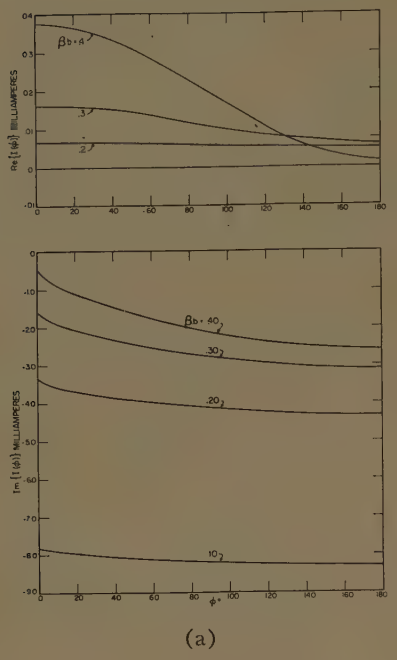

(a)

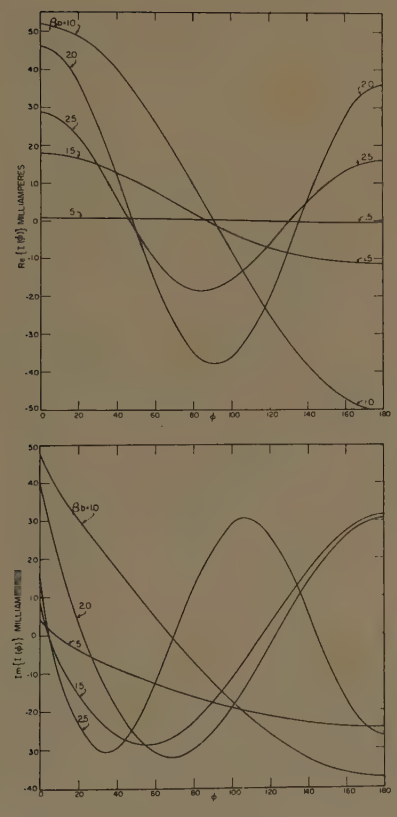

(b)

Fig. 19—(a) Real and imaginary components of current distributions on small loop antennas. $\Omega = 2 \ln (2\pi b/a) = 10$. (b) Real and imaginary components of current distributions on loop antennas. $\Omega = 2 \ln (2\pi b/a) = 10$.

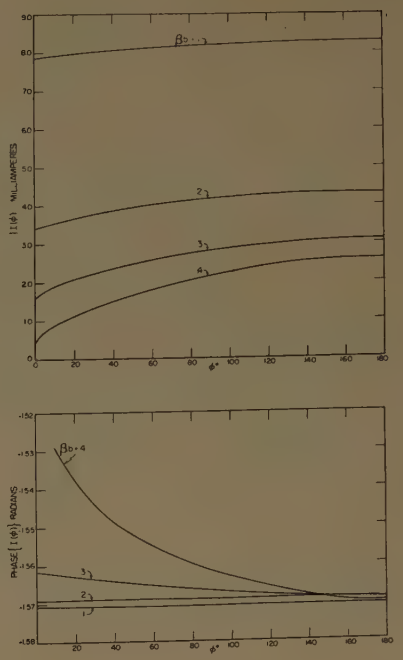

(a)

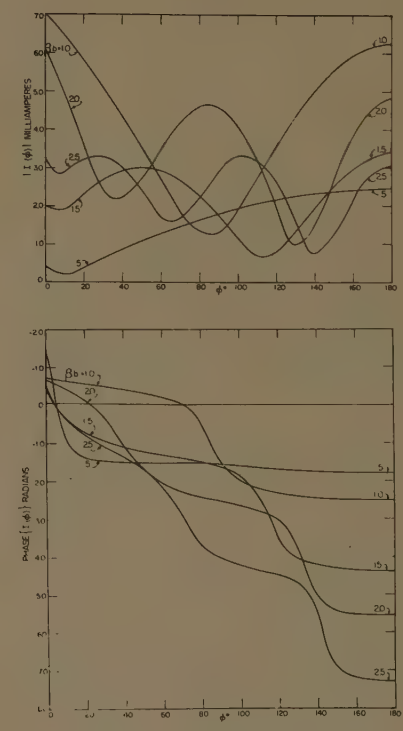

(b)

Fig. 20—(a) Magnitude and phase of current distributions on small loop antennas. $\Omega = 2 \ln (2\pi b/a) = 10$. (b) Magnitude and phase of current distributions on loop antennas. $\Omega = 2 \ln (2\pi b/a) = 10$.

Appendix

The several parameters that occur in Storer's formula (85) for the current in a circular loop are defined as follows:

$$\alpha_n = \frac{\beta b}{2}(K_{n+1} + K_{n-1}) - \frac{n^2}{\beta b} K_n \qquad \text{(A-1)}$$

where

$$K_{n+1} - K_n = \Omega_{2n+1}(2\beta b) + jJ_{2n+1}(2\beta b), \qquad n > 0 \quad \text{(A-2)}$$

$$K_0 = \frac{1}{\pi} \ln \frac{8b}{a} - \frac{1}{2}\left[\int_0^{2\beta b} \Omega_0(x)dx + j\int_0^{2\beta b} J_0(x)dx\right], \qquad \text{(A-3)}$$

$\Omega_{2n+1}(x)$ is the Lommel-Weber function of order $2n+1$ (tabulated in the Johnke-Emde Tables of Functions); $J_{2n+1}(x)$ is the Bessel function of the first kind and order $2n+1$. Graphs of the function α_n are in Figs. 16 and 17. The functions $J_1(\phi)$ and $J_2(\phi)$ are defined by the integrals,

$$J_1(\phi) = \int_0^{\infty} \frac{\ln\left(\frac{n_0}{4.5}\right)}{\ln\left(\frac{n_0}{4.5}\right) - \ln x} \cdot \frac{\cos(4.5\phi)}{x^2} dx \qquad \text{(A-4)}$$

$$J_2(\phi) = \int_1^{\infty} \frac{\cos(4.5\phi x)}{x^4} dx \qquad \text{(A-5)}$$

where $n_0 = (2b/a)\, e^{-\gamma}$, $\gamma = 0.5772 \cdots$. They are represented graphically in Fig. 18. Note that $J_2(0) = \frac{1}{3}$. The distributions of current as determined from (90) are shown in Figs. 19(a), 19(b) and 20(a), 20(b) for $\Omega = 10$ and $0.1 \leq \beta b \leq 1$.

Sidelobe Reduction by Nonuniform Element Spacing*

ROGER F. HARRINGTON†, MEMBER, IRE

***Summary*—A perturbational procedure for reducing the sidelobe level of discrete linear arrays with uniform amplitude excitation by using nonuniform element spacing is presented. The calculation of the required element spacings is quite simple. The method can reduce the sidelobe level to about $2/N$ times the field intensity of the main lobe, where N is the total number of elements, without increasing the beamwidth of the main lobe. Several examples are given.**

I. Introduction

THE principal uses of antenna arrays are 1) to provide power gain and 2), to give directive patterns. The first objective can be achieved by the so-called uniform array, which is an array of uniformly-spaced and uniformly-excited elements. However, the first sidelobe of a uniform array is only about 13.5 db down from the main lobe level. This is undesirable for many directive applications, such as in radar and in direction finding. The sidelobes can be reduced to any desired level by tapering the amplitude of the excitation of the elements.[1,2] However, tapering the excitation requires a complicated feed system, and also increases the main beamwidth. The use of arbitrary element positions for pattern synthesis purposes has been suggested by Unz.[3] A recent paper by King and others proposes the use of nonuniform element separation to reduce grating lobes.[4] These are secondary lobes equal in amplitude to the main lobe which can occur in uniform arrays with large element spacings. King also notes that some patterns have sidelobes below those for uniform arrays, and hence nonuniform element spacing can be used to reduce sidelobes.

This paper presents a method for reducing sidelobe levels by using nonuniform element spacing, while retaining uniform excitation. It is shown that the sidelobes can be reduced in height to approximately $2/N$ times the main lobe level, where N is the number of elements. At the same time the beamwidth remains essentially the same as for the uniform array.

II. Basic Theory

Fig. 1 shows the array geometry for the cases: (a) even number of elements, and (b) odd number of elements. The N elements are not necessarily equally

* Received by the PGAP, August 12, 1960; revised manuscript received, October 10, 1960. This work was sponsored by Rome Air Dev. Center under Contract No. AF30(602)-1640.

† Dept. of Elec. Engrg., Syracuse University, Syracuse, N. Y.

[1] S. A. Schelkunoff, "A mathematical theory of linear arrays," *Bell Syst. Tech. J.*, vol. 22, pp. 80–107; January, 1943.

[2] C. L. Dolph, "A current distribution which optimizes the relationship between beamwidth and sidelobe level," PROC. IRE, vol. 34, p. 335; April, 1946.

[3] H. Unz, "Linear arrays with arbitrarily distributed elements," IRE TRANS. ON ANTENNAS AND PROPAGATION, vol. AP-8, pp. 222–223; March, 1960.

[4] D. D. King, R. F. Packard, and R. K. Thomas, "Unequally spaced, broad-band antenna arrays," IRE TRANS. ON ANTENNAS AND PROPAGATION, vol. AP-8, pp. 380–385; July, 1960.

spaced, but are assumed to be symmetric about the array center. The excitation is such that all elements are fed equal amplitudes, and progressively phased so that the field from all elements adds in-phase in a direction θ_0, forming the main beam. Hence the phase of the nth element is

$$\alpha_n = -\frac{2\pi}{\lambda} d_n \cos\theta_0, \tag{1}$$

where λ is the wavelength and d_n is the distance of the nth element from the array center. In order to treat arrays with odd and even numbers of elements simultaneously, the following summation convention will be used. For an even number of elements

$$\sum_n \text{means} \sum_{n=1,3,5,\cdots}^{N-1}, \tag{2}$$

that is, summation extends over only odd integers smaller than the number of elements in the array. For an odd number of elements,

$$\sum_n \text{means} \sum_{n=0,2,4,\cdots}^{N-1}, \tag{3}$$

that is, summation extends over only even integers smaller than the number of elements in the array.

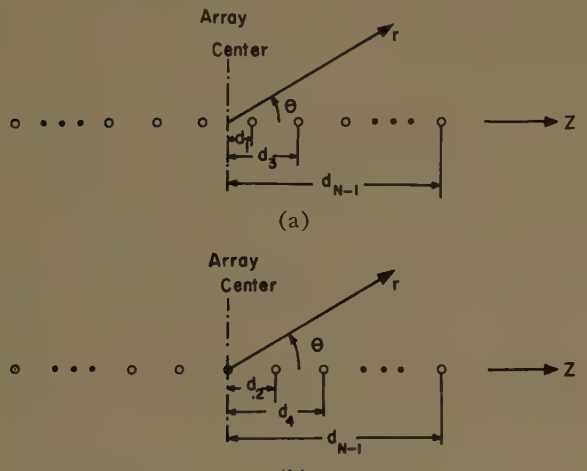

Fig. 1—Array geometry. (a) Even number of elements. (b) Odd number of elements.

If the elements are uniformly spaced a distance d apart, then $d_n = nd/2$, and the normalized field pattern is[5]

$$E_u = \frac{1}{N}\sum_n \cos(nu/2) = \frac{1}{N}\frac{\sin(Nu/2)}{\sin(u/2)}, \tag{4}$$

where

$$u = \frac{2\pi}{\lambda} d(\cos\theta - \cos\theta_0). \tag{5}$$

[5] J. D. Kraus, "Antennas," McGraw-Hill Book Co., Inc., New York, N. Y.; p. 76; 1950.

If the elements are nonuniformly spaced, a convenient "base separation" d can be picked, and the element spacing expressed as

$$d_n = \left(\frac{n}{2} + \epsilon_n\right) d. \tag{6}$$

In other words, ϵ_n is the fractional change from uniform spacing. The normalized field pattern is given by

$$E = \frac{1}{N}\sum_n \cos\left[\left(\frac{n}{2} + \epsilon_n\right) u\right]. \tag{7}$$

This can be put into a more convenient form by separating out the pattern of a uniform array having element separation equal to the base separation.

$$E = E_u - \frac{1}{N}\sum_n \left[\sin\epsilon_n u \sin n\frac{u}{2} + (1 - \cos\epsilon_n u)\cos n\frac{u}{2}\right], \tag{8}$$

where E_u is the uniform array pattern, given by (4).

The undesirable feature of the uniform array for directive purposes is that the sidelobes near the main beam ($u=0$) are too high. The summation term of (8) can be used to reduce these side lobes. If all $\epsilon_n u$ are assumed small, (8) reduces to

$$E = E_u - \frac{u}{N}\sum_n \epsilon_n \sin n\frac{u}{2}, \tag{9}$$

which can be rearranged to read

$$\sum_n \epsilon_n \sin n\frac{u}{2} = \frac{N}{u}(E_u - E). \tag{10}$$

The ϵ_n are then given by the formula for Fourier coefficients:

$$\epsilon_n = \frac{2N}{\pi}\int_0^{\pi} \frac{1}{u}(E_u - E)\sin n\frac{u}{2}\, du. \tag{11}$$

Hence, if one assumes a desired pattern E, fractional changes in element spacing from uniform spacing can be calculated by (11). The approximation is restricted to small $\epsilon_n u$, and minimizes the net mean square error in the desired $(E_u - E)/u$. Note that the fractional change in position of each pair of elements determines the amplitude of one term in the trigonometric series (10).

III. Method of Reducing Sidelobes

Fig. 2(a) shows the field pattern E_u for a uniform array, specifically for a 12-element array. Suppose it is desired to reduce the first sidelobe to the level of the second. The desired field E then follows the dashed curve of Fig. 2(a). The quantity $(E_u - E)/u$ is shown in Fig. 2(b). One can now evaluate (11) for the necessary changes in element spacing, which gives a least-mean-square approximation to Fig. 2(b). However, an even simpler procedure can be used, as follows.

Instead of the exact corrective term of Fig. 2(b), suppose an impulsive function is taken. To correct the first sidelobe level one can choose an impulse function to reduce the peak of the sidelobe, as represented by the heavy arrow in Fig. 3(a). Eq. (11) is a finite Fourier series; hence, the resultant corrective term will be a smoothed-out function, as shown in Fig. 3(a). The strength of the impulse function determines the amount of sidelobe reduction effected, and can be determined by trial. The resultant pattern is shown in Fig. 3(b). The necessary fractional changes in element position from uniform spacing are summarized by the table included in Fig. 3(b).

If one then wishes to reduce the second sidelobe, a second impulse function can be added to the corrective term. This is positioned at the new second sidelobe peak, which is slightly changed from its position for the uniform array. Fig. 4(a) represents by arrows the two impulse functions required to reduce the first two sidelobes. The curve of Fig. 4(a) shows the resultant smooth corrective term obtained from (11). Figure 4(b) shows the final nonuniform array pattern, with the first two sidelobes down more than 19 db from the main lobe level. The necessary fractional changes in element positions from uniform spacing are shown in the table included in Fig. 4(b). Note that the main beamwidth is virtually unchanged from that of the uniform array.

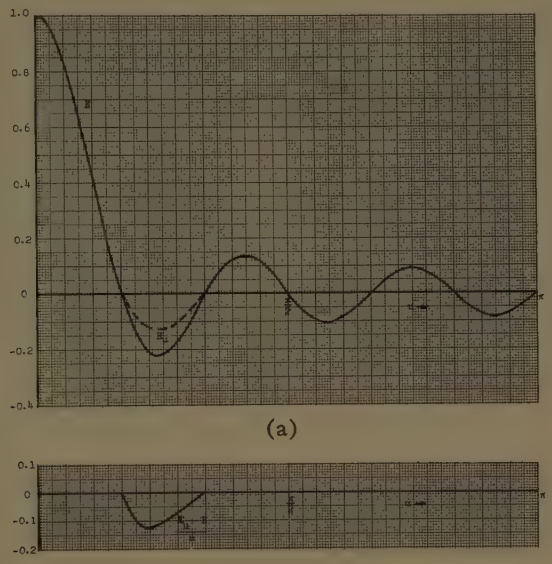

Fig. 2—(a) 12-element array. Uniform array field pattern E_u shown solid, desired pattern E shown dashed. (b) The function $(E_u-E)/u$.

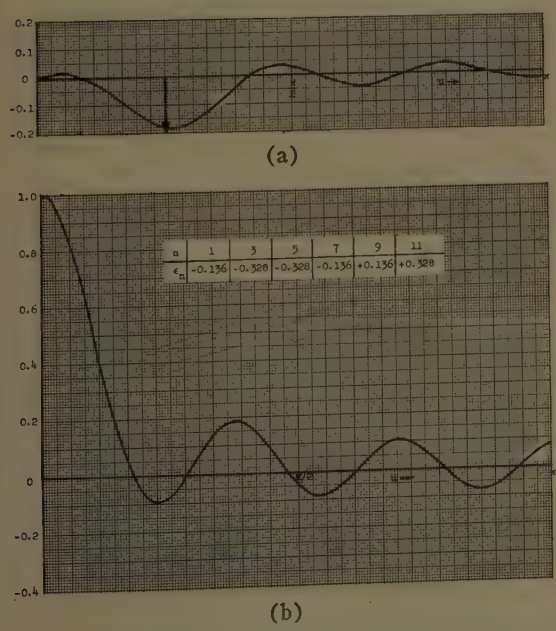

n	1	3	5	7	9	11
ϵ_n	-0.136	-0.328	-0.328	-0.136	+0.136	+0.328

Fig. 3—(a) The function $(E_u-E)/u$ to reduce the first side lobe; the impulsive approximation is represented by the arrow. (b) The resultant field pattern.

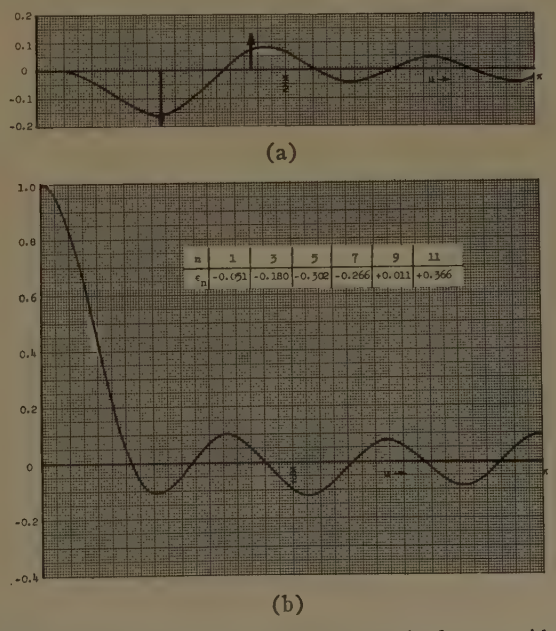

n	1	3	5	7	9	11
ϵ_n	-0.051	-0.180	-0.302	-0.266	+0.011	+0.366

Fig. 4—(a) The function $(E_u-E)/u$ to reduce the first two side lobes; the impulsive approximation is represented by the arrows. (b) The resultant field pattern.

The mathematical formulation of this method of sidelobe reduction is as follows. Let the corrective impulse functions be ordered 1, 2, 3 · · ·, counting from the origin, let u_k denote the position of the kth impulse, and let a_k denote the strength of the kth impulse. Then the impulsive corrective term is

$$\frac{E_u - E}{u} \approx \frac{1}{u} \sum_{k=1}^{K} a_k \, \delta(u - u_k), \tag{12}$$

where δ is the unit impulse function and K is the number of impulse functions used. Application of (11) to (12) gives

$$\epsilon_n = 2 \frac{N}{\pi} \sum_{k=1}^{K} a_k \frac{\sin \frac{n}{2} u_k}{u_k}. \tag{13}$$

The number of sidelobes that can be reduced by this method, as well as the amount of sidelobe reduction, is restricted by the condition that all $\epsilon_n u$ are assumed small in the derivation, at least over the range for which the correction is desired. The check on the validity of this assumption, and also the choice of a_k, are best made by trial.

In the design of large arrays, some time can be saved by reducing a number of sidelobes simultaneously, and then adding additional correction later if necessary. In the uniform array pattern the sidelobe maxima are positioned approximately at

$$u_k = \frac{\pi}{N} (2k + 1). \tag{14}$$

Hence, (14) gives the positions of the necessary impulse functions. Also, the sidelobes adjacent to the main lobe drop off as $1/u$, so the a_k of (13) can be assumed to behave in this manner. Then (12) becomes

$$\frac{E_u - E}{u} \approx A \frac{1}{u^2} \sum_{k=1}^{K} (-1)^k \, \delta \left[u - \frac{\pi}{N} (2k + 1) \right], \tag{15}$$

where A determines the amount of correction to be applied. Similarly, (13) becomes

$$\epsilon_n = 2A \left(\frac{N}{\pi} \right)^3 \sum_{k=1}^{K} (-1)^k \frac{\sin \frac{n\pi}{2N} (2k + 1)}{(2k + 1)^2}. \tag{16}$$

Both K (number of sidelobes reduced) and A (amount of reduction) are restricted by the assumption of smallness of $\epsilon_n u$. Again the final restriction on A and K should be found by trial. Experience has shown that sidelobes can be reduced to the level of those of E_u in the vicinity of $u = \pi/2$. At $u = \pi/2$ the sidelobe level of E_u is about $2/N$ times the main lobe level.

Reducing the sidelobe level in the region $u < \pi/2$ has but little effect in the region $\pi/2 < u < \pi$. However, in the region $\pi < u$, the sidelobes tend to become large. Fig. 5 shows the field pattern for the final 12-element nonuniform array designed above, carried out to $u = 2\pi$. All lobes are shown positive, as is conventional for field patterns. Note that the "grating lobe" that the uniform array would have at $u = 2\pi$ is absent from the nonuniform array pattern. This is the effect in which King, *et al.*, were interested.[4]

The reason for higher sidelobes in the region $u > \pi$ is evident from (9). The uniform array pattern E_u has odd or even symmetry about $u = \pi$, according as the number of elements N is even or odd, respectively. The corrective term of (10) is even about $u = \pi$ when E_u is odd (N even), and vice versa. Hence, from (9) it follows that a small decrease in a lobe at some $u = u_k < \pi$, results in a larger *increase* in the corresponding lobe at $u = 2\pi - u_k$. Hence, by decreasing sidelobe levels $u < \pi$, one necessarily increases them in the region $u > \pi$.

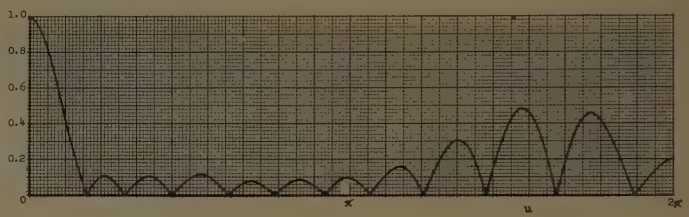

Fig. 5—The final 12-element nonuniform array pattern for $0 < u < 2\pi$. The ϵ_n are given in Fig. 4(b).

IV. Additional Examples

To further illustrate the method a 24-element array was considered. The uniform array pattern is shown in Fig. 6(a). The first four sidelobes were then simultaneously reduced, using (16). The result is shown in Fig. 6(b), and the necessary fractional changes in element positions are given in Table I. Note that the second sidelobe is higher than the others. This is a general characteristic of the method, and is due to the shift in position of this lobe toward the main lobe. To further correct the second sidelobe, an additional impulse function was added at the new second sidelobe position. The resultant field pattern is shown in Fig. 6(c), and the necessary fractional changes in element positions are given in Table II. Note that the sidelobe level is now down about 22 db from the main lobe, which agrees with the previous estimate of 20 log $2/N$.

To give a clearer picture of the character of the shift in position of the elements, Fig. 7 shows scale plots of the element positions for both the uniform array, Fig. 6(a), and the final nonuniform array, Fig. 6(c). Note that the elements are first shifted closer together, and then farther apart as one proceeds outward from the array center. This appears to be generally true, regardless of the number of elements. Fig. 6(d) shows the pattern for the same array in the range $\pi < u < 2\pi$.

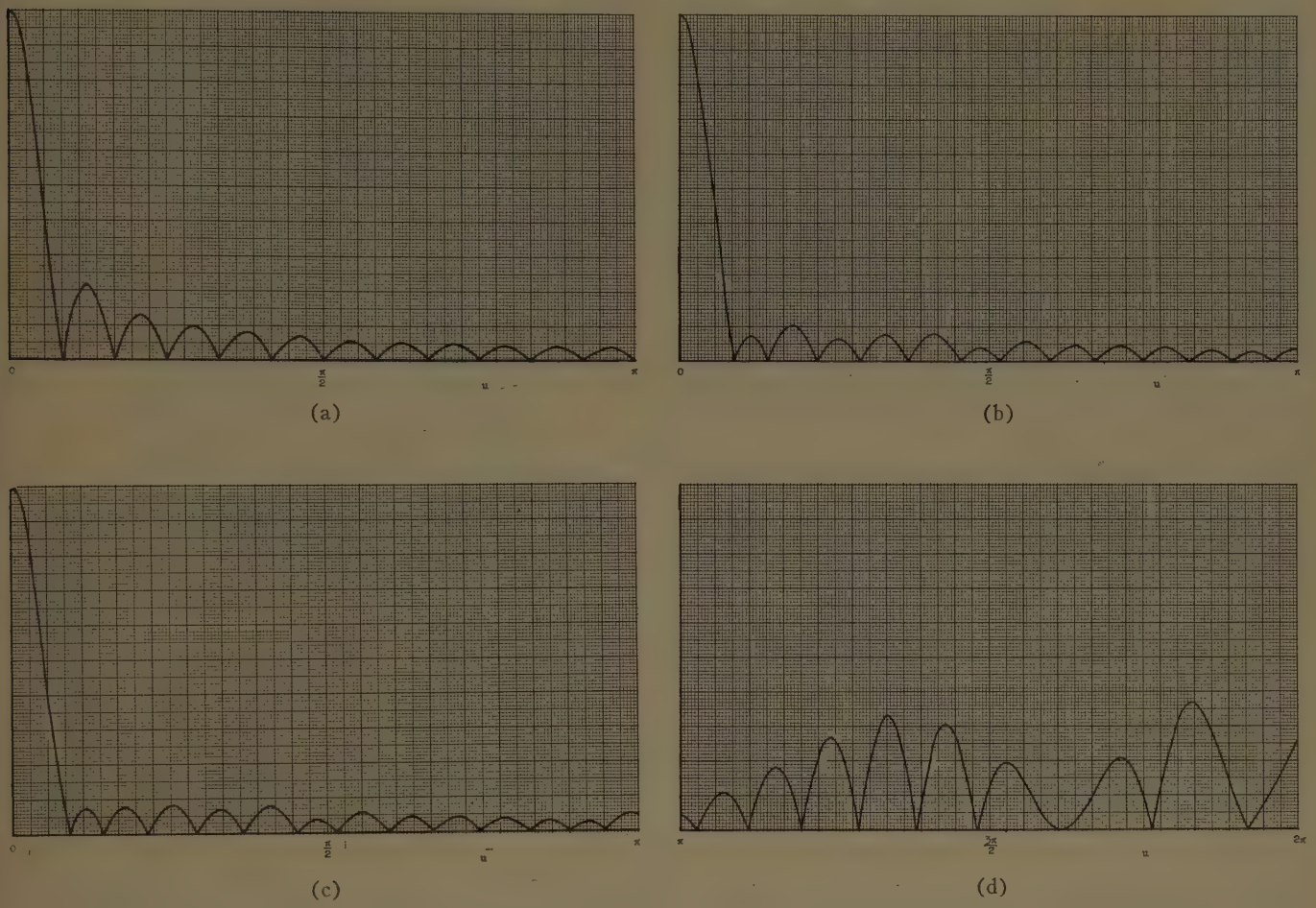

Fig. 6—(a) 24-element uniform array pattern. (b) The nonuniform array pattern obtained by simultaneously reducing the first four sidelobes. (c) Further reduction of the second sidelobe. (d) The pattern of (c) in the range $\pi < u < 2\pi$.

TABLE I

ϵ_n's FOR THE ARRAY OF FIG. 6(B)

n	1	3	5	7	9	11	13	15	17	19	21	23
ϵ_n	−0.077	−0.255	−0.457	−0.615	−0.662	−0.613	−0.552	−0.457	−0.223	+0.234	+0.813	+1.230

TABLE II

ϵ_n's FOR THE ARRAY OF FIG. 6(C)

n	1	3	5	7	9	11	13	15	17	19	21	23
ϵ_n	−0.048	−0.176	−0.354	−0.518	−0.603	−0.616	−0.622	−0.541	−0.328	+0.153	+0.780	+1.253

Fig. 7—Comparison of (a) uniform element spacing, which gives Fig. 6(a), with (b) nonuniform element spacing, which gives Figs. 6(c) and (d).

The amount of sidelobe reduction attainable by this method is still larger for end-fire arrays under the so-called "increased directivity" condition.[6] In this case the progressive phase shift between elements, given by (1), is made even greater than under ordinary end-fire conditions. In particular, an additional phase shift equal to $2.94/N$ is added to the phase shift needed for end-fire operation. In this case the point $u=0$ is never reached, and the main beam is lower in proportion to the sidelobes. Fig. 8(a) shows a uniform 24-element array pattern under the increased directivity condition. The first sidelobe is down less than 10 db from the main lobe. Fig. 8(b) shows the pattern of the nonuniform array of Fig. 7(b) under increased directivity conditions. All sidelobes are now down more than 18 db from the main lobe. While the array of Fig. 7(a) is close to the maximum end-fire directivity for uniform arrays, it is evident that even higher directivity could be obtained from the nonuniform array by further increasing the progressive phase shift.

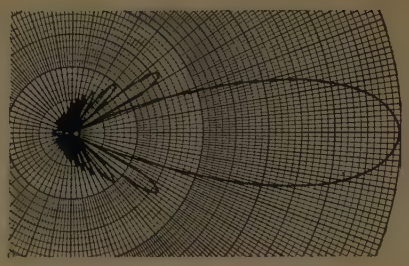

(a)

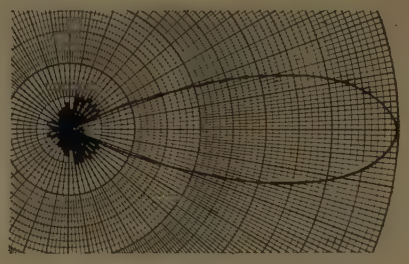

(b)

Fig. 8—Illustration of sidelobe reduction under the increased directivity condition. (a) Uniform array pattern. (b) Nonuniform array pattern.

V. Discussion

The above procedure for reducing sidelobe levels is relatively simple. Element positions can be calculated quite quickly by computers, even for large arrays. There are no simultaneous equations to solve, as is characteristic of other methods.[3] Also, control of the pattern at specific points is attained by the above method. The final patterns are, however, not optimum in the sense that Tchebycheff patterns are.[2] It appears unlikely that a simple optimization procedure can be devised for nonuniform arrays because of the nonlinear character of the basic equations with respect to element position. More work might be done along this line.

The amount of reduction in sidelobe level attainable is quite significant, especially for large arrays. The implementation of nonuniform element spacing in practice is often simpler than the commonly employed amplitude tapering. Also, the high-power capabilities of an array having all elements fed equally are better than when amplitude tapering is used. It appears that serious consideration should be given to sidelobe reduction by nonuniform element spacing whenever large arrays are designed.

[6] *Ibid.*, p. 81. Also, W. W. Hansen and J. R. Woodyard, "A new principle in directional antenna design," Proc. IRE, vol. 26, pp. 333–345; March, 1938.

CORRECTION

R. C. Hansen, author of "Gain Limitations of Large Antennas," which appeared on pages 490–495 of the September, 1960, issue of these Transactions, has called the following correction to the attention of the *Editor*.

In column 1, p. 495, formula 20,

$$F(u) = \frac{J_\gamma(\pi\sqrt{u^2 - C^2})}{[\pi\sqrt{u^2 - C^2}]^2},$$

should read

$$F(u) = \frac{J_\gamma(\pi\sqrt{u^2 - C^2})}{[\pi\sqrt{u^2 - C^2}]^\gamma}.$$

Photoconductive Modulation of Microwave Electric Fields*

W. E. BULMAN†, SENIOR MEMBER, IRE, B. C. POTTS‡, MEMBER, IRE, AND R. B. GREEN‡

Summary—**Thin films and coatings of photoconductive cadmium sulfide material are being used to modulate electric fields. This paper analyzes these films in terms of the physics involved and the effect upon microwave fields. Experimental procedures show the validity of the analyses and indicate possible applications of the principle. Practical significance of the technique is illustrated by experimentally determining the areas of a particular flat plate that produce the first sidelobe of the scattering pattern.**

Introduction

CERTAIN materials are known to yield substantial changes in conductivity upon irradiation by light of sufficiently small wavelength. This mechanism offers a method for producing periodic variations of the conductivity which leads to a modulation of the diffraction field when an electric field is incident upon the material. Such modulation has proven useful in microwave scattering measurements.

The principal use, to date, of photoconductive modulation has been that of modulating the energy being scattered from a small area of an object. The purpose, of course, is to "code" the scattered energy from the given area so that, in conjunction with a proper detection system, the contribution of the given area to the over-all scattering pattern of the object may be determined.

In general, thin films are used in practical measurements, as described above, so that the incident field is only slightly perturbed by the presence of the photoconductive modulator. The thin films, as small panels, have been analyzed by utilizing the concept of polarization currents to determine the problems involved in using the photoconductive modulator and the radiation patterns of the panels.

Experimental results of using photoconductive modulator panels have verified theoretical results as to the properties of the panels. Furthermore, the application of the photoconductive materials as coatings has led to some interesting results which indicate that the coatings may be of most practical interest in the future.

Phenomenological Theory

Photoconductivity is the increase in the electrical conductivity of a material caused by incident radiation. The effect is observable to some degree in almost all semiconductors and insulators. The direct effect of the radiation is to increase the number of mobile, or free, carriers in the material. The additional carriers then represent a change in conductivity. Upon removing the radiation, the carrier concentration will return to its equilibrium value in a period of time which varies from material to material and with the level of radiation. Although this, in general, explains the process, the phenomenon involved deserves to be treated in more detail.

If a photon is absorbed in a crystal of material it may have a high probability of producing a hole-electron pair, provided its energy $hf \geq E_g$; where h is Planck's constant, f is the frequency, and E_g is the energy gap between the valence and conduction bands. Both the hole and the electron will contribute to the conductivity until they combine with each other. The rate of change of electron concentration, n, for a uniform crystal is given by [1]

$$\frac{dn}{dt} = L - Anp = L - An^2, \tag{1}$$

where L is the number of photons absorbed per unit volume per unit time, A is the recombination coefficient, and p is the number of holes per unit volume. If we assume $n \simeq 0$ when $t = 0$, then from (1)

$$n = \sqrt{\frac{L}{A}} \tanh (\sqrt{LA}\, t) \tag{2}$$

now as $t \to \infty$, $n \to \sqrt{L/A}$.

If the light is suddenly removed at $t = T$, the decay of the added carrier concentration may be described by

$$n_0 = \frac{n_0}{1 + An_0(t - T)}, \tag{3}$$

where n_0 is the concentration of carriers at $t = T$.

It is important to note that material models with carrier trapping centers and with concentrations of impurities are not treated here in order to explain detailed photoconductive behavior. For our purpose it is sufficient to point out that the photoconductive mechanism provides a method by which the concentration of charge carriers can be altered significantly in a repetitive manner. This point of view is justified if the light intensities used cause the rate of excitation to be so high that these minor phenomena have little effect upon the maximum carrier density.

With the variation in the number of carriers considered, we can proceed to account for the change in σ, the conductivity, as a function of $N = n$.

The general case of conductivity may be illustrated by means of a calculation involving the free electron

* Received by the PGAP, January 12, 1960; revised manuscript received, July 13, 1960. This research was supported by the U. S. Air Force under Contract AF 33(616)-5341, in cooperation with the Wright Air Development Center of the Air Research and Development Command.

† Ohio Semiconductors, Inc., Columbus, Ohio.
‡ Antenna Lab., The Ohio State University, Columbus, Ohio.

when subjected to a time-dependent electric field. The net effect of collisions with the crystal lattice may be regarded as a damping force on the electronic motion. The equation of motion for such an electron then becomes[1]

$$m\frac{d^2\bar{r}}{dt^2}+\frac{m}{\tau}\frac{d\bar{r}}{dt}=e\bar{E}e^{-j\omega t}, \tag{4}$$

where

m = mass of the electron,
$\bar{r}$ = electronic displacement vector,
τ = time between scattering collisions,
e = electronic charge, and
$\bar{E}$ = electric field vector.

In the usual manner, a solution of the form $\bar{r}=\bar{A}e^{-j\omega t}$ is assumed.

In order to consider the current density, it is necessary to evaluate the electronic velocity, $v=d\bar{r}/dt$, and one finds

$$\bar{v}=\frac{d\bar{r}}{dt}=\frac{e\bar{E}}{m\tau\left(\omega^2+\frac{1}{\tau^2}\right)}+\frac{j\omega e\bar{E}}{m\left(\omega^2+\frac{1}{\tau^2}\right)}. \tag{5}$$

The current density is defined as the flow of charge per unit time through a unit area, $\bar{J}=Ne\bar{v}$; so now, by comparison with the definition of conductivity, $\bar{J}=\sigma\bar{E}$, and (5),

$$\sigma=\frac{Ne^2}{m\left(\omega^2+\frac{1}{\tau^2}\right)}\left\{\frac{1}{\tau}+j\omega\right\}. \tag{6}$$

Whether the real or imaginary part of the conductivity is dominant at a particular frequency depends on the relative value of ω and τ. In the case of cadmium sulfide, which is of primary interest in the experimental investigations covered by this paper, calculations based on a value of carrier mobility reported by Reynolds [2] yield a value of $\tau=2.8\times10^{-14}$ seconds. Now referring to (6), it can be seen that at $f=10$ kMc, $1/\tau\gg\omega$. Thus, at X band frequencies the electromagnetic conductivity of CdS is essentially real and may be represented by

$$\sigma=\frac{Ne^2\tau}{m}. \tag{7}$$

We have shown that as the excitation L varies, $N=n$ varies accordingly by (2) and (3), and the conductivity then varies as shown in (7). If we generalize the dielectric constant of the photoconductive material, we may write a complex dielectric constant

$$\epsilon^*=\epsilon+\frac{\sigma}{j\omega}=\epsilon\left(1-j\frac{\sigma}{\omega\epsilon}\right), \tag{8}$$

where ϵ is the real dielectric constant of the material. Thus, as σ is varied the imaginary part of the complex dielectric constant will change correspondingly.

On the basis of (2), (3), (7), and (8), we can theoretically predict that a periodic variation in the intensity of a light beam which impinges on a cadmium sulfide layer will produce a corresponding periodic variation in the complex dielectric constant, ϵ_1^*, of the layer.

Characteristics of Practical Materials

While the phenomenological theory of the photoconductor shows that modulation of microwaves is possible, experimental determination of the necessary conditions under which the photoconductive material should be operated is essential. The main difficulty is that single crystals of photoconductive materials are not generally available in practical sizes; thus, powders mixed in a resin matrix material are usually used. In preliminary studies, waveguide measurements were made on cadmium sulfide, lead sulfide, zinc sulfide, and silicon. While some effect was obtained in most cases, large changes in the microwave properties of cadmium sulfide at visible light frequencies resulted in the selection of this material for initial experiments.

The results of a 10.0-kMc RF transmission through a 4-inch square panel of cadmium sulfide as a function of light intensity are shown in Fig. 1 for the static case, *i.e.*, no light modulation. The panel used in this case consisted of a 0.007-inch layer of cadmium sulfide upon a 0.009-inch plastic sheet. The results of Fig. 1 show that a large nonlinear change in transmission occurred with increasing light intensity for low illumination. This nonlinear relationship was probably due to the presence of trapping levels in the cadmium sulfide. At higher light intensities, the transmission change became linear with light intensity, as expected from considerations of simple intrinsic photoconductors.

To determine the effect of the decay times associated with photoconductive cadmium sulfide, an experiment was performed using various light-modulation frequencies in the test arrangement of Fig. 2. The relative amplitude of the light modulation is shown in Fig. 3 as a function of frequency from 10 to 400 cps. From Fig. 3 it is apparent that in using this material, light-modulation frequencies of less than 30 cps should be used. Other materials which could be used at higher modulation frequencies had relatively low changes in microwave characteristics as a function of light intensity.

[1] For a similar development see J. A. Stratton, "Electromagnetic Theory," McGraw-Hill Book Co., Inc., New York, N. Y., p. 326; 1941.

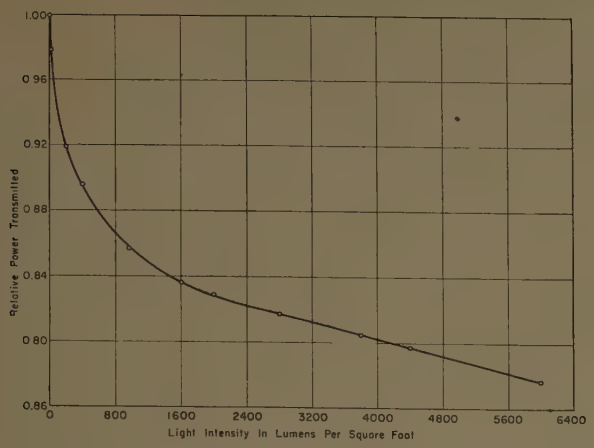

Fig. 1—10-kMc RF transmission through a 4-inch square panel coated with F2103 cadmium sulfide, as a function of light intensity.

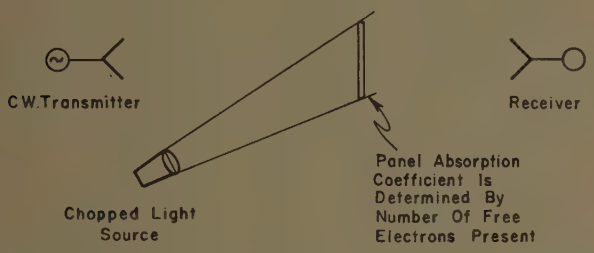

Fig. 2—Experimental arrangement for transmission studies.

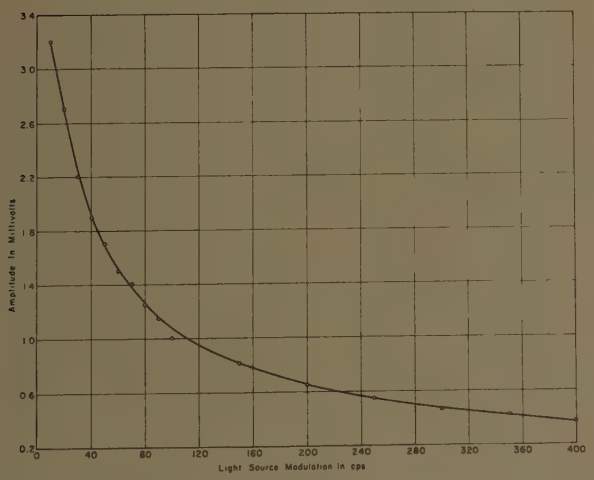

Fig. 3—Dependence of 10-kMc transmission characteristics of F2103 cadmium sulfide upon light-modulation frequency.

Volume Polarization Currents

To apply the above discussion to an analysis of the panel, the concept of polarization currents is used. A general discussion of this concept has been given by Rhodes [3] and the results will be reviewed here.

The total electric field $\boldsymbol{E}^t$ in the vicinity of a scattering object is given by the sum of the incident field $\boldsymbol{E}^i$ and the scattered field $\boldsymbol{E}^s$. Maxwell's equations in the object are:

$$\nabla \times \boldsymbol{E}^t = -j\omega\mu \boldsymbol{H}^t, \tag{9}$$

$$\nabla \times \boldsymbol{H}^t = j\omega\epsilon_1^* \boldsymbol{E}^t = j\omega\epsilon_0 \boldsymbol{E}^t + j\omega(\epsilon_1^* - \epsilon_0)\boldsymbol{E}^t, \tag{10}$$

where ϵ_1^* is the complex dielectric constant of the object. The term $j\omega(\epsilon_1^* - \epsilon_0)E^t$ is called the polarization current.

The scattered field $\boldsymbol{E}^s$ at any point may be obtained in terms of the polarization current as

$$\boldsymbol{E}^s = \frac{\epsilon_1^* - \epsilon_0}{4\pi\epsilon_0}\left[\omega^2\mu\epsilon_0 \int_V \boldsymbol{E}^{t'}\psi dv' + \int_S (\boldsymbol{n}\cdot\boldsymbol{E}^{t'})\nabla'\psi ds'\right], \tag{11}$$

where

$$\psi = \frac{e^{-j\beta_0 r}}{r},$$

r = distance from a point in the scatterer to a point P in space, and equaling

$$\sqrt{(x-x')^2 + (y-y')^2 + (z-z')^2},$$

β_0 = phase constant of free space $(2\pi/\lambda_0) = \omega\sqrt{\epsilon\mu}$, and
$\boldsymbol{n}$ = outward pointing normal.

The primes indicate operations with respect to the coordinates of integration, and Fig. 4 shows the geometry involved.

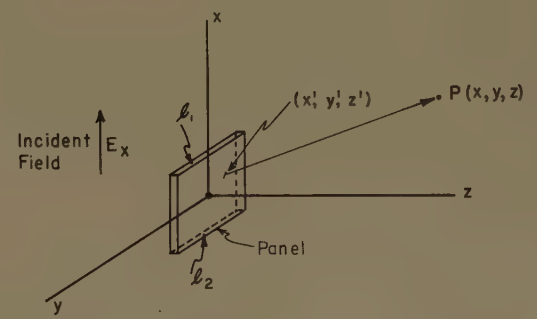

Fig. 4—Geometry for radiation from panel in terms of volume polarization currents.

For the low percentage modulation usually involved, the scattered field within the panel will be small compared to the incident field; this makes $E^t \sim E^i$ within the panel. Furthermore, for thin panels E^i is constant in the x direction within the panel and the volume integral may be replaced by a surface integral, and the surface integral by a line integral.

Using the approximations above, the scattered field becomes

$$\boldsymbol{E}^s = \frac{(\epsilon_1^* - \epsilon_0)}{4\pi\epsilon_0} tE^i\left[\beta^2\hat{x}\int_S \psi ds + \int_{l_1} \nabla'\psi dl - \int_{l_2} \nabla'\psi dl\right]. \tag{12}$$

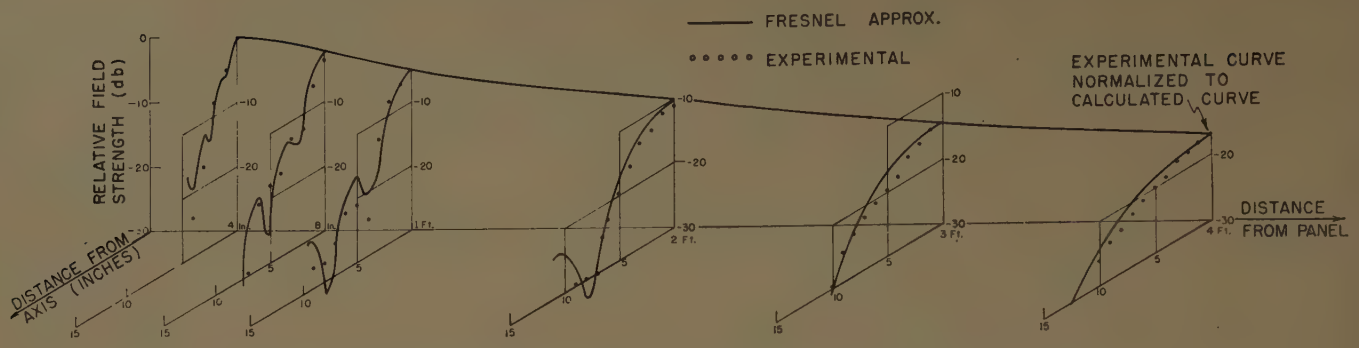

Fig. 5—Magnitude variation of the radiation pattern for a 4-inch square panel at 9.3 kMc.

It is apparent that the scattered field will contain a modulated portion when ϵ_1^* is modulated. If one solves for the E_x component of the field in the plane $x=0$, the following approximation may be obtained:

$$E_x \approx \frac{(\epsilon_1^* - \epsilon_0)tE^i\beta^2}{4\pi\epsilon_0}\left[\int_{-l/2}^{l/2}\int_{-l/2}^{l/2}\psi dx'dy'\right]. \quad (13)$$

Evaluation of the Radiation Integrals

By means of approximation, the integrands of the radiation integrals were reduced to $e^{-i\beta r}/r$. Integrals of this type may be evaluated approximately to varying degrees of accuracy by rather well-established methods [4]. By writing them in the form of Fresnel integrals, the calculated pattern of Fig. 5 was obtained. This is compared with experimental results obtained by probing behind a 4-inch square thin panel of cadmium sulfide material. As can be seen, there is good agreement between calculated and experimental results.

Experimental Determination of the Modulation Mechanism

The most direct method of determining the on-axis scattered field predicted by the polarization current analysis of the thin photoconductive panel is to measure the modulated component of the field from the front and back side of a panel, as shown in Fig. 6. The results of probing at the same spacing in front of and in back of the panel are shown in Fig. 7. These results indicate that the panel "radiates" equally in both directions as a result of the modulated polarization-current. Variations between the two patterns of Fig. 7 are probably due to the disturbance of the incident field by the probe horn.

Another measurement technique which eliminates the perturbation of the field by the horn may be used to justify the uniform polarization-current approach to the thin photoconductive panel. This method makes use of the standing-wave effect next to a flat conductor, as shown in Fig. 8.

Now if one assumes volume polarization currents, the radiated fields depend on panel excitation. Since the modulated components of the total or exciting field with the panel present are small compared to the unmodulated incident field, only excitation caused by the total unmodulated field need be considered. Restricting the discussion to panel-plate spacings d of less than $\lambda/2$, the excitation is given by $-2E_0 \sin 2\pi d/\lambda \sin \omega t$. The quantity $2E_0 \sin 2\pi d/\lambda$ gives the usual standing-wave magnitude caused by an incident wave E_0. The time dependence $-\sin \omega t$ is found from the fact that within the spacings considered, the phase of the standing wave is essentially constant and leads the phase of the incident field at the plate ($\cos \omega t$) by 90°.

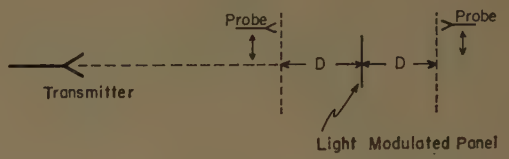

Fig. 6—Method of determining the radiation field of a photoconductive panel.

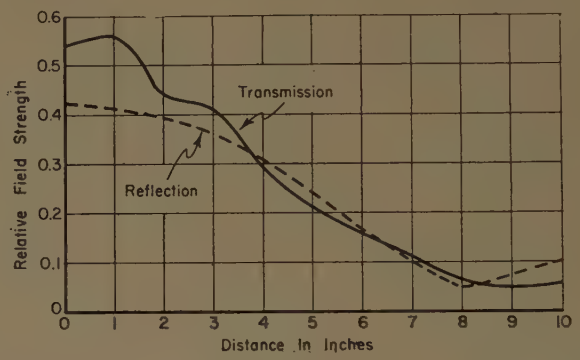

Fig. 7—The modulated fields of a 4-inch square photoconductive panel measured in parallel planes two feet on each side of the panel.

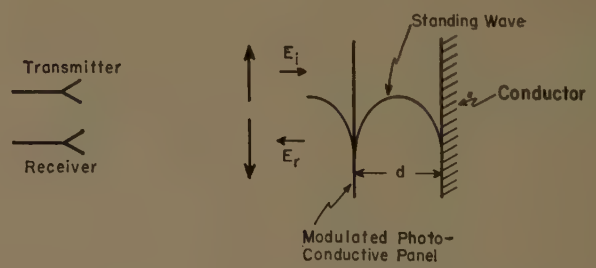

Fig. 8—Effect of standing wave on panel excitation.

The panel hypothetically "radiates" with equal intensity in both directions. Thus, the total field to the left of the panel is made up of the direct "radiation" to the left plus a reflected component related in phase by $(180° - 4\pi d/\lambda)$. The total field produced by the uniform volume polarization currents is then

$$E = -2\delta E_0 m(t) \sin\frac{2\pi d}{\lambda}\left[\sin' \omega t - \sin\left(\omega t - \frac{4\pi d}{\lambda}\right)\right] \quad (14)$$

where

δ = "radiation" efficiency,
$m(t)$ = modulation function, and
E_0 = magnitude of the incident field.

An experiment to determine if (14) does yield the correct result was conducted. The method used was to transmit an unmodulated field normal to a large flat plate, setting up a standing wave. The modulated panel was then moved various distances from the plate in the standing wave. At each distance the relative magnitude of the modulated component of the received field was recorded. The results are shown in Fig. 9 along with those calculated by (14). These results verify that the uniform polarization current approach to the thin photoconductive panel is valid.

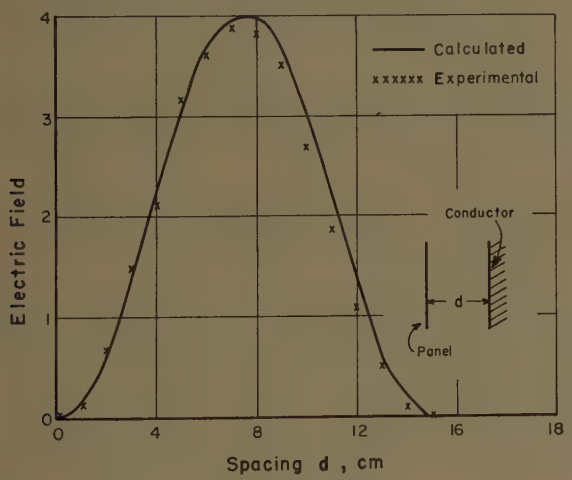

Fig. 9—Radiation field of panel.

The Modulated Window Technique

Pittman [5] investigated a modulated window technique which would modulate the incident electric field on small areas of a scattering body. Bulman [6] however, conceived the photoconductive film using cadmium sulfide that has been used successfully in this application. The methods of preparing these cadmium sulfide panels have been described by Crawford [7].

As described previously, the principle of the photoconductive modulated window is that it will "radiate" a modulated component proportional to the amplitude of the total field in the plane of the panel. When the panel is positioned relatively close to a complex scattering object and the object is illuminated by a plane wave, the signal detected at any aspect will consist of two components. Because the thin panel does not disturb the incident field appreciably, there is a large unmodulated component, and there is also a small modulated component "radiated" by the panel. If the two components are mixed in a crystal detector, which squares the sum of the two components, and the crystal output is fed through a selective amplifier, then the output of the amplifier can be shown to be

$$V_0 = kE_m E_u m(t) \cos\theta, \quad (15)$$

where

k = over-all gain constant,
E_m = magnitude of the modulated signal,
E_u = magnitude of the unmodulated signal,
$m(t)$ = modulation function, and
θ = phase difference between the modulated and modulated carriers.

The detected signal V_0 of (15) is actually of no value since the output of interest should be independent of the erratic E_u and θ for various aspects and yet proportional to $E_m m(t)$, which carries the amplitude information at the position of the panel. However, a method described by Richmond [8] substitutes a known reference signal for the unmodulated carrier, thus allowing E_u and θ to be controlled quite accurately. In this case, E_u may be treated as a constant and θ can be controlled by a phase shifter.

In preliminary applications of the photoconductive panel as a modulating window, the panel was moved across the scatterer in order to note the major scattering areas on complex objects for a given aspect. Many problems had to be solved before reliable data were obtained: methods of eliminating the direct "radiation" from the panel, for example, had to be affected; methods of resetting phase for each movement of the panel had to be eliminated; and, the resolving power of the panel had to be studied. The methods of solving these problems are the subject of another paper, and, in general, are still being studied and improved. The basic result to note, however, is that it is possible to modulate small portions of the total field surrounding a scattering object so that a more detailed picture of the scattering can be obtained, even though the detection problems involved require special instrumentation.

Photoconductive Coatings in Microwave Measurement

Although (14) predicts that no modulated component of the scattered field will exist when the modulated panel is placed directly in contact with a conducting object, photoconductive materials mixed with Eccofoam layers have been successfully employed as modulators when the target is directly coated with the ma-

terial. The basic difference is that with thick coatings, the volume polarization currents are no longer uniform. Certainly, such direct coatings disturb the normal scattered field from the object of interest, but experimental procedures will determine most readily the effect the coating will have on various shapes of scatterers.

To illustrate the use of the photoconductive modulator technique, an experiment involving the scattering from a flat plate is described. The conducting flat plate, 4.5 inches square, was coated with a quarter-wavelength thick, 4.8-inch square, coating of cadmium sulfide mixed in Eccofoam. The coating was covered with black paper masks which exposed the photoconductive coating only in certain areas, as shown in Fig. 10. For each masking condition, a scattering pattern of the flat plate was taken with the receiver at a bistatic angle of 30° and using a 30-cps modulation of the light source impinging on the panel. Noting the detection system was only sensitive to the modulated component of the scattered field, the magnitude of this return for each of the four conditions is also found in Fig. 10.

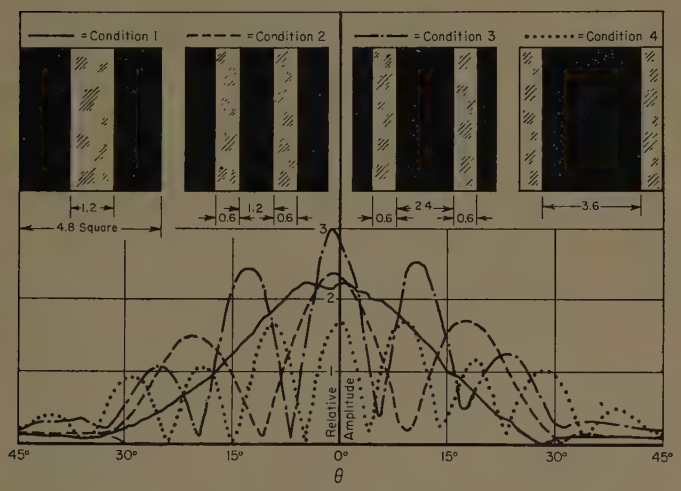

Fig. 10—Modulated scattering pattern of a flat plate when various areas are masked off from modulated light.

The real and imaginary part of the field was recorded for each condition at all angles of rotation of the flat plate. The four patterns corresponding to each condition were added vectorially and compared to the over-all scattering from the coated flat plate. The results are shown in Fig. 11, and they indicate that the scattering from the flat plate has been successfully attributed to four subareas. The results indicate that the scattering from the flat plate may be studied by breaking the total reflecting area down into any set of arbitrary subareas by the light modulation technique.

To illustrate the practical value of the above conclusion, the problem of sidelobe suppression for the flat plate is studied. By comparing the scattering contributions of the various conditions of Fig. 10 to the over-all scattering pattern of Fig. 11, it was noted that the so-called condition 3 made a very large contribution to the first sidelobe. Upon mathematically eliminating the contribution of this condition to the over-all scattering pattern, the pattern was altered to that of Fig. 12, where it is compared to the original pattern. Fig. 12 shows that the first sidelobe was reduced 7.2 db by destroying the scattering from the areas involved in condition 3.

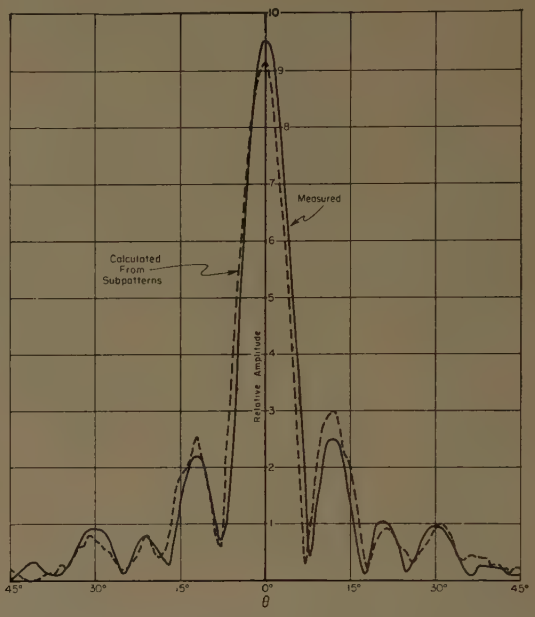

Fig. 11—Comparison of the measured scattering from a flat plate with that calculated from subpatterns as shown in Fig. 10.

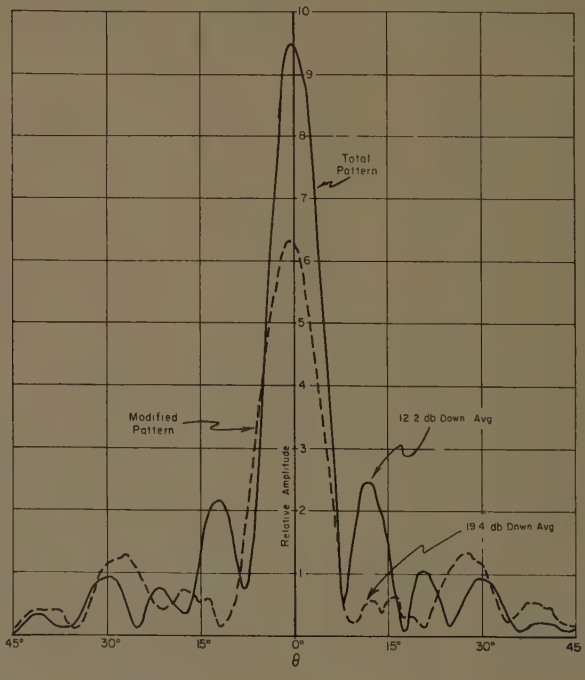

Fig. 12—Scattering pattern (bistatic angle 30°) of the flat plate with the field of condition 3 removed from the original pattern.

Conclusions

Photoconductive materials may be used to provide a medium for the interaction of visible or near-visible light frequencies and microwave electric fields. The applications of this principle are virtually unexploited, but photoconduction at microwave frequencies has been utilized successfully for amplitude modulators.

The concept of volume polarization currents for thin films of photoconductive materials allows for easy evaluation of the "radiation" patterns of the films when exposed to incident microwave radiation. With the patterns of the modulators known, the application of the thin photoconductive panels to the partial modulation of a scattered field for an object of interest may be analyzed.

The use of photoconductive modulators at the target creates a unique detection problem: discrimination between the modulated and the unmodulated scattering. This is generally accomplished, however, rather simply with a coherent detection system.

The results of measuring the scattering from a flat plate in four subpatterns illustrates that possibly many objects may be analyzed in detail by applying photoconductive coatings to the objects. This is possible because the scattering from the areas of the object that are illuminated with a modulated light will be "coded" and may be studied separately or in comparison to the scattering from the entire reflecting object.

Bibliography

[1] C. Kittel, "Introduction to Solid State Physics," John Wiley and Sons, Inc., New York, N. Y., 2nd ed., pp. 513–514; 1956.
[2] D. C. Reynolds, private communication.
[3] D. R. Rhodes, "An Investigation of Pulsed Radar Systems for Model Measurements," Antenna Lab., The Ohio State University, Columbus, Rept. No. 475–6; December, 1953.
[4] A. Hund, "Short Wave Radiation Phenomena," McGraw-Hill Book Co., Inc., New York, N. Y., vol. 2; 1952.
[5] C. W. Pittman, "A Modulating Window Technique for the Measurement of the Microwave Scattering from Complex Objects," Antenna Lab., The Ohio State University, Columbus, Rept. No. 777-3; June 1, 1958.
[6] W. E. Bulman, "Utilization of Photoconductivity in Electromagnetics," Antenna Lab., The Ohio State University, Columbus, Rept. No. 777-6; November 30, 1958.
[7] R. W. Crawford, "Memorandum on the Preparation of a Uniform, Thin, Cadmium Sulfide Panel," Antenna Lab., The Ohio State University, Columbus, Rept. No., 777–10; February 20, 1959.
[8] J. H. Richmond, "A modulated scattering technique for measurement of field distributions," IRE Trans. on Microwave Theory and Techniques, vol. MTT-3, pp. 13–15; July, 1955.
[9] W. E. Bulman, "Modulation of the Plane Wave Reflection Coefficient of a Semi-Infinite Dielectric Sheet Through Induced Conductivity," Antenna Lab., The Ohio State University Res. Foundation, Columbus, Rept. No. 777-2; May 1, 1958.
[10] R. Green, "Flare Spot Determination by Use of Photoconductive Panels," Antenna Lab., The Ohio State University Res. Foundation, Columbus, Rept. No. 777-14; May 31, 1959.
[11] B. Potts, "A Light-Modulated Panel Technique for Measuring Microwave Near-Fields," Antenna Lab., The Ohio State University Res. Foundation, Columbus, Rept. No. 777-16; July 31, 1959.
[12] Summary Engrg. Rept. Antenna Lab., The Ohio State University Res. Foundation, Columbus, Rept. No. 777–18; November 1, 1959.

Diffraction of a Plane Wave by an Infinite Slit in a Unidirectionally Conducting Screen*

S. R. SESHADRI†

Summary—**The scattering of a plane electromagnetic wave of wave number k, by an infinite slit (of width $2a$) formed by two unidirectionally conducting, semi-infinite coplanar screens of zero thickness is considered. By employing an integral equation procedure, a rigorous asymptotic solution is obtained up to order $(ka)^{-5/2}$. The currents induced on the screens and the first few terms in the transmission coefficient are evaluated. The similarity between this and the corresponding problem involving perfectly conducting screens is pointed out.**

* Received by the PGAP, January 23, 1960; revised manuscript received, November 25, 1960. This work was supported by Harvard University, Cambridge, Mass.

† Electronics Res. and Dev. Establishment, Bangalore, India. Formerly with Gordon McKay Lab., Harvard University, Cambridge, Mass.

Introduction

THE problem of diffraction of a plane electromagnetic wave by an infinite slit formed by two semi-infinite coplanar screens of zero thickness has been the subject of numerous past investigations, in all of which the screens are assumed to be perfectly conducting. In recent times interest has arisen in the study of diffraction by screens which are composed of fine parallel wires. Such a screen has been idealized by an infinitely thin disk which is perfectly conducting in one direction.

Toraldo di Francia[1] has studied the problem of diffraction of a plane wave by a small circular disk composed of fine parallel wires. Karp[2] has obtained closed form expressions for the electromagnetic field produced by the diffraction of a plane wave by a semi-infinite unidirectionally conducting half-plane. Radlow,[3] on the other hand, has treated the problem of a unidirectionally conducting half-plane for the incidence of a dipole field. The author has re-examined the diffraction of a plane wave by a unidirectionally conducting half-plane—the same problem that has been treated by Karp—by employing an integral equation procedure. The result of that study revealed the possibility of successfully using similar methods in obtaining rigorous solutions to the problems of diffraction by unidirectionally conducting planar obstacles possessing simple geometry. In this paper, diffraction by an infinite slit in a unidirectionally conducting screen is investigated by formulating it in terms of a Wiener-Hopf integral equation. Rigorous asymptotic solution of the integral equation is obtained by a method which is essentially the same as that first devised by Levine and Wu[4] in connection with their investigation of the problem of diffraction by a circular aperture.

Integral Equation Formulation of the Problem

The infinite slit is formed by two unidirectionally conducting semi-infinite screens $S_1(x<-a,\ -\infty<y<\infty,\ z=0)$ and $S_2(x>a,\ -\infty<y<\infty,\ z=0)$ where x, y, z form a right-handed rectangular coordinate system. It is convenient to introduce also a rotated system of coordinates ξ, η, z where

$$\begin{aligned}\xi &= x\cos\alpha + y\sin\alpha\\ \eta &= -x\sin\alpha + y\cos\alpha.\end{aligned}\tag{1}$$

The screen is assumed to be conducting in the direction ξ only. A plane electromagnetic wave

$$\begin{aligned}\boldsymbol{E}^i(\boldsymbol{r}) &= \boldsymbol{B}\exp\left[ik\hat{k}\cdot\boldsymbol{r}\right] = \boldsymbol{B}\exp\left[ik(l\hat{x}+m\hat{y}+n\hat{z})\cdot\boldsymbol{r}\right]\\ \boldsymbol{H}^i(\boldsymbol{r}) &= \hat{k}\times\boldsymbol{B}\exp\left[ik\hat{k}\cdot\boldsymbol{r}\right]\end{aligned}\tag{2}$$

is incident on the screen in the half-space $z<0$. $\boldsymbol{r}$ denotes the position vector of a point $P(x, y, z)$ in space. The direction of propagation of the incident wave is given by its direction cosines l, m and n. $\boldsymbol{B}$ is a prescribed constant vector, which, on account of the divergence relation, is subject to the condition

$$\boldsymbol{B}\cdot\hat{k} = 0\tag{3}$$

The harmonic time dependence $e^{-i\omega t}$, which is assumed for all the field components, is omitted throughout. The wave-number k is assumed to have a vanishingly small positive imaginary part, which is set equal to zero in the final formulas.

On account of the incidence of (2), there arises the total fields $\boldsymbol{E}(\boldsymbol{r})$, $\boldsymbol{H}(\boldsymbol{r})$ which satisfy the time harmonic Maxwell's equations

$$\nabla\times\boldsymbol{E}(\boldsymbol{r}) = ik\boldsymbol{H}(\boldsymbol{r})\tag{4a}$$

$$\nabla\times\boldsymbol{H}(\boldsymbol{r}) = -ik\boldsymbol{E}(\boldsymbol{r})\tag{4b}$$

$$\nabla\cdot\boldsymbol{E}(\boldsymbol{r}) = 0\tag{4c}$$

$$\nabla\cdot\boldsymbol{H}(\boldsymbol{r}) = 0\tag{4d}$$

in the exterior to the screen. The unidirectional conductivity of the screen is described by the following boundary conditions on the screens, *i.e.*, for $z=0$, $|x|>a$.

$$E_\xi(x, y, o) = 0\tag{5}$$

$$[H_\xi(x, y)] = H_\xi(x, y, o^+) - H_\xi(x, y, o^-) = 0\tag{6}$$

$$[E_\eta(x, y)] = 0.\tag{7}$$

Further, in order to have a unique solution, it is necessary to guarantee the quadratic integrability of $\boldsymbol{E}(\boldsymbol{r})$, $\boldsymbol{H}(\boldsymbol{r})$ at the edges of the two screens and thus impose appropriate edge conditions. In addition, the scattered fields $\boldsymbol{E}^d(\boldsymbol{r})$, $\boldsymbol{H}^d(\boldsymbol{r})$ are required to be outgoing at infinity.

The total electromagnetic field is conveniently split up as follows:

$$\begin{aligned}\boldsymbol{E}(\boldsymbol{r}) &= \boldsymbol{E}^i(\boldsymbol{r}) + \boldsymbol{E}^r(\boldsymbol{r}) + \boldsymbol{E}^d(\boldsymbol{r})\\ \boldsymbol{H}(\boldsymbol{r}) &= \boldsymbol{H}^i(\boldsymbol{r}) + \boldsymbol{H}^r(\boldsymbol{r}) + \boldsymbol{H}^d(\boldsymbol{r}) \qquad z<0,\end{aligned}\tag{8}$$

and

$$\begin{aligned}\boldsymbol{E}(\boldsymbol{r}) &= \boldsymbol{E}^t(\boldsymbol{r}) + \boldsymbol{E}^d(\boldsymbol{r})\\ \boldsymbol{H}(\boldsymbol{r}) &= \boldsymbol{H}^t(\boldsymbol{r}) + \boldsymbol{H}^d(\boldsymbol{r}) \qquad z>0,\end{aligned}\tag{9}$$

where $\boldsymbol{E}^i(\boldsymbol{r})$, $\boldsymbol{H}^i(\boldsymbol{r})$ are the incident fields given by (2); $\boldsymbol{E}^r(\boldsymbol{r})$, $\boldsymbol{H}^r(\boldsymbol{r})$, and $\boldsymbol{E}^t(\boldsymbol{r})$, $\boldsymbol{H}^t(\boldsymbol{r})$ are respectively the reflected and the transmitted fields appropriate to a complete screen with no slit; and $\boldsymbol{E}^d(\boldsymbol{r})$, $\boldsymbol{H}^d(\boldsymbol{r})$ are the scattered fields due to the presence of the infinite slit. For a complete screen with no aperture, the solution of (4) subject to the boundary conditions (5), (6) and (7) for the incidence of (2) is straightforward. However, it is convenient to decompose the incident wave into two components; one component has the magnetic vector and the other the electric vector transverse to the direction in which the screens are conducting. These components are named the E- and H-polarizations, respectively. Using (2) and (3), the two polarizations of the incident wave may be taken separately as:

[1] G. Toraldo di Francia, "Electromagnetic cross section of a small circular disc with unidirectional conductivity," *Il Nuovo Cimento*, series X, vol. 3, pp. 1276–1284; 1936.

[2] S. N. Karp, "Diffraction of a Plane Wave by a Unidirectionally Conducting Half-Plane," Inst. Math. Sciences, New York University, New York, N. Y., Res. Rept. No. EM. 108; 1957.

[3] J. Radlow, "Diffraction of a Dipole Field by a Unidirectionally Conducting Screen," Inst. Math. Sciences, New York University, New York, N. Y., Res. Rept. No. EM.105; 1957.

[4] H. Levine and T. T. Wu, "Diffraction by an Aperture at High Frequencies," Applied Math. and Statistics Lab., Stanford University, Stanford, Calif., Tech. Rept. No. 71; 1957.

E-polarization

$$\begin{aligned} \boldsymbol{E}^i(r) &= [(q^2+n^2)\hat{\xi} - pq\hat{\eta} - pn\hat{z}]e^{ik(p\xi+q\eta+nz)} \\ \boldsymbol{H}^i(r) &= [n\hat{\eta} - q\hat{z}]e^{ik(p\xi+q\eta+nz)} \end{aligned} \tag{10}$$

H-polarization

$$\begin{aligned} \boldsymbol{E}^i(r) &= [n\hat{\eta} - q\hat{z}]e^{ik(p\xi+q\eta+nz)} \\ \boldsymbol{H}^i(r) &= [-(q^2+n^2)\hat{\xi} + pq\hat{\eta} + np\hat{z}]e^{ik(p\xi+q\eta+nz)} \end{aligned} \tag{11}$$

where with the help of (1), it is seen that

$$\begin{aligned} p &= l\cos\alpha + m\sin\alpha \\ q &= -l\sin\alpha + m\cos\alpha. \end{aligned} \tag{12}$$

For a complete screen, (4) is easily solved subject to the boundary conditions (5), (6) and (7) to yield the following reflected and transmitted fields:

E-polarization

$$\begin{aligned} \boldsymbol{E}^r(r) &= [-(q^2+n^2)\hat{\xi} + pq\hat{\eta} - np\hat{z}]e^{ik(p\xi+q\eta-nz)} \\ \boldsymbol{H}^r(r) &= [n\hat{\eta} + q\hat{z}]e^{ik(p\xi+q\eta-nz)} \\ \boldsymbol{E}^t(r) &= 0 \\ \boldsymbol{H}^t(r) &= 0 \end{aligned} \tag{13}$$

H-polarization

$$\begin{aligned} \boldsymbol{E}^r(r) &= 0 \\ \boldsymbol{H}^r(r) &= 0 \\ \boldsymbol{H}^t(r) &= [n\hat{\eta} - q\hat{z}]e^{ik(p\xi+q\eta+nz)} \\ \boldsymbol{H}^t(r) &= [-(q^2+n^2)\hat{\xi} + pq\hat{\eta} + np\hat{z}]e^{ik(p\xi+q\eta+nz)}. \end{aligned} \tag{14}$$

It is interesting to observe that the screen is perfectly reflecting for the E-polarization and is totally transparent for the H-polarization. For the H-polarization, no net current is induced on the wires composing the screen and, hence, even with an infinite slit in the complete screen, the incident wave will be undisturbed. On the other hand, for the E-polarization of the incident wave, the perforation of an infinite slit in the complete screen produces, in addition to the specularly reflected fields, diffracted fields whose determination is now considered.

Because of the unidirectional conductivity, the density of the surface current on the screen has only a ξ-component. Define the surface current density on the illuminated side of the screen, $z=0^-$, as J^- and that on the shadow side of the screen, $z=0^+$, as J^+. Denote their sum as

$$J = J^- + J^+. \tag{15}$$

In the absence of the slit, it is obvious from (10), (12) and (13) that

$$\begin{aligned} J^+ &= 0 \\ J^- &= J^0 = 2ne^{ik(lx+my)}. \end{aligned} \tag{16}$$

In the presence of the slit, J^+ and J^- have different values from that given in (16). It is convenient to introduce

$$\begin{aligned} J^{-\prime} &= J^- - J^0 \\ J' &= J^t + J^{-\prime}. \end{aligned} \tag{17}$$

Since $J=0$ in the slit, it follows that

$$J' = -J^0 \tag{18}$$

for $|x| < a$.

It is evident that the entire diffracted field $[\boldsymbol{E}^d(r), \boldsymbol{H}^d(r)]$ is due to J' and can be derived from the vector potential

$$\boldsymbol{A}^d(r) = \frac{1}{4\pi}\int_{S1+S2+A} J'(\varrho')\,\frac{\exp[ik|r-\varrho'|]}{|r-\varrho'|}\,dS' \tag{19}$$

where ϱ denotes the position vector of a point in the x-y plane. Like the current, the vector potential $\boldsymbol{A}^d(r)$ has also only a ξ-component. It is known that $\boldsymbol{A}^d(r)$ satisfies the differential equation

$$(\nabla^2 + k^2)\boldsymbol{A}^d(r) = 0. \tag{20}$$

The diffracted magnetic field is obtained with the help of the relation

$$\boldsymbol{H}^d(r) = \nabla \times \boldsymbol{A}^d(r) \tag{21}$$

in the component form as

$$H_\xi{}^d(r) = 0 \tag{22a}$$

$$H_\eta{}^d(r) = \frac{\partial}{\partial z}A^d(r) \tag{22b}$$

$$H_z{}^d(r) = -\frac{\partial}{\partial \eta}A^d(r) \tag{22c}$$

where account is taken of the fact that the vector potential has only a ξ component. With (4b), the diffracted electric field is obtained as

$$E_\xi{}^d(r) = \frac{i}{k}\left(k^2 + \frac{\partial^2}{\partial\xi^2}\right)A^d(r) \tag{23a}$$

$$E_\eta{}^d(r) = \frac{i}{k}\frac{\partial^2}{\partial\xi\partial\eta}A^d(r) \tag{23b}$$

$$E_z{}^d(r) = \frac{i}{k}\frac{\partial^2}{\partial\xi\partial z}A^d(r). \tag{23c}$$

Owing to the geometrical identity of the half-spaces $z \lessgtr 0$, the vector potentials are identical at the corresponding points. It follows therefore from (22b) that $H\eta^d(r)$ at the corresponding points in the two half-spaces are equal in magnitude but opposite in sign.

Since on the planes $z=0^{\pm}$ the unit vectors $\hat{n}$ are also oppositely directed, the currents are identical. Therefore,

$$J^{+} = J^{-\prime} \tag{24}$$

so that

$$J' = 2J^{+} = 2J^{-\prime}. \tag{25}$$

Together with (16) and (18), (25) yields

$$J^{+}(\varrho) = -ne^{ik(lx+my)} \tag{26}$$

for $|x|<a$.

It is now desired to obtain an integral equation which specifies J^{+}. For that purpose conditions (5–7) must be made use of. However, taking account of the fact that the vector potentials $A^{d}(r)$ are identical at the corresponding points in the two half-spaces, together with (22a) and (23b), it is evident that (6) and (7) are automatically fulfilled. With the use of (19), (23a) and (25), it is obvious that

$$E_{\xi}{}^{d}(r) = \frac{i}{2\pi k}\left(k^2 + \frac{\partial^2}{\partial \xi^2}\right) \cdot \int_{S_1+S_2+A} J^{+}(\varrho') \frac{[ik|\, r-\varrho'\,|\,]}{|\, r-\varrho'\,|}\, dS' \tag{27}$$

Since the geometry of the problem is invariant with respect to y, it is clear that the dependence of all the field components on y arises on account of the incident wave and, hence, like the incident wave depends on y only through the phase factor e^{ikmy}. Hence set

$$E_{\xi}{}^{d}(r) = E_{\xi}{}^{d}(x, z)e^{ikmy}$$
$$J(\varrho) = J(x)e^{ikmy}. \tag{28}$$

Also from (1), it follows that

$$\frac{\partial}{\partial \xi} = \cos\alpha \frac{\partial}{\partial x} + \sin\alpha \frac{\partial}{\partial y}. \tag{29}$$

By substituting (28) and (29) in (27) and explicitly carrying out the integration with respect to y', it results that

$$E_{\xi}{}^{d}(x, z) = \frac{1}{2k}\left[k^2 + \left(\cos\alpha \frac{d}{dx} + ikm\sin\alpha\right)^2\right] \times \int_{-\infty}^{\infty} J^{+}(x')H_0{}^{(1)}[k_0\sqrt{(x-x')^2+z^2}\,]dx' \tag{30}$$

where

$$k_0{}^2 = k^2(1-m^2). \tag{31}$$

By imposing the boundary condition (5) in (30), the following integro-differential equation is obtained after some simplification:

$$\left(\frac{d}{dx} - ik_1\right)\left(\frac{d}{dx} + ik_2\right) \cdot \int_{-\infty}^{\infty} J^{+}(x')H_0{}^{(1)}[k_0|\, x-x'\,|\,]dx' = 0 \quad |x| > a \tag{32}$$

where

$$k_1 = k(\sec\alpha - m\tan\alpha)$$
$$k_2 = k(\sec\alpha + m\tan\alpha). \tag{33}$$

Note that k_1 and k_2 like k, have an imaginary part that is positive. The solution of (32) for the integral together with (26) and (28) yields the following integral equation:

$$\int_{-\infty}^{-a} J_1(x')H_0{}^{(1)}[k_0|\, x-x'\,|\,]dx' + \int_{a}^{\infty} J_2(x')H_0{}^{(1)}[k_0|\, x-x'\,|\,]dx' = n\int_{-a}^{a} e^{iklx'}H_0{}^{(1)}[k_0|\, x-x'\,|\,]dx' + Ce^{ik_1x} + De^{-ik_2x} \qquad |x| > a, \tag{34}$$

where C and D are the integration constants. Since there is no possible confusion, the superscript on J has been omitted.

The similarity between (34) and the integral equation for the diffraction by an infinite slit in a perfectly conducting screen is evident. For the later problem, it was found that an asymptotic solution in the form of a series in inverse powers of ka approximated satisfactorily the exact solution, with only the first few terms over a wide range of parameter ka (*i.e.*, $ka>2$). Hence, it is proposed to solve (34) asymptotically for large ka.

It is necessary to know the method for determining the integration constants C and D. For this purpose, the edge condition is to be used. For $\alpha\neq\pi/2$, the requirement that the currents at the ends of the wires composing the two screens should vanish, together with (17), (25) and (28), yields the following edge conditions:

$$J_1(x=-a) = -ne^{-ikla}$$
$$J_2(x=a) = -ne^{ikla} \qquad \text{for } \alpha \neq \frac{\pi}{2}. \tag{35}$$

For the special case $\alpha=\pi/2$, the integrated terms in (34) vanish and the condition (35) is no longer valid; nor is it required. For $\alpha=\pi/2$, the currents are parallel to the edges of the screens and therefore a comparison with the case of the perfectly conducting half-plane shows that the currents, near the edges, have a singularity of the form

$$J_1(x) \sim (-a-x)^{-1/2}$$
$$J_2(x) \sim (-a+x)^{-1/2} \qquad \text{for } \alpha = \frac{\pi}{2}. \tag{36}$$

But for other values of α $(0 \leq \alpha < \pi/2)$, the currents vanish at the edges as the square root of the distance therefrom, *i.e.*,

$$J_1(x) = (-a - x)^{1/2},$$

$$J_2(x) = (-a + x)^{1/2} \qquad \text{for } \alpha \neq \frac{\pi}{2}. \tag{37}$$

The conditions (36) and (37) which arise out of the requirement of the quadratic integrability of $\boldsymbol{E}(r)$, $\boldsymbol{H}(r)$ at the edges of the two screens, ensure the uniqueness of the solution.

Fourier Transform Solution of the Integral Equation

The integral equation (34) and the method for solving it are similar to those that have been encountered in the problem of diffraction by an infinite slit in a perfectly conducting screen. Hence, only the essential steps in the solution of (34) are given; for details, reference may be made to the previous work.[5] The solution presented here is valid only subject to the condition $a(k_0 \pm k1) \gg l$ and hence it breaks down for the value of n close to zero. However, a solution valid for n near zero is readily obtained by solving (34) using the technique developed by Levine[6] for treating the problem of diffraction by an infinite slit in a perfectly conducting screen.

By considering the diffraction process as due to the screen S_1, and modified by the presence of the screen S_2, and vice versa, the following two simultaneous integral equations specifying the current distributions (up to order $(ka)^{-5/2}$) on the two screens are easily derived:

$$\int_0^\infty \Big[J_1(-a-t')H_0^{(1)}[k_0 \mid t-t' \mid]dt'$$

$$+ \beta e^{ik_0(t+t')} J_2(a+t') \left\{ 1 - \frac{t}{4a} - \frac{t'}{4a} - \frac{i}{16k_0 a} \right\} dt' \Big]$$

$$= n \int_{-\infty}^{0} \Big[e^{-ikla} e^{-ikl t'} H_0^{(1)}[k_0 \mid t-t' \mid]dt'$$

$$+ \beta e^{ik_0(t+t')} e^{ikla} e^{ikl t'} \left\{ 1 - \frac{t}{4a} - \frac{t'}{4a} - \frac{i}{16k_0 a} \right\} dt' \Big]$$

$$+ Ce^{-ik_1 a} e^{-ik_1 t} + De^{ik_2 a} e^{ik_2 t} \qquad t > 0 \tag{38}$$

and

$$\int_0^\infty \Big[J_2(a+t')H_0^{(1)}(k_0 \mid t-t' \mid)dt'$$

$$+ \beta e^{ik_0(t+t')} J_1(-a-t') \left\{ 1 - \frac{t}{4a} - \frac{t'}{4a} - \frac{i}{16k_0 a} \right\} dt' \Big]$$

$$= n \int_{-\infty}^{0} \Big[e^{ikla} e^{ikl t'} H_0^{(1)}(k_0 \mid t-t' \mid)dt'$$

$$+ \beta e^{ik_0(t+t')} e^{-ikla} e^{-ikl t'} \left\{ 1 - \frac{t}{4a} - \frac{t'}{4a} - \frac{i}{16k_0 a} \right\} dt' \Big]$$

$$+ Ce^{ik_1 a} e^{ik_1 t} + De^{-ik_2 a} e^{-ik_2 t} \qquad \text{for } t > 0 \tag{39}$$

where

$$\beta = \frac{1}{\sqrt{\pi k_0 a}} e^{i(2k_0 a - \pi/4)}. \tag{40}$$

Eqs. (38) and (39) are of the Wiener-Hopf type, and may therefore be solved by the standard Fourier transform technique. Two functions $R(t)$ and $S(t)$, which are identically zero for $t > 0$ are added to the right-hand sides of (38) and (39), respectively, in order to make them valid for $t < 0$. If $J_1(-a-t)$ and $J_2(a+t)$ are defind to be zero for $t < 0$, (38) and (39), with $R(t)$ and $S(t)$ added to their right-hand sides become valid for all t from $-\infty$ to ∞. A complex Fourier transformation is applied (38), (39). While taking the transforms of the terms containing the factor $e^{ik_0(t+t')}$, integration is performed only between the limits of t from 0 to ∞. However, the contributions arising from the integral between the limits of t from $-\infty$ to 0, are added to the transforms of $R(t)$ and $S(t)$ to give respectively $\bar{R}(\zeta)$ and $\bar{S}(\zeta)$. The result of such a transformation is

$$\frac{2\bar{J}_1(-\zeta)}{\sqrt{k_0^2 - \zeta^2}} + \frac{\beta i \bar{J}_2(-k_0)}{k_0 - \zeta} + \frac{\beta}{16k_0 a} \frac{\bar{J}_2(-k_0)}{k_0 - \zeta}$$

$$+ \frac{\beta}{4a} \frac{\bar{J}_2(-k_0)}{(k_0 - \zeta)^2} + \frac{\beta \bar{J}_2'(-k_0)}{4a(k_0 - \zeta)}$$

$$= \frac{2ine^{-ikla}}{\zeta + i\epsilon + kl} \cdot \frac{1}{\sqrt{k_0^2 - \zeta^2}} + \frac{n\beta e^{ikla}}{(k_0 + kl)(k_0 - \zeta)}$$

$$- \frac{n\beta i e^{ikla}}{16k_0 a(k_0 + kl)(k_0 - \zeta)} - \frac{n\beta i e^{ikla}}{4a(k_0 + kl)(k_0 - \zeta)^2}$$

$$- \frac{n\beta i e^{ikla}}{4a(k_0 + kl)^2(k_0 - \zeta)} - \frac{Cie^{-ik_1 a}}{k_1 + \zeta} + \frac{Die^{ik_2 a}}{k_2 - \zeta}$$

$$+ \bar{R}(\zeta) \tag{41}$$

[5] S. R. Seshadri, "High-Frequency Diffraction of Plane Waves by an Infinite Slit," Cruft Lab., Harvard University, Cambridge, Mass., Sci. Rept. No. 20; 1958.

[6] H. Levine, "Diffraction by an Infinite Slit," Applied Math. and Statistics Lab., Stanford University, Stanford, Calif., Tech. Rept. No. 61; 1957.

and

$$\frac{2\bar{J}_2(\zeta)}{\sqrt{k_0^2-\zeta^2}}+\frac{\beta i\bar{J}_1(k_0)}{(k_0-\zeta)}+\frac{\beta}{16k_0a}\frac{\bar{J}_1(k_0)}{k_0-\zeta}$$

$$+\frac{\beta}{4a}\frac{\bar{J}_1(k_0)}{(k_0-\zeta)^2}-\frac{\beta\bar{J}_1'(k_0)}{4a(k_0-\zeta)}$$

$$=\frac{2ine^{ikla}}{\zeta+i\epsilon-kl}\cdot\frac{1}{\sqrt{k_0^2-\zeta^2}}+\frac{n\beta e^{-ikla}}{(k_0-kl)(k_0-\zeta)}$$

$$-\frac{n\beta i}{16k_0a}\frac{e^{-ikla}}{(k_0-kl)(k_0-\zeta)}-\frac{n\beta ie^{-ikla}}{4a(k_0-kl)(k_0-\zeta)^2}$$

$$-\frac{n\beta ie^{-ikla}}{4a(k_0-kl)^2(k_0-\zeta)}+\frac{Cie^{ik_1a}}{k_1-\zeta}-\frac{Die^{-ik_2a}}{k_2+\zeta}$$

$$+\bar{S}(\zeta) \tag{42}$$

where the primes denote differentiation with respect to ζ and

$$\int_0^\infty J_1(-a-t')e^{i\zeta t'}dt'$$

$$=\int_{-\infty}^0 J_1(-a+t')e^{-i\zeta t'}dt'=\bar{J}_1(\zeta) \tag{43}$$

and

$$\int_0^\infty J_2(a+t')e^{-i\zeta t'}dt'=\bar{J}_2(\zeta). \tag{44}$$

An iterative procedure is used to solve the transform relations (41) and (42). For that purpose, set

$$\begin{aligned}\bar{J}_1(\zeta)&=\bar{J}_1^{(0)}(\zeta)+\bar{J}_1^{(1)}(\zeta)\\ \bar{J}_2(\zeta)&=\bar{J}_2^{(0)}(\zeta)+\bar{J}_2^{(1)}(\zeta)\\ \bar{R}(\zeta)&=\bar{R}^{(0)}(\zeta)+\bar{R}^{(1)}(\zeta)\\ \bar{S}(\zeta)&=\bar{S}^{(0)}(\zeta)+\bar{S}^{(1)}(\zeta)\\ C&=C^{(0)}+C^{(1)}\\ D&=D^{(0)}+D^{(1)}\end{aligned} \tag{45}$$

where all the quantities with superscript 1 are order $(ka)^{-1}$ lower than with superscripts 0. By retaining all the higher-order terms in (41), and applying the familiar Wiener-Hopf procedure, it results that

$$\bar{J}_1^{(0)}(-\zeta)=\frac{ine^{-ikla}}{\zeta+i\epsilon+kl}\left(1-\sqrt{\frac{k_0-\zeta}{k_0+kl+i\epsilon}}\right)$$

$$+\frac{\sqrt{2k_0}}{\sqrt{k_0-\zeta}}\left(\frac{n\beta e^{ikla}}{2(k_0+kl)}-\frac{\beta i\bar{J}_2^{(0)}(-k_0)}{2}\right)$$

$$+\frac{D^{(0)}i\sqrt{k_0+k_2}\,e^{ik_2a}}{2}\frac{\sqrt{k_0-\zeta}}{(k_2-\zeta)}. \tag{46}$$

The value of $D^{(0)}$ in (46) is chosen in such a way to satisfy the edge condition (35). For that purpose, it is necessary to obtain $J_1(-a-t)$, from which (43) is obtained as

$$J_1^{(0)}(-a-t)=\frac{1}{2\pi}\int_{-\infty}^{\infty}\bar{J}_1^{(0)}(-\zeta)e^{i\zeta t}d\zeta \tag{47}$$

where the path of integration passes below the branch point $\zeta=k_0$ and the pole $\zeta=k_2$ of the integrand. By closing the path of integration in the lower half-plane, it is obtained that $J_1^{(0)}(-a-t)=0$ if $t<0$ (*i.e.*, $x>-a$) as is to be expected. By closing it in the upper half-plane, it may be easily derived that

$$J_1^{(0)}(-a-t)=-\frac{ine^{-ikla}}{\sqrt{k_0+kl}}$$

$$\cdot\left[-\frac{2\sqrt{k_0+kl}}{\sqrt{\pi}}e^{-i(klt-\pi/4)}\int_{\sqrt{(k_0+kl)t}}^{\infty}e^{is^2}ds+\frac{ie^{i(k_0t+\pi/4)}}{\sqrt{\pi}t^{1/2}}\right]$$

$$-\sqrt{2k_0}\left(\frac{n\beta e^{ikla}}{2(k_0+kl)}-\frac{\beta i\bar{J}_2^{(0)}(-k_0)}{2}\right)\frac{ie^{i(k_0t+\pi/4)}}{\sqrt{\pi t}}$$

$$-\frac{D^{(0)}i\sqrt{k_0+k_2}}{2}e^{ik_2a}\left[i\sqrt{k_0-k_2}\,e^{ik_2t}\right.$$

$$\left.-\frac{2\sqrt{k_0-k_2}}{\sqrt{\pi}}e^{i(k_2t+\pi/4)}\int_{\sqrt{(k_0-k_2)t}}^{\infty}e^{is^2}ds+\frac{i}{\sqrt{\pi}}\frac{e^{i(k_0t+\pi/4)}}{t^{1/2}}\right]. \tag{48}$$

From (35) it is clear that for $t=0$, $J_1^{(0)}(-a-t)$ has the finite value

$$J_1^{(0)}(-a-t)=-ne^{-ikla}\quad\text{for } t=0 \tag{49}$$

and hence $D^{(0)}$ in (48) is chosen to nullify the coefficient of $t^{-1/2}$. The value of $D^{(0)}$ is therefore easily seen to be

$$D^{(0)}=\frac{2e^{ik_2a}}{i\sqrt{k_0+k_2}}\left[\frac{ine^{-ikla}}{\sqrt{k_0+kl}}\right.$$

$$\left.-\sqrt{2k_0}\left(\frac{n\beta e^{ikla}}{2(k_0+kl)}-\frac{\beta i\bar{J}_2^{(0)}(-k_0)}{2}\right)\right]. \tag{50}$$

With (50), (46) becomes

$$\bar{J}_1^{(0)}(-\zeta)$$

$$=\frac{ine^{-ikla}}{\zeta+i\epsilon+kl}\left(1-\sqrt{\frac{k_0-\zeta}{k_0+kl}}\right)+\frac{P_1}{\sqrt{k_0-\zeta}}$$

$$-\left(\frac{ine^{-ikla}}{\sqrt{k_0+kl}}+P_1\right)\frac{\sqrt{k_0-\zeta}}{k_2-\zeta} \tag{51}$$

where

$$P_1=\sqrt{2k_0}\left(\frac{n\beta e^{ikla}}{2(k_0+kl)}-\frac{\beta i\bar{J}_2^{(0)}(-k_0)}{2}\right). \tag{52}$$

In a similar manner, (42) may be solved with the result

$$\bar{J}_2^{(0)}(\zeta) = \frac{ine^{ikla}}{\zeta + i\epsilon - kl}\left(1 - \sqrt{\frac{k_0 - \zeta}{k_0 - kl}}\right) + \frac{P_2}{\sqrt{k_0 - \zeta}} - \left(\frac{ine^{ikla}}{\sqrt{k_0 - kl}} + P_2\right)\frac{\sqrt{k_0 - \zeta}}{k_1 - \zeta} \tag{53}$$

where

$$P_2 = \sqrt{2k_0}\left(\frac{n\beta e^{-ikla}}{2(k_0 - kl)} - \frac{\beta i \bar{J}_1^{(0)}(k_0)}{2}\right). \tag{54}$$

By setting $\zeta = -k_0$ in both (51) and (53), two simultaneous equations in the unknowns $\bar{J}_1^{(0)}(k_0)$ and $\bar{J}_2^{(0)}(-k_0)$ are obtained; the result of solving the simultaneous equations, if only terms up to the order k^{-2} are retained, is

$$P_1 = \frac{\beta e^{ikla}(k_1 - kl)}{\sqrt{k_0 + kl}\,(k_1 + k_0)} + \frac{i\beta^2}{2}\frac{e^{-ikla}}{\sqrt{k_0 - kl}} \cdot \frac{(k_0 - k_1)(k_2 + kl)}{(k_0 + k_1)(k_2 + k_0)} - \frac{\beta^3 e^{ikla}(k_1 - kl)(k_0 - k_1)(k_0 - k_2)}{4\sqrt{k_0 + kl}\,(k_1 + k_0)^2(k_0 + k_2)} \tag{55}$$

and

$$P_2 = \frac{\beta e^{-ikla}(k_2 + kl)}{\sqrt{k_0 - kl}\,(k_2 + k_0)} + \frac{i\beta^2 e^{ikla}(k_0 - k_2)(k_1 - kl)}{2\sqrt{k_0 + kl}\,(k_0 + k_2)(k_1 + k_0)} - \frac{\beta^3 e^{-ikla}(k_2 + kl)(k_0 - k_2)(k_0 - k_1)}{4\sqrt{k_0 - kl}\,(k_2 + k_0)^2(k_0 + k_1)}. \tag{56}$$

The second iteration in the solution of the transform relations (41) and (42) is easily carried out, and the result, when only terms up to the order $k^{-5/2}$ are retained is

$$\bar{J}_1^{(1)}(-\zeta) = P_3\left[\frac{1}{\sqrt{k_0 - \zeta}} - \frac{\sqrt{k_0 - \zeta}}{k_2 - \zeta}\right] + \frac{P_5}{(k_0 - \zeta)^{3/2}} \tag{57}$$

and

$$\bar{J}_2^{(1)}(\zeta) = P_4\left[\frac{1}{\sqrt{k_0 - \zeta}} - \frac{\sqrt{k_0 - \zeta}}{k_1 - \zeta}\right] + \frac{P_6}{(k_0 - \zeta)^{3/2}} \tag{58}$$

where

$$P_3 = -\frac{\beta}{8a}\left[\frac{2ink_0e^{ikla}}{(k_0 + kl)^2\sqrt{k_0 - kl}} - \frac{2ink_0e^{ikla}}{(k_1 + k_0)^2\sqrt{k_0 - kl}} - \frac{ine^{ikla}}{2(k_0 + kl)\sqrt{k_0 - kl}} + \frac{ine^{ikla}}{2(k_1 + k_0)\sqrt{k_0 - kl}}\right] \tag{59}$$

$$P_4 = -\frac{\beta}{8a}\left[\frac{2ink_0e^{-ikla}}{(k_0 - kl)^2\sqrt{k_0 + kl}} - \frac{2ink_0e^{-ikla}}{(k_2 + k_0)^2\sqrt{k_0 + kl}} - \frac{ine^{-ikla}}{2(k_0 - kl)\sqrt{k_0 + kl}} + \frac{ine^{-ikla}}{2(k_2 + k_0)\sqrt{k_0 + kl}}\right] \tag{60}$$

$$P_5 = -\frac{\beta ink_0e^{ikla}}{4a\sqrt{k_0 - kl}}\left[\frac{1}{k_0 + kl} - \frac{1}{k_1 + k_0}\right] \tag{61}$$

$$P_6 = -\frac{\beta ink_0e^{-ikla}}{4a\sqrt{k_0 + kl}}\left[\frac{1}{k_0 - kl} - \frac{1}{k_2 + k_0}\right]. \tag{62}$$

High-Frequency Currents on the Screens

With the knowledge of $\bar{J}_1(-\zeta)$ and $\bar{J}_2(\zeta)$, it is possible to determine all the quantities of physical interest in this problem. In this section, expressions for the high-frequency currents on the screens S_1 and S_2 are obtained. Since the current distribution $J_1(x)$ is obtainable from $J_2(x)$ by the symmetry considerations, it is necessary to evaluate $J_2(x)$ only. With (45), (53) and (58) it follows that

$$\bar{J}_2(\zeta) = \frac{ine^{ikla}}{\zeta + i\epsilon - kl}\left(1 - \sqrt{\frac{k_0 - \zeta}{k_0 - kl}}\right) - \frac{ine^{ikla}}{\sqrt{k_0 - kl}}\frac{\sqrt{k_0 - \zeta}}{k_1 - \zeta} + (P_2 + P_4)\left[\frac{1}{\sqrt{k_0 - \zeta}} - \frac{\sqrt{k_0 - \zeta}}{k_1 - \zeta}\right] + \frac{P_6}{(k_0 - \zeta)^{3/2}}. \tag{63}$$

Using (44), (63) is easily inverted to yield

$$J_2(x) = \frac{ine^{ikla}}{\sqrt{k_0 - kl}}\left[\frac{2\sqrt{k_0 - kl}\,e^{i[kl(x-a)+\pi/4]}}{\sqrt{\pi}}\int_{\sqrt{(k_0-kl)(x-a)}}^{\infty} e^{is^2}ds + i\sqrt{k_0 - k_1}\,e^{ik_1(x-a)} - \frac{2\sqrt{k_0 - k_1}\,e^{i[k_1(x-a)+\pi/4]}}{\sqrt{\pi}}\int_{\sqrt{(k_0-k_1)(x-a)}}^{\infty} e^{is^2}ds\right]$$
$$+ (P_2 + P_4)\left[i\sqrt{k_0 - k_1}\,e^{ik_1(x-a)} - \frac{2\sqrt{k_0 - k_1}\,e^{i[k_1(x-a)+\pi/4]}}{\sqrt{\pi}}\int_{\sqrt{(k_0-k_1)(x-a)}}^{\infty} e^{is^2}ds - \frac{2P_6}{\sqrt{\pi}}(x - a)^{1/2}e^{i[k_0(x-a)+\pi/4]}\right]$$
$$\text{for } x > a. \tag{64}$$

It is interesting to note that the first term in (64) is the current distribution appropriate to the isolated screen S_2 in the absence of the screen S_1 and the next two terms are the interaction currents induced on the screen S_2 due to the presence of the screen S_1. Also, as x approaches the edge $x=a$, the first term approaches the constant value $-ne^{ikla}$ as it should, and the next two terms vanish. Further, (64) is not valid $\alpha=\pi/2$, when k_1, k_2 become infinite. To obtain $J_2(x)$ for $\alpha=\pi/2$, (63) is simplified for $k_1=\infty$ and then inverted, with the result

$$J_2(x)=\frac{ine^{ikla}}{\sqrt{k_0-kl}}\left[\frac{2\sqrt{k_0-kl}\,e^{i[kl(x-a)+\pi/4]}}{\sqrt{\pi}}\int_{\sqrt{(k_0-kl)(x-a)}}^{\infty}e^{is^2}ds-\frac{ie^{i[k_0(x-a)+\pi/4]}}{\sqrt{\pi(x-a)}}\right]-\frac{(P_2+P_4)ie^{i[k_0(x-a)+\pi/4]}}{\sqrt{\pi(x-a)}}$$
$$-\frac{2P_6}{\sqrt{\pi}}(x-a)^{1/2}e^{i[k_0(x-a)+\pi/4]}\qquad\text{for } x>a,\quad \alpha=\frac{\pi}{2}\cdot \tag{65}$$

Note that as x tends to a, the current becomes infinite as $(x-a)^{-1/2}$.

The Series for the Transmission Cross Section

For the E-polarization of the incident wave, it is proper to define transmission cross section in the same way as for an infinite slit in a perfectly conducting screen, since the transmission of power takes place entirely through the slit even in the case when the slit is formed by two coplanar semi-infinite unidirectionally conducting screens. In conformity with the usual practice, the transmission cross section σ per unit length of the slit is defined as the ratio of the power passing through unit length of the slit to the incident power per unit area. The transmission coefficient which is equal to the transmission cross section divided by the area $2a$ of the slit per unit length, is easily obtained with the knowledge of $\bar{J}_1(-\zeta)$ and $\bar{J}_2(\zeta)$ through the use of the following relation:

$$t=n-\frac{1}{2a}\,\mathrm{Re}\,[e^{ikla}\bar{J}_1(kl)+e^{-ikla}\bar{J}_2(kl)]. \tag{66}$$

The substitution of (51), (53), (55), (56), (57–62), in (66) yields the following expression for the transmission coefficient:

where

$$m_1=1-m^2$$
$$c_1=\sec\alpha-m\tan\alpha$$
$$c_2=\sec\alpha+m\tan\alpha. \tag{68}$$

Although the use of (57–62) gives t correctly up to and including order $(ka)^{-5/2}$, the $(ka)^{-5/2}$ term is omitted in (67) in order to avoid a lengthy expression.

It is interesting to observe that the transmission coefficient (67), for the two special cases $\alpha=\Delta$ and $\alpha=\pi/2$ becomes equal to those of an infinite slit in a perfectly conducting screen respectively corresponding to the H- and E-polarizations.[5,7] This interesting observation is easily demonstrated for the case of normal incidence ($l=0$, $m=0$, $n=1$) for which (66) yields

$$t=1-\frac{(1-\cos\alpha)\cos(2ka-\pi/4)}{\sqrt{\pi}\,(ka)^{3/2}}$$
$$+\frac{(1-\cos\alpha)(1-\sec\alpha)\sec\alpha\sin 2(2ka-\pi/4)}{2\pi(1+\sec\alpha)^2(ka)^2}$$
$$+\frac{(1-\cos\alpha)\sec\alpha(1-\sec\alpha)^2\cos 3(2ka-\pi/4)}{4\pi^{3/2}(1+\sec\alpha)^3(ka)^{5/2}}$$
$$+\frac{3(1-\cos\alpha)\sin(2ka-\pi/4)}{16\sqrt{\pi}\,(ka)^{5/2}}$$
$$+\frac{(1-\cos\alpha)\sin(2ka-\pi/4)}{4\sqrt{\pi}\,(1+\sec\alpha)^2(ka)^{5/2}}$$
$$-\frac{(1-\cos\alpha)\sin(2ka-\pi/4)}{16\sqrt{\pi}\,(1+\sec\alpha)(ka)^{5/2}}$$
$$-\left(1-\frac{1}{1+\sec\alpha}\right)\frac{\sin(2ka-\pi/4)}{4\sqrt{\pi}\,(ka)^{5/2}}\cdot \tag{69}$$

[7] S. R. Seshadri, "High Frequency Transmission Coefficient of an Infinite Slit in a Plane Screen," Cruft Lab., Harvard University, Cambridge, Mass., Sci. Rept. No. 17; 1958.

$$t=n-\frac{1}{(ka)^{3/2}}\left[\left(\frac{1}{\sqrt{m_1+l}}-\frac{\sqrt{m_1+l}}{c_2+l}\right)\frac{(c_1-l)\cos[2ka(1+l)-\pi/4]}{2\sqrt{\pi m_1}\,\sqrt{m_1+l}\,(c_1+m_1)}\right.$$
$$\left.+\left(\frac{1}{\sqrt{m_1-l}}-\frac{\sqrt{m_1-l}}{c_1-l}\right)\frac{(c_2+l)\cos[2ka(1-l)-\pi/4]}{2\sqrt{\pi m_1}\,\sqrt{m_1-l}\,(c_2+m_1)}\right]$$
$$+\frac{1}{(ka)^2}\left[\left(\frac{1}{\sqrt{m_1+l}}-\frac{\sqrt{m_1+l}}{c_2+l}\right)\frac{(m_1-c_1)(c_2+l)\sin 2(2ka-\pi/4)}{4\pi m_1\sqrt{m_1-l}\,(m_1+c_1)(c_2+m_1)}\right.$$
$$\left.+\left(\frac{1}{\sqrt{m_1-l}}-\frac{\sqrt{m_1-l}}{c_1-l}\right)\frac{(m_1-c_2)(c_1-l)\sin 2(2ka-\pi/4)}{4\pi m_1\sqrt{m_1+l}\,(m_1-c_2)(c_1+m_1)}\right]+0[(ka)^{-5/2}] \tag{67}$$

For $\alpha=0$, (69) becomes

$$t = 1 - \frac{\sin(2ka - \pi/4)}{8\sqrt{\pi}\,(ka)^{5/2}} \tag{70}$$

and, for $\alpha=\pi/2$

$$t = 1 - \frac{\cos(2ka - \pi/4)}{\sqrt{\pi}\,(ka)^{3/2}} - \frac{\sin 2(2ka - \pi/4)}{2\pi(ka)^2} + \frac{1}{4\sqrt{\pi}\,(ka)^{5/2}}\left[\frac{\cos 3(2ka - \pi/4)}{\pi} - \frac{7\sin(2ka - \pi/4)}{4}\right]. \tag{71}$$

It is now clear that the transmission coefficients (70) and (71) are equal to those of an infinite slit in a perfectly conducting screen corresponding to H- and E-polarizations.

It is observed that the diffraction pattern in the far field can be easily evaluated with the knowledge of the Fourier transforms of the current distribution on the two semi-infinite screens. Details of the determination of the far field are omitted in order to save space.

ACKNOWLEDGMENT

The author is indebted to Prof. R. W. P. King and Dr. T. T. Wu for their help and encouragement.

Refraction Compensation in a Spherically Stratified Ionosphere*

STEPHEN M. HARRIS†, MEMBER, IRE

Summary—**For satellite orbit determinations, it is necessary to know the range to the satellite with great accuracy. The presence of the ionosphere with a frequency-dependent index of refraction produces errors in range measurements made by either CW (Doppler) or pulse radio techniques. A measurement scheme is proposed that gives the instantaneously-corrected range for a spherically stratified ionosphere without recourse to any further assumptions about the electron density profile. The corrected range is given by the average of the CW and pulse range measurements and is free of the first-order error contributed by the inverse frequency-squared term in the refractive index. This scheme is shown to be slightly more effective than a scheme combining the results of two CW range measurements. Expressions are also derived for the higher-order residual errors which remain after the proposed compensation, and the expressions for the variation in arrival angle with frequency are given. These expressions depend upon the integrated effect of the free electrons; consequently, a calculation with a simple profile should yield typical results. The compensated range error and the residual errors are given for a satellite at a height of 640 km, arrival angles in the first quadrant, and at a frequency of 100 Mc. This compensation scheme cancels all but a few per cent of the original range error.**

I. INTRODUCTION

WITH the advent of man-made orbital satellites, we have the possibility of communication through the ionosphere and further. When radio transmissions are used for an accurate determination of orbital parameters, the refractive effects of the ionosphere must be allowed for and, if possible, nullified.

This paper concerns a scheme for instantaneous elimination of the first-order refraction effect that occurs because of the presence of the free electrons in the ionosphere. Tropospheric effects and their possible methods of compensation are not discussed.

It is well known that in a region with free electrons the complex refractive index is given by the Appleton-Hartree equation;[1] at VHF much greater than f_0 (*e.g.*, at least 100 Mc), the absorption and magnetic effects are quite small and the refractive index (all real) is approximately given by

$$n^2 = \left(1 - \frac{\omega_0^2}{\omega^2}\right), \tag{1}$$

where ω_0 and ω are the angular values of the plasma frequency and operating frequency, respectively. Consider a ray propagating through the ionosphere to a receiving station on the earth. (Fig. 1.)

The phase velocity u of the ray traveling from S to T (or T to S) is

$$u = c/n, \tag{2}$$

where n is the index of refraction along the path and c is the velocity of propagation in vacuo. The phase range (electrical length along the ray) from S to T is

$$R_p(\omega) = c\tau_p = \int_S^T n(\omega)\,ds, \tag{3}$$

where ds is an element of path length and τ_p is the phase time delay. The actual path must be determined by finding the extremal given by Fermat's principle.

* Received by the PGAP, February 1, 1960; revised manuscript received July 11, 1960. This work was supported in part by the Air Force Cambridge Research Center, under contract AF 19(604)-5905.

† Hermes Electronics Co., Cambridge, Mass.

[1] S. K. Mitra, "The Upper Atmosphere," The Asiatic Society, Calcutta, India, p. 186; 1952.

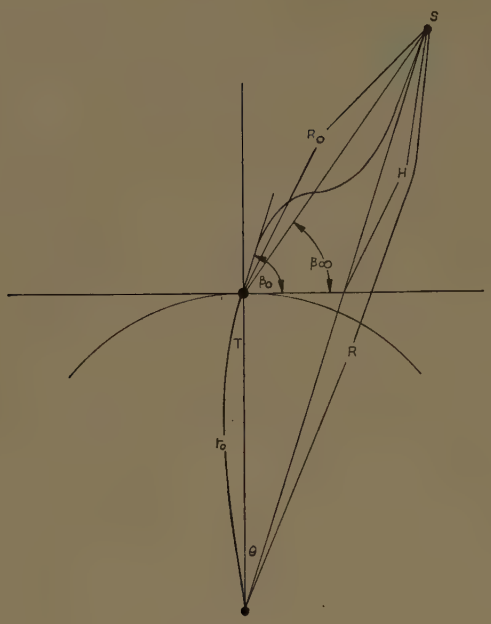

Fig. 1—Ray path geometry.

II. Refraction Compensation Schemes

Since the refractive effect of the ionosphere is small at these frequencies, let us expand n in powers of $1/\omega^2$. (Magneto-ionic effects will introduce odd powers of $1/\omega$, cf. Sec. IV.) Then $R_p(\omega)$ can be written as

$$R_p(\omega) = R_0 - \frac{A}{\omega^2} - \frac{C}{\omega^4} - \cdots . \tag{4}$$

At VHF, the phase range $R_p(\omega)$ will always be less than the straight-line distance R_0 between S and T since the phase velocity is always greater than c.

If two closely spaced frequencies are transmitted from S to T, we may then speak of the velocity of the group (or of the envelope of the modulation). Then the time delay of the group[2] is

$$\tau_g = \frac{d\phi}{d\omega} = \frac{d(\omega\tau_p)}{d\omega}, \tag{5}$$

and the group (or pulse) range is

$$R_g = R_0 + \frac{A}{\omega^2} + \frac{3C}{\omega^4} . \tag{6}$$

If we then average the group and phase measurements,

$$R_{\text{corr}} = \frac{R_g + R_p}{2} = R_0 + \frac{C}{\omega^4}, \tag{7}$$

the resultant quantity will be free of the first-order $(1/\omega^2)$ refraction term.

[2] W. P. Wilson, "Group delay and group velocity," *Electronic and Radio Engr.*, vol. 36, pp. 145–146; April, 1959.

For a body moving with respect to the receiving station on the earth but slowly in relation to the speed of light, the body can be imagined as being successively fixed at positions along the orbit, and at each instant of time the preceding analysis holds. Consequently, this correction scheme can also be utilized to correct the range rate for ionospheric effects. The phase range rate $\dot{R}_p$ is proportional to the measured Doppler signal, while $\dot{R}_g$ is just the time derivative of a group-type range measurement.

If we utilize only phase (Doppler) measurements, we can also provide correction for the refraction effect proportional to $1/\omega^2$ if two separated frequencies are employed. Let us say $\omega_1 = \omega$ from the previous calculation and $\omega_2 = \alpha\omega$ where α is a rational fraction less than 1. Then R_{corr}, the corrected range, is

$$R_{\text{corr}} = \frac{R_p(\omega) - \alpha^2 R_p(\alpha\omega)}{1 - \alpha^2} = R_0 + \frac{C}{\omega^4}\frac{1}{\alpha^2} . \tag{8}$$

For example, if the second frequency is $\frac{2}{3}$ the first frequency, the $1/\omega^4$ residual-error term is 2.25 that which it was for the group-phase correction scheme. Thus, the group-phase scheme is superior to the two-frequency phase scheme although both residual errors are of the same order of magnitude.

III. Expressions for the Ionospheric Effects (No Magnetic Field)

We should like to evaluate the constants A and C for certain specific cases. Consider a locally spherical earth and a spherically stratified ionosphere with a height-dependent index of refraction. Then, for the spherically symmetric medium, the well-known generalization for Snell's law is

$$n(r)r\cos\beta(r) = n_0 r_0 \cos\beta_0 = k(\omega) \tag{9}$$

where

$n(r)$ = index of refraction at radial distance r,
n_0 = index of refraction at the earth's surface,
r_0 = radius of the earth,
$\beta(r)$ = angle between the ray path and the normal to the radius vector at radial distance r,
$k(\omega)$ = constant for a given frequency.

Rewriting (9) with $r = r_0 + h$, we have for Snell's law

$$n'(h)(1 + h')\sec\beta_0 = \sec\beta \tag{10}$$

where

$$n'(h) = \frac{n(h)}{n_0},$$

$$h' = \frac{h}{r_0} .$$

We wish to separate from sec β_0 that part which is frequency-independent. This will facilitate the evaluation of the range integral

$$R_p = c\tau_p = \int_{\text{path}} n ds. \tag{11}$$

When converted into an integral dependent on height, apparent elevation angle, andrefr active index[3] $n'(h)$, (11) becomes

$$R_p = n_0 \int_{h=0}^{H} n'^2(h)(1 + h') \sec \beta_0 \cdot [(1 + h')^2 n'^2(h) \sec^2 \beta_0 - 1]^{-1/2} dh, \tag{12}$$

where H is the altitude of the vehicle. Let us assume that sec β_0 is expandable in the following series

$$\sec^2 \beta_0 = \sec^2 \beta_\infty \left(1 + \frac{a}{\omega^2} + \frac{c}{\omega^4} + \cdots\right), \tag{13}$$

where β_∞ is the elevation angle of arrival for a ray from S to T if there were no ionosphere present (at $\omega \to \infty$). Since the basic dependent variable is $1/\omega^2$, only even powers appear in the expansion.

The coefficient a, a constant which in (13) gives the variation of arrival angle with radio frequency, can be evaluated from the expression[4] for the true central angle θ where

$$r_0\theta = \int_{h=0}^{H} \frac{1}{1 + h'} [(1 + h')^2 n'^2(h) \sec^2 \beta_0 - 1]^{-1/2} dh, \tag{14}$$

since $r_0\theta$ is a constant for a given satellite geometry and is independent of frequency.

After some algebraic substitution and expansion, keeping terms to order $1/\omega^4$, the following solutions for the coefficients result:

$$a = \frac{\int_{h=0}^{H} \frac{\omega_0^2 z dz}{(z^2 - 1)^{3/2}}}{\int_{h=0}^{H} \frac{z dz}{(z^2 - 1)^{3/2}}}, \tag{15}$$

$$A = \frac{r_0 n_0}{2 \sec \beta_\infty} \int_{h=0}^{H} \omega_0^2 \frac{z dz}{\sqrt{z^2 - 1}}, \tag{16}$$

$$C = \frac{r_0 n_0}{8 \sec \beta_\infty} \left[\int_{h=0}^{H} \omega_0^4 \frac{z dz}{\sqrt{z^2 - 1}} + \int_{h=0}^{H} \frac{z dz}{(z^2 - 1)^{3/2}} (\omega_0^4 - a^2) \right], \tag{17}$$

where $z(h) = (1 + h') \sec \beta_\infty$ and $n_0 \approx 1$ approximately at the earth's surface.

[3] J. R. Bauer, W. C. Mason, and F. A. Wilson, "Radio refraction in a Cool Exponential Atmosphere," Lincoln Lab., Tech. Rept. No. 186, eq. (10); (ASTIA 202331.) August 27, 1958.

[4] *Ibid.*, eq. (13).

IV. Effects of Magnetic Fields

When magnetic fields exist in the region of propagation, we must refer to the Appleton-Hartree equation for the refractive index.[5] With absorption neglected, we distinguish two cases: 1) quasi-longitudinal propagation where the magnetic field is essentially directed along the path of propagation, and 2) quasi-transverse propagation where the field is essentially normal to the direction of propagation.

It is seen that for quasi-longitudinal propagation a $(1/\omega^3)$ term arises in the refractive index. Eqs. (13) and (4) can be rewritten to include this $(1/\omega^3)$ effect. We have neglected the second-order magnetic contribution to the $1/\omega^4$ term. It is much smaller than any of the previously included terms. Rewriting (4) for this case, we get

$$R_p(\omega) = R_0 - \frac{A}{\omega^2} - \frac{B}{\omega^3} - \frac{C}{\omega^4}. \tag{18}$$

The previous type of analysis can be carried out. We find that (15) through (17) remain unchanged, and in addition

$$B = \frac{r_0 n_0}{2 \sec \beta_\infty} \int_{h=0}^{H} \frac{z dz}{(z^2 - 1)^{1/2}} \omega_0^2 \omega_L \tag{19}$$

where ω_L is the longitudinal angular gyrofrequency.

V. Results

We note that the coefficients A, B and C which give the range error resulting from the ionosphere are functions which depend upon the integrated effect of the electron density. Consequently, small changes in the electron density vs height profile should not greatly alter the results, provided that the total electron content in the column of unit cross section remains constant.

Let us take as an ionospheric model one that is spherically stratified with a rectangular distribution (Fig. 2) such that

$$\begin{aligned} f_0^2 &\equiv 0 && 0 \le h < H_m - Y_m, \\ f_0^2 &= 80.5 N_{\max} && H_m - Y_m \le h < H_m + Y_m, \\ f_0^2 &\equiv 0 && H_m + Y_m \le h < H, \end{aligned}$$

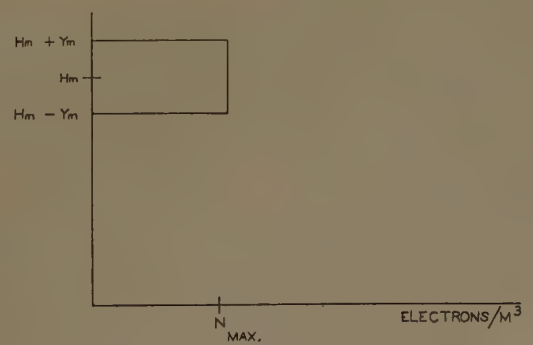

Fig. 2—Height vs electron density.

[5] Mitra, *op. cit.*, pp. 188–189.

where

f_0 = critical frequency,
N = electron density (m^{-3}),
H_m = height of layer where level of ionization is maximum,
Y_m = semithickness of the layer,

Fig. 3 gives the range error vs elevation angle (β_∞) for the following typical case:

$f_0 = 10$ Mc,
$f = 100$ Mc,
$Y_m = 150$ km,
$H_m = 300$ km,
$r_0 = 6400$ km (earth radius),
$H = 640$ km (satellite height),
$H_0 = 50$ ampere-turns/meter.

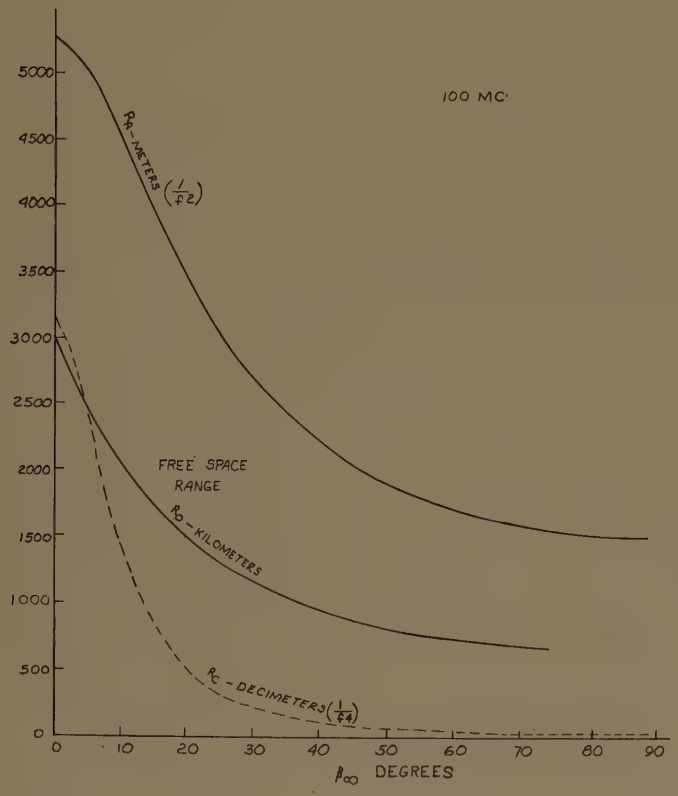

Fig. 3—Range and range errors vs elevation angle ($at\ \omega \to \infty$).

The critical frequency $f_0 = 10$ Mc represents that of a fairly active daytime ionosphere.[6] The magnetic-field intensity $H_0 = 50$ ampere-turns/meter (≈ 0.63 gauss) represents a maximum value for the earth's magnetic-field intensity.

[6] Mitra, *op. cit.*, pp. 290–291.

From Fig. 3, for elevation angles of 0°, 30°, 90° (β_∞), we give Table I, where

$$R_A = \frac{A}{\omega^2},$$

$$R_B = \frac{B}{\omega^3} \text{ (term from quasi-longitudinal propagation)},$$

$$R_0 = \frac{C}{\omega^4}.$$

TABLE I
RANGE AND RANGE ERRORS AS A FUNCTION OF ELEVATION ANGLE AND FREQUENCY

R	β_∞					
	0°		30°		90°	
	100 Mc	200 Mc	100 Mc	200 Mc	100 Mc	200 Mc
R_0 km	2930	2930	1140	1140	640	640
R_A [$\propto (1/f^2)$] m	5240	1310	2675	669	1500	375
R_B [$\propto (1/f^3)$] m	92	12	47	6	26	3.3
R_C [$\propto (1/f^4)$] m	313	20	22	1.4	4	.25

Thus, for the given satellite at an elevation angle (β_∞) of 30° at 200 Mc, we have a true range of 1140 km with a group range error of 685.2 m, of which only 16.2 m remain after compensation.

VI. Conclusions

We have introduced a means for compensating the first-order refractive effects of the ionosphere. Implementation of this idea would furnish a corrected range measurement based on the average of a pulse and a CW (Doppler) range measurement, without any assumptions regarding ionospheric parameters except that the index of refraction admits of expansion in a power series in frequency. This condition exists when the propagation frequency is many times the critical (plasma) frequency. While the discussion here concerns range measurements, the same results and mathematical development can be applied to the range rates which are the quantities more frequently measured in practice. From theoretical calculations, the error in range after compensation should be only a few per cent of the error existing prior to compensation.

Acknowledgment

The author is indebted to R. J. Davisson and Dr. S. Stein for their guidance and their many stimulating discussions.

Scatter Communications with Radar Chaff*

R. A. HESSEMER, JR.†, MEMBER, IRE

Summary—**The first part of this paper is concerned with finding an analytical expression for the scattering cross section of chaff oriented randomly within a vertical cone. The dipoles are allowed to take on all the angles within this cone. A vertically-polarized receiver is assumed off on the horizon and the transmitter on the ground below the chaff. The cross section is a function of the conical angle of the configuration and the angle between a normal to the ground and the incident electric field from the transmitter. Fig. 2 is a plot of the scattering cross section as a function of these two angles.**

Half-wave chaff randomly distributed within a conical angle about a vertical is not the most effective ensemble, but is a practical one at the lower frequencies. Cutting all these half-wave dipoles into very short ones makes it practical to place them in a horizontal position which has an ensemble gain over the conical but a reradiation loss, since short dipoles are less effective scatters than half-wave ones. The second part of this paper compares the reradiation loss and horizontal ensemble gain.

I. Introduction

THIS PAPER investigates the possibility of establishing moderate range communications for short intervals of time between non-line of sight points by using a large number of metallic half-wave dipoles (chaff), placed at a modest altitude somewhere between, used as the scattering element.

The initial chaff altitude has to be sufficient to allow line of sight propagation from it to both antennas. Chaff falls at the rate of several hundred feet per minute, and additional height of this amount above that needed for line of sight is required. For points separated some 200 miles, the line of sight altitude is 20,000 feet for smooth earth.

The transmission loss depends directly on the scattering ability of the chaff, which in turn depends on the length of the chaff dipoles and the arrangement of these dipoles in the ensemble. Half-wave resonant dipoles are considered first. The ensemble configuration is a random orientation of chaff within a vertical cone. The dipoles are allowed to take on all the angles within this cone. This particular configuration prompted Spogen[1] to suggest the possibility of using chaff dipoles much shorter than a half wave, but oriented in a horizontal plane. The hope was that the scattering loss due to the short dipoles would be balanced out by the gain of the superior configuration.

II. Transmission Equation

The transmission equation gives the relationship between the power radiated by the transmitter antenna and the maximum power available at the receiver antenna terminals. It is similar to the radar equation, except that here the transmitter and receiver are at separate locations and hence can be at different distances from the scattering target.

The transmission equation can be derived as follows: The effective transmitter radiated power P_2 incident to the chaff is

$$P_2 = \frac{P_1 G_1 \bar{\sigma}}{4\pi r_1^2}, \tag{1}$$

where

P_1 = transmitter-radiated power,
r_1 = effective distance from transmitter antenna to chaff,
$\bar{\sigma}$ = average cross section of the chaff,
G_1 = average transmitter antenna gain in the direction of the chaff.

The cross section of the chaff σ[2] is by definition that area intercepting that amount of power which, when scattered isotropically, produces an echo equal to that observed from the target, for chaff σ is a fluctuating quantity. Here we use the average value and discuss the amount and frequency of this fluctuation in the section on chaff characteristics.

From the definition of σ, the incident power to this area as given in (1) must be scattered isotropically[3] to give the correct amount of power at the receiver. Thus, the power available at the receiving antenna terminal is

$$P_3 = \frac{P_2 A_3}{4\pi r_2^2} \tag{2}$$

where

A_3 = effective area of the receiving antenna,
r_2 = effective distance between the chaff and the receiving antenna.

* Received by the PGAP, June 27, 1960; revised manuscript received, September 7, 1960. The research described in this paper was sponsored by the Signal Corps, Fort Huachuca, Ariz., under Contract DA-36-039-SC-80146 with the Appl. Res. Lab., University of Arizona, Tucson.

† Elec. Engrg. Dept., University of Arizona, Tucson.

[1] L. R. Spogen, Jr., Appl. Res. Lab., University of Arizona, Tucson, private communication.

[2] Isotropic scattering is merely a convenient and standard way of defining σ. Any type of scattering could be used to define σ, though each type gives a different value. The isotropic scattering used here to define σ in no way forces or constrains the real chaff actually to scatter energy isotropically. In fact, it does not; see (23).

[3] D. E. Kerr, "Propagation of Short Radio Waves," McGraw-Hill Book Co., Inc., New York, N. Y., p. 33; 1951.

The effective area A of an antenna is related to its gain G as follows:

$$A = \frac{\lambda^2 G}{4\pi}. \tag{3}$$

Eqs. (1)–(3) can be combined to give the transmission equation

$$P_3/P_1 = \frac{G_1 G_3 \lambda^2 \bar{\sigma}}{(4\pi)^3 (r_1 r_2)^2}. \tag{4}$$

The net transmission attenuation can be calculated from the above equation once the system parameters of antenna gains, signal frequency, chaff effective area, and distances from chaff to both antennas are given. This attenuation is the amount that the available power P_3 at the receiver terminals is below the power P_1 radiated by the transmitting antenna.

III. Chaff Characteristics

A. Scattering Cross Section

The scattering cross section can be expressed analytically as

$$P_3 = \frac{P_2 \sigma}{4\pi r^2} \tag{5}$$

where

P_2 = incident power per square meter to the chaff,
P_3 = scattered power per square meter at the receiver,
r = distance from chaff to receiver.

For a given target, σ generally depends on its orientation with respect to both the incident wave and the receiver. This point is examined in more detail later. For now, it is only necessary to realize that σ is a function in spherical coordinates of the two angles θ and ϕ.

For a single chaff dipole the scattered power per square meter at a receiver distance away r is

$$P_3 = \frac{P_d G'}{4\pi r^2}, \tag{6}$$

where

P_d = power in the dipole collected from the incident wave and then reradiated,
G' = gain of the dipole in the direction of the receiver.

For a short-circuited resonant half-wave dipole,[4]

$$P_d = 4AP_2 \tag{7}$$

where

$A = \lambda^2 G/4\pi$ = antenna effective area,
λ = wavelength.

Substitution of (7) into (6) gives

$$P_3 = \frac{4AP_2G'}{4\pi^2}. \tag{8}$$

Equating (8) and (5) and solving for σ gives

$$\sigma = 4AG_d = \frac{\lambda^2 GG'}{\pi}. \tag{9}$$

Eq. (5) gives the value for σ only for resonant dipoles. Since σ is a function of angles, it should also be written as

$$\sigma(\theta, \phi) = \frac{\lambda^2}{\pi} G(\theta, \phi) G'(\theta', \phi'). \tag{10}$$

The dipoles in the chaff ensemble are assumed to be in a state of motion, fluttering and dispersion, such that the total scattered signal has a Rayleigh amplitude as a function of time. Under these conditions, the average power from the ensemble is just the sum of the average power per dipole. This average power is a time average found by allowing the dipole to assume all the allowable positions in the configuration. For half-wave dipoles the scattering cross section equation using spherical coordinates is

$$\bar{\sigma} = \frac{N\lambda^2}{A\pi} \int_0^{\phi} \int_0^{\theta} G(\theta, \phi) G'(\theta', \phi') \sin\theta d\theta d\phi, \tag{11}$$

and

$$A = \int_0^{\phi} \int_0^{\theta} \sin\theta d\theta d\phi, \tag{12}$$

where $G(\theta, \phi)$ and $G'(\theta', \phi')$ are the respective dipole gains in the direction of the transmitter and receiver, and N represents the number of dipoles in the ensemble.

B. Physical Properties

Chaff[5] has been used during war time as a means of establishing a large reflecting area to radar waves. The chaff was made from thin aluminum foil strips approximately one-half-wavelength long. Packages, each containing several thousand dipoles, were released from bombers and allowed to disperse in the air and float downward.

The first chaff which was made bent when packaged bundles of it were thrown into the slip stream of the airplane. Such bending caused some of the strips to become tangled into small masses that reflected little of the

[4] J. D. Kraus, "Antennas," McGraw-Hill Book Co., Inc., New York, N. Y., p. 47; 1950.

[5] D. Fink, "Radar countermeasures," *Electronics*, vol. 19, pp. 92–97; January, 1946.

radar wave and also fell quite rapidly. In addition, adjacent strips of the smooth foil stuck to one another, preventing rapid dispersal. To solve these problems, the foil was embossed and then crimped along its length. This chaff proved to be highly dispersive and fell at the rate of about 150 feet per minute. It was designed for 450 to 600 Mc and thus was 10 to $11\frac{1}{2}$ inches long. The weight of 1000 dipoles was only 2 ounces.

Studies made during the war on the 450- to 600-Mc chaff show that its rate of fall depends on its orientation in space. Horizontal dipoles fall about two thirds as fast as vertical dipoles. It is thought that dipoles shaped regularly fall in a near horizontal position. Dipoles that are irregular initially, or bent in the dispersal, are thought to fall predominantly in a near vertical position. Kuiper[6] gives rates of fall from 150 to 500 feet per minute depending on the type of chaff as well as its orientation in space.

The 450- to 600-Mc chaff dispersed about equally into the vertical and horizontal positions. This is in marked contrast with the results for two-inch dipoles at 3000 Mc.[7] The horizontal dipoles (3000 Mc) returned more power than the vertical dipoles by a factor of 12 to 15 db. This increase is thought to occur because the two-inch dipoles are quite regular and tend to resist bending, compared to the 10- to $11\frac{1}{2}$-inch chaff, and hence fall predominantly in a horizontal position.

C. Location of the Chaff

The optimum location of the chaff depends upon the criteria used. One criterion is to locate the chaff so as to minimize the product r_1r_2 in (4) for a given transmitter-receiver separation.

Assume that for a given transmitter-receiver separation the sum of r_1+r_2 is essentially constant when the chaff is placed somewhere between. Then the product r_1r_2 decreases as the chaff is moved from a central point toward one of the antennas. This is easy to demonstrate with numbers. Let r_1 and r_2 each be 5; their sum is 10, and their product 25. Now, let r_1 be 7 and r_2 be 3; their sum is still 10, but their product is now only 21. When r_1 is increased still more to 9 and r_2 reduced to 1, the product is now only 9. Under these conditions, the chaff should be as near one antenna as possible.

The earth's curvature makes it necessary to elevate the chaff. Thus, the optimum chaff location seems to be directly over one of the antennas at an altitude sufficient for line of sight propagation to the other antenna. From a practical viewpoint, this makes the chaff placement rather straight forward.

The chaff altitude depends on the rate at which it falls, the desired communication time, as well as the height needed for line-of-sight communications. The elevation needed for line-of-sight conditions, using a 4/3 earth-radius correction factor, is

$$h = D^2/2, \tag{13}$$

where

h = altitude in feet,
D = line-of-sight distance in miles.

A 200-mile separation between transmitter and receiver requires a minimum chaff altitude of 20,000 feet above a smooth earth. Irregular earth at the antenna farthest from the chaff, as well as the chaff rate of fall, makes it necessary to increase this altitude by an appropriate amount.

IV. Calculation of the Scattering Cross Section

Fig. 1 shows the positions of the two antennas with respect to the chaff origin. The chaff dipoles are assumed to be randomly oriented within the cone about the z axis bounded by a constant value of θ. The scattering cross section for a single fixed dipole within the cone is

$$\sigma(\theta, \phi) = \frac{\lambda^2}{\pi} G(\theta, \phi)G'(\theta', \phi'), \tag{14}$$

where $G(\theta, \phi)$ accounts for the chaff dipole gain including polarization with respect to the transmitting antenna and $G'(\theta', \phi')$ with respect to the receiving antenna. The angles θ and ϕ are the angles the chaff dipole makes with the x, y, z coordinates, while the angles θ' and ϕ' are with respect to the x', y', z' coordinates.

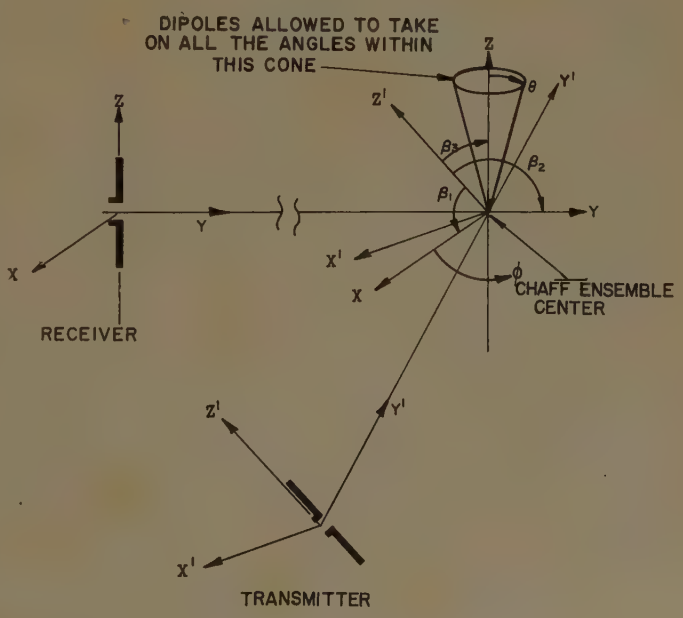

Fig. 1—Basic coordinate system.

[6] G. P. Kuiper, "A Study of Chaff Echoes at 515 Mc," Radio Res. Lab., Harvard University, Cambridge, Mass., Rept. 411–73, p. 1; December 19, 1943.
[7] *Ibid.*, p. 15.

For a half-wave chaff dipole, the gain in the direction of the transmitting antenna is

$$G(\theta, \phi) = 1.64\left[\frac{\cos(\pi/2 \sin\theta)}{\cos\theta}\right]^2. \quad (15)$$

This expression for antenna gain does not lend itself to analytical integration or to a transformation in coordinates. The pattern for a short dipole is

$$G(\theta, \phi) = 1.5 \cos^2\theta. \quad (16)$$

This expression is manageable analytically without great effort. The pattern of a short dipole is slightly wider than that for a half-wave dipole, but the error involved is not appreciable, probably being in the order of a few tenths of a decibel. The gain of a chaff dipole in the direction of the receiving antenna is

$$G'(\theta', \phi') = 1.5 \cos^2\theta'. \quad (17)$$

To evaluate the integral for $\bar{\sigma}$ in (11), it is necessary to transform one set of coordinates to the other. Here the primed coordinates are transformed back to the original coordinates. That is, $G'(\theta', \phi')$ is expressed as a function of θ and ϕ, the unprimed coordinates. This transformation[8] is standard and goes as follows: Let R be the length of a chaff dipole. Its projections on the original coordinates are

$$R_x = R \sin\theta \cos\phi, \quad (18a)$$

$$R_y = R \sin\theta \sin\phi, \quad (18b)$$

$$R_z = R \cos\theta. \quad (18c)$$

Adding primes to all the values except R makes (18) valid for the primed coordinate system. That is,

$$R_x' = R \sin\theta' \cos\phi', \quad (19a)$$

$$R_y' = R \sin\theta' \sin\phi', \quad (19b)$$

$$R_z' = R \cos\theta'. \quad (19c)$$

The projection on the z' axis can also be expressed as

$$R_z' = R_x \cos\beta_1 + R_y \cos\beta_2 + R_z \cos\beta_3. \quad (20)$$

Eqs. (17), (18), (19c) and (20) yield the following expression for $G(\theta', \phi')$ in terms of the unprimed coordinates and the rotational angles β_1, β_2, and β_3:

$$G'(\theta', \phi') = 1.5[(\sin\theta \cos\phi \cos\beta_1)^2 + (\sin\theta \sin\phi \cos\beta_2)^2 + (\cos\theta \cos\beta_3)^2 + \text{cross-product terms}]. \quad (21)$$

Each cross-product term contains one of the following: $\sin\phi \cos\phi$, $\cos\phi$, or $\sin\phi$. Each of these integrates to zero when ϕ goes from 0° to 360°, as it does for the conical configuration of chaff considered here. Thus, the cross-product terms are omitted in the work that follows.

Substitution of (16) and (21) into (11) yields a solution for the scattering cross section. The integrals with respect to ϕ are

$$\int_0^{2\pi} \cos\phi^2 = \pi, \qquad \int_0^{2\pi} \sin\phi^2 = \pi.$$

Thus the expression becomes

$$\bar{\sigma} = \frac{N\lambda^2(1.5)^2}{A}\int_0^{\pi}[\sin^3\theta \cos^2\theta \cos^2\beta_1 + \sin^3\theta \cos^2\theta \cos^2\beta_2 + 2 \cos^4\theta \sin\theta \cos^2\beta_3]d\theta. \quad (22)$$

For the particular cone angle of 90° representing spherically random chaff, the scattering cross section becomes

$$\bar{\sigma} = 0.048N\lambda^2[1 + 2 \cos^2\beta_3], \quad (23)$$

since

$$\cos^2\beta_1 + \cos^2\beta_2 + \cos^2\beta_3 = 1. \quad (24)$$

The scattering cross section for other values of θ is shown in Fig. 2 in db relative to the value of (13) when $\cos\beta_3$ is unity.

V. Calculation of the Transmission Loss

The transmission loss is found from (4). Letting the antenna gains be unity and the scattering cross that for random spherical chaff, the normalized loss L_n is

$$L_n = \frac{0.14N\lambda^4}{(4\pi)^3(r_1r_2)^2}.$$

This normalized loss is shown in Fig. 3. Actual scattering cross sections with respect to random spherical chaff are given in Fig. 2. The ordinate values are added or subtracted from the normalized loss to give the actual loss exclusive of antenna gains.

VI. Horizontal Chaff

Half-wave chaff randomly distributed within a conical angle about a vertical is not the most effective configuration but is a practical one for, say, 100 Mc where a half-wave dipole is about 5 feet long. Cutting all these half-wave dipoles into very short ones makes it practical to place them in a horizontal position, which has a configuration gain over the conical but a reradiation loss since short dipoles are less effective scatterers than half-wave ones.

The configuration or scattering cross section is considered first; then the reradiation difference, and finally a comparison.

A. Scattering Cross Section

In Fig. 1, let the chaff be randomly oriented in the $x-z$ plane; now rotate the drawing so that the $x-z$ plane becomes horizontal. This makes the angle ϕ always zero, and the integral [see (11)] for the average cross section reduces to

$$\bar{\sigma} = \frac{N\lambda^2}{A\pi}\int_0^{\pi} G(\theta, \phi)G'(\theta', \phi')d\theta, \quad (25)$$

[8] O. W. Eshbach, "Handbook of Engineering Fundamentals," John Wiley and Sons, Inc., New York, N. Y., pp. 2, 72; 1936.

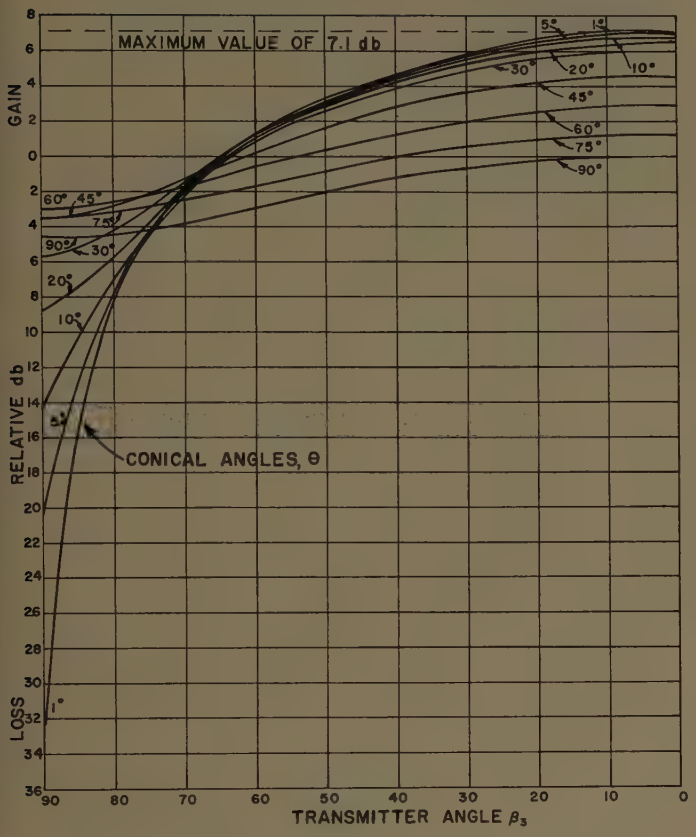

Fig. 2—Scattering cross section $(\bar{\sigma}/(N\lambda^4)$ vs conical and transmitter angles.

$$L_N = \frac{0.14N\lambda^4}{(4\pi)^3 (r_1 \cdot r_2)^2}$$

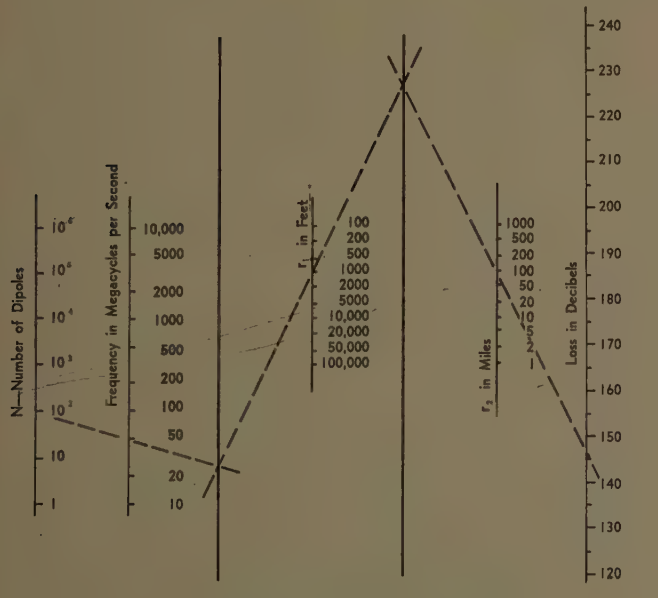

Fig. 3—Normalized transmission loss.

and

$$A = \int_0^{\pi} d\theta = \pi.$$

Substitution of (16) and (21) into (25) yields

$$\bar{\sigma} = \frac{N\lambda^2(1.5)^2}{\pi^2} \int_0^{\pi} [(\sin\theta \cos\theta \cos\beta_1)^2 + (\cos^2\theta \cos\beta_3)^2 + (2 \sin\theta \cos^3\theta \cos\beta_1 \cos\beta_3)]d\theta. \quad (26)$$

The third term integrates to zero and the first two are

$$\int_0^{\pi} \sin^2\theta \cos^2\theta \cos^2\beta_1 d\theta = \frac{\pi}{8} \cos^2\beta_1$$

$$\int_0^{\pi} \cos^4\theta \cos^2\beta_3 d\theta = \frac{3\pi}{8} \cos^2\beta_3.$$

Thus the integral is

$$\bar{\sigma} = 0.09\lambda^2 \cos^2\beta_1 + 0.27\lambda^2 \cos^2\beta_3. \quad (27)$$

With the use of (24), this becomes

$$\bar{\sigma} = 0.27\lambda^2 - 0.27\lambda^2 \cos^2\beta_2 - 0.18\lambda^2 \cos^2\beta_1, \quad (28)$$

which has a maximum value of

$$\bar{\sigma} = 0.27\lambda^2 \quad (29)$$

when both β_1 and β_2 are 90°. This value compares with the zero ordinate value of $0.14\lambda^2$ in Fig. 2; thus it represents about a 2.9-db gain over the zero scale in Fig. 2.

B. Short Dipole Reradiation

A short dipole compared to a half-wavelength is not too effective at absorbing and reradiating electromagnetic energy. The object of this section is to find quantitatively the amount of this decrease compared to a half-wave resonant dipole. Orientation is not a factor in this calculation; therefore let both dipoles be rotated so as to intercept the maximum power from an incident plane wave. The current at the midpoint of the dipole is

$$I_{sc} = \frac{V_{oc}}{z_a},$$

where

$V_{oc} = EL'$,
E = incident electric field strength,
L' = effective length of the dipole,
Z_a = dipole impedance, $R+jX$.

The power reradiated by the dipole is

$$P_d = I_{sc}^2 R$$

$$P_d = \frac{(EL')^2 R}{(R+jX)^2}. \quad (30)$$

Let L_1 be the length of a half-wave resonant dipole and L_2 the length of a short dipole. In comparing the reradiation ability, assume that the short dipoles outnumber the half-wave dipoles so that the same total footage of each type exists. That is, for every half-wave dipole let there be m short dipoles when $m=L_1/L_2$. A half-wave resonant dipole has zero reactance and a radiation resistance of about 70 ohms. With these values, the radiated power ratio H/S becomes

$$\frac{H}{S}=\frac{(L_1')^2}{(L_2')^2}\,\frac{(R_2+jX_2)^2}{m70R_2}. \tag{31}$$

The effective lengths are

$$L_1'=\frac{2L_1}{\pi}=0.64L, \qquad L=\lambda/2, \tag{32a}$$

$$L_2'=\frac{2L_2}{3}=0.67L, \qquad L\ll\lambda/2. \tag{32b}$$

Effective lengths are defined in Jordan[9] with current distributions as given by Schelkunoff and Friis.[10] Eq. (32b) represents the limiting value for infinitely short dipoles.

The ratio now becomes

$$\frac{H}{S}=\frac{m(R_2+X_2)^2}{76R_2}. \tag{33}$$

The radiation resistance of short dipoles is

$$R=80\pi^2\left(\frac{L'}{\lambda}\right)^2. \tag{34}$$

Substitution of (32b) for the effective length gives

$$R=350\left(\frac{L_2}{\lambda}\right)^2. \tag{35}$$

The reactance of a dipole depends on its shape as well as its length-to-width ratio. Jordan[11] and Schelkunoff[12] both show curves of reactance vs length for several length-to-width ratios. The curve in Jordan labeled $r_0/r_\lambda=0.001$ and the one in Schelkunoff for $a/b=70.7$ are about the same. Both of these represent for a flat dipole a length-to-width ratio in the range of 20 to 35. Smaller ratios reduce the reactance but are not thought to be practical. Table I lists the reactances, resistances, and the H/S ratio for various lengths L_2 of short flat dipoles.

[9] E. C. Jordan, "Electromagnetic Waves and Radiating Systems," Prentice-Hall, Inc., New York, N. Y., p. 333; 1950.
[10] S. A. Schelkunoff and H. T. Friis, "Antennas, Theory and Practice," John Wiley and Sons, Inc., New York, N. Y., p. 242; 1952.
[11] Jordan, *op. cit.*, p. 364.
[12] S. A. Shelkunoff, "Advanced Antenna Theory," John Wiley and Sons, Inc., New York, N. Y., p. 118; 1952.

C. Comparison of Reradiation Loss and Horizontal Ensemble Gain for Short Dipoles

The reradiation loss of short dipoles is merely a measure of their decreased ability to scatter electromagnetic energy compared to half-wave dipoles. The same footage of material is used in both cases; thus, short dipoles one-tenth the length of a half-wave dipole are ten times more numerous in their ensemble. This loss is listed in Table I for various lengths of short dipoles.

The short dipoles are assumed to be randomly distributed in a horizontal pattern, whereas the half-wave dipoles have a random distribution within a fixed angle about a vertical axis. The scattering ability of the horizontal ensemble is 8.6 db better than a 30° conical ensemble and increases rapidly with a decrease in polar angle. Other values of conical angles are shown in Fig. 2 for $\beta_3=90°$, remembering that the horizontal ensemble has a value 2.9 db above the zero axis.

Fig. 4 is a plot of the reradiation loss as a function of short dipole length. The horizontal ensemble gain over various conical angles is also indicated on the curve. For example, short dipoles 0.2λ long have a reradiation loss of 26.8 db and the horizontal ensemble has a gain of this same amount over a conical ensemble of somewhat less than 5°.

TABLE I
RERADIATION LOSS FACTORS

L_2	m	R_2	X_2	H/S	
0.4λ	1.25	56.0	140	6.5	8.2 db
0.2λ	2.5	14.0	450	480	26.8 db
0.15λ	3.3	7.9	560	1700	32.3 db
0.10λ	5.0	3.5	830	13×10^3	41.1 db
0.05λ	10.0	0.9	1600	440×10^3	56.4 db

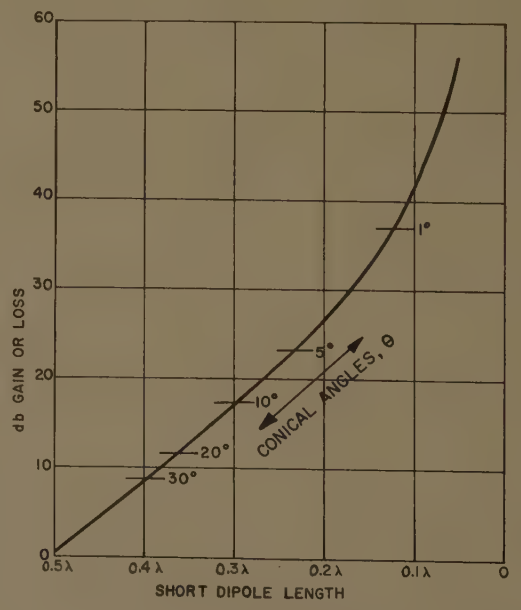

Fig. 4—Reradiation loss and horizontal ensemble gain for short dipoles, where $\beta_3=90°$.

VII. Conclusions

The first part of this report was concerned with finding an analytical expression for the scattering cross section of chaff oriented randomly within a vertical cone. A vertically polarized receiver is assumed off on the horizon and the transmitter on the ground below the chaff. The cross section is a function of the conical angle of the configuration and the angle between a normal to the ground and the incident electric field from the transmitter. Fig. 2 is a plot of the scattering cross section as a function of these two angles. The values are all relative to the same number of dipoles placed in a spherical random ensemble. Fig. 3 is a nomogram for finding the transmission loss for a spherical random ensemble. The necessary corrections to the conical ensemble are obtained from Fig. 2.

Half-wave chaff randomly distributed within a conical angle about a vertical is not the most effective ensemble but is a practical one at the lower frequencies. Cutting all these half-wave dipoles into very short ones makes it practical to place them in a horizontal position which has an ensemble gain over the conical but a reradiation loss since short dipoles are less effective scatters than half-wave ones. The second part of this report compared the reradiation loss and horizontal ensemble gain. Fig. 4 is a plot of the loss as a function of the short dipole length. The horizontal ensemble gain over various conical angles is also indicated on the curve.

Diffraction by a Slit*

ROBERT PLONSEY†, SENIOR MEMBER, IRE

Summary—**The electric field diffracted by a strip caused by an incident cylindrical wave with E parallel to the edge, at various angles of incidence, is measured in a parallel plane medium. The field is compared with that computed from geometrical optics currents and with the addition of equivalent line currents at the edges. The edge "line currents" improve the geometrical optics current field particularly at oblique incidence.**

I. Introduction

A SOLUTION to the problem of the diffraction of electromagnetic waves by a strip was first given by Morse and Rubinstein.[1] In their method of solution the strip is considered as the limiting case of an elliptical cylinder, and an eigenfunction solution is developed. This result is expressed in the form of an infinite series involving Mathieu functions.

Because of the inadequate tabulation of Mathieu functions and also because of the slowness of convergence for large arguments, the above solution has been cumbersome to use, and satisfactory approximate techniques have been sought. Thus, from an analysis of the induced currents on a strip of width λ/π and $2\lambda/\pi$ caused by normal plane wave incidence and with E parallel to the edge, Moullin and Phillips[2,3] characterized the diffracted field as due to geometrical optics currents plus equivalent line currents at the edge. In this formulation they followed an approach originally suggested by Braunbek.[4,5]

Moullin and Phillips noted that the currents near the edges of a strip are very similar to that near the edge of a half plane, provided the strip is $2\lambda/\pi$ or greater in width. By examining the "deviation from geometrical optics" currents for the half plane, the author[6] developed a more generalized "edge current" which permits consideration of oblique incidence. We summarize this development below.

Considering the geometry in Fig. 1, the Sommerfeld

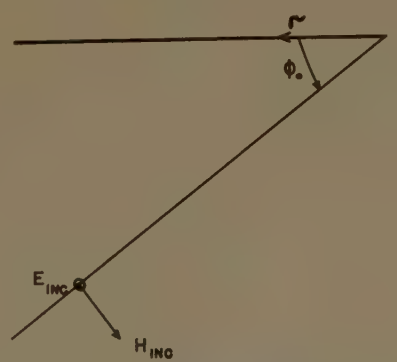

Fig. 1—Half-plane geometry.

* Received by the PGAP, May 31, 1960; revised manuscript received, August 1, 1960.

† Elec. Engrg. Dept., Case Institute of Technology, Cleveland, Ohio.

[1] P. M. Morse and P. J. Rubinstein, "The diffraction of waves by ribbons and by slits," *Phys. Rev.*, vol. 54, pp. 895–898; December, 1938.

[2] E. B. Moullin and F. M. Philips, "On the current induced in a conducting ribbon by the incidence of a plane electromagnetic wave," *Proc. IEE*, vol. 99, pp. 137–150; July, 1952.

[3] E. B. Moullin, "On the current induced in a conducting ribbon by a current filament parallel to it," *Proc. IEE*, vol. 101, pp. 7–17; February, 1953.

[4] W. Braunbek, "Neue Näherungsmethode für die Beugung am eben Schrim," *Z. Physik*, vol. 127, No. 4, pp. 381–390; 1950.

[5] W. Braunbek, "Zur Beugung an die Kreisscheibe," *Z. Physik*, vol. 127, No. 4, pp. 405–415; 1950.

[6] R. Plonsey, "Diffraction by cylindrical reflectors," *Proc. IEE*, vol. 105, pp. 312–317; January, 1958.

solution[7] gives a current distribution as follows, if the incident electric field has an amplitude $\sqrt{\mu/\epsilon}$. We obtain

$$K = -2\sin\phi_0 e^{jkr\cos\phi_0}\frac{e^{j\pi/4}}{\sqrt{\pi}}\cdot\left[\int_{-\infty}^{-\sqrt{2kr}\cos\phi_0/2} e^{-jt^2}dt - \int_{-\infty}^{\sqrt{2kr}\cos\phi_0/2} e^{-jt^2}dt\right] + 2\sqrt{\frac{2}{\pi}}\sin\frac{\phi_0}{2}\frac{e^{-j(kr+\pi/4)}}{\sqrt{kr}}, \quad (1)$$

where K is the surface current density. This result is obtained by equating the surface current to the discontinuity in the tangential magnetic field at the surface of the half plane. The quantity in the brackets of (1) can be written

$$[\ ] = -\int_{-\sqrt{2kr}\cos\phi_0/2}^{\sqrt{2kr}\cos\phi_0/2} e^{-jt^2}dt = -2\int_0^{\sqrt{2kr}\cos\phi_0/2} e^{-jt^2}dt = -\sqrt{\pi}\,e^{-j(\pi/4)} + 2\int_{\sqrt{2kr}\cos\phi_0/2}^{\infty} e^{-jt^2}dt. \quad (2)$$

Eq. (1) can now be written

$$K = K_{g0} - 4\sin\phi_0 e^{jkr\cos\phi_0}\frac{e^{j\pi/4}}{\sqrt{\pi}}\int_{\sqrt{2kr}\cos\phi_0/2}^{\infty} e^{-jt^2}dt + 2\sqrt{\frac{2}{\pi}}\sin\frac{\phi_0}{2}\cdot\frac{e^{-j(kr+\pi/4)}}{\sqrt{kr}}, \quad (3)$$

where $K_{g0}=2\sin\phi_0\exp(jkr\cos\phi_0)$ is the geometrical optics current. The two remaining terms in (3) give the "deviation current" K_D. The integral in (3) is a Fresnel integral for which we have the following asymptotic expansion for large argument:

$$F(x) = \int_x^{\infty} e^{-jt^2}dt = -\frac{j}{2x}\left(1 + \frac{j}{2x^2} + \cdots\right)e^{-jx^2}\quad x\to\infty.$$

The leading term of this expansion when substituted into (3) cancels the third term of that expression. The final result is

$$K_D \sim -\frac{\sin\frac{\phi_0}{2}\,e^{-j(kr-\pi/4)}}{\sqrt{2\pi}(kr)^{3/2}\cos^2(\phi_0/2)}. \quad (4)$$

Eq. (4) yields K_D asymptotically for large (kr). Since the deviation currents decrease rather rapidly [*i.e.*, $O(r^{-3/2})$] from the edge, the field produced by these currents can be ascribed to an equivalent line current at the edge. The "line current" will be non-isotropic. Remaining details are in a previous paper.[6] An effort to confirm experimentally the usefulness of this analysis is given in this paper and in one by Silver and Chang.[8] In both cases the effort fails, partly because the "line currents" are not very large, and the geometrical optics currents alone give good results.

When an incident wave is oblique to an infinite strip, the edge effect is enhanced, as reference to (4) would confirm. Such a conclusion is also clear if we consider edge-on incidence where geometrical optics predict no perturbation at all. Consequently a strip, excited by a line current for different inclinations of the strip, was considered. The geometry is illustrated in Fig. 2. The primary source is a line current; consequently the incident wave is cylindrical, but was treated as being locally plane at the edges. The electric field was measured over a circular path whose center is at the line source and was compared to that calculated from geometrical optics currents, $K_{g0}=2\sin\phi_0\exp(jkr\cos\phi_0)$, with and without the edge correction of (4).

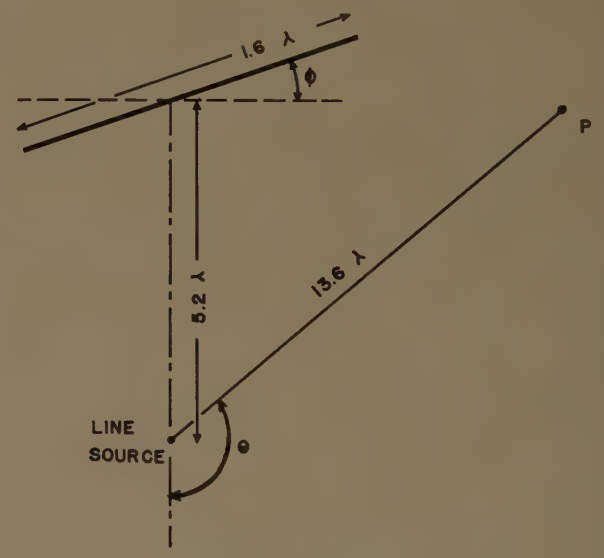

Fig. 2—Geometry for diffraction by a strip.

The measurements were performed in a parallel plane region as described previously.[6] The strip reflector was cut from solid brass so that it has a "U" shaped cross section and was 0.020 inch thick, and 1.6 λ at 9375 Mc. It was equipped with shim stock spring contacts to the upper and lower parallel planes. Accuracy was believed to be ±0.2 db. Calculations required the use of Fresnel integrals and, subject to the assumptions in setting up the model, were essentially precise. It should be noted that a reference field intensity, such as the incident field,

[7] A. Sommerfeld, "Optics," Academic Press, Inc., New York, N. Y., pp. 249–265; 1954.

[8] W. Chang and S. Silver, "Current Distributions on Circular Cylindrical Reflectors," Electronic Res. Lab. Ser., University of Calif., Berkeley, No. 6, Issue No. 193; August, 1957.

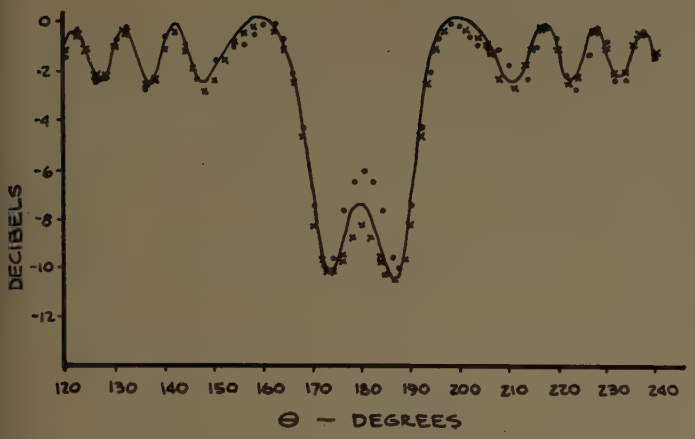

Fig. 3—Electric field pattern for strip with "normal incidence" cylindrical wave, as measured. ($\phi=0$; frequency=9375 Mc.) **0**=geometrical optics, ***X***=edge currents added.

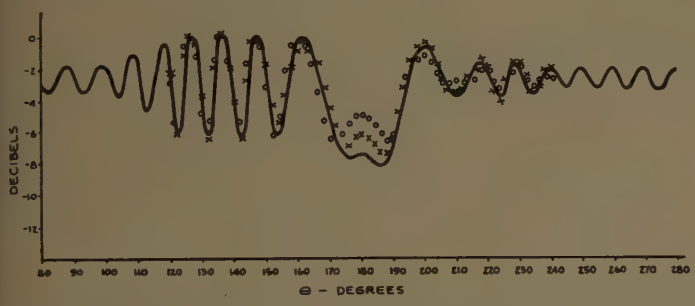

Fig. 4—Electric field pattern for inclined strip due to incident cylindrical wave, as measured. ($\phi=60°$; frequency 9375 Mc.) (See Fig. 2 for geometry.) **0**=geometrical optics. ***X***=edge currents added.

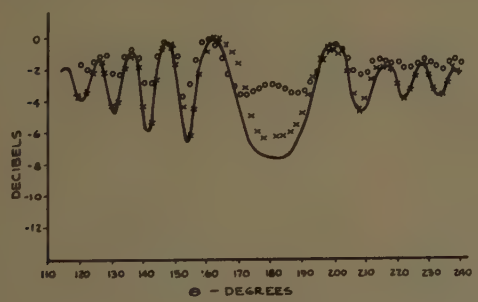

Fig. 5—Electric field pattern for inclined strip due to incident cylindrical wave, as measured. ($\phi=75°$; frequency=9375 Mc.) (See Fig. 2 for geometry.) ***X***=corrected, **0**=geometrical optics.

was not established. Consequently, only relative values in the measured curves of Figs. 3–5 were actually obtained and in each case a reference was arbitrarily established so that the closest agreement with the calculations resulted.

Fig. 3 corresponds to normal plane wave incidence and confirms the above remarks that the geometrical optics currents alone give good results. Figs. 4 and 5 are for oblique incidence and illustrate how the field calculated from geometrical optics currents becomes inaccurate as the angle of incidence increases. The measurements are given by the solid curve while points calculated from geometrical optics are shown by circles; those points whose calculation includes an edge-current correction are denoted by x.

They also indicate that inclusion of edge currents under these conditions will improve the calculated pattern. It is possible that this technique will be useful in predicting the edge effect of an arbitrarily shaped cylindrical reflector.

Acknowledgment

The experimental work and a portion of the computations were carried out at the Electronics Research Laboratory of the University of California at Berkeley. This activity was sponsored by the Office of Naval Research Contract N7-Onr-29529. The remaining work was performed at the Case Institute of Technology, Cleveland, Ohio, sponsored by the Electronics Research Directorate of the Air Force Cambridge Research Center, Cambridge, Mass., under contract AF 19(604)-3887. Mrs. Ceres Schroer at Berkeley and Hwei-Piao Hsu at Case performed the bulk of the computations.

The author wishes to acknowledge his indebtedness to Professor S. Silver of the University of California for his interest in and guidance of this work.

communications

Matrix Relations for a Linear Array with Dipole Elements in the Fresnel Zone*

This communication is an extension of a previous paper[1] to the Fresnel region. The electric dipole elements are shown to be arbitrarily distributed along the x axis, in Fig. 1. The magnetic field at the observation point $P(\rho_l; \psi_l; \phi)$ due to the dipole element A_l at position $x=x_l$ will be

$$H_{\phi l} = A_l\left[\frac{i}{(k\rho_l)^2} - \frac{1}{(k\rho_l)}\right]\sin\psi_l e^{-ik\rho_l}. \quad (1)$$

Using Stratton's definition for spherical Hankel functions of the second kind,[2] (1) may be rewritten as

$$H_{\phi l} = A_l h_1^{(2)}(k\rho_l)\sin\psi_l. \quad (2)$$

By adding the contributions of all the dipole elements in Fig. 1, and using elementary trigonometric considerations, one gets from (2) the total magnetic field

$$H_\phi = kR\sin\theta\sum_{l=0}^{L} A_l\frac{h_1^{(2)}(k\rho_l)}{k\rho_l} \quad (3)$$

where A_l is the complex amplitude (amplitude and phase) of dipole l.

The addition theorem given by Morse and Feshbach[3] (given originally by Gegenbauer, Sonine and Watson[4]) is

$$\frac{h_1^{(2)}(k\rho_l)}{k\rho_l} = \frac{1}{kR}\sum_{n=0}^{\infty}(2n+3)\frac{j_{n+1}(kx_l)}{kx_l} \cdot h_{n+1}^{(2)}(kR)T_n^1(\cos\theta), \quad (4)$$

where $j_n(kx_l)$ and $h_n^{(2)}(kR)$ are the spherical Bessel and Hankel functions and $T_n^1(\cos\theta)$ is the Gegenbauer polynomial of the first order as defined by Morse and Feshbach.[3]

Defining the Fresnel region pattern $F(\theta; R_0)$ at any sphere, $R=R_0$ by

$$H_\phi = \frac{ie^{-ikR_0}}{kR_0}F(\theta; R_0) = h_0^{(2)}(kR_0)F(\theta; R_0), \quad (5a)$$

where the far zone (Fraunhofer region) pattern $F(\theta)$ will be

$$F(\theta) = \lim_{R_0\to\infty} F(\theta; R_0). \quad (5b)$$

It may be expanded as follows by using the orthogonality property of the Gegenbauer polynomials:[3]

$$F(\theta; R_0) = \sin\theta\sum_{n=0}^{\infty}(2n+3)\alpha_n(R_0)T_n^1(\cos\theta). \quad (6)$$

Substituting (4) in (3) and (6) in (5a), one gets the relationships

$$\alpha_n(R_0) = \gamma_{n+1}(R_0)\sum_{l=0}^{L} A_l\frac{j_{n+1}(kx_l)}{kx_l}, \quad (7)$$

where

$$\gamma_{n+1}(R_0) = \frac{h_{n+1}^{(2)}(kR_0)}{h_0^{(2)}(kR_0)} \quad \text{for} \quad n \geq 0.$$

In case of a far zone pattern $R_0\to\infty$, one gets[2]

$$\lim_{R_0\to\infty}\gamma_{n+1}(R_0) = i^n. \quad (8)$$

Since (7) holds for every $n\geq 0$, it may be rewritten in the following matrix form:

$$\left[\frac{\alpha_n(R_0)}{\gamma_{n+1}(R_0)}\right] = \left[\frac{j_{n+1}(kx_l)}{kx_l}\right], \quad A_l]. \quad (9)$$

The importance of finding the Fraunhofer far zone pattern from measurements in the Fresnel region has been pointed out previously.[5,6] Eqs. (7) and (9) give this possibility for antenna arrays made of dipole elements.

H. Unz
Elec. Engrg. Dept.
University of Kansas
Lawrence, Kan.

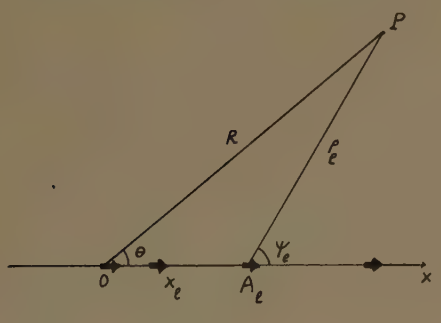

Fig. 1.

* Received by the PGAP, October 4. This work was done while the author was a consultant for the Rad. Lab., University of Michigan, Ann Arbor, during summer 1958.

[1] H. Unz, "Linear arrays with arbitrarily distributed elements," IRE TRANS. ON ANTENNAS AND PROPAGATION, vol. 8, pp. 222–223; March, 1960.

[2] J. A. Stratton, "Electromagnetic Theory," McGraw-Hill Book Co., Inc., New York, N. Y., p. 405; 1941.

[3] P. M. Morse and H. Feshbach, "Methods of Theoretical Physics," McGraw-Hill Book Co., Inc., New York, N. Y., pp. 782–783, 1574; 1953.

[4] G. N. Watson, "Bessel Functions," Cambridge Univ. Press, Cambridge, Eng., p. 363; 1944.

[5] R. W. Bickmore, "Fraunhofer pattern measurement in the Fresnel region," *Canad. J. Phys.*, vol. 35, pp. 1299–1308; 1957.

[6] D. K. Cheng, "On the stimulation of Fraunhofer radiation patterns in the Fresnel region," IRE TRANS. ON ANTENNAS AND PROPAGATION, vol. 5, pp. 399–402; October, 1957.

Multiple-Parameter Presentation of Radar Meteor Echoes*

A circuit is given enabling the range, time of occurrence, duration, maximum amplitude, and amplitude variations in radar echoes from meteor trails to be presented on a single-beam oscillograph.

I. Introduction

Radar echoes from a single meteor trail, using—if desired—a common-antenna array, give information on the range, time of occurrence, duration, maximum amplitude, and amplitude variations. The work presented here enables all these parameters to be presented on a single-beam oscillograph, suitable for photographic recording.

The intensity-modulated presentation normally used in radar for meteor patrol purposes was used in the present equipment. The system operated conventionally at 69.0 Mc, transmitting pulses of 90-kw peak power and 16-μsec width, at a pulse-recurrence frequency of 150 per second. The linear receiver had a noise figure of 1.95 db. The positive-going echo output from the receiver was applied to the grid of a cathode-ray tube, giving spot brightening of a nearly blacked out time-base.

II. Addition of Echo Amplitude Presentation

A. General Considerations

In principle, all that is required to show echo amplitude is to add the receiver-output pulse waveform to the linear sweep voltage, with accelerated film motion if necessary. A circuit to achieve this, in which the pulse voltage accelerates the electron beam, causing reduced intensity or a "hole" in the time base, of length proportional to the echo amplitude, has been given by Pineo and Peck.[1] With this arrangement, however, it is possible that the hole will be partly filled in by the next time-base trace moving over the same part of the cathode-ray tube screen, if the amplitude or range is altering at a greater rate than the film motion. Also, their pulse amplifier feeds directly into the low-output impedance of a cathode follower, which must restrict the available voltage output if a linear copy of the signal amplitude is to be maintained. These facts, together with the wish to use positive modulation, led to the development of the following circuit.

B. The Additive Mixer

When a cathode follower is required to accept large negative-voltage waveforms, its quiescent current must be high. To avoid this, and since the existing sweep generator output is negative-going, two "anode followers" are used in cascade (Fig. 1). The first anode follower adds the pulse and sweep voltages without mutual interference, and the second inverts the compound-sweep waveform. Since the sweep-generator output has undergone two phase reversals at unity gain, there is no change in its polarity or magnitude. (A double-pole switch is sufficient to remove the amplitude parameter. Since the output impedance of the anode followers is very low, the stray capacitance across the switch contacts is of no consequence.)

With simple mixing, the intensity of the pulse trace is proportional to the instantaneous pulse amplitude, and consequently there is no clear indication of where the pulse begins to accelerate the time base. It therefore becomes necessary to delay the pulse input to the mixing circuit until the intensity has risen sufficiently, by application of the pulse to the grid of the oscillograph tube, make the time base visible. A principal advantage of the circuit is that in the absence of an echo there is no bright-up, and consequently no problem arises due to subsequent time-base sweeps overlying the wanted signal.

The various waveforms and time relationships are shown in Fig. 2. The delay required is of the order of half the pulse length, or about 13 μsec, which can readily be achieved by a simple integrating circuit. If all echoes are assumed to be of the same width, then the integrated output will be a linear function of the input amplitude. This constancy of width is reasonably true for all but the longest duration echoes, when errors may arise due to widening of the received pulse by winds which distort the meteor trail.[2] Such echoes are few in number.

In order to facilitate echo recognition in the absence of amplitude presentation, a square wave is used to displace alternate time bases; synchronous echoes therefore appear in duplicate. This facility has been retained, resulting in the appearance of echoes, as in Fig. 3. It was thought that this "jitter" might still be necessary to identify the shortest duration echoes, but it is now apparent that the presence of linear bright-up alone would be adequate for recognition of such echoes.

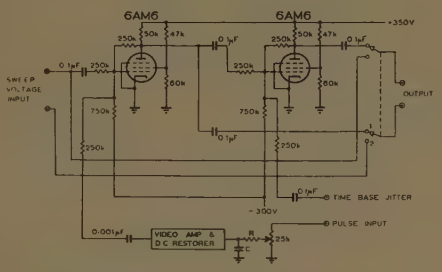

Fig. 1—Circuit diagram of additive mixer.

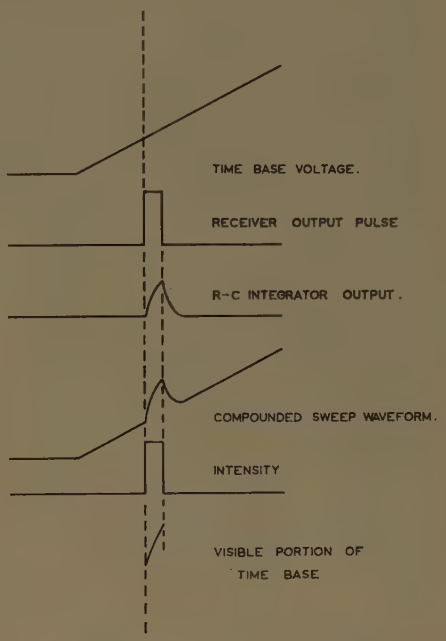

Fig. 2—Time relationship of signals applied to oscilloscope tube.

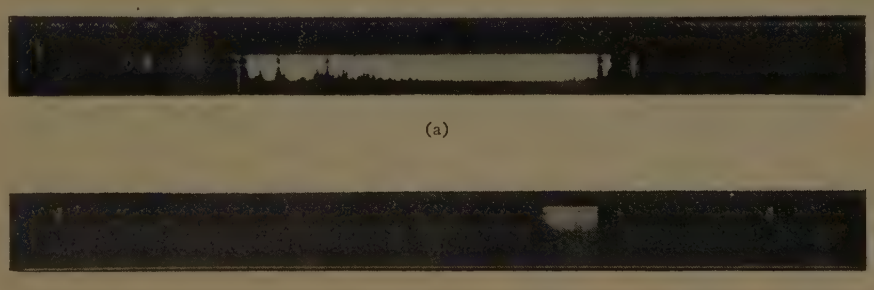

(a)

(b)

Fig. 3—Echo presentation. Range increases vertically downwards and time increases from right to left. Both traces cover one minute of recording. (a) Four echoes, with the main echo showing amplitude saturation and deep fading. (b) Four typical echoes.

Initial maximum amplitude and range data were used to calculate line densities of electron concentration in meteor trails, and these values were then converted to meteor magnitudes.[3] The range of magnitudes observed is a function of the equipment. In the work for this note, meteor magnitudes between 7 and 11 were simply recorded in this way.

C. Ellyett
A. C. Stanbury
University of Canterbury
Christchurch, New Zealand

* Received by the PGAP, October 21, 1960. The work for this note was carried out in part under Contract AF64(500)-6 of the AF Cambridge Res. Center, Cambridge, Mass.

[1] V. E. Pineo and R. C. Peck, "A circuit for simultaneously recording the range, amplitude and duration of radar-type reflections," *Rev. Sci. Instr.*, vol. 22, pp. 112; February, 1951.

[2] J. S. Greenhow, "A radio echo method for the investigation of atmospheric winds at altitudes of 80 to 100 km," *J. Atmos. Terrest. Phys.*, vol. 2, pp. 282–291, 1952.

[3] T. R. Kaiser, "Radio echo studies of meteor ionization," *Phil. Mag.*, Suppl., vol. 2, pp. 495–544; October, 1953.

Amplitude Comparison Error of a Signal Received by Two Circularly-Polarized Antennas Due to Off-Axis Ellipticity*

Target location by post-detection beam-interpolation amplitude comparison is a simple method of tracking, provided that the beamshape of each antenna in the receiver array is identical and known as a function of angle, and most important, that the antennas are linearly polarized and have a common plane of polarization. In an application where it is necessary to have circularly-polarized receiving antennas, amplitude comparison is erroneous, due to the fact that the polarization of any circularly polarized antenna increases in ellipticity as a function of angle off-axis. (See Fig. 1.)

Consider only two identical antennas, spaced and oriented such that the angular beam spacing is δ and the crossover is located at $\theta=\delta/2$ with respect to the first element. (See Fig. 2.) The axial ratio r is then different for each antenna for any $0\leq\theta\leq\delta$.

Since the antennas are angularly displaced, the normalized far field amplitudes are related as

$$\bar{F}_2(\theta) = \bar{F}_1(\theta - \delta). \tag{1}$$

If one considers elliptical polarization, it is convenient to define a unit polarization vector,

$$1_P = \frac{1_\phi' + 1_\theta'(jr)}{\sqrt{1+r^2}}, \tag{2}$$

where $j=\sqrt{-1}$ denotes time quadrature. If one further considers a polarization or tilt angle τ of the major axis of polarization ellipse, then (2) becomes

$$1_P = \frac{1_\phi(\cos\tau + jr\sin\tau) + 1_\theta(\sin\tau - jr\cos\tau)}{\sqrt{1+r^2}}. \tag{3}$$

The complex voltage or current induced by an elliptically polarized wave incident upon a receiving antenna is

$$\left.\begin{matrix} I_R \\ V_R \end{matrix}\right\} \propto 1_{PT}\cdot 1_{PR}^{*,1,2} \tag{4}$$

where the subscripts T and R refer to transmitted and received signals and the asterisk (*) denotes complex conjugate. Thus, the normalized post-detection voltage amplitude comparison is

$$\Delta = \frac{\left| 1_{PT}\cdot\bar{F}_1^* \right|}{\left| 1_{PT}\cdot\bar{F}_2^* \right|}, \tag{5}$$

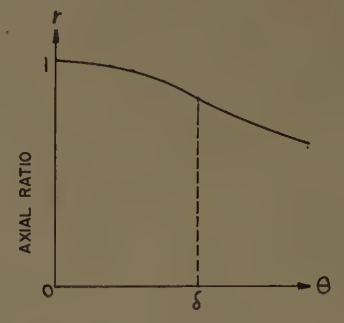

Fig. 1—Axial ratio.

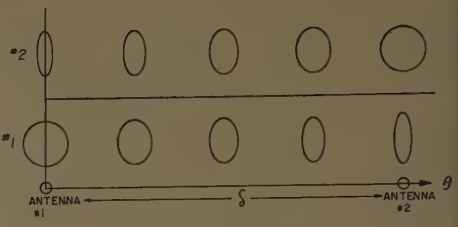

Fig. 3—Ellipticity variation.

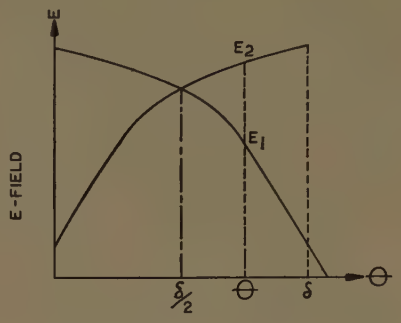

Fig. 2—Beam overlap for amplitude comparison.

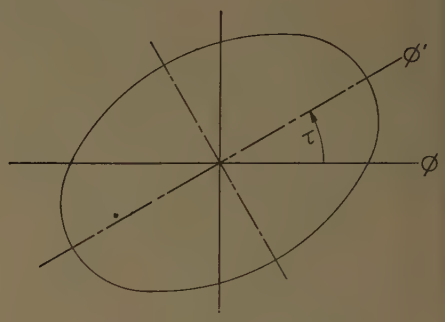

Fig. 4—Polarization angle.

where

$$\bar{F}_K^* = 1_{PK}{}^*F_K, \tag{6}$$

$$\Delta = \sqrt{\frac{(1+r_2^2)}{(1+r_1^2)}}\,\frac{\left|(1+r_Tr_1)\cos(\tau_T-\tau_1)+j(r_1+r_T)\sin(\tau_T-\tau_1)\right|}{\left|(1+r_Tr_2)\cos(\tau_T-\tau_2)+j(r_2+r_T)\sin(\tau_T-\tau_2)\right|}\,\frac{F_1}{F_2}, \tag{7}$$

taking the absolute value

$$= \sqrt{\left[\frac{1+r_2^2}{1+r_1^2}\right]\left[\frac{(1+r_Tr_1)^2-(1-r_T^2)(1-r_1^2)\sin^2(\tau_T-\tau_1)}{(1+r_Tr_2)^2-(1-r_T^2)(1-r_2^2)\sin^2(\tau_T-\tau_2)}\right]}\,\frac{F_1}{F_2}. \tag{8}$$

Thus, if the antennas are identically polarized, *i.e.* $\tau_1=\tau_2$ and $\tau_T-\tau_1=\tau$, it is noted that normal amplitude comparison,

$$\Delta = \frac{F_1}{F_2}, \tag{9}$$

exists, except when the receiving antennas are elliptically polarized.

Polarization		Δ for $\tau_1=\tau_2$
Transmitter	Receiver	
Linear	Elliptical	$\frac{F_1}{F_2}\left[\frac{1+r_2^2}{1+r_1^2}\right]^{1/2}\left[\frac{1-(1-r_1^2)\sin^2\tau}{1-(1-r_2^2)\sin^2\tau}\right]^{1/2}$
Circular	Elliptical	$\frac{F_1}{F_2}\,\frac{(1+r_1)}{(1+r_2)}\left[\frac{1+r_2^2}{1+r_1^2}\right]^{1/2}$
Elliptical	Elliptical	(8)
All other combinations		$\frac{F_1}{F_2}$

* Received by the IRE, November 17, 1960.

[1] M. L. Kales, "Part III—elliptically polarized waves and antennas," PROC. IRE, vol. 39, pp. 544–549; May, 1951.

[2] M. L. Kales and J. I. Bohnert, "Elliptically polarized waves," Naval Res. Lab., Washington, D. C. Rept. No. 3686.

H. B. QUERIDO
Electronics Div.
Westinghouse Electric Corp.
Baltimore, Md.

Octave-Bandwidth Feed Horn for Paraboloid*

This note describes a broadband feed horn[1] which, when mounted at the focal point of a parabolic dish, yields equal E- and H-plane radiation patterns. The aperture of the feed horn (Fig. 1) is circular in cross section and operates on the fundamental TE_{11}-waveguide mode. Single-mode operation of the TE_{11} over a wide frequency range was obtained by quadruple-ridge loading of the circular waveguide feeding the horn.

An antenna consisting of a horn mounted at the focal point of a parabolic dish of $f/D=0.42$ was constructed to check the radiation patterns of the complete antenna. The results of these tests showed that the E- and H-plane patterns taken at the frequencies of 15.1 and 30.2 kMc have identical half-power beamwidths of 1.2 degrees with the principal-plane sidelobes at least −23 db down from the main beam. The antenna, consisting of the feed horn mounted at the focal point of the parabolic dish, is shown in Fig. 2.

The secondary radiation patterns of the antenna were measured on a 1100-foot antenna range at the frequencies of 15.1 and 30.2 kMc, and are shown in Fig. 3. It can be seen from these patterns that, at both frequencies, the E- and H-plane patterns have

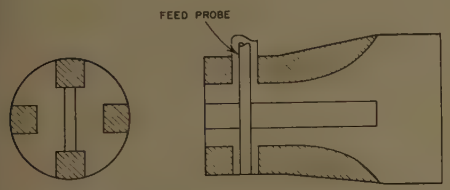

Fig. 1—Schematic diagram of the quadruply-ridged circular-waveguide antenna feed horn.

Fig. 2—Photograph of the parabolic antenna.

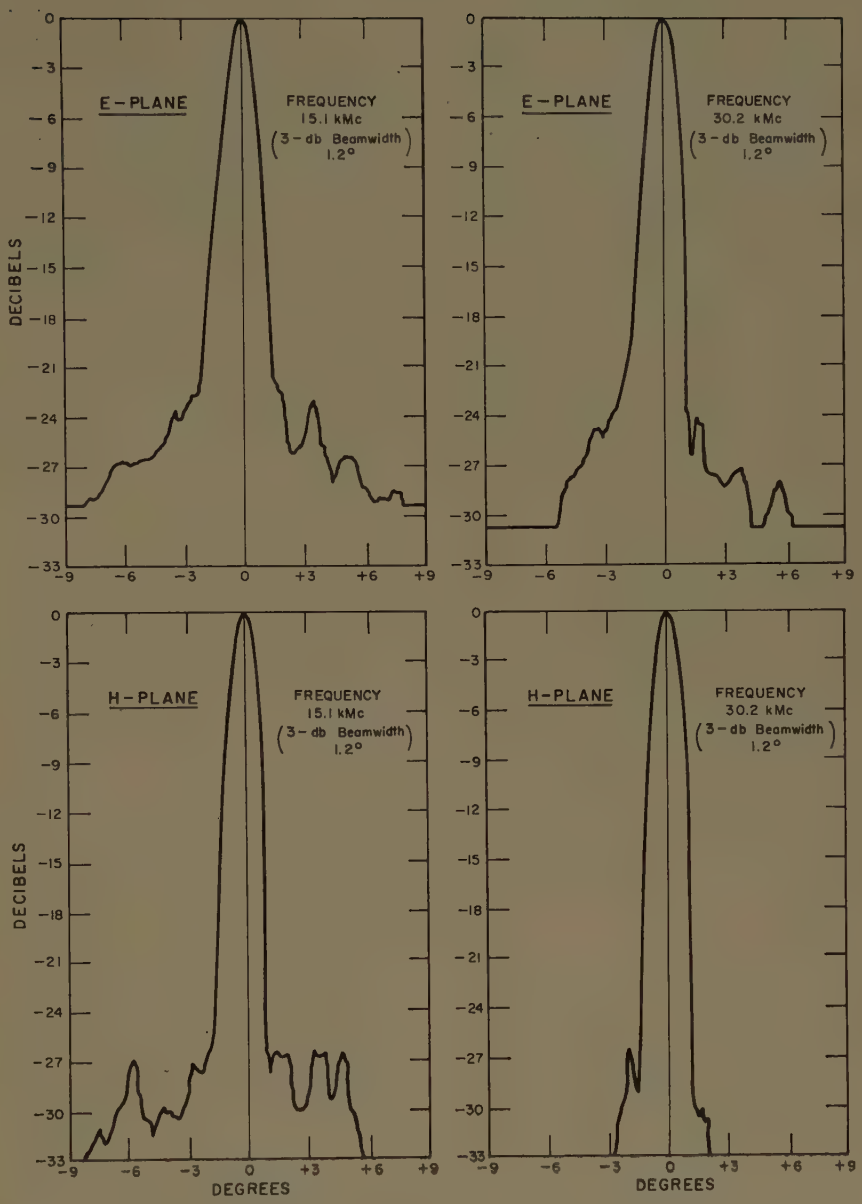

Fig. 3—E- and H-plane radiation patterns of the parabolic antenna.

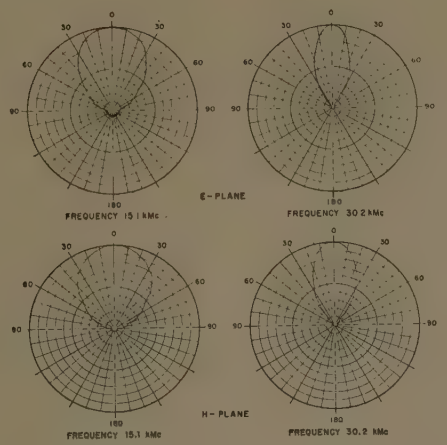

Fig. 4—E- and H-plane amplitude radiation patterns of the feed horn.

* Received by the PGAP, October 27, 1960.

[1] J. K. Shimizu, "Overseas Auroral Propagation Experiments," Final Rept., pt. 2, Stanford Res. Inst., Menlo Park, Calif., Contract AF30(602)-1871, SRI Project 2604; March 19, 1960.

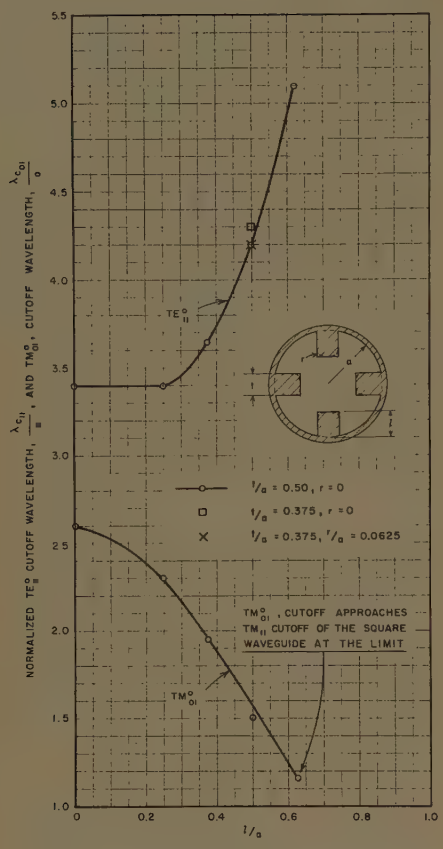

Fig. 5—Normalized quadruply-ridged circular waveguide TE_{11} and TM_{01}—cut-off wavelength (t/a=0.50).

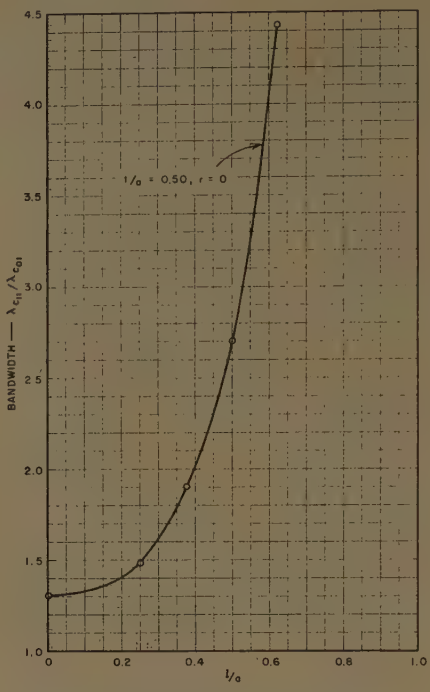

Fig. 6—Bandwidth of the quadruply-ridged circular waveguide (t/a=0.50).

equal half-power beamwidths of 1.2 degrees with all the sidelobes at least −23 db down from the main beam. These radiation patterns were produced with a quadruply-ridged primary feed horn having a cylindrical aperture 0.587 inch in diameter. This aperture corresponds to 0.75 λ_L, where λ_L is the free-space wavelength at the lower operating frequency.

The primary E- and H-plane radiation patterns of the feed horn alone, taken at 15.1 and 30.2 kMc, are shown in Fig. 4. The E- and H-plane patterns of the horn at 15.1 kKc show that the patterns are approximately 10 db down from the main beam at the angle of ±61.5 degrees. This angle corresponds to the edge of the parabolic dish with a focal-length-to-diameter ratio of f/d=0.42. At the frequency of 30.2 kMc, the aperture opening of the horn of 0.587-inch diameter corresponds to 1.50 λ_h, where λ_h is the free-space wavelength at the higher operating frequency. It can be seen from Fig. 4 that the pattern in the E plane is sharper than the H-plane pattern,[2] with the sidelobe levels at least −20 db down within the angle of ±61.5 degrees.

To be able to propagate a single TE_{11} mode over at least a 2:1 frequency range in a circular waveguide, some means of suppressing the higher-order modes is required. When exciting the TE_{11} mode in a circular waveguide with the feed probes arranged as shown in Fig. 1, the first of these higher-order modes that will tend to destroy the desired feed-horn pattern will be the TM_{01}. The TM_{01} mode was suppressed by ridge-loading the circular waveguide.

In order to determine the effects on the cutoff frequencies of the TE_{11} and the TM_{01} modes as the ridge dimensions are varied, a quadruply ridged cavity was constructed and tested as a band-pass filter. The cross section of the cavity was constructed so that the length l and thickness t of the ridges could be varied. The results of these tests are shown in Fig. 5. In Fig. 6, the ratio of the two cutoff wavelengths is plotted as a function of the ratio l/a. This ratio corresponds to the bandwidth available between the cutoff of the TE_{11} mode and the cutoff of the TM_{01} mode. The data presented in Fig. 5 are for the case when t/a=0.50, and the TE_{11}-mode cutoff wavelengths for several other combinations of ridge thickness and length have been measured by Chait and Sakiotis.[3]

With a quadruple-ridge-loaded circular horn mounted at the focal point of a parabolic dish, it was possible to obtain equal beamwidth patterns at the two discrete frequencies, which are separated one full octave. Although the antenna described in this note was specifically designed to operate at 15.1 and 30.2 kMc, the feed horn for this antenna is capable of propagating a single TE_{11} mode over the frequency range from 12 to 36.2 kMc. The design data which are included in this paper show that it is possible to design a horn of this type to operage over a frequency band of more than 4:1.

A quadruple-ridge-loaded horn of this type may find many uses as a broad-band horn as well as a feed to yield a constant-beamwidth secondary pattern when mounted at the focal point of a parabolic dish.

ACKNOWLEDGMENT

The author wishes to acknowledge the help and advice received in the course of the work from Dr. E. M. T. Jones and Dr. R. C. Honey.

J. K. SHIMIZU
Stanford Res. Inst.
Menlo Park, Calif.

On the Definition of the Effective Aperture of Antennas*

According to IRE *Standards on Antennas* published in 1948, the aperture area, henceforth referred to as the effective aperture, of an antenna is defined as $\lambda^2 D/4\pi$ where D denotes the directivity of the antenna. It is currently well known among antenna engineers that if we define the effective aperture as

$$A = \frac{P_r}{S^i} = \frac{\text{power received}}{\text{incident power density}}, \quad (1)$$

then the quoted definition applies only to the optimum case where the incident field has a polarization matched to that of the vector effective height of the antenna, aside from the condition that the load impedance is also matched to the antenna impedance. Since the previously mentioned *Standards* is a little obsolete anyway, we would like to introduce a revised definition for that term which has a broader coverage.

In the general case where the polarizations and the impedances are not matched, one may evaluate the value of P_r/S^i as contained in (1) and derive the following formula for A, namely,

$$A = pq\frac{\lambda^2 D(\theta, \phi)}{4\pi} \quad (2)$$

where

$D(\theta, \phi)$ = directivity of the antenna defined in the direction of incidence of the incident field (θ, ϕ),
q = impedance mismatching factor

$$= \frac{4RR_L}{(R+R_L)^2+(X+X_L)^2},$$

[2] G. C. Southworth, "Principles and Applications of Waveguide Transmission," D. Van Nostrand Co., Inc., New York, N. Y., pp. 404–407; 1960.

[3] H. N. Chait and N. G. Sakiotis, "Broad-band ferrite rotators using quadruply-ridged circular waveguide," IRE TRANS. ON MICROWAVE THEORY AND TECHNIQUES, vol. MTT-7, pp. 38–41; January, 1959.

* Received by the PGAP, November 7, 1960. Part of this research was performed under Contract AF 33(616)-7614, sponsored by Wright Air Dev. Div., Wright-Patterson Air Force Base, with the Ohio State University Res. Foundation.

$Z_L = R_L + jX_L$ = load impedance,
$Z = R + jX$ = antenna impedance defined at the load terminals,
p = polarization mismatching factor

$$= \frac{|\boldsymbol{h}\cdot\boldsymbol{E}^i|^2}{|\boldsymbol{h}|^2|\boldsymbol{E}^i|^2},$$

$\boldsymbol{h} = h_\theta\hat{\theta} + h_\phi\hat{\phi}$ = vector effective height of the antenna,

$\boldsymbol{E}^i = E_\theta{}^i\hat{\theta} + E_\phi{}^i\hat{\phi}$ = incident electric field.

As shown by Deschamps,[1] the polarization mismatching factor can be described in a very neat form by means of the Poincaré sphere; that is,

$$p = \cos^2\delta \tag{3}$$

where 2δ denotes the angular distance between the two polarization states corresponding to that of $\boldsymbol{h}$ and $\boldsymbol{E}^{i*}$ (conjugate of $\boldsymbol{E}^i$) as defined on the Poincaré sphere. In terms of the polarization ratios defined by

$$\frac{h_\phi}{h_\theta} = te^{j\beta} \quad \text{and} \quad \frac{E_\phi{}^i}{E_\theta{}^i} = se^{j\alpha}, \tag{4}$$

p is given by

$$p = \frac{1 + s^2t^2 + 2st\cos(\alpha+\beta)}{(1+s^2)(1+t^2)}. \tag{5}$$

Polarization matching corresponds to $\alpha = -\beta$ and $s = t$, as first pointed out by Yeh.[2] The use of (2) as the definition of the effective aperture of an antenna removes the restrictions imposed upon by the old one. If one deals with a matched load, then $q = 1$ and the corresponding effective aperture will be denoted by

$$A_m = \frac{p\lambda^2 D(\theta,\phi)}{4\pi}. \tag{6}$$

If the polarizations are also matched, then $p = 1$, and the corresponding effective aperture will be denoted by

$$A_{mm} = \frac{\lambda^2 D(\theta,\phi)}{4\pi}. \tag{7}$$

Finally, if the incident field is incident upon in the direction of maximum directivity, D, of the receiving antenna, we have the optimum case, *i.e.*,

$$A_{op} = \frac{\lambda^2 D}{4\pi}. \tag{8}$$

From (1) and (2), it is also relatively simple to derive the transmission formula of Friis as applied to the unmatched cases. Thus, if we substitute (9),

$$S^i = \frac{P_t D_t(\theta,\phi)}{4\pi r^2}, \tag{9}$$

into (1), and use the formula for A as given by (2), the following relation is obtained.:

$$\frac{P_r}{P_t} = pq\left(\frac{\lambda}{4\pi r}\right)^2 D_t(\theta,\phi) D_r(\theta,\phi) \tag{10}$$

where r and t denote, respectively, the parameters pertaining to the receiving and the transmitting antennas. Finally, it may be mentioned here that if the incident field is randomly polarized, the average value of p as evaluated on the Poincaré sphere is simply equal to $\frac{1}{2}$ which can be verified as follows:

$$\begin{aligned}\bar{p} &= \frac{1}{4\pi}\int\int p\,d\Omega \\ &= \frac{1}{4\pi}\int_0^\pi\int_0^{2\pi}\cos^2\frac{\theta'}{2}\sin\theta'\,d\theta'\,d\phi' \\ &= \frac{1}{2}.\end{aligned} \tag{11}$$

The average value of A_m as applied to the case of a matched load is then given by

$$\bar{A}_m = \frac{\lambda^2 D(\theta,\phi)}{8\pi} \tag{12}$$

which is independent of the state of polarization of the receiving antenna.

The author gratefully acknowledges the suggestion of Dr. Robert G. Kouyoumjian of integrating p on the Poincaré sphere in evaluating the average value of A_m for a randomly polarized wave.

Chen To Tai
Antenna Lab.
Dept. of Elec. Engrg.
The Ohio State University
Columbus, Ohio

[1] G. A. Deschamps, "Geometrical representation of the polarization of a plane electromagnetic wave," Proc. IRE, vol. 39, pp. 540–544; May, 1951.
[2] Yung-Ching Yeh, "The receiving power of a receiving antenna and the criteria for its design," Proc. IRE, vol. 37, pp. 155–158; February, 1949.

Correction of the Astigmatism of a Spherical Diffraction Reflector*

In a previous paper[1] a particular type of reflector antenna was described which allows the scanning of large angles by only moving the feeder. This antenna has a general spherical shape, but its reflecting surface is constituted by zones of confocal paraboloids, suitably spaced with respect to one another. Such an antenna, which must operate at a given wavelength (design wavelength), presents the following characteristics:

1) The spherical aberration vanishes over the whole aperture.
2) The coma is identically zero to any order in the aperture and to the first order in the field angle.

A model of this antenna to operate at $\lambda = 3.2$ cm has been built and tested at the Centro Microonde.[2] Other models with different values of the parameters have been built and tested by Ramsey and Jackson[3] and by Provencher.[4]

The results of the experimental tests were in excellent agreement with the theory developed on the basis of parageometrical optics.[1] On the basis of the tests carried out on our mirror, one can conclude that a field angle of $\pm 20°$ is effectively covered. This limit is essentially due to the astigmatism, which affect the system to the same extent as in any conventional smooth mirror.

It is well known that the astigmatism is a function of the field angle and that it is measured by the distance between the two astigmatic foci. The effect of the astigmatism may be reduced by placing the feeder at the "best focus" (defined as the midpoint between the two astigmatic foci). However, this is a compromise, giving only a partial correction.

It occurred to us that the effect of the astigmatism can be completely eliminated by means of a particular type of feeder. The feeder is simply constituted by two open rectangular waveguides of different dimensions, the smaller one being fitted into the larger one, as shown in Fig. 1. The smaller waveguide can be longitudinally shifted so as to vary the distance d from its mouth to the mouth of the larger waveguide. The smaller waveguide may have a square cross section which is useful for changing the direction of polarization of the field. The larger waveguide may be simply constituted by two parallel plates.

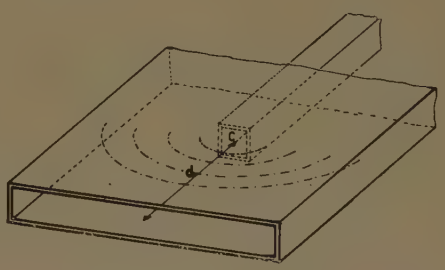

Fig. 1.

When the smaller waveguide is fed, it gives rise to a cylindrical wave in the space between the two mouths. This cylindrical wave is diffracted at the mouth of the larger waveguide and spreads into a fan. The net result is an "astigmatic wave" with its two foci at the mouths of the two waveguides if the mode within the larger waveguide is TEM. For any other mode corresponding to a refractive index n the distance apart of the two foci is d/n. The astigmatism can be varied simply by varying the distance d.

Fig. 2 shows a picture of the feeder which was built for testing the diffraction reflector. The cross sections of both waveguides are 2.3×2.3 cm and 2.5×40 cm, respectively, and d can vary between 0 and 12 cm.

* Received by the PGAP, November 4, 1960. This research has been sponsored by the Air Res. and Dev. Comm., U.S.A.F., under Contract AF 61(052)-234, through the European Office, A.R.D.C.
[1] L. Ronchi and G. Toraldo di Francia, "An application of parageometrical optics to the design of a microwave mirror," IRE Trans. on Antennas and Propagation, vol. AP-6, pp. 129–133; January, 1958.
[2] G. Toraldo di Francia, L. Ronchi, and V. Russo "Experimental test of a stepped-zone mirror for microwaves," IRE Trans. on Antennas and Propagation, vol. AP-7, pp. 125–131; December, 1959.
[3] J. F. Ramsey and J. A. C. Jackson, "Wide-angle scanning performance of mirror aerials," *Marconi Rev.*, vol. 19, pp. 119–140; July–October, 1956.
[4] J. A. Provencher, "Experimental study of a diffraction reflector," IRE Trans. on Antennas and Propagation, vol. AP-8, pp. 331–336; May, 1960.

Fig. 2.

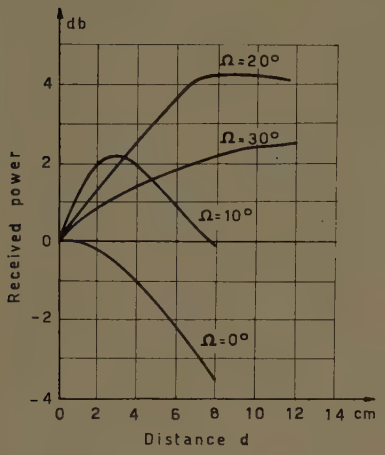

Fig. 3.

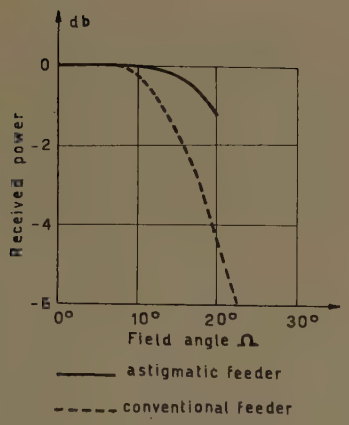

Fig. 4.

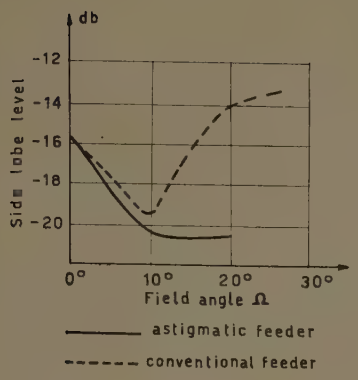

Fig. 5.

The position of the two foci has been texted experimentally by determining the radiation centers of the emerging wavefronts for different values of the distance d and the two different polarizations. A slight discrepancy with the prediction appeared only in the TE case where an effective index $n=0.7$ is found instead of the computed value $n=0.6$. This discrepancy may be justified by taking into account the "spherical aberration" of the emerging wavefront due to the refraction at the plane mouth of the larger waveguide.

A set of measurements with this feeder has been carried out on the diffraction reflector described by Toraldo di Francia.[2]

First the long mouth of the feeder was brought to coincide with the tangential Sturm line,[5] as previously determined by a conventional feeder. For each of a set of values of the field angle Ω, the power received, P, was plotted as a function of the distance d. The results are shown in Fig. 3. It appears that the curve for $\Omega=0°$ has a maximum at $d=0$ and the curve for $\Omega=10°$ has a maximum at $d=2.5$ cm, while for $\Omega=20°$ the maximum corresponds to $d=10$ cm. These values coincide with the theoretical predictions for the astigmatism.

The width of the main lobe turns out to be the same as that found with a conventional feeder. However, as shown in Fig. 4, the power collected by the astigmatic feeder (solid line) considerably exceeds that collected by the conventional feeder at the best focus (broken line), as soon as the field angle exceeds about 15°. Another gratifying result is illustrated in Fig. 5, which shows the behavior of the first sidelobe level for the conventional (broken line) and the astigmatic (solid line) receivers. The latter presents an incredibly small sidelobe level from $\Omega=10°$ upwards.

In conclusion, the astigmatic feeder appears to improve substantially the performance of the diffraction reflector.

V. Russo
G. Toraldo di Francia
Centro Microonde
Florence, Italy

[5] P. F. Checcacci, L. Ronchi, V. Russo, and G. Toraldo di Francia, "Design, Development and Test of an Advanced, Fixed Position Radio Astronomy Antenna," Centro Microndе, Florence, Italy, USAF contract AF 61(052)-234 April, 1960.

Stochastic Processes and Beyond-the-Horizon Propagation*

Introduction

The theoretical literature on the subject of tropospheric scatter propagation is extensive and growing at an ever-increasing rate. In view of this, it is of interest to analyze the assumptions common to most theoretical ventures.

* Received by the PGAP , November 17, 1960.

There are at present two different possible approaches to the problem of beyond-the-horizon propagation. The first is the classical or nonstatistical form in which the beyond-the-horizon field is assumed to result from repeated coherent refraction and diffraction of the original wave. The most recent application of this method was made by Tukizi.[1] His results appear to check with the experiments quoted; however, his model for the dielectric profile is open to serious question. The second method is statistical in nature and assumes that beyond-the-horizon field is due to scattering by turbulence in the antennas' common volume. This method was first proposed by Booker and Gordon in 1950.[2] The method is well summarized by Wheelon in a recent paper.[3] In general, it is possible to conclude that the classical diffraction theory has failed to explain the experimental results while the statistical theory of scattering by turbulence appears to have succeeded, given a particular model for the turbulence.

This letter is concerned with a critical analysis of the question of wave propagation in or through a region of space characterized by a stochastic process.

General Theory

Let a source and observer be located in a space bounded by the surface at infinity and surface of the earth. Let the dielectric constant and conductivity of the earth V_1 be deterministic, and let the dielectric constant of V_2 be a stochastic process in *both* space and time. If the time rate of change in the stochastic process $\epsilon(\boldsymbol{r}, t)$ is bounded such that

$$\max \left\langle \left| \frac{\dot{\epsilon}}{\epsilon} \right| \right\rangle \ll \omega_0 \qquad (1)$$

where ω_0 is the carrier frequency of the source, then the homogeneous wave equation for the electric field intensity is similar in form for all space.

$$\nabla \times \nabla \times \boldsymbol{E} + \mu\epsilon\ddot{\boldsymbol{E}} = 0. \qquad (2)$$

There are *three* possible cases of interest which depend on the statistical nature of the dielectric constant:

1) $\epsilon_1(\boldsymbol{r}, t)$ is a *strictly* stationary process. A strictly stationary stochastic process is one whose distributions remain the same in all regions of space and time.[4] In this case, it is possible to define a new process $\Delta\epsilon$ such that

$$\Delta_1\epsilon(\boldsymbol{r}, t) = \epsilon_1(\boldsymbol{r}, t) - \langle\epsilon\rangle \qquad (3)$$

where the bracket represents an ensemble average. It is evident that the expectation of $\Delta_1\epsilon$ will vanish everywhere and that $\langle\Delta_1\epsilon(\boldsymbol{r}_1, t_1)\Delta\epsilon_1(\boldsymbol{r}_2, t_2)\rangle$ is a true covariance.

Substituting (3) into (2) we note that the

[1] O. Tukizi, "Diffraction theory of tropospheric propagation near and beyond the horizon," IRE Trans. on Antennas and Propagation, vol. AP-7, pp. 261–273; July 1959.

[2] H. G. Booker, and W. E. Gordon, "A theory of radio scatterihg by the troposphere," Proc. IRE, vol. 38, pp. 401–412; April, 1950.

[3] A. D. Wheelon, "Radio Wave Scattering by Tropospheric Irregularities," *J. Research, Natl. Bur. Standards*, vol. 63D, pp. 205–233; September–October, 1959.

[4] J. L. Doob, "Stochastic Processes," John Wiley and Sons, Inc. New York, N. Y.; 1953.

wave equation may be written as

$$\nabla \times \nabla \times \boldsymbol{E} + \mu\langle\epsilon\rangle\ddot{\boldsymbol{E}} = -\mu\Delta\epsilon_1(\boldsymbol{r}, t)\ddot{\boldsymbol{E}}. \quad (4)$$

Since the process $\epsilon_1(\boldsymbol{r}, t)$ is strictly stationary, it follows that its expectation $\langle\epsilon\rangle$ is independent of both space and time. It therefore follows that the solution of the homogeneous equation

$$\nabla \times \nabla \times \boldsymbol{E} + \mu\langle\epsilon\rangle\ddot{\boldsymbol{E}} = 0$$

must correspond to the classical diffraction theory for a homogeneous atmosphere.

The assumption of stationarity is common to nearly all statistical models for the analysis of "scatter" propagation.[4]

As noted by Wheelon,[4] the theoretical prediction of the distance dependence of scatter links assumes that the mean squared dielectric fluctuations are some function of altitude. In particular,

$$\langle\Delta\epsilon^2\rangle \sim \left(\frac{d\epsilon_0}{dh}\right)^2. \quad (5)$$

This is clearly a violation of the original assumption of statistical stationarity for the stochastic process $\epsilon(\boldsymbol{r}, t)$.

From this it is evident that a strictly stationary stochastic process is clearly *incorrect* in the case of the earth's troposphere.

2) $\epsilon_2(\boldsymbol{r}, t)$ is a wide-sense stationary process. A stochastic process is stationary in the wide sense if[4]

$$\langle|\epsilon(\boldsymbol{r}, t)|^2\rangle < \infty \quad \text{for all } \boldsymbol{r} \text{ and } t$$

and if the covariance function

$$\langle\epsilon(\boldsymbol{r}_1, t_1)\epsilon(\boldsymbol{r}_2, t_2)\rangle$$

is independent of *both* time and space. It is of interest to note that the expectation may still be positional or time dependent, or both.

In the application of this type of process to the problem of scatter propagation in the troposphere, it can be shown that what was said previously for ϵ_1 is true here as well.

3) $\epsilon_3(\boldsymbol{r}, t)$ is a nonstationary random process. The description of a nonstationary process will, in general, depend on its form. Clearly, in the case of the troposphere, it would be both necessary and sufficient to define a process ϵ_3 such that

$$\begin{aligned}\langle\epsilon_3\rangle &= \text{mean dielectric profile}\\ \langle\epsilon_3(\boldsymbol{r}_1, t_1)\epsilon_3(\boldsymbol{r}_2, t_2)\rangle &= \text{function of altitude, time and } |\boldsymbol{r}_2 - \boldsymbol{r}_1|. \end{aligned} \quad (6)$$

Since the process is nonstationary, the ensemble average will, in general, be a function of time and space. This is consistent with the known altitude dependence of the dielectric profile and the variation from month to month. It is of interest to note that if the process ϵ_3 is gaussian, then (6) completely determines the process.

The above conditions are useful in defining the process ϵ_3 but unfortunately they cannot be used to simplify the vector wave equation. This follows, since $\langle\epsilon\rangle$ may itself be a random but slowly varying function of space and time. In view of this, Green's function of the homogeneous equation

$$\nabla \times \nabla \times \boldsymbol{E} + \mu\langle\epsilon_3\rangle\ddot{\boldsymbol{E}} = 0$$

would itself be a stochastic process rather than deterministic, as required.

One possible way of eliminating the difficulties introduced by a nonstationary process is to use the notions of time statistics. Let any member of the process ϵ_3 represent the conditions prevalent in a physical world similar to our own. Then the ensemble of all such worlds starting with different initial conditions would constitute a random process in space and time.

Let the ensemble average of the process ϵ_3 be denoted by $\langle\epsilon_3\rangle$. Let the time average over some interval T be denoted by $\overline{\epsilon_3^T}$. It is evident that

$$\langle\overline{\epsilon_3^T}\rangle = \langle\overline{\epsilon_3}^T\rangle = \text{average profile for the interval } T.$$

This is just the standard atmosphere if T equals one year.

We are now in a position to define a new process $\Delta\epsilon_3$ such that

$$\Delta\epsilon_3(\boldsymbol{r}, t) = \epsilon_3(\boldsymbol{r}, t) - \langle\overline{\epsilon_3(\boldsymbol{r}, t)^T}\rangle. \quad (7)$$

It follows that

$$\langle\overline{\Delta\epsilon_3(\boldsymbol{r}, t)^T}\rangle = 0$$

where the time interval T is arbitrary. Since the ensemble average of the time average of the process ϵ_3 is independent of time within the interval $(t, t+T)$, it follows that the covariance function of the process $\Delta\epsilon_3$ as defined by (7) is typical of the class of locally homogeneous processes in space first considered by Silverman.[5] From the above discussion, it is also evident that the Green function of

$$\nabla \times \nabla \times \boldsymbol{E} + \mu\langle\overline{\epsilon_3^T}\rangle\ddot{\boldsymbol{E}} = 0$$

is deterministic and indeed a solution of the classical diffraction problem for the case of an inhomogeneous atmosphere. In view of this, the solution of

$$\nabla \times \nabla \times \boldsymbol{E} + \mu\langle\overline{\epsilon_3^T}\rangle\ddot{\boldsymbol{E}} = -\mu\Delta\epsilon_3(\boldsymbol{r}, t)\ddot{\boldsymbol{E}} \quad (8)$$

would constitute a true solution of the problem of scattering by a nonstationary dielectric noise.

For the sake of future analysis it is of importance to note that the process $\Delta\epsilon$ as defined by (7) may be written as the sum of two generally dependent processes. For example, let

$$\Delta\epsilon_3 = \Delta\epsilon' + \Delta\epsilon'' \quad (9)$$

where

$$\Delta\epsilon'(\boldsymbol{r}, t) = \epsilon_3(\boldsymbol{r}, t) - \overline{\epsilon_3(\boldsymbol{r}, t)^T} \quad (10)$$

and

$$\Delta\epsilon''(\boldsymbol{r}, t) = \overline{\epsilon_3(\boldsymbol{r}, t)^T} - \langle\overline{\epsilon_3(\boldsymbol{r}, t)^T}\rangle. \quad (11)$$

It is evident from these definitions that the process $\Delta\epsilon'$ is a measure of the difference between the dielectric constant and its time average in one world while the process $\Delta\epsilon''$ is a measure of the difference between the time average in one world and the ensemble average of the time average in all worlds.

Physically, this may be interpreted as follows: Let a "layer" be defined by the random process $\Delta\epsilon''$ such that the time interval $t, t+T$ corresponds to the "lifetime" of the layer. It follows that the random variable $\Delta\epsilon'$ is just a measure of random variations relative to these "layers."

In order to apply the nonstationary theory introduced above to the earth's troposphere, it is necessary to establish the cross-covariance function between the process $\Delta\epsilon'$ and $\Delta\epsilon''$. Gossard's recent experimental paper[6] concludes that intensity and scale size increase with altitude as one proceeds through a mixed (unstable) layer, but that scale size and intensity decrease sharply with height through a stable layer. Surely this indicates that the processes $\Delta\epsilon'$ and $\Delta\epsilon''$ are well correlated.

The above notions will be used by the author to analyze the problem of beyond-the-horizon propagation. Results of this analysis will be published in the near future.

DIMITRI S. BUGNOLO
Bell Telephone Labs., Inc.
Holmdel, N. J.

[5] R. A. Silverman, "Locally Stationary Random Processes," New York University, N. Y., Research Report No. MME-2; April, 1957.

[6] E. E. Gossard, "Power spectra of temperature humidity and refractive index from aircraft and tethered balloon measurements," IRE TRANSACTIONS ON ANTENNAS AND PROPAGATION, vol. AP-8, pp. 186–200; March, 1960.

Further Reply to Comments by Leon Peters, Jr. and F. C. Weimer*

First of all I wish to express my complete agreement with Muchmore's comments on this problem,[1] which successfully refute the implications of the paper by Peters and Weimer.[2] There is, furthermore, some additional factual information which bears on the practical significance of the theory under discussion which is most helpful in further invalidating the criticism of Peters and Weimer. Studies were performed by Systems Laboratories Corporation, Los Angeles, Calif. (now a Division of Electronic Specialty Company) for Hughes Aircraft Company, Los Angeles,[3] in analyzing radar reflection data from model measurements performed by Radiation Incorporated, Melbourne, Fla., and comparing these results with the theoretical results of Siegel's group at the University of Michigan, Ann Arbor, on a variety of military jet aircraft. This study was, in fact, motivated by a suspicion that actual aircraft echoes are not Rayleigh distributed. The results of this study are most interesting and for the military jet aircraft considered can be summarized as follows.

* Received by the PGAP, November 17, 1960.

[1] R. B. Muchmore, "Reply to comments by Leon Peters, Jr. and F. C. Weimer," IRE TRANS. ON ANTENNAS AND PROPAGATION, vol. AP-9, pp. 112–113; January, 1961.

[2] L. Peters, Jr. and F. C. Weimer, "Concerning the assumption of random distribution of scatterers as a model of an aircraft for tracking radars," IRE TRANS. ON ANTENNAS AND PROPAGATION, vol. AP-9, pp 110–112; January, 1961.

[3] Subcontract P.O. 4-56136-FC-38-4.

1) The theoretical results of Siegel's group provide a valid description of the radar echo in no more than 20° of azimuth out of 360° at S and X band. In this 20° a few large reflectors do dominate the radar echo and the echo is indeed not Rayleigh distributed. Furthermore, the echo here is large.

2) In the remaining 340° the echo *analyzed over 5° intervals in azimuth* is remarkably Rayleigh and is considerably larger than the predictions of Siegel's group. This difference we attribute to the jet motors which were not even considered by Siegel's group. Thus the motors dominate the echo over most aspect angles and the Rayleigh distribution can be attributed to their complicated internal structure.

3) The motors were modeled imperfectly, *i.e.*, with insufficient internal detail, but the measured echo was still remarkably Rayleigh everywhere, with slowly changing mean value with angle. Throwing caution to the winds we speculate that the real motors produce echoes which, if anything, are even closer to a Rayleigh distribution and this due to their more complicated structure.

It should be evident from these results that the Rayleigh distribution in this particular practical application does not proceed from a regular structure tailored to produce it, but is the result of several complex concave and convex structures with a strong possibility of multiple internal reflections. In this case the randomly phased scatterer model is the only nontrivial explanation possible.

R. H. De Lano
Systems Labs.
Div. of Electronic Specialty Co.
Los Angeles, Calif.

Comparison Between Theoretical and Experimental Radar Cross Sections of Aircraft*

Despite De Lano's comments to the contrary,[1] the results of our group have yielded good agreement between theory and experiment for the radar cross sections of aircraft for the past several years.

In the late forties the results obtained at X and S band were good to about 10 db. In the early fifties the results improved so that without the use of digital computers, differences between theory and experiment were reduced to about 6 db. Now, at the frequencies discussed (X and S band), we have obtained and can obtain agreement to within about 2 or 3 db. The differences have decreased, not only because of improvements in the theory, but also because of improvements in experimental technique and in our ability to make models.

* Received by the PGAP, December 8, 1960.

[1] R. H. De Lano, "Further reply to comments by Leon Peters, Jr. and F. C. Weimer," this issue, pp. 227–228.

Differences of 2 or 3 db reduce the problem to an academic one, as experience has shown that thousands of engineering changes are made on an aircraft before it changes its name. Many of these changes affect the cross section by an amount greater than the 2- or 3-db differences mentioned above.

De Lano's comments are incorrect on many scores. It is true that our initial results on the B-47 were off by as much as 6 db at nose-on aspects for the blueprint of the B-47 we then used in our calculations. This was within the theoretical tolerance we placed on the methods we were using. John Hult of the RAND Corporation first pointed out the significances of the jet engines, and we quickly improved our calculations. Long after our calculations were improved, many scientists continued to criticize our original results, never recognizing that our results were as good as desired for the purpose for which they were computed. The tendency increased to use howitzers to shoot down clay pigeons. That is, people wanted us to compute cross sections to $\pm\frac{1}{2}$ db when they would not know how to use results better than ± 3 db, especially since a change in aspect easily swamps any small errors in calculations at a single aspect.

I challenge De Lano to compare our results for the B-57 obtained well before any experiments were made with the later experiments. He will find they completely refute his findings.

Since De Lano has brought me into this discussion by name, I have answered it myself. However, it would be wrong if I did not point out that our methods of computing cross sections have improved because of the many helpful analyses of Kennaugh, Kouyoumjian and Peters of The Ohio State University and those of Crispin and his coworkers at the Radiation Laboratory of The University of Michigan, as well as the work of many other investigators in this field.

K. M. Siegel
Dept. of Elec. Engrg.
University of Michigan
Ann Arbor, Mich.

Reply to Comments by R. H. De Lano*

We disagree with three statements De Lano[1] makes in his comments: 1) most important, 5 degrees is the proper interval in which to observe the target, 2) jet motors are the major contributors over 340° out of 360° of azimuth, and 3) Muchmore[2] has successfully refuted our "implications."

The rate of change of aspect of a jet in normal flight conditions is usually considerably less than one degree per second. Therefore, about 0.5° would be the appropriate interval in which to observe the target, assuming the time response of the servo to be no more than one second. For such aspect intervals, the echo area of the typical target is no longer Rayleigh distributed.

The case of the jet motors cannot be detailed here because of classification but is a problem that personnel at this laboratory including one of these authors has considered in considerable detail.[3–6] The apparent radar center of the jet motor has also been measured,[6] and its characteristics differ drastically from those suggested by De Lano. On the basis of this experience, let us state that De Lano is completely wrong when he assumes the jet motors are the major source of echo area for these 340° of azimuth.

The source of echo area for complex targets has been studied at this laboratory and while the results cannot be published for reasons of classification, the list of reports[7–10] indicates that this problem has not been considered lightly.

In concluding this letter, we emphasize that the echo area of typical targets is not Rayleigh distributed over the proper aspect interval. Therefore, the methods of De Lano and Muchmore can not yield the correct results. Furthermore, even if the echo area had been Rayleigh distributed, one cannot be assured that their methods are applicable as has been shown by an example.

L. Peters, Jr.
F. C. Weimer
Antenna Lab.
The Ohio State University
Columbus, Ohio

* Received by the PGAP, December 13, 1960.

[1] R. H. De Lano, "Further reply to comments by Leon Peters, Jr. and F. C. Weimer," this issue, pp. 227–228.

[2] R. B. Muchmore, "Reply to comments by Leon Peters, Jr. and F. Weimer," IRE Trans. on Antennas and Propagation, vol. AP-9, pp. 112–113; January, 1961.

[3] R. G. Kouyoumjian and C. C. Maneri, "Memorandum Discussing the Effects of Air Intakes on the Echo Measurements of Jet Aircraft," Antenna Lab., The Ohio State University Res. Foundation, Columbus, Ohio, Rept. No. 601-21; prepared under Contract AF 33(616)-2546, Air. Res. and Dev. Command, Wright Air Dev. Ctr., Wright-Patterson AFB, Ohio, ASTIA Doc. No. AD 139 232; July 19, 1957.

[4] W. E. Bulman, "Association of the 600-Megacycle Radar Back-Scattering Characteristics with the Physical Structure of the B-47 Aircraft," Antenna Lab., The Ohio State University Res. Foundation, Rept. No. 601-20, prepared under Contract AF 33(616)-2546, ASTIA Doc. No. AD 144 426; August 31, 1957.

[5] W. E. Bulman, "Investigation of Angular Scattering Cross Section of the B-47 Aircraft at a Simulated Frequency of 250 Megacycles," Antenna Lab., The Ohio State University Res. Foundation, Rept. No. 601-27, prepared under Contract AF (33(616)-2546, ASTIA Doc. No. AD 152 785; November 30, 1957.

[6] J. R. Copeland and L. Peters, Jr., "The Effect of Polarization of the Echo Area and Scintillation of the F-86 Aircraft at Several Frequencies," Antenna Lab., The Ohio State University Res. Foundation, Rept. No. 601-28, prepared under Contract AF 33(616)-2546 ASTIA Doc. No. AD 150 184; November 30, 1957.

[7] L. Peters, Jr., "Location of Scatterers on a Complex Target by Means of Tracking Radar Systems," Antenna Lab., The Ohio State University Res. Foundation, Rept. No. 777-1; prepared under Contract AF 33(616)-5341, Air Res. and Dev. Command, Wright Air Dev. Ctr., Wright-Patterson AFB, ASTIA Doc. No. AD 162 696; March 15, 1958.

[8] D. E. Lewis, "Location of Radar Scattering Centers by Optical Means," Antenna Lab., The Ohio State University Res. Foundation, Rept. No. 777-8, prepared under Contract AF 33(616)-5341, ASTIA Doc. No. AD 307 759; February 28, 1959.

[9] D. E. Lewis, "Location of Scatterers on the B-47 Aircraft and Other Complex Targets," Antenna Lab., The Ohio State University Res. Foundation, Rept. No. 777-12, prepared under Contract AF 33(616)-5341, ASTIA Doc. No. AD 314 349; March 20, 1959.

[10] L. Peters, Jr., "Location of Flare Spots by Modeling Techniques," Antenna Lab., The Ohio State University Res. Foundation, Rept. No. 777-13, prepared under Contract AF 33(616)-5341, ASTIA Doc, No, Ad 313 159; June 30, 1959.

Reply to Comments by R. B. Muchmore*

In our original communication[1] we have shown that the apparent radar center does not wander for two cases:

1) the two-point target when the echo area of the individual scatterers is equal regardless of their relative phases,
2) the uniform line source with a linear phase distribution.

As we pointed out, the statistical methods would predict that the apparent phase center does wander. The reason for this discrepancy is that the original condition set forth by DeLano,[2] that the target be composed of an infinite number of statistically independent amplitudes and phases, has not been satisfied. The uniform line source discussed above has a Rayleigh distributed far field over a wide range of aspects. On the basis of this example, we concluded that DeLano's original condition could not be relaxed to that of a target whose echo area is Rayleigh distributed.

The mathematical singularity appearing in the solutions for the apparent radar center ϵ_0 for both a two point scatterer and for a line scatterer is not significant. For the cases we have considered, the apparent radar center must lie at the midpoint of the target, as Muchmore[3] has agreed. Only when no voltage is received can this differ. If the radar receives no voltage, it can not locate the radar center whether or not there is a mathematical singularity. In other words, even though the phase front is shifted 90°, the radar can not tell this because it receives no signal. The pertinent limit in this case is a physical one. At some time the received signal falls just below the threshold level of the receiver and is no longer detectable. At this time, however, the radar signal is still finite and the apparent radar center is fixed at the midpoint of the target. Whatever happens as this signal progresses to an absolute zero has no physical significance. It will be recalled that we stated that the apparent radar center does wander and we have correlated theoretical calculations with experiment. The point is that computations using the statistical methods insofar as these cases are concerned are not correct because the target fails to satisfy the original assumptions. The two-point target may be altered such that the apparent radar center does wander. We have no assurances that statistical methods would yield correct results unless DeLano's original criterion is satisfied, particularly when an example that fits the criterion of a Rayleigh distributed echo area has been given, however improbable that example may be, for which incorrect results are obtained. This is particularly true for the two-point target where the magnitude of the echo area of the individual scatterers differ as there is not a sufficient number of scatterers.

Muchmore has misinterpreted our example for the two-point scatterer. We have considered the case of two scatterers with equal amplitudes but with arbitrary, not fixed, phases. Indeed this is in agreement with the original assumption of DeLano as described above and, for small changes of aspect angle, is correct for the typical target.

Several examples of radar targets that might be point scatterers insofar as a tracking radar is concerned include:

1) Triple bounce corner reflector for which the reflections appear to come from the apex,
2) The sphere for which reflections seem to come from the point at normal incidence,
3) Any smoothly curved surface with radii of curvature, large with respect to wavelength, for which reflections appear to come from the point at normal incidence. In this case, the point wanders slowly and magnitude changes as a function of the angle of incidence but not in a random manner.

In relation to the line scatterer, it would appear that Muchmore makes our point quite neatly when he gives the example of reflections occurring from the vertical stabilizer and four motor nacelles; *i.e.*, all other reflections are negligible. However, there is usually not such a large number of dominant scatterers.

This last viewpoint leads to what we believe is the proper approach; *i.e.*, the properties of typical targets need to be studied and when the original conditions of DeLano are satisfied for the appropriate time interval, the statistical approach is applicable. Otherwise, it is necessary to study the motion of the apparent radar center as a function of time to determine the scintillation properties. This approach has been used by R. B. Feagin and Dr. R. B. Watson at the University of Texas.

L. Peters, Jr.
F. C. Weimer
Antenna Lab.
The Ohio State University
Columbus, Ohio

* Received gy the PGAP, December 13, 1960.

[1] L. Peters, Jr. and F. C. Weimer, "Concerning the assumption of random distribution of scatterers as a model of an aircraft for tracking radars," IRE Trans. on Antennas and Propagation, vol. AP-9, pp. 110–112; January, 1961

[2] R. H. De Lano, "Further reply to comments by Leon Peters, Jr. and F. C. Weimer," this issue, pp. 227–228.

[3] R. B. Muchmore, "Reply to comments by Leon Peters, Jr. and F. C. Weimer," IRE Trans. on Antennas and Propagation, vol. AP-9, pp. 112–113; January, 1961.

Some Variations in Log-Periodic Antenna Structures*

Two types of simple log-periodic zig-zag structures are shown in Figs. 1 and 2. Fig. 1 shows an unbalanced tapered strip structure on a small sectoral image plane with the plane of polarization perpendicular to the image plane. Fig. 2 shows a balanced essentially planar version of wire or rod zig-zag conductors.

Sample *E*- and *H*-plane relative-power patterns of the unbalanced structure of Fig. 1 are shown in Figs. 3 and 4; of the balanced

* Received by the PGAP, November 20, 1960.

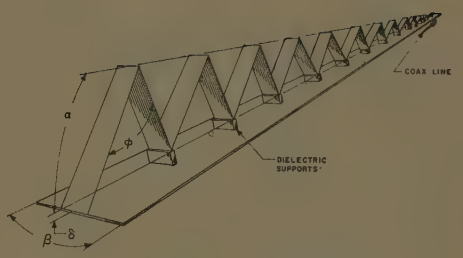

Fig. 1—Unbalanced strip zig-zag.

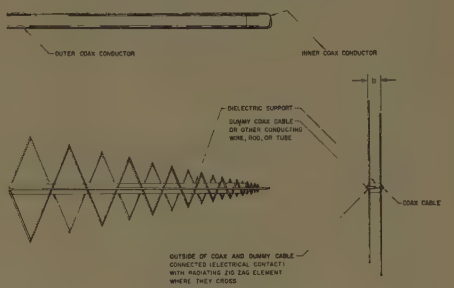

Fig. 2—Balanced planar zig-zag.

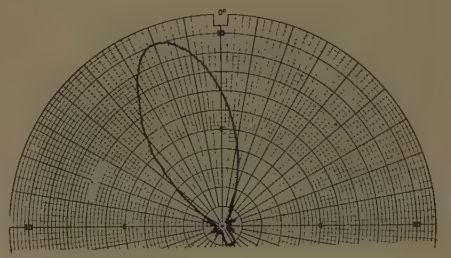

Fig. 3—Typical *E*-plane pattern of unbalanced strip zig-zag on 19° sectorial image plane.

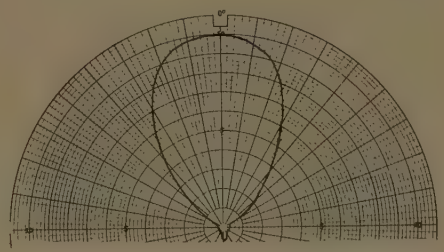

Fig. 4—Typical *H*-plane pattern of unbalanced strip zig-zag on 19° sectorial image plane.

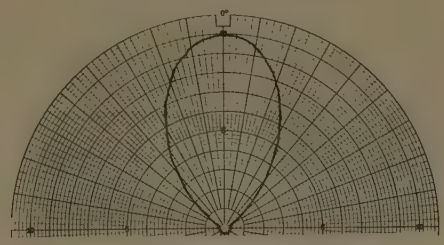

Fig. 5—Typical *E*-plane pattern of balanced planar zig-zag.

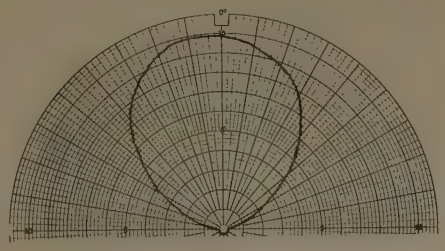

Fig. 6—Typical *H*-plane pattern of balanced planar zig-zag.

structure in Figs. 5 and 6. Both antennas can be designed to easily fold up into a neat package. Fig. 7 shows a variation of Fig. 2. It will be noted that, when fed with a balanced line, the balanced zig-zag structure does not require conducting members conductively coupled to the center points of the radiators as in the case when fed by an unbalanced line located in a corresponding position. Nor are the straight longitudinal conducting sections required in the case where the unbalanced line is integrated into the radiating sections instead of being brought into the structure by the standard method shown in Fig. 2. One method is to run the coaxial line inside of tubular zig-zag radiators. Another method is to run the coax alongside the conductors as indicated in Fig. 7, the outer coax conductor being at least spot conductively coupled to the radiators, for instance, at each vertex of the zig-zag.

The dimensionless ratio τ for all structures is given by

$$\tau = \left[\frac{1 - \tan\frac{\alpha}{2}\tan\frac{\phi}{2}}{1 + \tan\frac{\alpha}{2}\tan\frac{\phi}{2}}\right]^2,$$

which is also the length ratio of any straight zig-zag element to the next larger parallel element.

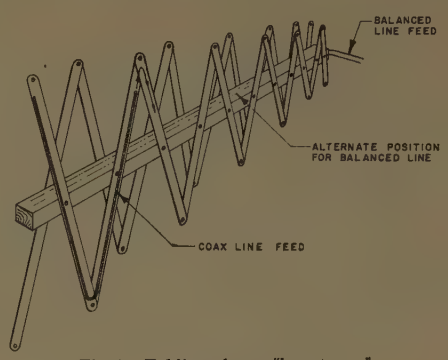

Fig. 7—Folding planar "lazy-tongs" zig-zag log-periodic.

Note that either radiator in Fig. 7 may be folded in the same fashion as a lazy-tongs mechanism.

Not only does the removal of the conducting rods simplify the antenna structure for some applications, but also it raises the characteristic impedance of the antenna. This latter characteristic makes the structure more easily adaptable to the nominally higher impedances of balanced two wire lines such as used in current television applications.

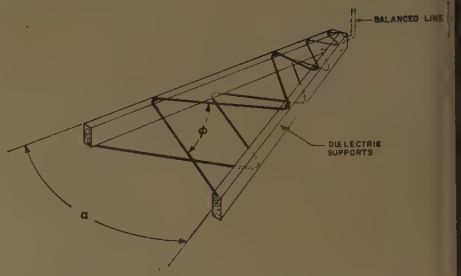

Fig. 8—Planar wire zig-zag log-periodic.

It is logical that this should be so, since removal of the two parallel conductors greatly decreases the distributed shunt capacity along the antenna. For instance, the mean R_0 of the structure of Fig. 2 was increased from about 85 ohms to approximately 230 ohms by simply removing the two parallel conductors. The b dimension was 1 inch, radiator diameter $\frac{1}{8}$ inch, $\tan \alpha/2 = 1/6$, $\phi = 45°$. Fig. 8 shows a planar balanced zig-zag constructed of flexible cable or wire, the vertices supported by structurally stiff dielectric members.

J. W. Carr
Missiles and Space Div.
Lockheed Aircraft Co.
Sunnyvale, Calif.

Contributors

Warren E. Bulman (A'52–SM'57) was born in Woodville, Ala. on January 3, 1923. He received the B.A. degree in physics from Berea College, Berea, Ky. in 1948, and the M.S. degree in physics from Purdue University, Lafayette, Ind., in 1951. He received the Ph.D. degree from The Ohio State University, Columbus, in 1958.

W. E. Bulman

From 1950–1951 he was employed at the National Bureau of Standards. From 1951 to 1955 he was engaged in solid-state physics and electronics research activities at Battelle Memorial Institute, Columbus, Ohio. From 1955 to 1958 he was engaged in research in electromagnetics and microwaves with the Antenna Laboratory of The Ohio State University, where he is now a consultant.

He has been President of Ohio Semiconductors, Inc., in Columbus since its inception in 1956.

Dr. Bulman is a member of Sigma Xi, the American Physical Society, and the Electrochemical Society.

❖

Samarendramohon Dasgupta was born on September 3, 1922, in Bengal, India. He received the B.S. degree in physics, with honors, in 1942, and the M.S. degree in applied physics (electronics) in 1944, from the University of Calcutta, Calcutta, India.

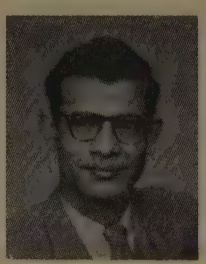

S. Dasgupta

Following his studies, he joined the department of electrical engineering at the Indian Institute of Science, Bangalore, India, as a research assistant, and worked in the radio direction finding project until 1947. In 1948 he joined the staff of the Ceylon Technical College, Colombo, Ceylon, as a lecturer in electrical communication engineering. After a year's stay there, he became assistant professor at the Government Engineering College, Jabalpur, India, and subsequently became a reader at the same institution. In 1956, on study leave from India, he joined the department of electrical engineering at the University of Illinois, Urbana. After receiving the Ph.D. degree in 1959 from this university, he returned to India to teach at the Government Engineering College, Jabalpur.

Dr. Dasgupta is a member of Pi Mu Epsilon, and an associate member of the Institute of Electrical Engineers, London.

❖

R. B. Green was born in Des Moines, Iowa, on July 15, 1936. He received the B.S. degree in electrical engineering from Iowa State University in 1958, and the M.S. degree in electrical engineering from The Ohio State University, Columbus, in 1959.

Since 1958, he has been associated with the Antenna Laboratory of the electrical engineering department of the Ohio State University, where he is currently a research associate working on radar scattering problems.

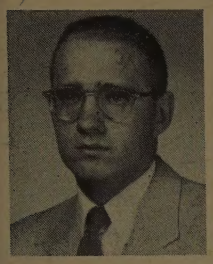

R. B. GREEN

Mr. Green is a member of Pi Mu Epsilon, Eta Kappa Nu, Tau Beta Pi, and Phi Kappa Phi, and is associated with Sigma Xi.

❖

Peter W. Hannan (S'49–A'49–M'55–SM'59) was born on February 19, 1927 in New York, N. Y. He served in the United States Navy during 1945 and 1946, and received the B.S. degree in engineering from Stevens Institute of Technology, Hoboken, N. J., in 1948. He received the M.S. degree in electrical engineering in 1950 from the University of Pennsylvania, Philadelphia, Pa.

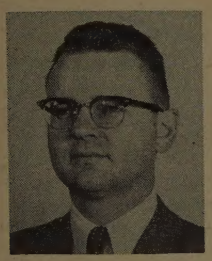

P. W. HANNAN

Since 1949, he has been a member of the staff of Wheeler Laboratories, Inc., Long Island, N. Y. His early work was performed at the Great Neck facility, and involved the design of microwave waveguide components. Subsequently his field of interest evolved into microwave antennas, and he has been responsible for several designs which are now in service. At present he is a senior development engineer at the Smithtown antenna facility, where he is engaged in consultation on a number of microwave antennas.

❖

Roger F. Harrington (S'48–A'53) was born in Buffalo, N. Y., on December 24, 1925. He received the B.E.E. degree in 1948 and the M.E.E. degree in 1950, both from Syracuse University, Syracuse, N. Y., and the Ph.D. degree in 1952 from The Ohio State University, Columbus, Ohio.

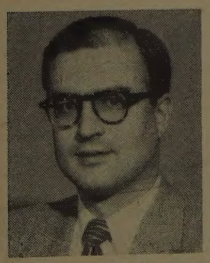

R. F. HARRINGTON

From 1945 to 1946, Dr. Harrington served as an instructor at the Naval Radio Materiel School, Dearborn, Mich., and from 1948 to 1950, he was employed as an instructor and research assistant at Syracuse University. While studying at The Ohio State University, he served as a research fellow in the Antenna Laboratory. Since 1952, he has been on the faculty of Syracuse University, currently as professor of electrical engineering.

Dr. Harrington is a member of Tau Beta Pi, Sigma Xi, and the American Association of University Professors.

❖

Stephen M. Harris (S'55–M'58) was born in New York, N. Y., on March 24, 1934. He received the bachelor's degree in engineering physics from Cornell University, Ithaca, N. Y., in 1956, and the M.S. degree in electrical engineering from Stanford University, Stanford, Calif., in 1957.

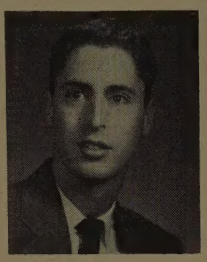

S. M. HARRIS

During his graduate studies at Stanford, he was a research and teaching assistant in the department of electrical engineering. From 1957 to 1959, he was associated with the Maynard Laboratory of the Raytheon Company, Maynard, Mass., where he studied the accuracy requirements and performance characteristics for a CW Doppler radar navigator. Since 1959, he has been on the technical staff of Hermes Electronics Company, Cambridge, Mass., where he has worked in the fields of radio propagation and communications systems design.

❖

Charles W. Harrison, Jr. (SM'57) was born on September 15, 1913, in Farmville, Va. He attended the U. S. Coast Guard Academy, New London, Conn., and received the B.S.E. and E.E. degrees in 1939 and 1940, respectively, from the University of Virginia, Charlottesville. He received the M.S. degree in communication engineering in 1942 from Harvard University, Cambridge, Mass., and, under the sponsorship of the ONR, received the M.E. and Ph.D. degrees in applied physics from Harvard in 1952 and 1954, respectively.

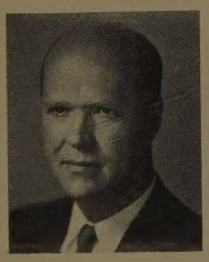

C. HARRISON, JR.

He completed the Navy course in radar engineering at the Massachusetts Institute of Technology, Cambridge, in 1942, and subsequently was engaged in lecturing to officers of the Armed Forces assigned to the radar schools at Harvard and at Princeton University, Princeton, N. J., for several years. He has had four tours of duty in the Electronics Design and Development Division, Bureau of Ships; two at the U. S. Naval Research Laboratory; one at the Signal Corps Engineering Laboratories (Evans Signal Laboratory); one at the Philadelphia Naval Ship Yard; one as Electronics Officer, Staff of Commander Operational Development Force; and one on the Staff of the Chief, Armed Forces Special Weapons Project. He left active service as a Commander in the regular Navy in 1957 to join the Scientific Staff of the Sandia Laboratory, Albuquerque, N. M.

Dr. Harrison is a member of the Research Society of America, the American Scientific Affiliation, URSI, and Sigma Xi. He is a Registered Professional Engineer in Virginia, the District of Columbia, and Massachusetts.

❖

Robert A. Hessemer, Jr. (S'48–A'50–M'55) was born in Montesano, Wash. on June 20, 1923. He received the B.S.E.E. degree in 1947 from the University of Washington, Seattle, and the M.S. and Ph.D. degrees in 1948 and 1953, respectively, from Stanford University, Stanford, Calif.

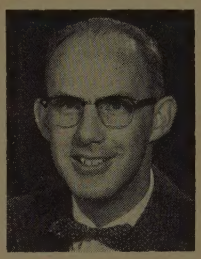

R. A. HESSEMER

He was an instructor in electrical engineering at the University of New Mexico Albuquerque, from 1948 to 1950 and an assistant professor from 1952 to 1955. From 1953 to 1955 he was a consultant to Sandia Corporation, Albuquerque, N. M., on problems associated with radar terrain return at near-vertical incidence. From 1956 to 1959 he was a consultant to the Radio Corporation of America on problems associated with simulation of communication systems. In 1955 he joined the University of Arizona, Tucson, as professor of electrical engineering, where he is presently engaged in teaching and research in microwave theory and antennas.

Dr. Hessemer is a member of Tau Beta Pi and Sigma Xi.

❖

Kenneth S. Kelleher (M'48–SM'51) was born on December 25, 1922, in Richmond, Va. He received the B.A. degree in mathematics from the University of North Carolina, Chapel Hill, in 1943, and the M.A. degree in mathematics from the University of Maryland, College Park, in 1948.

K. S. KELLEHER

From 1943–1953, he served in the Microwave Optics Section of the Naval Research Laboratory, Washington, D. C. He was Project Manager in charge of the Antenna and Countermeasures Sections at Melpar, Inc., Falls Church, Va., from 1953 to 1958. Since 1958, he has been the President of Aero Geo Astro Corporation, Alexandria, Va.

Mr. Kelleher is a member of the American Rocket Society and of Commission 6 of URSI. In 1958, he was given the Professional Achievement Award to the Outstanding Young Applied Scientist at the Engineers and Architects Day Observance in Washington, D. C.

Ronold W. P. King (A'30–SM'43–F'53) was born in Williamstown, Mass., on September 19, 1905. He received the B.A. degree in 1927 and the M.S. degree in 1929, both from the University of Rochester, Rochester, N. Y., where he majored in physics. He received the Ph.D. degree from the University of Wisconsin, Madison, in 1932, after having done graduate work at the University of Munich, Munich, Germany, and Cornell University, Ithaca, N. Y.

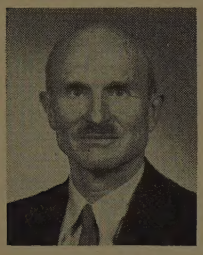

R. W. P. KING

He served as teaching and research assistant at the University of Wisconsin in 1932–1934, and as instructor and assistant professor of physics at Lafayette College, Easton, Pa., from 1934 to 1937. The year 1937–1938, he spent in Germany as a Guggenheim Fellow. In 1938 he joined the faculty of Harvard University, Cambridge, Mass., where he advanced to the rank of professor in 1946. He is now Gordon McKay Professor of applied physics at Harvard University. Again in 1958, he was a Guggenheim Fellow, studying and traveling abroad.

Dr. King is a Fellow of the American Physical Society and the American Academy of Arts and Sciences, a corresponding member of the Bavarian Academy of Sciences, and a member of the American Association of University Professors, the American Association for the Advancement of Science, Phi Beta Kappa, and Sigma Xi.

❖

Y. T. Lo, for a photograph and biography, please see page 122 of the January, 1961 issue of these TRANSACTIONS.

❖

Robert Plonsey (A'47–S'54–M'56–SM'60) was born in New York, N. Y. on July 17, 1924. He received the B.E.E. degree from Cooper Union, New York, in 1943, the M.E.E. degree from New York University, New York, in 1948, and the Ph.D. degree from the University of California, Berkeley, in 1956.

R. PLONSEY

From 1943 to 1944 he worked as junior radio engineer for Hazeltine Electronics Corporation, Little Neck, L. I., N. Y. After receiving his degree from New York University, he was a staff member at Polytechnic Research and Development, Brooklyn, N. Y. from 1948 to 1949. In 1953 he was appointed research assistant at the Antenna Laboratory, University of California, Berkeley. From 1955 to 1957 he served on the faculty of the University of California as an acting assistant professor in electrical engineering. Since 1957 he has been at the Case Institute of Technology, Cleveland, Ohio, where he is associate professor of electrical engineering. His work has been in the field of electromagnetic theory.

Dr. Plonsey is a member of Sigma Xi.

❖

Byron C. Potts was born in Springfield, Ohio, on October 2, 1930. He received the B.E.E. and M.S. degrees in electrical engineering from The Ohio State University, Columbus, in 1959.

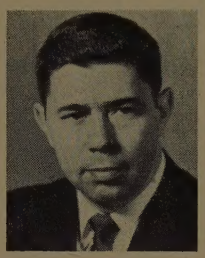

B. C. POTTS

Since 1959 he has been employed as a research associate at the Antenna Laboratory of the electrical engineering department of The Ohio State University, working in the fields of microwave scattering, upper-atmosphere physics, and electromagnetic propagation.

Mr. Potts is a member of Tau Beta Pi and Eta Kappa Nu, and is an associate of Sigma Xi.

❖

S. R. Seshadri was born on October 25, 1928, in Madras, India. He received the M.S. degree in physics in 1951 from the University of Madras, India, and he earned the diploma in electrical communication engineering in 1953 from the Indian Institute of Science, Bangalore, India. In 1959, he received the Ph.D. degree in applied physics from Harvard University, Cambridge, Mass.

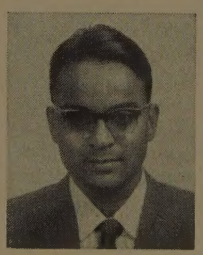

S. R. SESHADRI

From 1954 to 1955 he served as a lecturer in electronics at the Madras Institute of Technology. He was a research fellow in electronics at Harvard University in 1960, and is presently with the Electronics Research and Development Establishment, Bangalore.

Dr. Seshadri is a member of Sigma Xi.

H. E. Shanks, for a photograph and biography, please see page 532 of the September, 1960, issue of these TRANSACTIONS.

❖

Eugene D. Sharp (S'54–A'55–M'57) was born on October 29, 1931, in Greeley, Colo. He received the B.S. degree in 1954 and the M.S. degree in 1956, both in electrical engineering from Stanford University, Stanford, Calif. In 1954–1955, he was employed by the Air Research Organization, Inc., Tullahoma, Tenn., and during 1955–1956, he was a teaching assistant in electrical engineering at Stanford University. From 1956 to 1958, he was a project officer at the Rome Air Development Center, Griffiss AFB, Rome, N. Y., working in the Antenna Development Section.

E. D. SHARP

In 1958, he joined the staff of Stanford Research Institute, Menlo Park, Calif., where he has been working on a study of electronic scanning antennas, ECM antennas, and high-power waveguide filters. He is studying for the Ph.D. degree in electrical engineering at Stanford University, on a part-time basis under the Honors Cooperative Program.

Mr. Sharp is a member of Tau Beta Pi.

❖

J. Paul Shelton, Jr. (M'56) was born on December 24, 1931, in Detroit, Mich. He attended Rollins College, Winter Park, Fla., from 1949 to 1952, and received the B.S. degree in physics from The Ohio State University, Columbus, in 1953.

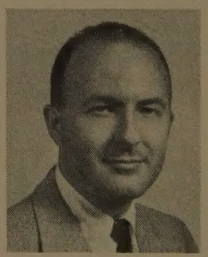

J. P. SHELTON, JR.

From 1953–1954, he served as Technical Editor at the Applied Physics Laboratory, Silver Spring, Md., and 1954–1958, he was Consulting Project Engineer for the Antenna Section at Melpar, Inc., Falls Church, Va. He was part-time mathematics instructor at the University of Virginia Extension, Arlington, from 1957 to 1958. From 1958 to 1960 he was a Staff Consultant at the Aero Geo Astro Corporation, Alexandria, Va. In the fall of 1960, he left the AGA Corporation to help found Radiation Systems, Inc., Alexandria, Va., where he is a member of the Senior Staff.

INSTITUTIONAL LISTINGS

The IRE Professional Group on Antennas and Propagation is grateful for the assistance given by the firms listed below, and invites application for Institutional Listing from other firms interested in the field of Antennas and Propagation.

AERO GEO ASTRO CORP., 1200 Duke St., Alexandria, Va.
Space Instrumentation; Antennas; Transponders; Command Receivers; Augmenters; Telemetry; Radar

ANDREW CORPORATION, P.O. Box 807, Chicago 42, Ill.
Antennas, Antenna Systems, Transmission Lines, Development and Production

ANTLAB, INC., 6330 Proprietors Rd., Worthington, Ohio
Antenna Pattern Range Systems—Recorders & Mounts, & Telemetry Servo Pedestals

BLAINE ELECTRONETICS, INC., 14757 Keswick St., Van Nuys, Calif.
Antennas, Paraboloids, Scale Models, Antenna Radiation Pattern Measurement Towers

DEVELOPMENTAL ENGINEERING CORP., Leesburg, Va.; Boston, Mass.; Boulder, Colo.; Washington, D C.
Antenna Research, Design & Evaluation-Propagation Studies & Communications Systems Engineering

DORNE & MARGOLIN, INC., 29 New York Ave., Westbury, L. I., N. Y.
Research, Development and Manufacture—Antenna and Microwave Technology

FXR, Inc., 25–26 50th St., Woodside 77, N. Y.
Precision Microwave Test Equip., High Power Microwave Electronics, Microwave Components & Instrumentation

GABRIEL ELECTRONICS, Division of The Gabriel Company, Main & Pleasant Sts., Millis, Mass.
Research, Engineering and Manufacture of Antenna Equipment for Government and Industry

HUGHES AIRCRAFT COMPANY, Florence and Teale Sts., Culver City, Calif.
Res., Dev., Mfg.: Radar Systems & Components; Antennas, Tubes, Radomes, Solid-State Devices

I-T-E CIRCUIT BREAKER CO., Special Products Div., 601 E. Erie Ave., Philadelphia 34, Pa.
Design, Development and Manufacture of Antennas, and Related Equipment

JANSKY & BAILEY, INC., 1339 Wisconsin Ave., N.W., Washington, D. C.
Complete Engineering Services for Antennas and Propagation Programs

MARK PRODUCTS CO., 5439 W. Fargo Ave., Skokie, Ill.
Antennas for Two-Way Communications, Grid Parabolas, Research & Development

TECHNICAL APPLIANCE CORP., 1 Taco St., Sherburne, N. Y.
Des., Dev., & Mfg.: Antennas & Antenna Systems for Communications, Telemetry, & Tracking

WEINSCHEL ENGINEERING COMPANY, INC., Kensington, Md.
Antenna Pattern Receivers; Bolometer Amplifiers; Microwave Sources; Insertion Loss Measuring Systems

WHEELER LABORATORIES, INC., Great Neck, N. Y.; Antenna Lab., Smithtown, N. Y.
Consulting Services, Research and Development, Microwave Antennas and Waveguide Components

The charge for Institutional Listing is $50 for one issue or $200 for six consecutive issues (one year). Application may be made to the Technical Secretary, The Institute of Radio Engineers, Inc., 1 East 79th Street, New York 21, N. Y.